All-optical processing using cross-phase modulation

James Ashley Harrison

Doctor of Philosophy

Aston University

October 2005

Aston University

All-optical Processing Using Cross-Phase Modulation

James Ashley Harrison

Doctor of Philosophy
October 2005

The following thesis presents results obtained from both numerical simulation and laboratory experimentation (both of which were carried out by the author). When data is propagated along an optical transmission line some timing irregularities can occur such as timing jitter and phase wander. Traditionally these timing problems would have been corrected by converting the optical signal into the electrical domain and then compensating for the timing irregularity before converting the signal back into the optical domain. However, this thesis posses a potential solution to the problem by remaining completely in the optical domain, eliminating the need for electronics. This is desirable as not only does optical processing reduce the latency effect that their electronic counterpart have, it also holds the possibility of an increase in overall speed.

A scheme was proposed which utilises the principle of wavelength conversion to dynamically convert timing irregularities (timing jitter and phase wander) into a change in wavelength (this occurs on a bit-by-bit level and so timing jitter and phase wander can be compensated for simultaneously). This was achieved by optically sampling a linearly chirped, locally generated clock source (the sampling function was achieved using a nonlinear optical loop mirror). The data, now with each bit or code word having a unique wavelength, is then propagated through a dispersion compensation module. The dispersion compensation effectively re-aligns the data in time and so thus, the timing irregularities are removed. The principle of operation was tested using computer simulation before being re-tested in a laboratory environment.

A second stage was added to the device to create 3R regeneration. The second stage is used to simply convert the timing suppressed data back into a single wavelength. By controlling the relative timing displacement between stage one and stage two, the wavelength that is finally produced can be controlled.

Additional key words and phrases

Nonlinear optics, cross-phase modulation, wavelength conversion, nonlinear optical loop mirror.

Acknowledgements

There are several people that should be thanked who have provided valuable support for the duration of this thesis. I would firstly like to thank Professor Keith Blow for all his help and backing throughout my time at Aston University. I should also say a big thank you to all of the staff in the Photonics Research Group at Aston University. Many valuable discussions took place with many different members. I would also like to thank Corning who were the case sponsor for the duration of the PhD. Corning also gave me the opportunity to work at the Corning Research Centre in Ipswich. This proved to be an invaluable experience where much was learnt. All of the experimental results shown in this thesis were obtained after experimentation at Corning Research Centre. Thus, my thanks goes to all the staff there for generating such an unforgettable experience. Special mention should go to Doctor Alistair Poustie who was my industrial supervisor. He taught me so much, I don't know where I would have been without him.

I would finally like to thank again Professor Blow and Doctor Poustie who demonstrated so much more than simple academic guidance, both providing much needed friendship.

for Mum and Dad, thanks for everything

Chapter 1 - Introduction to Optical Communications

1.1 Introduction

Since the advent of telegraphy in the 1830's [1, 2] the modern telecommunications industry has grown at a tremendous rate. The importance and need to be able to directly communicate at will on a global scale has become paramount in modern society. This was made possible by the birth of the telephone. However, an increase in demand for capacity (more and more simultaneous telephony) and the introduction of the internet (by connecting computers together, it has meant that it is possible to transmit large amounts data over a telephone line) has meant that the traditional "twisted copper pair" communication system is fast becoming obsolete. The demand for an increase in bandwidth lead to the discovery in the 1970's that light could be propagated along an optical fibre with a loss of less than 20dB/km [3] (at the time of discovery this was often referred to as a "light pipe") and that this propagated light could be encoded with data. It was clear from an early stage that this new optical fibre technology would be able to overcome many of the limitations of coaxial copper electrical system where the key development in the industry has been the dramatic improvement in optical fibre technology, both in terms optical loss and dispersion.

Certainly another important factor in the growth of optical communications was the technological advancements in the optical amplifier domain which involved the use of doping silica or fluoride fibres with rare-earth ions such as erbium. Developments like

these have meant that it was now possible to consider the high bandwidth possibilities of optical communications.

1.2 Optical fibres

Before we go any further it is important that we firstly discuss some of the properties of optical fibre. Any typical optical communications system will consist of a lightwave transmitter (clearly electronics of some sort will be associated with this section), a transmission medium (we would assume optical fibre) and finally a receiver.

An optical fibre consists of a dielectric core (usually doped silica) of a high refractive index which is then surrounded by a cladding which has a lower refractive index than the core [2]. A typical cross-section of SMF is shown in Figure 1.1 (not shown is the protective coating that usually covers optical fibres which simply protects the fibre from breakage or excessive bending. This can come in many different forms and have many different thicknesses. It is important that optical fibres are protected in this manner because the excessive attenuation caused by severe bending of the fibre could lead to a drop below a given threshold at the receiver and thus causing an increase in transmitted errors. We should also note that the protective coating can be used to shield the fibre from interference, when multiple fibres are "bundled" together, the transmission light, an electromagnetic field, is prone to leaking from one fibre to another).

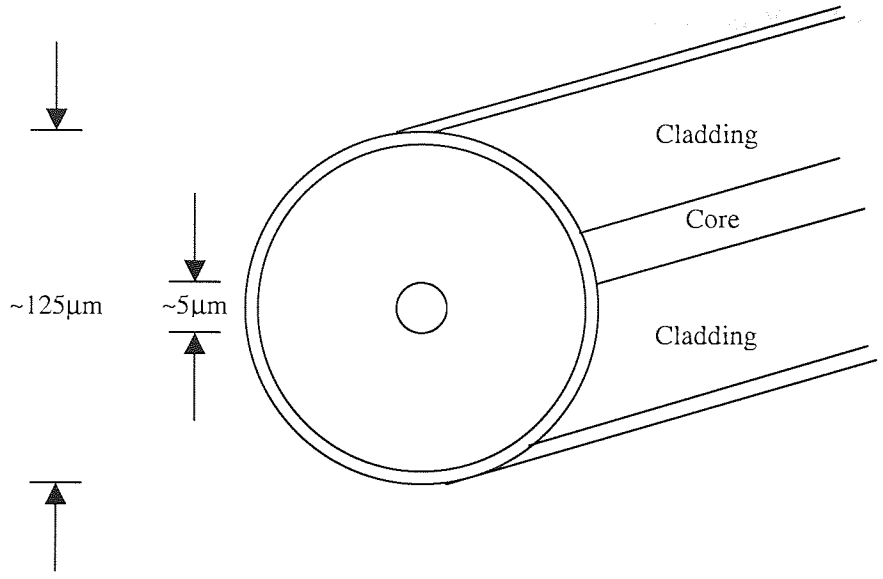

Figure 1.1: A typical cross-section of standard mode fibre (SMF). The core would typically have a diameter of 2-10μm

As the core of the fibre has a higher refractive index than the cladding the light can be contained within the optical fibre. The fibre itself can be described by using the following two parameters, the relative core cladding index difference, Δ, and the normalised frequency, V [4] where:

$$\Delta = \frac{n_1 - n_2}{n_1} \qquad (1.1)$$

$$V = k_0 a\left(n_1^{\,2} - n_2^{\,2}\right)^{\frac{1}{2}} \qquad (1.2)$$

n_1 and n_2 are the refractive indices of the core and cladding respectively and k_0 is the wavenumber:

$$k_0 = \frac{2\pi}{\lambda} \qquad (1.3)$$

Single mode fibre has a typical normalised frequency value such that $V < 2.405$. Because of the laws of total internal reflection [5], light can be guided through the optical fibre. If a wave is incident at an interface which bisects two media of differing refractive index, n_1 and n_2, and has an angle of incidence of $\theta_1 = \theta_2$, then:

$$n_1 \sin\theta_c = n_2 \qquad (1.4)$$

and the refracted wave just grazes the interface of the two media and the angle is known as the critical angle, θ_c. If the angle of incidence is greater than θ_c, then there is no refracted wave and it is for these angles that we have total internal reflection. If we now transpose this to the more specific case of an optical fibre and re-arranging equation 1.4 we get:

$$\theta_c = \sin^{-1}\left(\frac{n_2}{n_1}\right) \qquad (1.5)$$

as before, any angle of incidence (at the core-cladding interface) greater than θ_c will result in total internal reflection. Assuming that we have a cylindrical and symmetrical fibre cross-section (as in the case of SMF, Figure 1.1), the wave will undergo the same total internal reflection at the lower interface and thus, the wave will be guided along the fibre. This phenomenon will still occur, even if the fibre is bent, so long as the angle of incidence is not less than the critical angle (Figure 1.2).

(Of course the phenomenon of total internal reflection in order to "guide" light around corners is nothing new. It was first demonstrated by John Tyndall et al in 1854 [6]. Even back in 1854 Tyndall also speculated back then that it might be possible to create stable structures that would one day be able to carry light, an early idea which later turned into the optical fibre which gave birth to the optical communications industry).

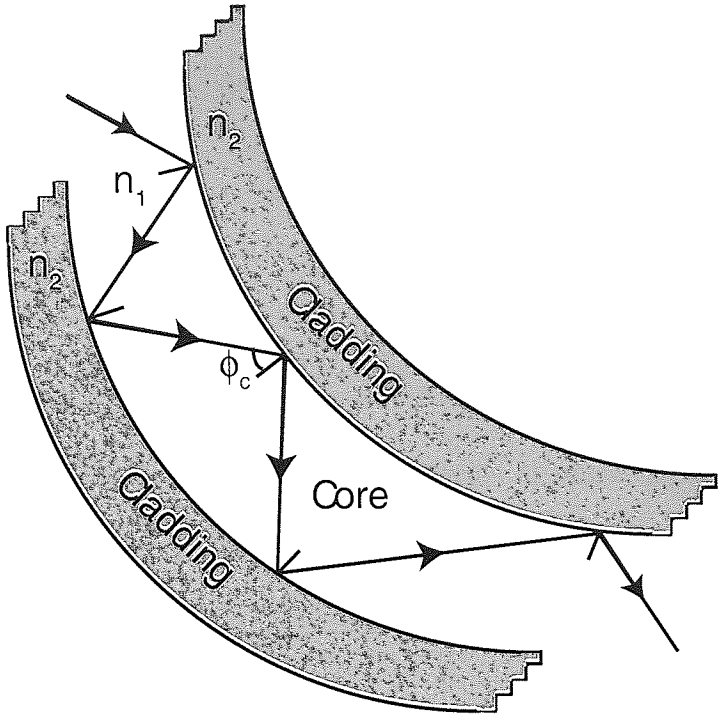

Figure 1.2: Optical rays enter at one end of a curved piece of optical fibre (core and cladding are not drawn to scale). Because of the effects of total internal reflection, light propagates through the fibre

Note, some of the other properties of the fibre such as attenuation, dispersion and nonlinearity will be discussed in the following chapters.

1.3 Digital transmission over optical fibre

Throughout the following thesis data will be transmitted along an optical fibre. This will be both computer simulated as well as seen in a laboratory environment. Thus, we can think of a transmitted signal as series of 1's and 0's (where a 1 is represented by the

presence of a data pulse and a 0 is represented by the absence of a data pulse). At the end of a transmission system there would typically be some sort of photo detector and receiver where a decision threshold level would need to be set (this threshold level is used to determine the difference between a 1 and a 0. If the measured energy within the bit slot at the receiver is greater than the threshold level a 1 is deemed present. If the energy measured is less than the threshold setting, a 0 is deemed to be present). Because of the way that we "measure" the data, if the propagated data channel undergoes some level of degradation, such as attenuation or dispersion (section 1.4 and section 1.6 respectively), there may not be the required power at the receiver. When this happens a 1 will fall below the threshold setting and will be assumed to be a 0 and so thus, the initial codeword will be changed and so errors will have occurred during transmission. However, when data propagates along any optical fibre if the peak power is too high the signal will also suffer degradation due to nonlinear effects (section 1.7). Because of the fine balancing act, careful consideration is required when choosing the power of codeword which is to be transmitted. It is for this reason that throughout most transmission links there will be some sort of device used to correct for any degradations that have occurred to the integrity of the transmitted data. Amplification, dispersion compensation and regeneration are commonplace.

In any optical communications system it is important to decide on the modulation format that is to be used. Usually data is applied by applying a codeword or data pattern to an external modulator (in some cases the laser itself can be directly modulated) which in turn modulates a channel of pulses. The two most commonly used formats are return-to-zero (RZ) and nonreturn-to-zero (NRZ) [4]. The RZ format occurs when each pulse, representing a 1, is firstly shorter than the bit period and secondly its amplitude returns to

zero before the bit period is over. On the other hand, in the NRZ format the bit slot remains full for the entire bit period and the amplitude is not returned to zero. Throughout this thesis, the RZ modulation format is always used.

1.4 Fibre Loss

Although dispersion and the nonlinearity in optical fibre may limit the performance of an optical communications system, fibre loss represent yet another limiting factor. It is for this reason that most lightwave systems use optical fibre as the transmission medium [7, 8]. The level of attenuation has dropped significantly in recent years with a level of 0.2dB/km being the norm for single mode fibre (SMF, the most commonly used transmission fibre) operating at a transmission wavelength of 1550nm.

Under what we will call "general" conditions the average optical power, P, of a bit stream propagating inside an optical fibre is given by:

$$\frac{dP}{dz} = -\alpha P \qquad (1.6)$$

where α is the attenuation coefficient. If P_{in} is now the power launched into a fibre of length L, the output power, P_{out}, can be calculated using equation 1.7.

$$P_{out} = P_{in} \exp(-\alpha L) \qquad (1.7)$$

which can be expressed in dB/km (which is the most common units used to describe attenuation) as:

$$a_{(dB/km)} = -\frac{10}{L}\log_{10}\left(\frac{P_{out}}{P_{in}}\right) \qquad (1.8)$$

It should be noted that the loss of an optical fibre is not constant for all wavelengths, the loss is wavelength dependant. A simple sketch depicting the loss profile is shown in Figure 1.3.

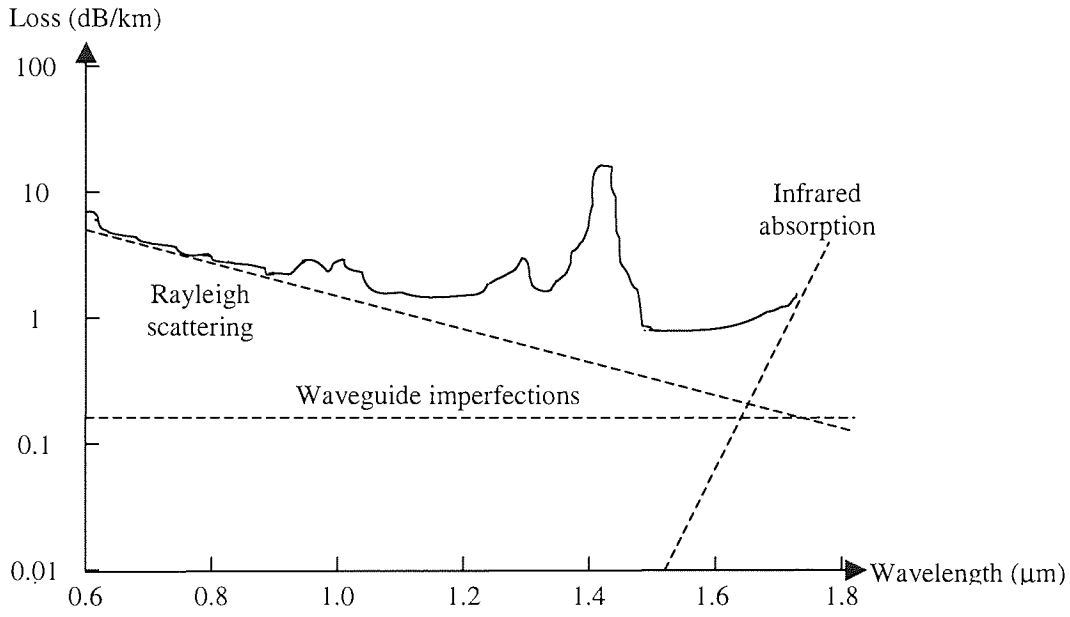

Figure 1.3: The loss profile of a silica based single mode fibre

The two most important loss mechanisms are material absorption and Rayleigh scattering [9-11]. Material absorption can be split into two categories, intrinsic absorption and extrinsic absorption. Intrinsic absorption losses correspond to absorption by the fused silica. On the other hand extrinsic absorption is caused by the presence of materials such as transient metal ions (Fe^{2+}, Cu^{2+}, Cr^{3+} to name a few) which absorb strongly in the wavelength range of 0.6-1.6μm. However, one of the main sources of extrinsic absorption is due to the presence of water vapour where the OH^- ions, which are dissolved in the glass, causing vibrational resonance. Rayleigh scattering arises from local microscopic

fluctuations in density because the silica molecules move randomly when the silica is in its molten state and then freeze in place during the fibre fabrication. These density fluctuations lead to random variations in the refractive index. The variations are on a scale smaller than the optical wavelength and when light is scattered in this manner it is referred to as Rayleigh scattering.

1.5 Derivation of the nonlinear Schrödinger equation

In order to be able to study most of the nonlinear effects which occur when a short pulse (~10ns to 10fs depending on power) propagates along a length of fibre we require a mathematical model. The nonlinear Schrödinger equation, or NLSE, is derived from Maxwell's equations [12-17] and describes pulse propagation within a dispersive medium. However, it is not prudent to perform or show a rigorous derivation in this thesis as many versions can be found in suitable textbooks and journals [18-22].

When optical pulses propagate along optical fibre, both dispersive and nonlinear effects occur which influence the temporal profile of the pulse as well as its associated optical spectrum. To investigate such phenomenon we start at the basic wave equation:

$$\nabla^2 E - \frac{1}{c^2}\frac{\partial^2 E}{\partial t^2} = \mu_0 \frac{\partial^2 P_L}{\partial t^2} + \mu_0 \frac{\partial^2 P_{NL}}{\partial t^2} \qquad (1.9)$$

c is the speed of light, μ_0 is the permeability of free space and P_L and P_{NL} are the linear and nonlinear parts of the induced polarisation. It is important that at this stage we make the following assumptions. Firstly P_{NL} is taken as only a small perturbation of P_L (this is

because the nonlinear changes are fairly small). Secondly, the optical field is assumed to maintain its polarisation along the propagation length within the optical fibre (clearly this is unlikely to be the case as the fibre's polarisation will change as the fibre is handled). Finally, the optical field is assumed to be quasi-monochromatic ($\Delta\omega/\omega_0 << 1$, where $\Delta\omega$ is the spectral width and ω_0 the central frequency). The electric field equation is now written as:

$$E(r,t)=\frac{1}{2}\hat{x}[E(r,t)\exp(-i\omega_0 t)+c.c] \qquad (1.10)$$

$\hat{x}$ is polarisation unit vector propagating light and c.c is complex conjugate (note, P_L and P_{NL} can be written in a similar way). By assuming that we have an instantaneous nonlinear response, the molecular vibrations, or Raman effect, can be ignored (no $\chi^{(3)}$ term) and so by applying a Fourier transform to equation 1.10 we get:

$$\tilde{E}(r,\omega-\omega_0)=\int_{-\infty}^{\infty}E(r,t)\exp[i(\omega-\omega_0)t]dt \qquad (1.11)$$

which satisfies the Helmholtz equation:

$$\nabla^2\tilde{E}+\varepsilon(\omega)k_0^2\tilde{E}=0 \qquad (1.12)$$

k_0 is the wavenumber (equation 1.3) and $\varepsilon(\omega)$ is the dielectric constant. The dielectric constant can be used to define refractive index, $\tilde{n}$, such that:

$$\tilde{n}=n+n_2|E|^2 \qquad (1.13)$$

$$n_2=\frac{3}{8n}\mathrm{Re}\left(\chi^{(3)}_{xxxx}\right) \qquad (1.14)$$

where n_2 is the nonlinear index coefficient. Equation 1.12 is now solved by using the separation of variables method to leave:

$$\tilde{E}(r,\omega-\omega_0)=F(x,y)\tilde{A}(z,\omega-\omega_0)\exp(i\beta_0 z) \qquad (1.15)$$

where $\tilde{A}(z,\omega)$is a slowly varying function of z and β_0 is the propagation constant. For the case of single mode fibre, F(x,y) corresponds to the modal distribution of the fundamental mode within the fibre. Substituting equation 1.12 into equation 1.15 gives:

$$\frac{\partial\tilde{A}}{\partial z}=i[\beta(\omega)+\Delta\beta-\beta_0]\tilde{A} \qquad (1.16)$$

Thus, each spectral component within the pulse envelope will suffer from a phase shift who's magnitude is both frequency and intensity dependant as it propagates. We now go back to the time domain by taking the inverse Fourier transform of equation 1.16 where it is useful to expand $\beta(\omega)$ in a Taylor series about the carrier frequency ω_0:

$$\beta(w)=\beta_0+(\omega-\omega_0)\beta_1+\frac{1}{2}(\omega-\omega_0)^2\beta_2+\frac{1}{6}(\omega-\omega_0)^3\beta_3+... \qquad (1.17)$$

where:

$$\beta_n=\left[\frac{\partial^m\beta}{\partial\omega^m}\right]_{\omega=\omega_0} \qquad (1.18)$$

If the spectral width, $\Delta\omega << \omega_0$ then the cubic and higher order terms are negligible and can be ignored because of the quasi-monochromatic assumption that was made earlier. If however, propagation is to be considered when the carrier frequency is close to the zero-dispersion wavelength then third order dispersion may well need to be considered.

By substituting $\beta(\omega)$, talking the inverse Fourier transform and evaluating $\Delta\beta$ the propagation equation can be found:

$$\frac{\partial A}{\partial z}+\beta_1\frac{\partial A}{\partial t}+\frac{i\beta_2}{2}\frac{\partial^2 A}{\partial t^2}+\frac{\alpha}{2}A=i\gamma|A|^2A \qquad (1.19)$$

where α is the fibre loss, the nonlinearity is given by n_2 and the nonlinear parameter, γ, is defined by using the effective core area, A_{eff}:

$$\gamma = \frac{n_2 \omega_0}{c A_{eff}} \qquad (1.20)$$

It can therefore clearly be seen that γ is dependant on the fibre parameters and than by simply either increasing the refractive index of the fibre or decreasing the core effective area, the nonlinearity of the fibre can be increased. In order to further simplify equation 1.19, we can make a frame of reference which moves along with the pulse at the same group velocity, v_g, by making the transform:

$$T = t - \frac{z}{v_g} \equiv t - \beta_1 z \qquad (1.21)$$

Applying this to equation 1.19 gives us a simply version of the nonlinear Schrödinger equation (NLSE):

$$i\frac{\partial A}{\partial z} + \frac{i\alpha}{s}A - \frac{\beta_2}{2}\frac{\partial^2 A}{\partial T^2} + \gamma|A|^2 A = 0 \qquad (1.22)$$

The second, third and fourth term determine the effects of loss, group velocity dispersion and the nonlinearity of the fibre [23]. For completeness, the more complex, generalised nonlinear Schrödinger equation (GNLSE) is also included (equation 1.23):

$$\frac{\partial A}{\partial z} + \frac{\alpha}{2}A + \frac{i\beta_2}{2}\frac{\partial^2 A}{\partial T^2} - \frac{\beta_3}{6}\frac{\partial^3 A}{\partial T^3} = i\gamma\left(|A|^2 A + \frac{i}{\omega_0}\frac{\partial}{\partial T}\left(|A|^2 A\right) - T_R A\frac{\partial |A|^2}{\partial T}\right) \qquad (1.23)$$

There are two more equations which will become quite useful. Depending on the initial pulse width, T_0, and peak power, P_0, of a pulse, either dispersive or nonlinear effects will dominate in propagation. Thus, two length scales are introduced, L_D, the dispersion length:

$$L_D = \frac{T_0^2}{|\beta_2|} \qquad (1.24)$$

and the nonlinear length, L_{NL}:

$$L_{NL} = \frac{1}{\gamma P_0} \qquad (1.25)$$

The dispersion length and the nonlinear length provide the length scales over which the dispersive or nonlinear effects become important.

1.6 Dispersion

In general, the optical frequency, ω, of an electromagnetic wave will have an effect on the response of the medium when the wave interacts with the bound electrons of the dielectric (this is referred to as chromatic dispersion). Chromatic dispersion is related to the resonant frequencies at which the transmission medium absorbs the electromagnetic wave through the oscillation of the bound electrons. Thus, we can say that because of the frequency dependence of the bound electrons, different wavelengths will actually travel at different speeds along an optical fibre. This is clearly a significant issue as no source will be truly monochromatic and so a large "spreading" of optical pulses after propagation along an optical fibre can occur. This can seriously affect of a high speed optical communications system where closely spaced pulses, 1's, broaden and merge with one another or even fill a 0 slot causing errors to occur in the received signal.

Thus, the envelope of an optical pulse moves at the group velocity whilst β_2 represents the dispersion of the group velocity and is responsible for the actual pulse broadening and can be related to the dispersion parameter, D, in the following way:

$$D = \frac{d\beta_1}{d\lambda} = -\frac{2\pi c}{\lambda^2}\beta_2 \qquad (1.26)$$

where n_g is the group index, v_g is the group velocity and:

$$\beta_1 = \frac{1}{v_g} = \frac{n_g}{c} \qquad (1.27)$$

If the wavelength of the channel propagated is such that:

$$\lambda < \lambda_D \qquad (1.28)$$

the fibre is said to exhibit normal dispersion ($\beta 2 > 0$). In this normal-dispersion regime, we see that the higher frequency components of the optical pulse travel slower than the low frequency components of the same optical pulse and so either broadening or shortening occurs. When:

$$\lambda > \lambda_D \qquad (1.29)$$

then the fibre is said to exhibit anomalous dispersion ($\beta 2 < 0$) and so the lower frequency components travel slower than the high frequency components and again, the pulse will either broaden or shorten, depending on the system parameters. As the pulse changes duration, it also becomes chirped. A similar effect is seen when more than one channel (and therefore each channel must have its own unique wavelength) is propagated along a fibre at once. In this case, the two pulses will experience different levels of dispersion and so will propagate at different speeds. This effect is known as walk-off and the walk-off length, L_w, is defined by:

$$L_w = \frac{T_0}{|d_{12}|} \qquad (1.30)$$

with:

$$d_{12} = \beta_1(\lambda_1) - \beta_1(\lambda_2) \qquad (1.31)$$

λ_1 and λ_2 are the centre wavelengths of the two pulses and T_0 is the pulse width.

1.7 Fibre nonlinearity

The nonlinear coefficient for silica fibre is relatively low. However, because of not only the potentially long propagation distances involved in optical communications, but also the high peak powers which may be involved, nonlinear effects do happen (of course sometimes we actually want them to happen, as is the case when we are trying to purposefully shape the pulse). They can be therefore very important in optical communication systems with one of the main nonlinear process being nonlinear refraction. This near instantaneous effect gives rise to several different phenomena including self phase modulation and cross phase modulation [24-26].

When an optical pulse travels through a fibre, the high intensity portions of the pulse encounter a higher refractive index than the lower intensity portions (equation 1.18). This intensity dependant refractive index effect is known as self phase modulation (SPM) [27-29]. Self phase modulation occurs when $L << L_D$ and $L \geq L_{NL}$ (equations 1.24 and 1.25

respectively). Here the pulse evolution will be governed by nonlinear effects and the dispersion contribution will be negligible. Thus:

$$\frac{L_D}{L_{NL}} = \frac{\gamma P_0 \tau_0^{\ 2}}{|\beta_2|} >> 1 \qquad (1.32)$$

If the spectrum broadens without a corresponding increase in temporal width, frequency chirping occurs with lower frequencies in the leading edge and higher frequencies in the trailing edge. This is because the broadening of the optical spectrum generates new frequencies within the pulse which will ultimately lead to an increase in broadening (because of the effects of dispersion).

We can now write the normalised amplitude of the field in the following way:

$$\frac{\partial U}{\partial z} = \frac{ie^{\alpha z}}{L_{NL}}|U|^2 U \qquad (1.33)$$

with L_{NL} being the nonlinear length (equation 1.25), γ is the nonlinear parameter (equation 1.21) and α is the attenuation (the attenuation needs to be considered here as when the pulse is attenuated, the size of the intensity dependant refractive index also decreases). Equation 1.33 is now integrated to give:

$$U(L,T) = U(0,T)\exp[i\phi_{NL}(L,T)] \qquad (1.34)$$

where U(0,T) is the field amplitude when there is zero propagation distance and:

$$\phi_{NL}(L,T) = |U(0,T)|^2 \left(\frac{L_{eff}}{L_{NL}}\right) \qquad (1.35)$$

where:

$$L_{eff} = \frac{[1-\exp(-\alpha L)]}{\alpha} \qquad (1.36)$$

Thus, the nonlinear phase shift increases with fibre length, L. The effective length, L_{eff}, is shorter than L and defines the distance over which the phase shift would occur in a loss-less system. The effect that self phase modulation has on the frequency chirp (or instantaneous frequency across the pulse), for a Gaussian pulse, can now be calculated to be:

$$\partial\omega(T) = \frac{\partial\phi_{NL}}{\partial T} = -\left(\frac{L_{eff}}{L_{NL}}\right)\frac{\partial}{\partial T}\left|U(0,T)\right|^2 \qquad (1.37)$$

Cross phase modulation (XPM), however, occurs when two or more channels propagate along the same length of optical fibre [30-35]. It is the nonlinear phase shift which is induced by one field on to another field where the two fields have different wavelengths, direction or even state of polarisation. The total electric field of two channels at frequencies ω_1 and ω_2 propagating along the same axis and in the same direction with the same polarisation state is given by:

$$E = \frac{1}{2}\hat{x}\left[E_1\exp(-i\omega_1 t) + E_2\exp(-i\omega_2 t) + c.c\right] \qquad (1.38)$$

c.c represents the complex conjugate. We can also define the nonlinear phase shift for the field at ω_1 as:

$$\phi_{NL} = n_2 k_0 L\left(\left|E_1\right|^2 + 2\left|E_2\right|^2\right) \qquad (1.39)$$

$$\phi_j^{NL}(z) = \left(\frac{\omega_j}{c}\right)\Delta n_j z = n_2\left(\frac{\omega_j}{c}\right)\left(\left|E_j\right|^2 + 2\left|E_{3-j}\right|^2\right)z \qquad (1.40)$$

which takes contributions from both SPM and XPM. If we were to now assume that if we were to have two channels, at differing wavelengths, but with identically intense optical fields, the contribution of XPM to the overall nonlinear phase shift will be double that of SPM [36].

In reality it is unlikely that we can assume that two channels exist in the same polarisation state. In order to be able to consider the case where two optical fields are orthogonally polarised, we must first define an arbitrarily polarised optical field, equation 1.41, for an elliptically polarised input wave.

$$E(r,t)=\frac{1}{2}\left(\hat{x}E_x+\hat{y}E_y\right)\exp(-i\omega_0 t)+c.c \qquad (1.41)$$

where E_x and E_y are defined as the complex amplitudes of the orthogonal polarisation states of the field at ω_0 (the carrier frequency). One of the polarisation states will effect the other, which will result in a relative change in refractive index and so the nonlinear birefringence is given by [37]:

$$\Delta n_x = n_2\left(\left|E_x\right|^2+\frac{2}{3}\left|E_y\right|^2\right) \qquad (1.42)$$

$$\Delta n_y = n_2\left(\left|E_y\right|^2+\frac{2}{3}\left|E_x\right|^2\right) \qquad (1.43)$$

In equations 1.42 and 1.43, the first term on the right hand side is the contribution that the SPM makes and the second term causes XPM. This is because the nonlinear phase shift which is acquired by one polarisation component is dependant on the intensity of the other polarisation component. The effect of the nonlinear birefringence is therefore to change the state of the aforementioned elliptically polarised light, which results in a nonlinear polarisation rotation. This in turn causes a self-induced change in the polarisation of the higher intensity section of the pulse compared to the low intensity section of the pulse and thus, pulse shaping can occur.

If we now take the case where a Gaussian pulse is zero chirp, the dispersion induced broadening does not depend on the sign of β_2 and so the pulse broadens by the same

amount in both the normal and anomalous regime [38]. However, it is important that we realise that the propagation of a Gaussian pulse changes once a chirp has been applied to it [39](a pulse is said to be chirped if the carrier frequency changes with time). The initial field can be expressed in the following way:

$$A(0,t) = A_0 \exp\left[-\frac{1+iC}{2}\left(\frac{t}{T_0}\right)^{2m}\right] \qquad (1.44)$$

where A_0 is the peak amplitude, C is the frequency chirp (note, when C = 0 there is said to be no chirp and the pulse is transform limited) [40], and:

$$T_{FWHM} = 2(\ln 2)^{\frac{1}{2}} T_0 \qquad (1.45)$$

when m = 1, we have a chirped Gaussian pulse, as m controls the pulse shape (as m gets larger, the pulse shape tends towards that of a rectangle with sharp leading and trailing edges). Thus, the instantaneous frequency increases linearly from the leading edge to the trailing edge for C > 0 (also known as up-chirp or positive chirp) yet decreases when C < 0, down-chirp (or negative chirp). When the carrier wavelength is far from the zero-dispersion wavelength (which implies that there is negligible contribution from β_3) we obtain:

$$A(z,t) = \frac{A_0}{\sqrt{Q(z)}} \exp\left[-\frac{(1+iC)t^2}{2T_0^2 Q(z)}\right] \qquad (1.46)$$

where:

$$Q(z) = 1 + \frac{(C-i)\beta_2 z}{T_0^2} \qquad (1.47)$$

from this we see that a Gaussian pulse remains Gaussian through propagation but its duration, chirp and amplitude change (the change is caused by Q(z)). Note, changes in the pulse duration are governed by the broadening factor:

$$\frac{T_1}{T_0} = \left[\left(1 + \frac{C\beta_2 z}{T_0^2} \right)^2 + \left(\frac{\beta_2 z}{T_0^2} \right)^2 \right]^{\frac{1}{2}} \qquad (1.48)$$

where T_1 is the half-width.

1.8 Optical loop mirrors and optical processing

There are several different types of optical loop mirror some of which share similar optical switching properties, including the Mach-Zehnder and Michelson interferometer and Sagnac loop mirror. These have many useful applications including the sensing of external parameters such as pressure, temperature and magnetic fields [41-43]. Light can be caused to "switch" when there is a change in the phase of the light or data propagating through single mode fibre (in terms of sensing, the phase change is caused by the change in an external parameter). When the power levels are large enough for nonlinear effects, such as SPM and XPM to occur (section 1.7), a phase change occurs and light is switched.

The Sagnac loop (or interferometer) [44-47] can also be used to switch light (because of the phase change caused by the nonlinear effects in the fibre). A single length of fibre is folded back on itself and connected to an optical coupler to form a loop Figure 1.4 [48].

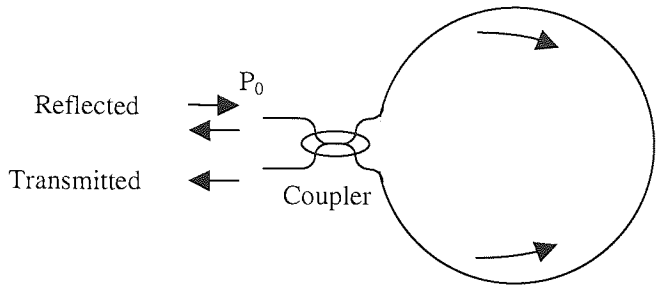

Figure 1.4: Schematic diagram of a basic all-optical Sagnac interferometer acting as a nonlinear optical loop mirror

The optical field enters the coupler and is split into two. The phase difference between the two counter-propagating fields determines if the beam is to be reflected or transmitted by the loop. If a 3dB coupler is used (also known as a 50:50 coupler as the light will be spit evenly in two with 50% of the light propagating in either direction) then the signal is completely reflected and the device simply acts as a perfect mirror (hence the name, nonlinear fibre loop mirror). Thus, the transmittivity of the loop can be seen to be dependant on the splitting ratio of the coupler. By taking the transfer matrix of a basic optical coupler the transmitted field of the loop is found to be:

$$\begin{pmatrix} A_t \\ A_r \end{pmatrix} = \begin{pmatrix} \sqrt{\rho} & i\sqrt{1-\rho} \\ i\sqrt{1-\rho} & \sqrt{\rho} \end{pmatrix} \begin{pmatrix} A_f' \\ A_b' \end{pmatrix} \qquad (1.49)$$

where:

$$\rho = \cos^2(\kappa l_c) \qquad (1.50)$$

Thus, the transmittivity of the Sagnac loop is given by:

$$T_S = 1 - 2\rho(1-\rho)\{1 + \cos[(1-2\rho)\gamma P_0 L]\} \qquad (1.51)$$

This demonstrates that when $\rho = 0.5$, T_s equals 0 and the loop is 100% reflective because there is no relative nonlinear phase difference between the two arms (a perfect loop mirror). However, if the $\rho \neq 0.5$, the loop mirror will act differently at low powers compared to that of high powers. As the input power, P_0, increases, so does the nonlinear effects and a phase shift is induced, caused by SPM. When there is a π phase difference between the two arms 100% transmission occurs (no light exits from the reflected arm of the loop):

$$\pi = \frac{|1-2\rho|\lambda P_0 L}{(2m-1)} \qquad (1.52)$$

where m is an integer and represents the order of the switching peak (so one would usually assume that m = 1 as this is the case which requires the least amount of power to switch) [49]. Because of the high peak power required to obtain π switching, we would usually expect a short pulse to be used. However, this can lead to distortions as only the central part of the pulse will have a large enough peak power to achieve the switching and so pulse distortion will occur. The switching point of the loop can also be lowered by introducing further offset or asymmetry to the loop by placing either amplification or attenuation in one arm [50]. In the case of amplification, one side of the loop will be amplified entering the loop whilst the other side will be amplified when exiting the loop. Because the intensities of the fields are different throughout propagation through the loop, the differential phase shift can be quite large. If the clockwise wave is now amplified by a factor G and assuming complete transmission, equation 1.51 now becomes:

$$P_0 = \frac{2\pi}{[(G-1)\gamma L]} \qquad (1.53)$$

A second channel, at a different wavelength, can now be added to the simple Sagnac loop after the coupler, on one side of the mirror only (this is often called a control, pump or

clock). When this happens, the control is injected into the loop mirror so that it propagates in only one direction and through XPM (section 1.7) induces a nonlinear phase shift in only one of the propagating waves whilst the other is unaffected. Thus, the control signal is used to unbalance the interferometer in the same was applying gain (equation 1.53) and so the loop can actually be made using any splitting ratio (including 0.5).

Considering a sech control pulse with:

$$A_P(T) = \sqrt{P_0}\,\mathrm{sec}\,h\left(\frac{T}{T_0}\right) \qquad (1.54)$$

The phase shift becomes [51]:

$$\phi_{XPM}(\tau) = \left(\frac{\gamma P_P}{\delta_\omega}\right)[\tanh(\tau) - \tanh(\tau - \delta_\omega)] \qquad (1.55)$$

with:

$$\tau = \frac{T}{T_0} \qquad (1.56)$$

and:

$$\delta_\omega = \frac{d_\omega L}{T_0} \qquad (1.57)$$

The relative phase difference is not only time dependant but its shape is also affected by the group velocity mismatch. The walk-off (equation 1.30) between the two pulses experiencing XPM will always be a problem resulting in low levels of XPM. This can either be avoided by using orthogonally polarised control and data or arranging for the two channels to experience the same group velocity (this requires careful selection of the fibres zero dispersion wavelength). By exploiting the two different switching characteristics, self

switching (SPM) and controlled switching (XPM), the loop mirror can be found to have many different applications.

1.9 Regeneration

The "regeneration" of data has the potential to be very useful indeed. It has applications in both long-haul transmission systems (for example, transatlantic links) and metro style networks (a network which may link an entire city together). If regeneration is not used, during transmission data will degrade (because of effects like dispersion, attenuation and maybe even nonlinear pulse shaping) and so some alternative method to regeneration is used. Clearly some of this can be achieved using optical amplification and dispersion compensation. However, regeneration offers a neat single box solution to the problem [52].

Regeneration of optical data can be achieved using a nonlinear optical loop mirror (NOLM). 2R regeneration [53-55] occurs when data is injected into the fibre coupler of a simple NOLM. The data is split into two paths and co and counter propagation occurs around the loop simultaneously. It is arranged such that one side will see a different peak power (either attenuation or amplification is used in one side of the loop to achieve this) and so a phase shift occurs back in the coupler such that only the high powered section of the data is transmitted and low powered reflected and so thus, zero noise suppression occurs [section 1.8]. By taking this a stage further and adding an extra clock source, wavelength conversion can be applied and 3R regeneration is possible. Wavelength conversion occurs because the data pattern is effectively "mapped" onto a new clock

source which is then used as the new data source [section 1.8] [56]. However, because the wavelength conversion happens as a result of XPM inside the NOLM, long lengths of nonlinear fibre are required. This leads to instability and the system becomes very sensitive to temperature fluctuations. By replacing the nonlinear fibre with an SOA, these instabilities can be removed and wavelength conversion is still possible [57, 58].

A slightly different technique for regeneration using a NOLM involves splitting the problem into three separate stages. Firstly the zero noise is suppressed using the first NOLM before a second NOLM is used to apply wavelength conversion where the data is mapped onto the local clock source before a final third NOLM is used to suppress the zero noise once again [59].

As well as using an SOA as the nonlinear element in a TOAD, a different and much more compact/practical solution is to use the SOA as the nonlinear element in a Michelson Interferometer (the Michelson Interferometer is simply a Sagnac loop that has been "unfolded"). This approach lends itself to integration onto a "photonic chip" and so we are left with a polarisation-independent monolithically integrated Michelson Interferometer [60-62]. The are two main advantages to this type of device. Firstly and most importantly is its physical size. Integrated devices are designed such that they can be packaged in conventional style photonic packaging and are generally less than 5cm in size and only require a couple of simple external controllers to operate. Secondly, because of their physicality's the devices are very stable and tolerant to extrinsic fluctuations such as temperature or movement. These features are extremely attractive from a practical point of view where simple integration into a network is of the up most importance.

There are alternatives to the previous approaches. For example, electro-absorption modulator (EAM) based devices can be used for optical regeneration. In this type of device the EAM is used to produce wavelength conversion where the original degraded data is mapped onto a new local clock wavelength. The data is launched, along with the clock, into the EAM and because of the cross-absorption effect in the EAM the data emerges at the new wavelength and is hence, regenerated. A second wavelength conversion is then applied so that the final emitted data is back at the original wavelength [63-66]. There is a serious limiting factor in this type of scheme and that is that the response time of the EAM itself will ultimately govern the maximum repetition rate of the device (although the response time of EAM's is ever increasing, current commercial limits are around 40Gbit/s) where as a fibre based device, such as the afore mentioned NOLM, has the potential to operate at much higher data rates as the fundamental limiting factor is the response time of the nonlinear silica fibre [67].

One should also note that by combining the use of an EAM and an SOA, nonreturn-to-zero, NRZ regeneration can also be achieved. An EAM is used to convert an NRZ signal into an RZ signal and thus the timing jitter significantly reduced. By converting back from RZ to NRZ (using an SOA) the amplitude jitter can also be removed and the regeneration is complete [68].

1.10 Single or multiple channels?

There are at the moment two different schools of thought when talking about optical communications. The first says that the more different optical wavelengths (also referred to as channels) the better. This is a potential easy way of increasing bandwidth and therefore the capacity of a transmission link. By choosing an appropriate level of dispersion, WDM couplers and amplifier spacing, it is possible to maintain and balance a transmission link (called a dispersion map) with multiple channels [69, 70]. Although this technique increases the capacity of a system, it isn't without its problems. Inter-channel interactions and nonlinearities have to be compensated for and the appropriate dispersion map chosen (as different wavelengths propagate at different speeds along the fibre). Thus, it is not simply a case of "adding channels" when we want to increase the capacity of a system. The second option is to concentrate on having one, single channel with an increased repetition rates [71, 72]with laboratory experiments heading towards multi-terabit transmission speeds [73] with the aim of practical installation as soon as possible. It should be pointed out however, that often in order to reach these record figures, the same techniques are often employed for single channel, as that of a multi-channel system. However, the an alternative approach is to use such techniques as 2R/3R regenerators and profile re-shapers in order to maintain and balance the system [74-83]. The limitation of this technique is that it usually only used on single channel systems as each channel would require a 3R regenerator, which potentially increases the components in a system (there are however, some 3R regenerators that can work with more than one channel at once, thus reducing component costs [84]). In order for optical networking to progress in the future, all-optical networks will have to be realised [85-91]. The current trend in optical networking is to electronic routers at each node in the network, however, this leads to

potential bottlenecks with the need to convert from the optical domain into the electrical domain and then back again adding large latency. The obvious solution to this problem is to keep the signal in the optical domain. In order to do this we need both optical routers and optical regenerators (whereby it would be possible to regenerate the signal at the same time that it is being routed) which would increase the efficiency of the network. It is in fact along this route that the following thesis progresses starting with a fundamental process, all-optical timing jitter [92, 93]/phase wander reduction and then finally all-optical 3R regeneration.

1.11 Discussion

The basic theoretical and numerical considerations which govern the propagation of light, or data, along an optical fibre have been presented within this section of the thesis. The nonlinear Schrödinger equation was derived which resulted in the formulation of the generalised nonlinear Schrödinger equation. Numerical analysis of nonlinear effects were also discussed, which included self phase modulation and cross phase modulation. Finally the way in which optical loop mirrors operate was analysed numerically. It is now possible, with the knowledge and theoretical tools contained within this chapter, to analyse the following simulation and experimental chapters.

Chapter 2 - Phase wander reduction, proof of principle using optical filters

2.1 Introduction

In this chapter we will start to investigate the principle of timing jitter and phase wander reduction. The results contained within the following chapter were completely generated using the commercially available computer simulation tool, VPI. There is an important distinction that needs to be made between the aforementioned timing jitter and phase wander. Timing jitter can be thought of as the variation in temporal displacement between adjacent bits which acts on each individual bit (the RMS noise which drives timing jitter is incoherent). For timing jitter suppression to occur, the amount of timing jitter must be significantly shorter than the timing window (the maximum/potential timing window is defined by the pulse duration of the chirped clock pulse. In order for the timing irregularities to be suppressed, the incoming data must temporally align with the chirped clock pulse inside the NOLM. If this does not occur, the timing irregularities will remain after propagation through the system). Alternatively, low frequency noise, phase wander, is caused by extrinsic, non-optical variations, such as environmental variations, which result in a physical change in say propagation distance. This results in an overall "timing offset" of the entire train of pulses or codeword. In order for phase wander suppression to occur the data pulses must fall somewhere inside the chirped clock pulse duration. This means that a significantly larger amount of phase wander can be corrected for compared to that of timing jitter.

The basic principle of operation is thus; take an incoming data stream (which suffers from either timing jitter or phase wander), at wavelength λ_0, and dynamically convert it to a new wavelength (the new wavelength is determined by the temporal displacement caused by either the timing jitter or phase wander). This is achieved by using a sampling function to sample a locally generated, linearly chirped, temporally square clock pulse (there are several different ways in which the wavelength conversion can occur [57, 94-96]). If we make the assumption that the "centre" or ideal timing position is the centre of the chirped clock pulse, we can assign a new wavelength to the individual data pulse depending on whether it is "early" or late". If the pulse is early, τ_1, the output after dynamic wavelength conversion, is assigned to λ_1. Conversely, if the pulse is late, τ_2, the output generated will be at λ_2. This principle is illustrated in the following diagram (Figure 2.1). The variation in colour represents the change in frequency across the linearly generated chirped pulse.

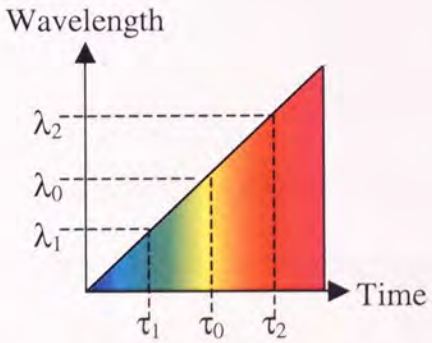

Figure 2.1: Schematic diagram showing the "dynamic wavelength conversion" and "temporal mapping" of the linearly chirped optical pulse

From the previous diagram we can obtain the following set of conditions:

$$\begin{aligned} \tau_1 &< \tau_0 < \tau_2 \\ \lambda_1 &< \lambda_0 < \lambda_2 \end{aligned} \qquad (2.1)$$

The speed at which light propagates along an optical fibre is dependant upon its wavelength and as such, once the dynamic wavelength conversion has taken place, a pulse with wavelength λ_2 will propagate faster than that of one with wavelength λ_0. Conversely, a pulse at wavelength λ_1 will propagate slower than that of one at λ_0. Thus, by using an appropriate and pre-determined amount of dispersion compensation (the dispersion compensation module can take many forms, for example a fibre Bragg grating, FBG, or dispersion compensating fibre, DCF) after the wavelength conversion section, the temporal displacement will be resolved and the timing jitter or phase wander suppressed. Because this scheme operates on a bit-by-bit level, both timing jitter (short time scale) and phase wander (long time scale) will be suppressed simultaneously. Figure 2.2 shows a block diagram illustrating the make up of the device.

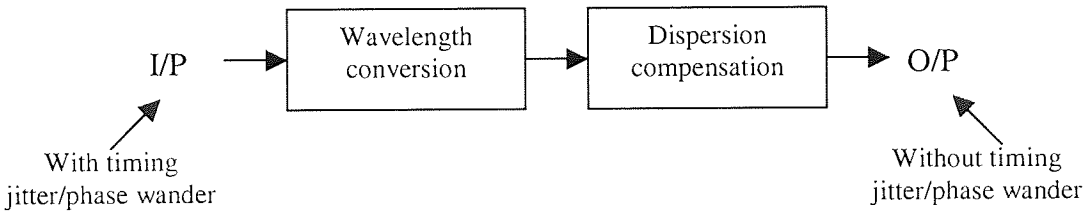

Figure 2.2: Block diagram demonstrating the principle of operation of the jitter reduction/phase wander suppression scheme

In the previously discussed scheme, it was shown that the jitter reduction system, in its simplest form, can be thought of a simple wavelength conversion scheme followed by a dispersion compensation module. Thus, it should be possible to re-create the effect of optical sampling by using a system of filters (this will replace the need to simulate the more complicated optical sampling function). Here we take the already generated linearly chirped clock pulse and use an optical filter to "slice out" a specific section of the chirped

pulse. The discrete frequency, Δf_n, is then assigned a discrete optical timing delay, $\Delta\tau_n$, ensuring that each frequency has a unique timing delay. As long as both Δf and $\Delta\tau$ have uniform independent increments, we can assume that this is analogous to the previously described system. The outputs are then re-combined together and propagated through a dispersion compensation module. Providing that the dispersion is chosen appropriately, the variation in timing displacement caused by the optical timing delays can be removed (it should be noted here again that there should be no confusion when talking about the dispersion compensation. The sign of the dispersion compensation needs to compensate for the variation in sampled frequency, in reality this means that if we change the sign of the chirped pulse, we need to change the sign if the dispersion slope in the dispersion compensation module) this principle is illustrated in Figure 2.3.

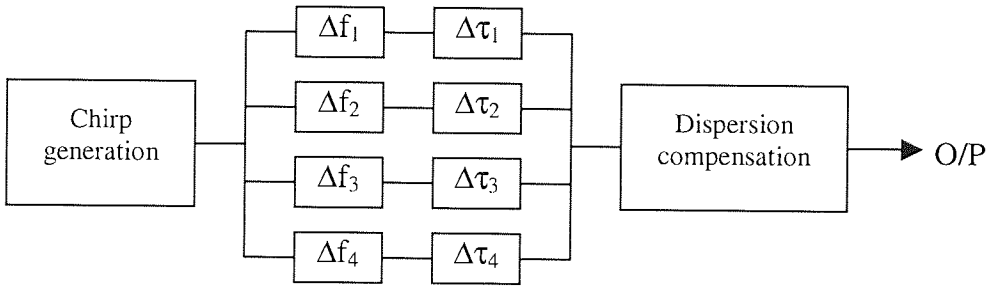

Figure 2.3: Schematic illustrating basic principle of the jitter suppression scheme. The filtering section replaces the optical AND gate

In order for timing jitter reduction to work correctly, it is important that we actually have as temporally "square" a clock pulse as possible. This is simply because if the pulse is not square in time (for example, if it were Gaussian), although wavelength conversion would still be possible, any timing jitter would be converted into amplitude jitter. We can now look at the case where we have a Gaussian shaped, locally generated, linearly chirped

clock pulse. The exact same principle that has been previously discussed will occur, the timing jitter will undergo wavelength conversion but at the expense of amplitude jitter. In the following schematic we are superimposing on top of each other the effect of early, ideal and late timing displacement.

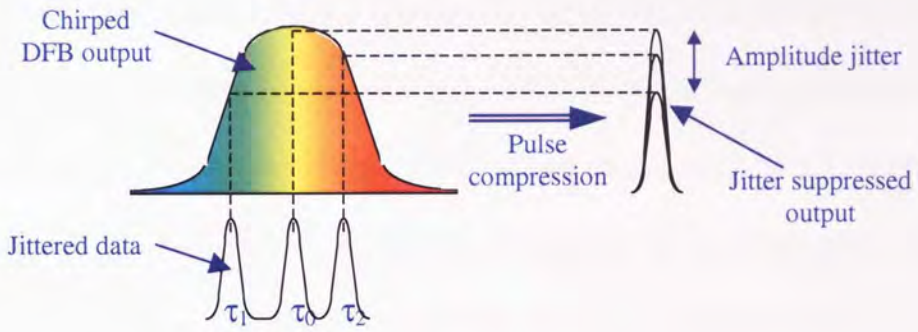

Figure 2.4: Schematic diagram depicting how a variation in timing jitter can translate into amplitude jitter for a non-square clock pulse. The change in colour represents the different frequency components of the chirped pulse

Figure 2.4 demonstrates how after wavelength conversion has taken place, the "early" pulse is assigned a specific output power, however, the remaining two pulses both are assigned to two different peak powers (or amplitudes). This will have the effect of significantly adding amplitude jitter to the output of the system, which will result in the final eye diagram having a significant reduction in performance, degradation to the overall BER of the system will occur.

2.2 Chirp Pulse Generation

The first thing to be considered is "how do we actually generate the desired linearly chirped, locally generated optical clock pulse?" There are several possible ways of achieving this, for example, a split contact distributed feedback (DFB) laser, could be used. However, this requires careful fabrication in order to achieve the desired properties and achieving a linear chirp can be especially difficult. Fibre Bragg gratings, FBG's, can also be used but the same problems as before may be encountered [97]. One could also use a semiconductor optical amplifier, SOA [98], to generate the linear chirp, but this dynamic component will then require an external power source. In this thesis we will concentrate on another method, that of using a length of nonlinear fibre to generate the linearly chirped clock pulse. By propagating a high peak powered optical pulse (the initial optical pulse used throughout this thesis will either be a Gaussian or Hyperbolic Secant, whose peak power can be increased by shortening the duration of the pulse) along nonlinear fibre. Through the effects of SPM (chapter 1.7) the pulse changes temporal profile and a chirp is developed [99]. The amount of broadening and chirp can be controlled by either changing the peak power of the initial pulse, or by changing the length of the nonlinear fibre, thereby changing the overall propagation length. This principle is demonstrated by simulating an input pulse propagating through a 1km length of Sumitomo nonlinear fibre (the parameters of which can be found in Appendix C). In order to maintain consistency, the initial power of the Gaussian pulse was kept constant throughout the simulation and then passed through an erbium doped amplifier, EDFA, which was immediately filtered in order to remove the amplified spontaneous emission, ASE. This was then propagated along the aforementioned nonlinear fibre and the output filtered before going into both a sampling oscilloscope and an optical spectrum analyser, OSA. A basic schematic diagram

of the simulation is shown in Figure 2.5 (note, it is important that the ASE of the EDFA is filtered out so that we are left with the spectral profile of the original clock).

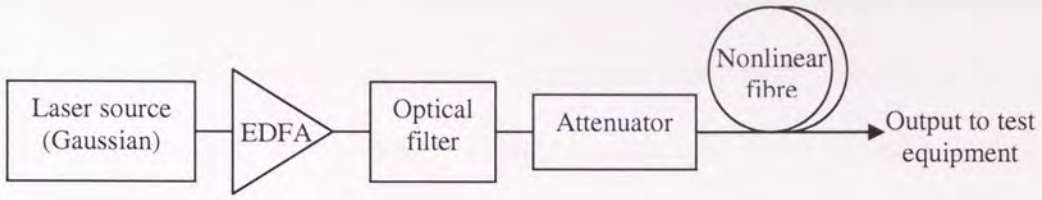

Figure 2.5: Basic schematic of the simulation. Using the attenuator, the average input power to the nonlinear fibre can be controlled

Although it is the peak power that causes the nonlinear effects, if the input pulse doesn't change in duration then simply changing the optical average power will have the same effect of increasing the peak power. The results of the simulation are shown Figure 2.6.

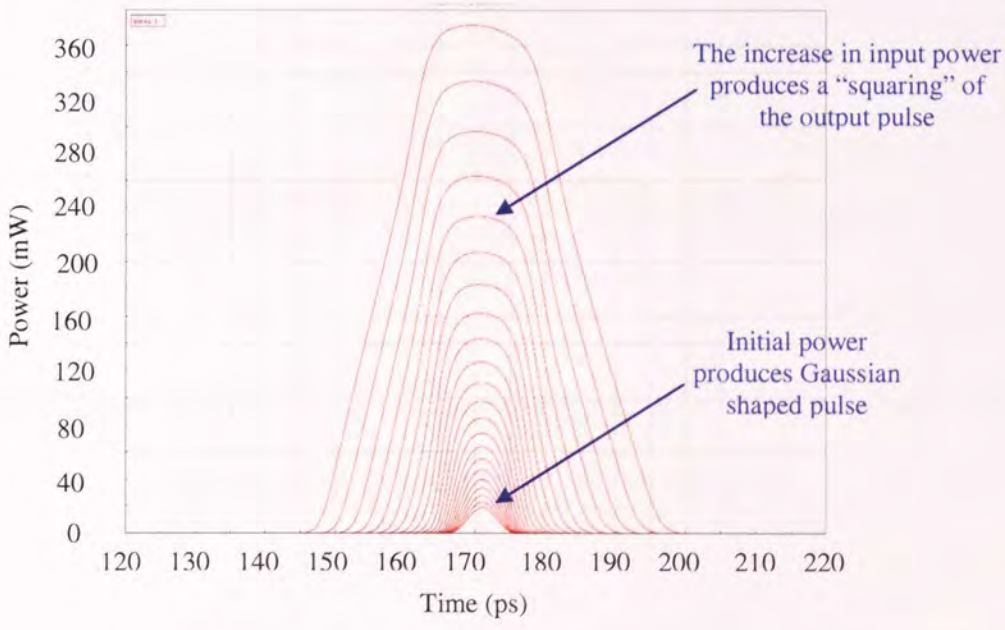

Figure 2.6: The increase in input power to the nonlinear fibre results in SPM changing the temporal profile of the output pulse

Not only does the pulse change shape (in the time domain), the FWHM also increases, this is exactly what we require and is known as nonlinear pulse broadening. It should of course be noted at this point that it can be seen in Figure 2.6 that the pulses are by no means "square" in temporal profile. The pulse shape has been seen before and achieving a completely square pulse is impossible so compromises have to be made. It is possible, by careful tailoring of the fibre properties, to improve on the results, however, in order to keep the simulations realistic, this is not done. We can now look at the corresponding optical spectrums (Figure 2.7).

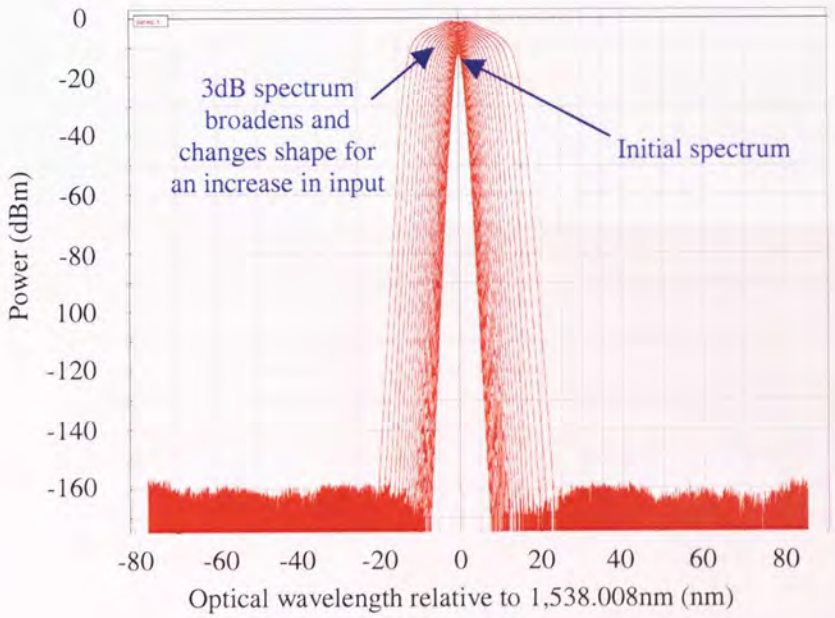

Figure 2.7: Corresponding optical spectrum to Figure 2.6. As the input power to the nonlinear fibre increases, the spectrum broadens

The change in the time domain profile of course has a corresponding change in the optical spectrum. This now gives us an optical profile which guarantees the desired square pulse profile.

We now consider what happens when we add another length of nonlinear optical fibre to the system. The fibre chosen was again nonlinear Sumitomo fibre which has very similar properties to the previously used Sumitomo fibre. The exact parameters used are shown in Appendix C, section 8.3. Thus, in addition to the 1km of Sumitomo fibre, the second length of Sumitomo fibre (which has a length of 1.2km) is simply added onto the end of the first piece of fibre. This gives a total propagation length of 2.2km of nonlinear fibre. This extra length of fibre should increase the nonlinear effects and so a lower peak input power will be required to achieve the same amount of pulse shaping. This principle is demonstrated in the following figure.

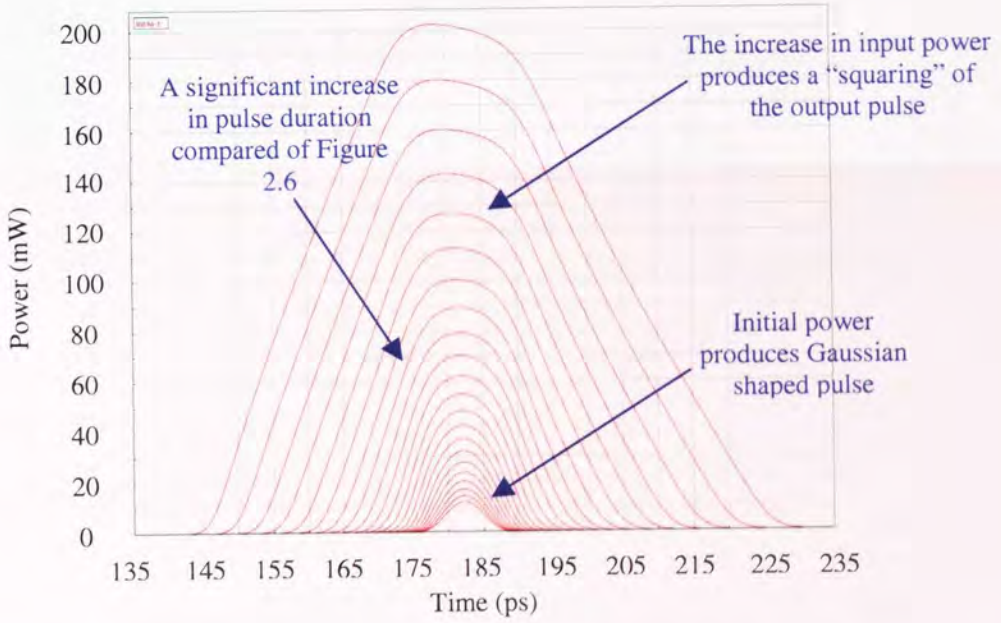

Figure 2.8: Temporal profile of output of system using 2.2km of nonlinear fibre

There is however a problem when using an extended length of nonlinear fibre and that is that the effects of dispersion will start to dominate rather than the nonlinear effects. We find that although the pulse still broadens, the pulse shaping or "squaring" effect (caused by the SPM) is minimised and thus, a compromise needs to be found. As before, the

length and parameters of the second length of nonlinear fibre were chosen to reflect real fibre that would be obtainable and useable for the forthcoming laboratory based experiments.

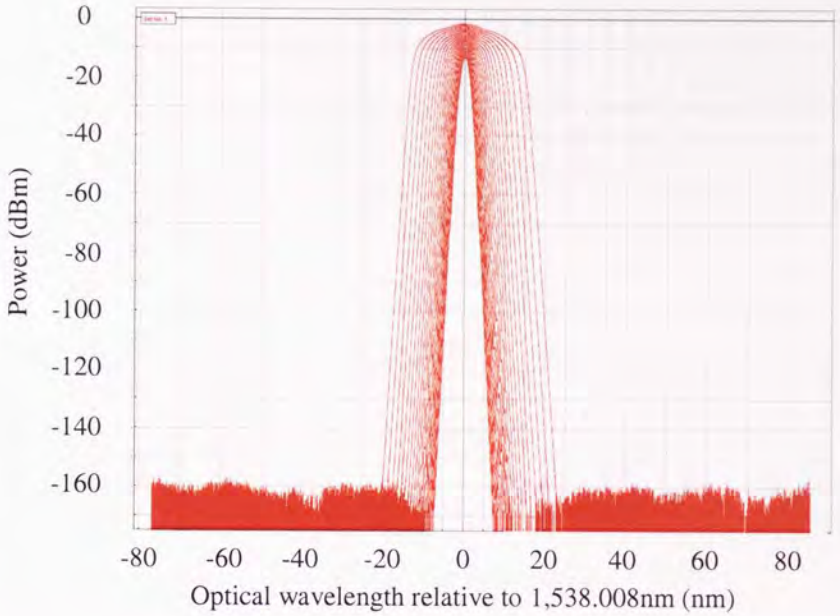

Figure 2.9: Spectral profile of output of system using 2.2km of nonlinear fibre

We do still however, see the same characteristic shape in the optical spectrum. This implies that we still have the nonlinear broadening and pulse shaping.

We can now directly compare the pulse broadening for both of the previous two cases, 1km and 2.2km of nonlinear fibre. This is achieved by simply measuring the full width half maximum, FWHM, in the time domain for each of the cases. These results are shown in Figure 2.10. This demonstrates that as the input power to the nonlinear fibre is increased, the pulse duration of the output increases. As the input power increases, the difference between the broadening in the two cases becomes more and more apparent.

However, as earlier stated, "pulse tails" (the pulse sides become less vertical) results in some deviation from the desired square temporal profile.

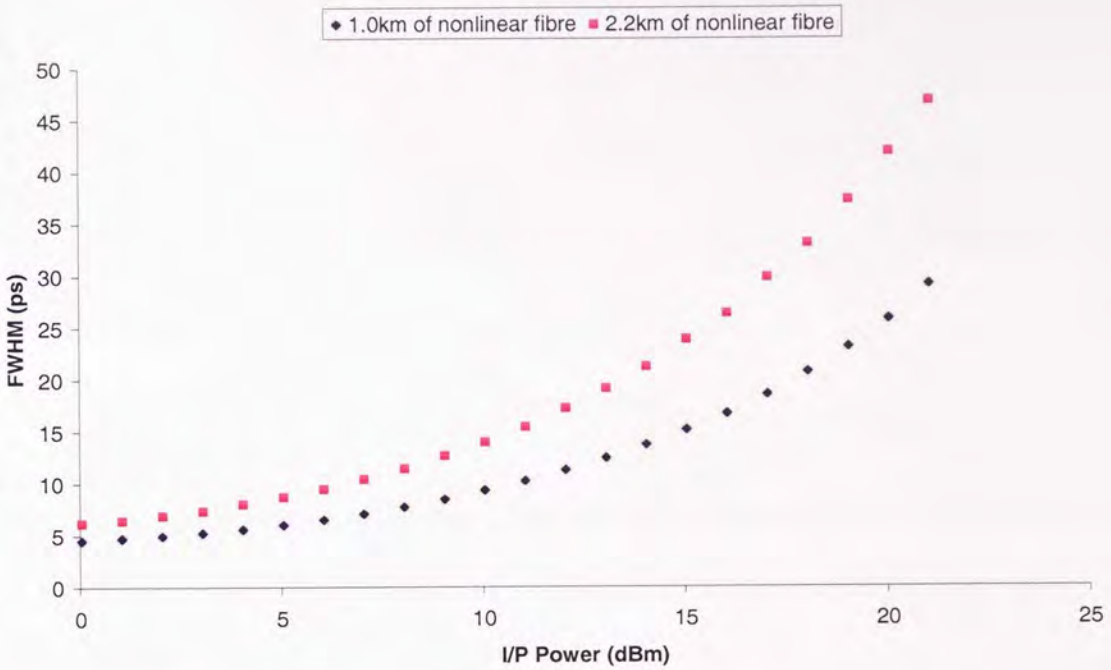

Figure 2.10: By increasing the propagation length through the nonlinear fibre, a lower input power produces greater temporal broadening

However, Figure 2.11 shows that there is very little to differentiate between the two cases when we are measuring the 3dB bandwidths of the optical spectrums. This is because of the domination of the dispersion, which was discussed earlier. In the case of the 2.2km of nonlinear fibre, if the broadening was due to the nonlinear coefficient, we would expect that this curve would increase at a greater rate than that of the 1km length of fibre.

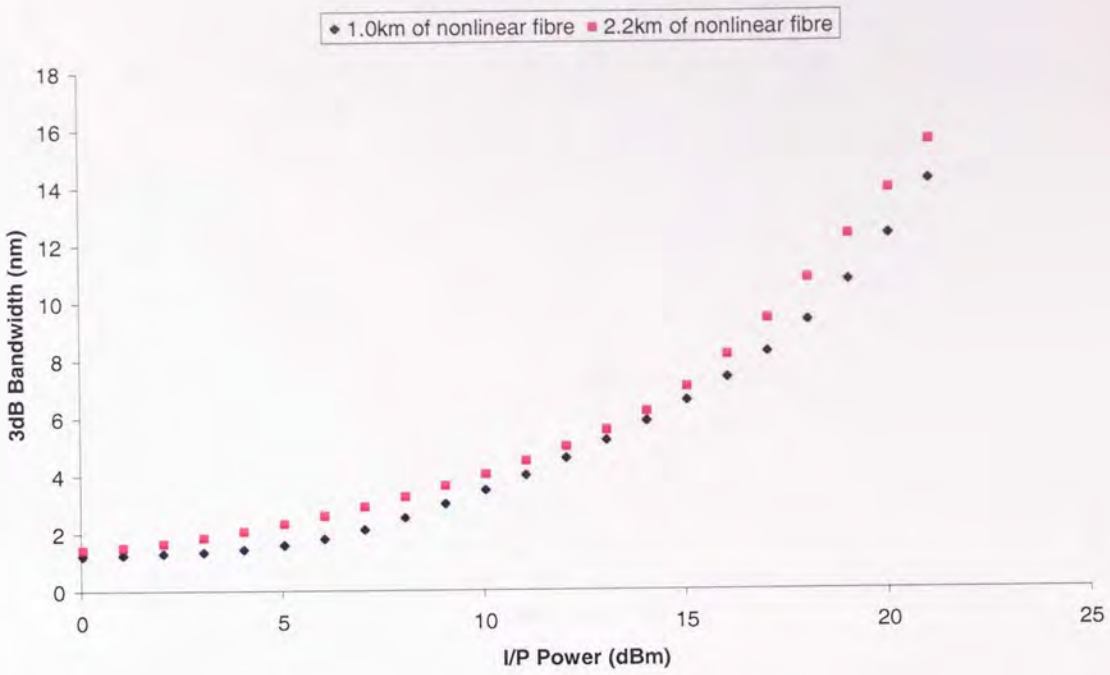

Figure 2.11: The corresponding (Figure 2.10) spectral broadening of the output pulse. The increase in input power increases the 3dB bandwidth for both of the two cases

We should also discuss at this point what happens if we do indeed alter the fibre type and increase the nonlinear coefficient of the fibre. The simplest way to achieve this is to decrease the core size of the fibre. In the following simulation, the same schematic as before (Figure 2.5) was used with just the original, 1km of nonlinear fibre. However, the input power to the nonlinear fibre remained constant at an average power of 50.61mW and initial pulse duration of 3.0ps. For each sweep of the simulation, the core effective area was decreased, thereby increasing the nonlinearity of the fibre. The simulation results shown in Figure 2.12 shows that as the core size decreases, the nonlinearity increases which means that there is significantly more nonlinear broadening happening. This has two effects, firstly the top of the pulse profile becomes flatter and second, the pulse duration is increased dramatically. These effects can also be seen in the corresponding optical spectrum. As the effective area decreases, the 3dB bandwidth increases.

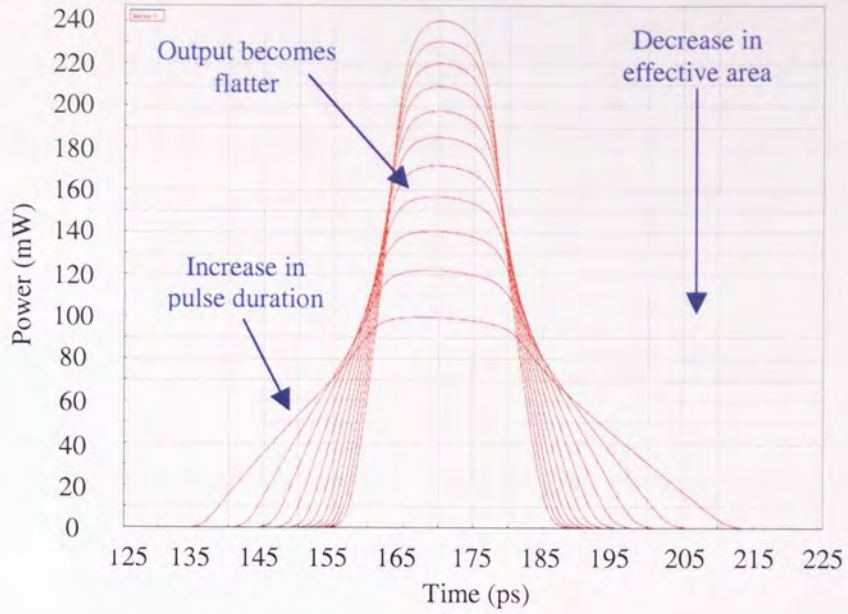

Figure 2.12: By decreasing the effective area of the nonlinear fibre, the nonlinear element is increased and the pulse becomes progressively more distorted and the pulse broadens further

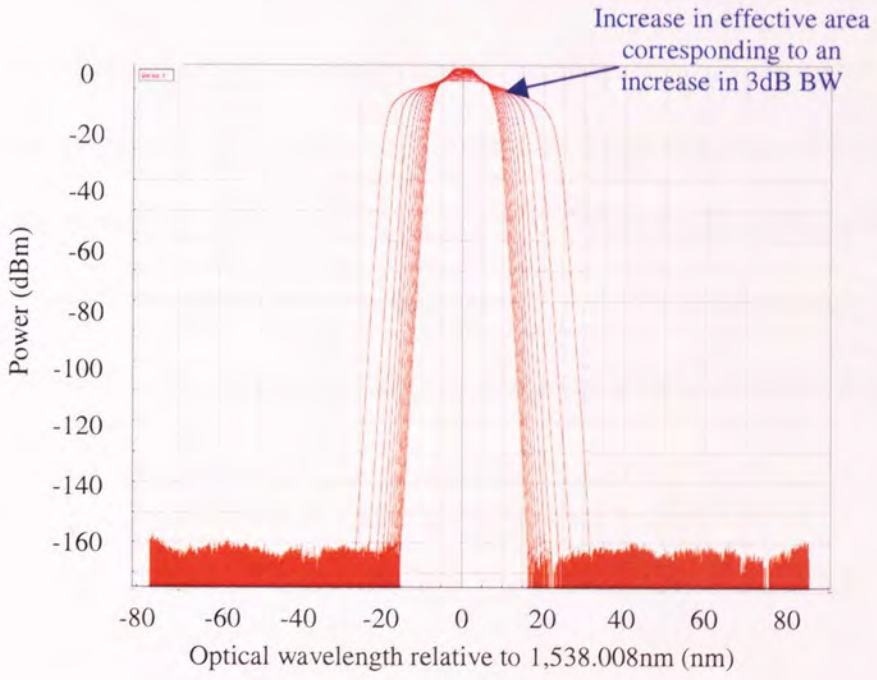

Figure 2.13: The optical spectrum (corresponding to Figure 2.12) increases as the nonlinearity of the fibre increases

Thus, the properties of the chirped pulse can be controlled by either increasing the incident power to the fibre, increasing the length of the nonlinear fibre or by changing the nonlinearity of the fibre. By tailoring these factors, we can control the generation of the chirped pulse.

2.3 Optical filtering to demonstrate the principle of operation

We can now verify the basic principle of operation by again, using the VPI simulation tool. We take the previously generated linearly chirped pulse (section 2.2) of 18.60ps duration and split the output into five equal paths (note, a conventional optical splitter was not used here, instead an optical node was used which makes four identical copies of the signal without any loss in optical power or added timing delay). The first sampled pulse, Δf_1, is then propagated along a short length of "perfect" optical fibre (we define the perfect optical fibre as one where there is no attenuation or dispersion, thus, we don't have to take any of these potentially adverse effects). We will define the f_1 as the "start" of our phase wander, $\Delta\tau_1$=0.00ps. Each additional frequency will be offset in time from this first sample. Thus, each new frequency has an additional 2.88ps of timing delay added thus,

$$\begin{aligned} \Delta\tau_1 &= 0 \\ \Delta\tau_2 &= \Delta\tau_1 + x \end{aligned} \qquad (2.2)$$

Thus;

$$\Delta\tau_n = \Delta\tau_{n-1} + x \qquad (2.3)$$

where x = determined time constant.

The five filtered channels are then propagated through SMF (which is used as the dispersion compensation element of the simulation). Although five individual lengths of fibre provided the dispersion compensation, these actually represent just one single fibre. Figure 2.14 shows the VPI schematic which was used to generate the following results.

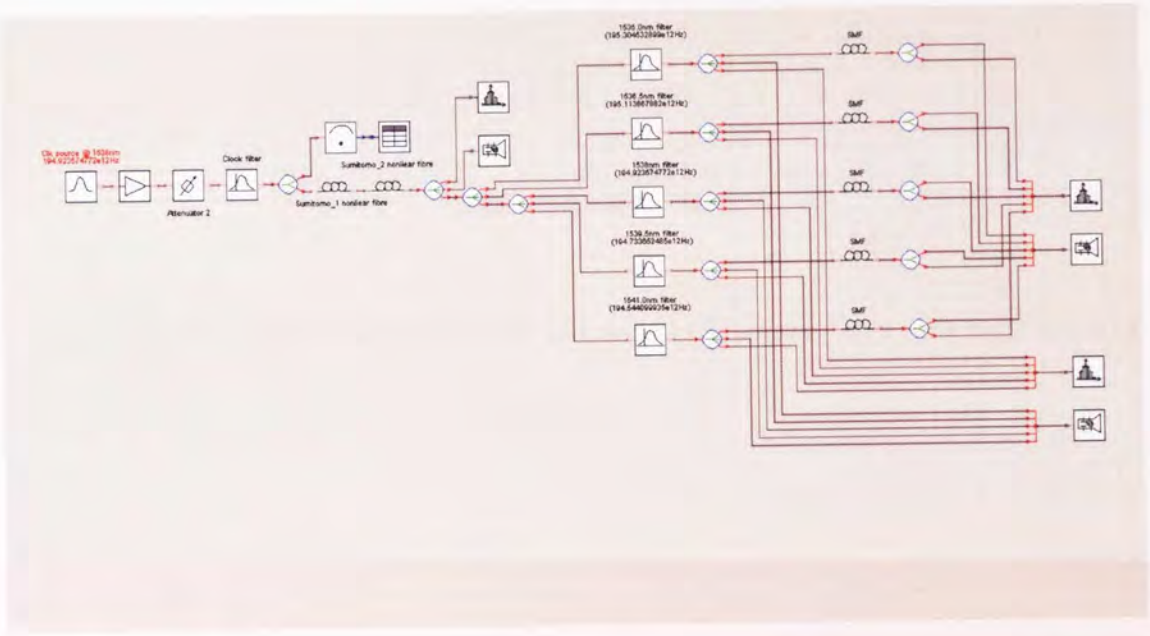

Figure 2.14: VPI Schematic showing the configuration used to demonstrate the filtering technique

(Note, for the following simulations the second, 1.2km of nonlinear fibre was turned off leaving just 1km of nonlinear fibre). The chirped clock source was generated using an initial average input power of 50.61mW and initial FWHM of 3.00ps at a wavelength of 1538nm. This produced a chirped clock pulse with a FWHM of 18.60ps and a 3dB bandwidth of 8.26nm.

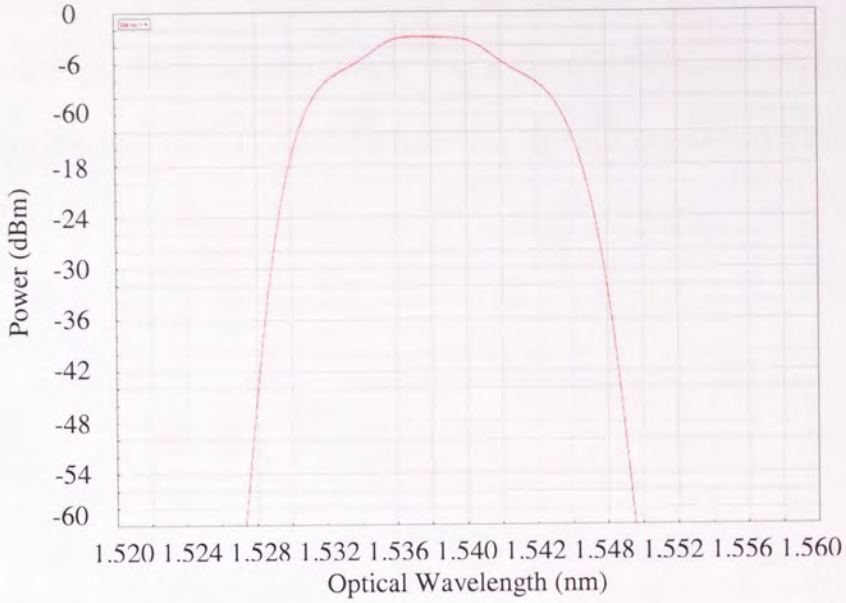

Figure 2.15: The optical spectrum of the chirped clock source has a 3dB bandwidth of 8.26nm

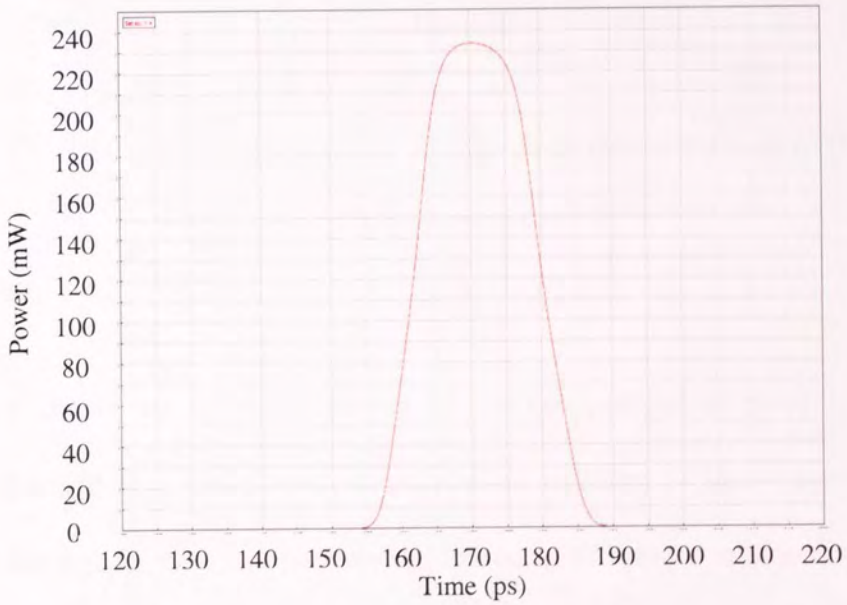

Figure 2.16: The temporal profile of the initial clock source (corresponding to Figure 2.15) shows an almost "square" profile

The clock source was then "sampled" using five 187GHz optical filters of with the first filtering at 1535nm. Each successive filter has a wavelength increase of just 1.4nm. This produces five discrete pulses each of which has its own individual timing displacement (Figure2.17)

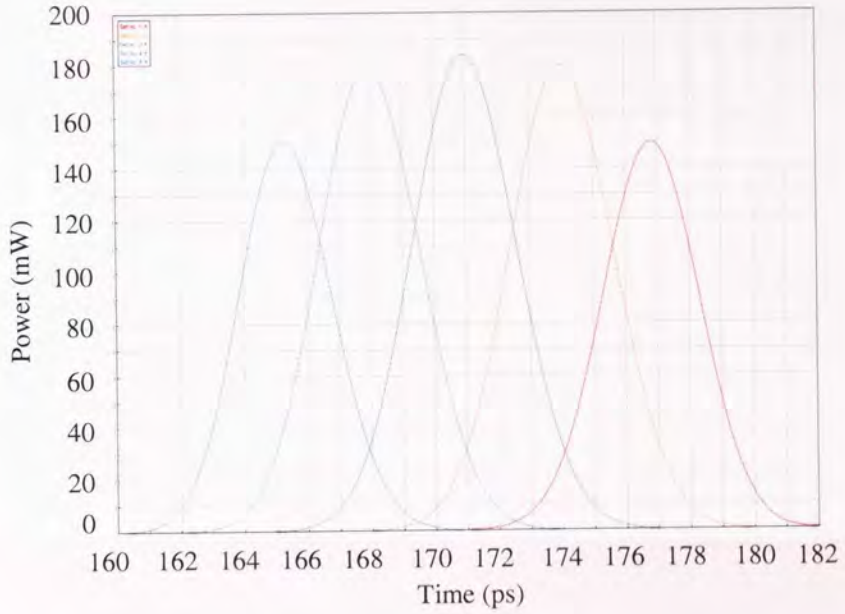

Figure 2.17: An input phase wander of 11.52ps is produced because of the five optical filters

Figure 2.17 shows the temporal output of the delayed pulses prior to the dispersion compensation (all five have been superimposed together to show how there is phase wander at the input). This can now be compared to the output of the entire system, post dispersion compensation (Figure 2.18) after propagation through 135m of SMF (this value was obtained from previous simulations). As we can see, the initial timing delay, or phase wander, of 11.52ps is virtually completely removed with a final phase wander of only 0.24ps. This would imply that in a "real" system, with a chirped pulse duration of 18.60ps,

we could compensate for as much as 11.52ps of phase wander. Unfortunately, amplitude jitter is generated due to the profile of the chirped clock source. Because the temporal profile of the clock is not square, filtering at the edge of the clock produces clock pulses with a lower peak power compared to filtering in the centre of the clock.

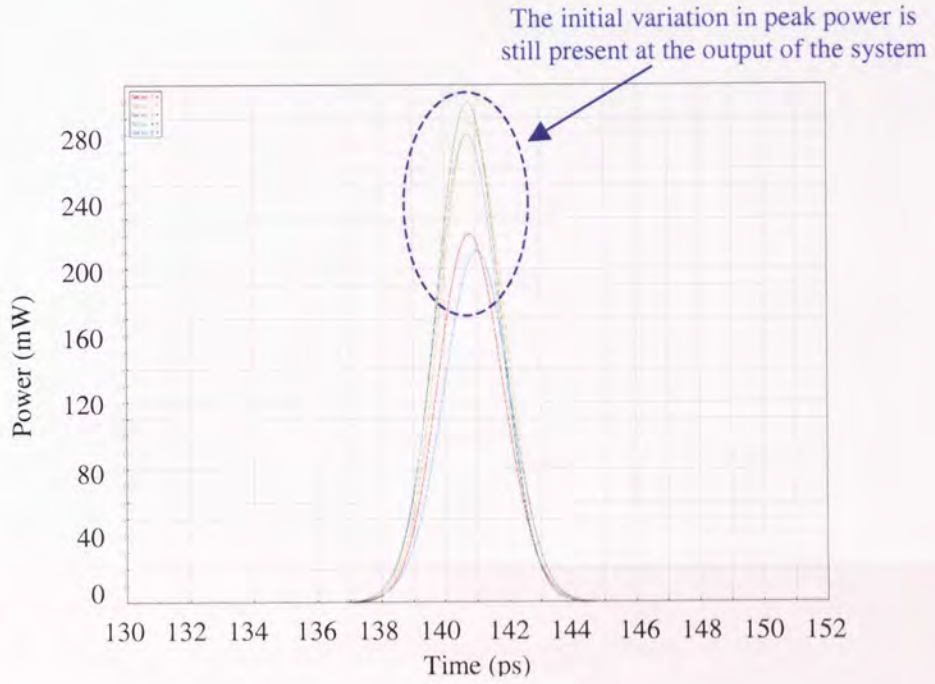

Figure 2.18: After dispersion compensation, the output phase wander is reduced to only 0.24ps

The level of dispersion compensation is critical in the timing jitter/phase wander reduction scheme. To illustrate this, the previous simulation was repeated with all the same parameters with one exception. The level of dispersion compensation is changed and the length of SMF increased by just 10m to 145m.

Even with this small increase in dispersion (as a result of the increase in SMF) the phase wander at the output of the system has increased from 0.24ps to 1.08ps. As the level of

dispersion gets further from the ideal, the amount of phase wander at the output will increase. This demonstrates how precisely the dispersion needs to be chosen in order to achieve maximum phase wander reduction.

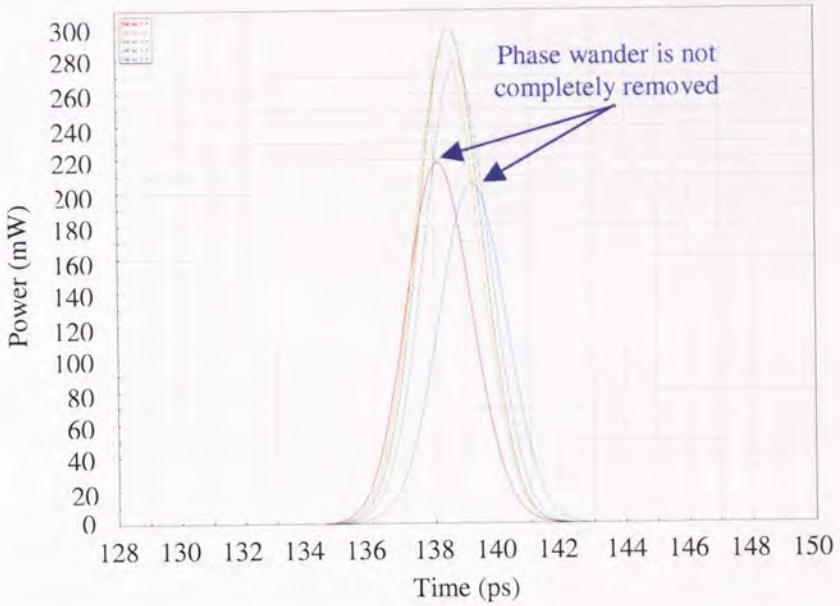

Figure 2.19: With an incorrect level of dispersion compensation the phase wander at the output of the system can not be reduced as much as it was previously

The dispersion compensation value is now reset so as to provide maximum dispersion compensation (SMF = 135m). The two outer optical filters which were used to generate Figure 2.17 are increased to 1533.5nm and 1542.5nm and the simulation repeated This increase is equivalent to now having a total of 17.35ps of input phase wander. Because the filters now sample at the edges of the chirped clock source we find that not all of the increase in applied phase wander can be successfully removed. However, we do see that the centre channels are compensated for in the same way as Figure 2.18. Now the outer two new channels have lower peak powers than previously and their temporal positions no longer align. The phase wander that remains at the end of the system is now 1.28ps. This

demonstrates that not only do we require exactly the correct level of dispersion compensation, we also have to set a limit to how much phase wander we will try and compensate for.

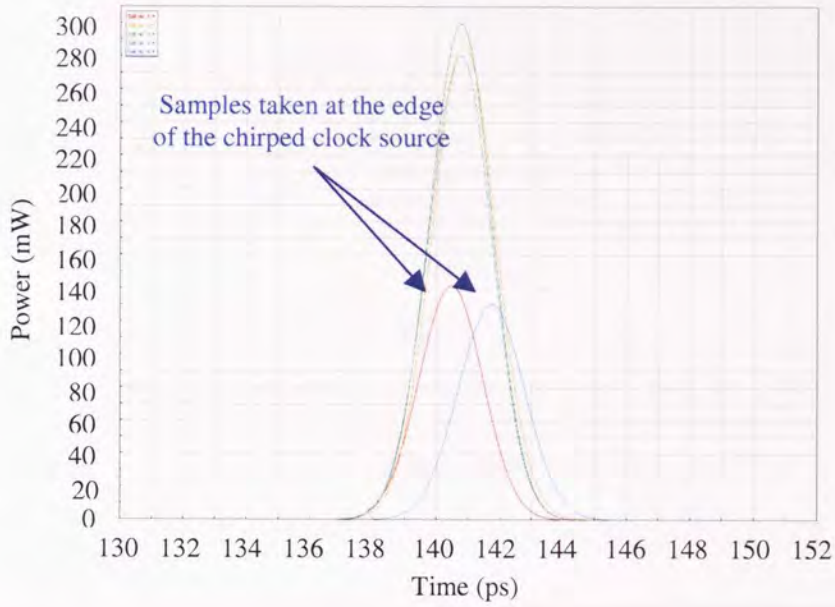

Figure 2.20: Sampling the clock at the edges of the pulse means that the dispersion phase wander cannot be reduced as much as in Figure 2.18

By increasing the clock's initial power, the FWHM of the chirped clock is increased from 18.60ps to 58.84ps. It was found that to successfully remove most of the applied phase wander, the level of dispersion compensation required was reduced to 129m and the previous simulation repeated. With the new broader clock, the further two channels can now be suppressed leaving a final phase wander after propagation through the system of 0.47ps (Figure 2.21). We should also notice that the variance in peak power has also been reduced.

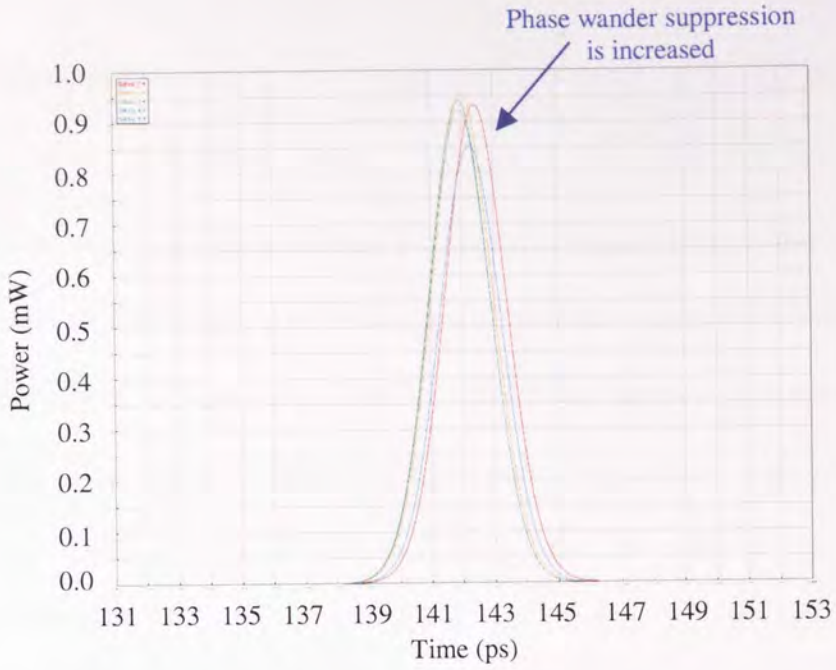

Figure 2.21: The increase in chirped clock duration means that the phase wander can now be reduced further and so there now is less phase wander after the system compared to Figure 2.19

This illustrates one of the limitations of this particular system, the filtering must fall within the centre portion of the chirped pulse in order for full phase wander to be compensated for. Clearly this is only indicative of this analogous system. Although it may appear as though simply increasing the chirped pulse spectrum will instantly remedy this problem, it would be impractical to think that the width of the chirped pulse can be increased without limitation.

2.4 Discussion

Several things have been demonstrated during this chapter. Firstly, the basic principle of operation has been explained. An explanation of how the system would work and why was discussed. Secondly, it was shown that by careful and precise considerations, a linearly chirped clock pulse could be generated by propagating a short, high powered Gaussian pulse along a length on nonlinear fibre. Not only can the slope of the chirped pulse be controlled, but also the temporal profile. It was clearly difficult to obtain a perfectly square temporal profile which would be the ideal.

An analogy to the sampling properties of an optical AND gate was also formulated and demonstrated. By using a simple optical filter to "slice out" a specific portion of the chirped clock pulse discrete wavelengths can be generated. These were then propagated through a dispersion compensating module (standard single mode fibre in this case) where it was shown that the applied phase wander could be reduced. This proved to be a useful tool in determining the feasibility of the proposed scheme without having to simulate a complete optical loop mirror.

Chapter 3 - Phase wander reduction using a NOLM

3.1 Introduction

In the previous chapter we demonstrated the "basic principle of operation" using the optical communication and network modelling tool VPI. However, in the previous chapter an analogy was used to demonstrate the principle. Simple optical filtering generated the wavelength shift and then dispersion compensation was used to remove the phase wander that had been applied at the input. In this chapter it will be shown that a nonlinear optical loop mirror (NOLM) can be simulated in the VPI and then used to apply wavelength shift to a data source which contains phase wander [100-102]. Not only can we use VPI to model the NOLM, it can also be used to show that applied phase wander can be removed from a data channel by compensating for the applied wavelength shift using dispersion compensation. This means that we can fully simulate the timing jitter/phase wander reduction scheme. The results contained within the following chapter were entirely obtained using computer simulation.

3.2 Self-Switching Characteristics of a Nonlinear Optical Loop Mirror

Using computer simulation to model a nonlinear optical loop mirror (NOLM) is not trivial. One would assume that in order to simulate the effects of a NOLM one would need to be able to backward-propagate optical signals through a fibre whilst at the same time, along the same piece of optical fibre, have forward propagation. This is simply not

possible with many software packages. However, there is a way around this problem in VPI. Contained within VPI are certain modules that would appear to allow bi-directional simultaneous propagation within the required components (such as bi-directional couplers and bi-directional fibres). On closer inspection we actually find that these components are split into two, one section deals with forward propagation and the other section deals with backward propagation, illustrated in Figure 3.1. This will now enable us to be able to construct what we would call a standard NOLM.

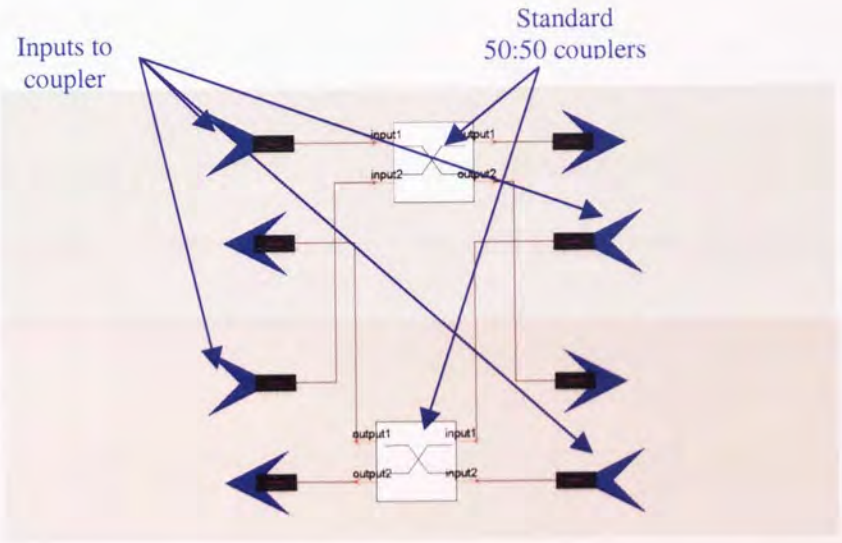

Figure 3.1: Break-down of bi-directional coupler found within the VPI modelling software tool. One coupler actually contains two couplers joined together to allow bi-directional propagation

The "bi-directional" coupler works by having two independent paths, one forward and one backward. The interactions are then considered within each of the two separate standard couplers and the combined optical fields considered.

As we can now "effectively" propagate in two different directions at once, it is possible to construct a standard NOLM. It should be mentioned that although in the schematic, Figure 3.2, a NOLM is used, VPI actually simulates the Mach-Zehnder version of the interferometer. This will not affect the results as any optical loop mirror could have been used. After construction, the NOLM is tested and checked that it operates in the conventional manner. It should be noted at this point that we can actually turn off the effects of polarisation and therefore remove any polarisation dependant properties of the NOLM and the nonlinear fibre. Thus, polarisation is not considered in any of the following simulations.

A simple NOLM was constructed using 1km of standard single mode fibre (SMF) to provide the nonlinear element which is required to achieve switching and the bi-directional coupler arrangement used.

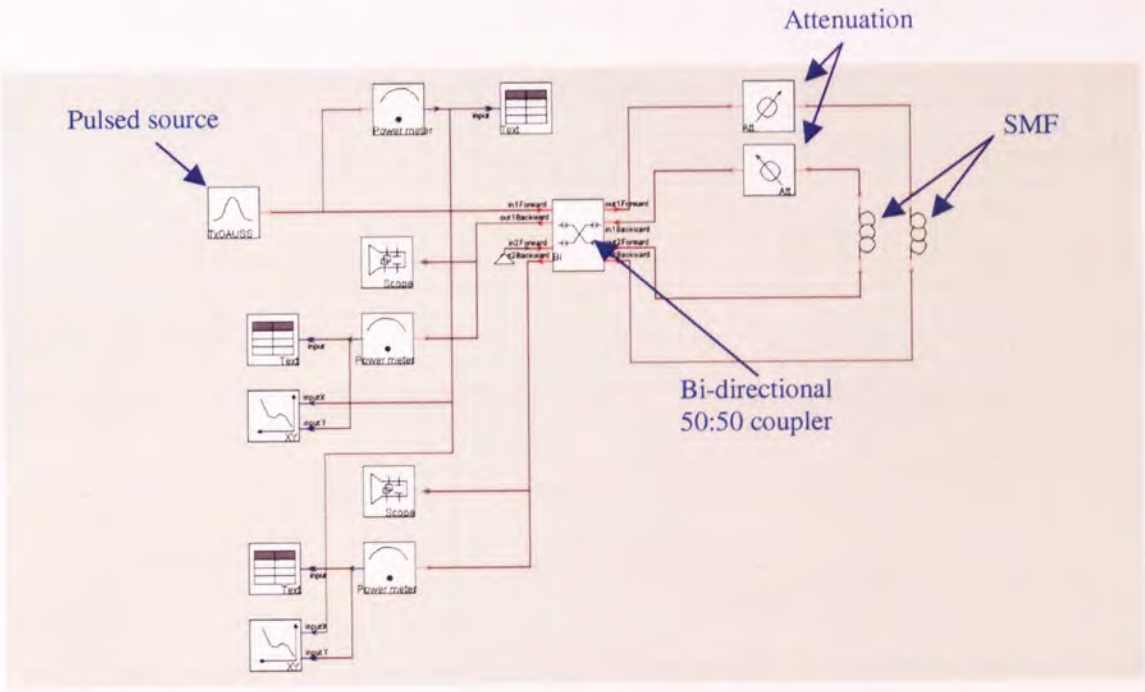

Figure 3.2: Schematic diagram showing a basic NOLM configuration. Using this configuration the self-switching characteristics can be investigated

By varying the input power of the data source that is to be propagated through the system and measuring the output power produced at both arms of the NOLM (reflection and transmission), the self-switching characteristic of the NOLM can be obtained. For the NOLM to be able to switch, the two arms (forward and backward propagation) need to be unbalanced. This can be achieved by either changing the coupling factor of the NOLM (i.e. the splitting ration of the input coupler) or unbalancing one side of the NOLM by adding either attenuation or amplification. The maximum achievable extinction ratio is reached with a 50:50 coupling ratio (0.5) and so it is usually more desirable to unbalance the loop whilst maintaining a 50:50 split. Amplification may seem like the obvious choice, by adding amplification we can increase the output power of the NOLM. However, this will add unwanted ASE into the system. It is for this reason that attenuation has been chosen. By varying the level of attenuation, the NOLM is manipulated to be more unbalanced. The more unbalanced the loop, the lower the level of input power required to achieve π switching, Figure 3.3 and Figure 3.4. We also see that as the loop becomes more and more unbalanced, the extinction ratio also increases.

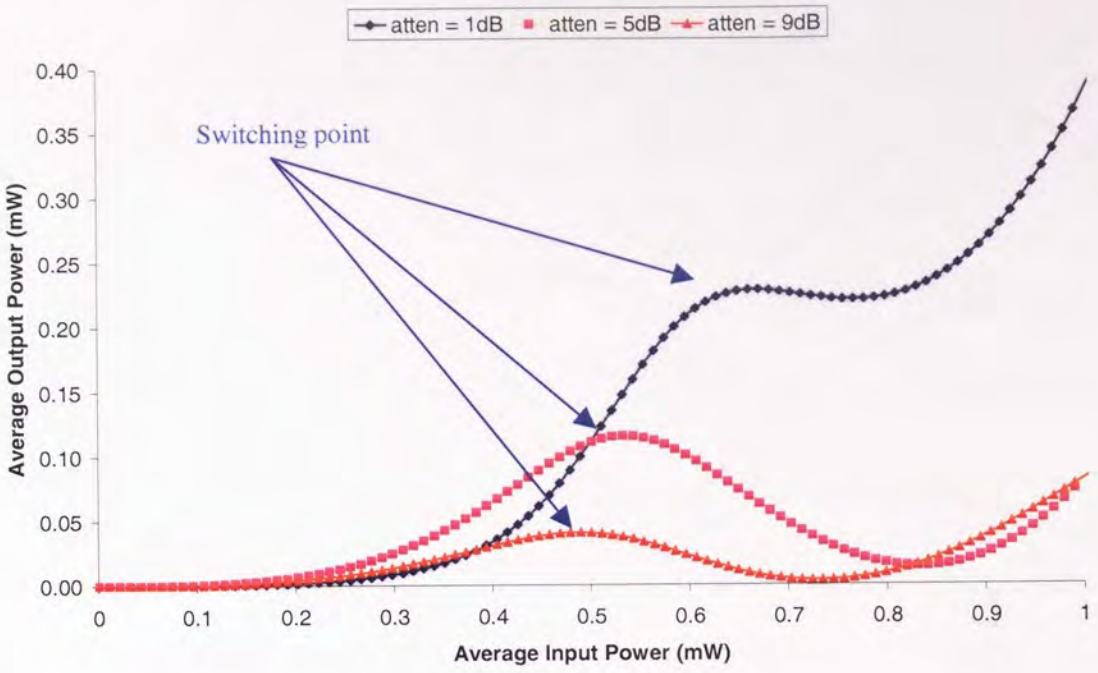

Figure 3.3: Self-switching characteristics of a nonlinear optical loop mirror. A full π phase shift is achieved as the input power to the NOLM increases for the transmission arm of the NOLM

By changing the length of the SMF, the nonlinear element of the NOLM can be changed (there are other ways to do this such as increasing the fibre's nonlinear coefficient or reducing the core diameter of the fibre). The effect of changing the nonlinearity of the NOLM is illustrated in both Figure 3.5 and Figure 3.6 (note, the coupling factor of the NOLM remained at 0.5 and the attenuation on one side of the loop was kept constant at 5dB).

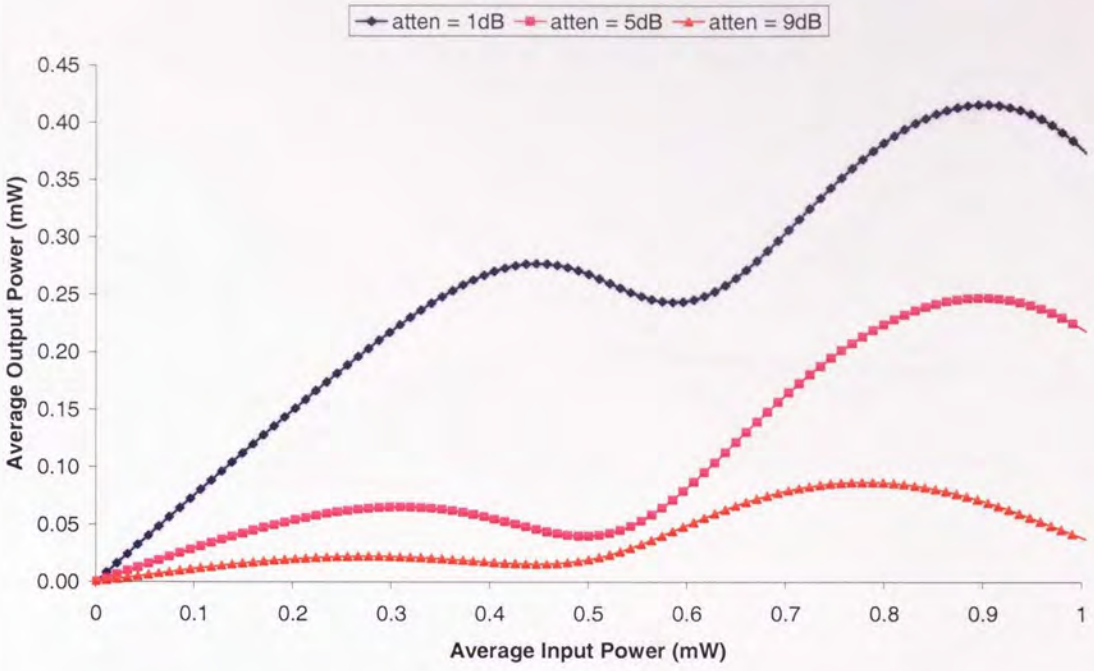

Figure 3.4: Self-switching characteristics of a nonlinear optical loop mirror. A full π phase shift is achieved as the input power to the NOLM increases for the reflection arm of the NOLM

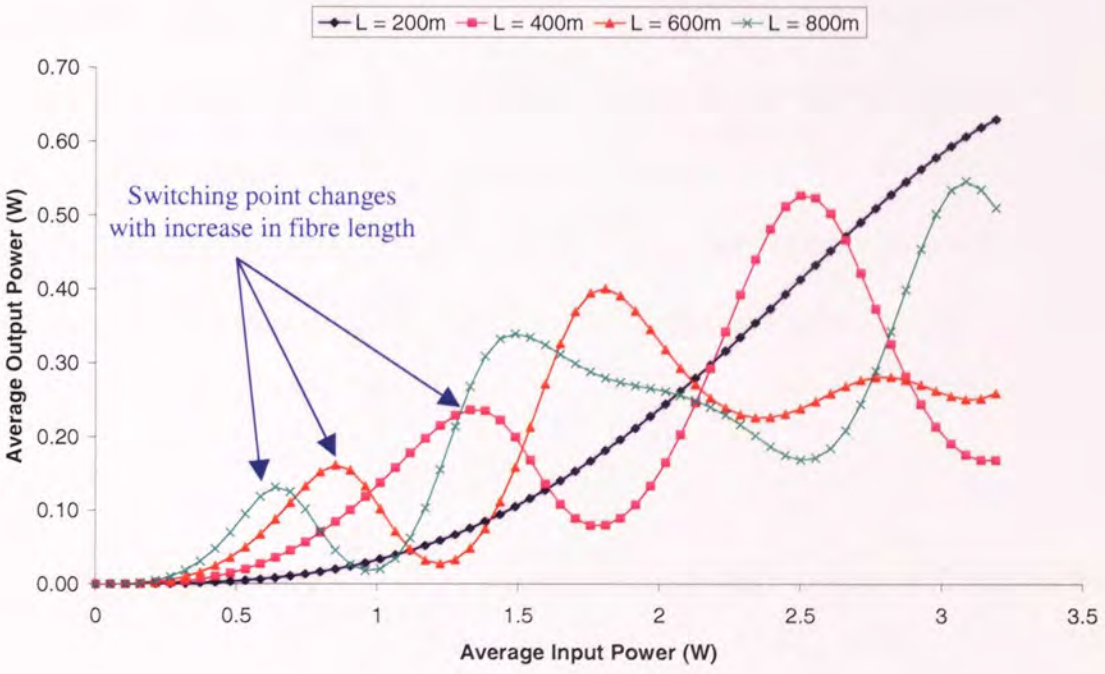

Figure 3.5: Self-switch characteristics (transmission) of the NOLM. A full π phase shift is achieved as the input power to the NOLM increases

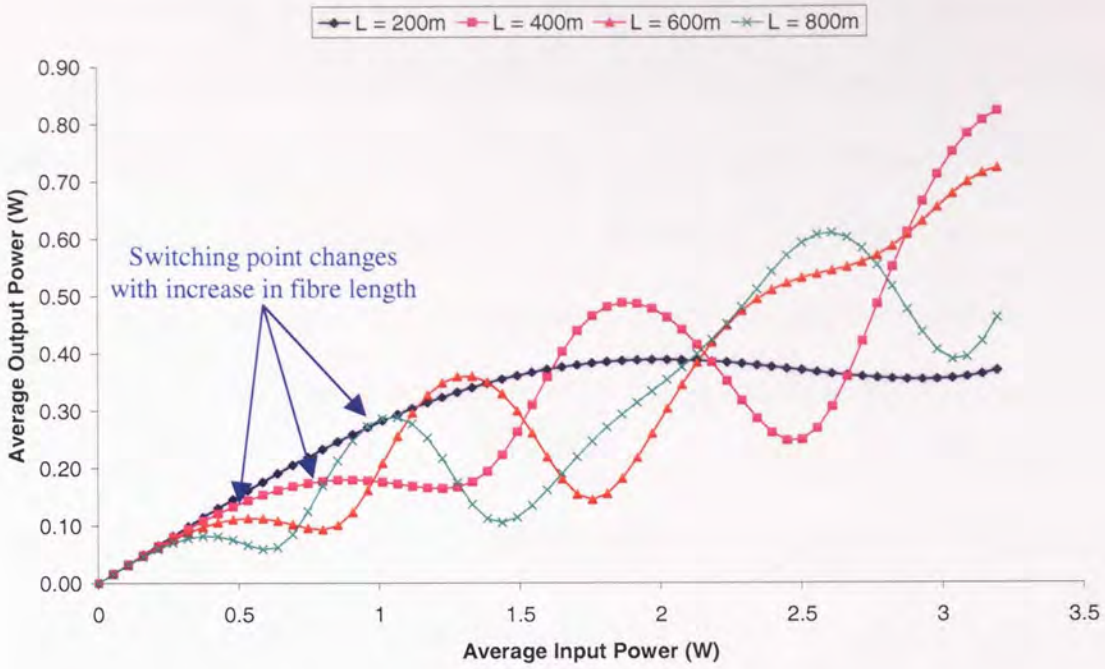

Figure 3.6: Self-switch characteristics (reflection) of the NOLM. A full π phase shift is achieved as the input power to the NOLM increases

As the fibre increases in length, the power required to achieve switching (a π phase change) decreases accordingly. This means that the self-switching characteristics of the NOLM can be tailored to fit several specific requirements. By careful manipulation of both the coupling factor and fibre length, switching can not only be made to occur at a very specific input power, but also a very specific extinction ratio.

3.3 Controlled switching using a Nonlinear Optical Loop Mirror

Another characteristic of a NOLM is its ability to switch light between one arm and another in the presence or absence of an additional control channel. This process is analogous to the function that an electronic logic AND gate produces. "Switching" (we

will define switching as light being emitted from the transmission arm of the loop) is only achieved when there is a control present, in the absence of a control pulse, the light is simply reflected. However, in order to achieve the maximum efficiency of the loop, a π phase difference is required between the two arms of the said loop. This is achieved by simply increasing the input power of the control in order to find the maximum transmitted power. Figure 3.7 shows a schematic diagram of the simulation used.

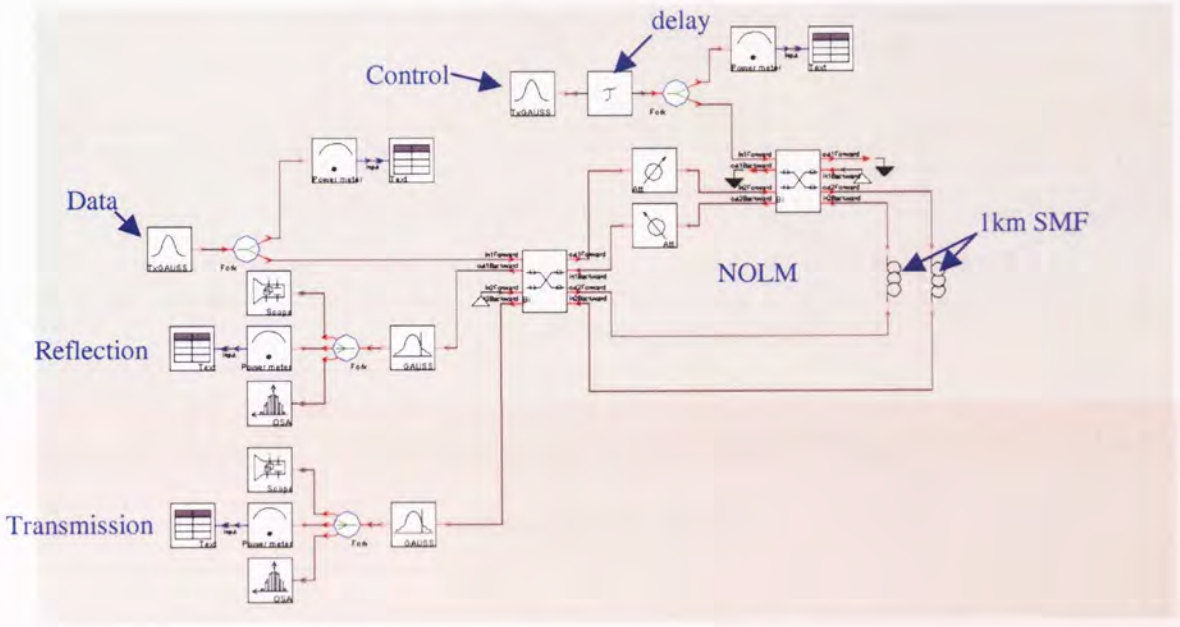

Figure 3.7: Schematic diagram showing a "controlled switch" NOLM configuration. Polarisation is not considered in this simulation

The timing offset between the two pulses (the data and the control) was set at 75ps. The data consisted of a pulse with a Gaussian profile, 0.5W of peak power and a FWHM of 10ps (with a central operating wavelength of 1558nm). The control also had a Gaussian profile with a FWHM of 10ps but had a central operating wavelength of 1538nm. As before, the fibre used in the loop was a 1km length of SMF and the loop had a coupling factor of 0.5 with 5dB of attenuation in one side. With $\Delta\tau$ = 75ps, the data was left

constant but the control power increased. The output produced in both the reflected and transmitted arms of the NOLM was measured and is shown in Figure 3.8.

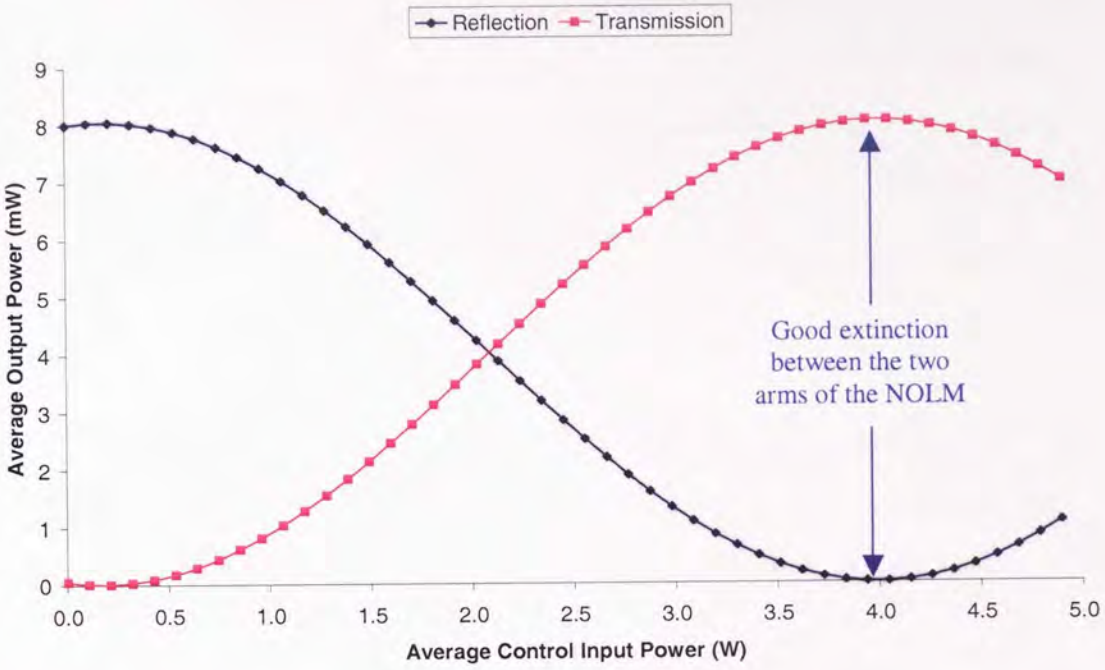

Figure 3.8: Controlled switching characteristic for a fixed timing offset between the data and the control channel.

It can be seen from the above graph, Figure 3.8, that when the output of one of the arms, say the reflected arm, is at a maximum, that at the other arm there is little or no output power at all. Whilst all other parameters remain constant, if the control pulse power is increased (note, the data power remains constant throughout the simulation) then the output appears to gradually switch from one arm to another before finally, all of the power is in the transmission arm. There is of course a point in the centre where the output power is equally split with 50% of the power in each arm and so the NOLM effectively acts like a simple 50:50 coupler. If the control power were to be increased even further, we would

see the output would switch back to the reflection arm of the NOLM. This pattern will continue whilst ever the control power is increased.

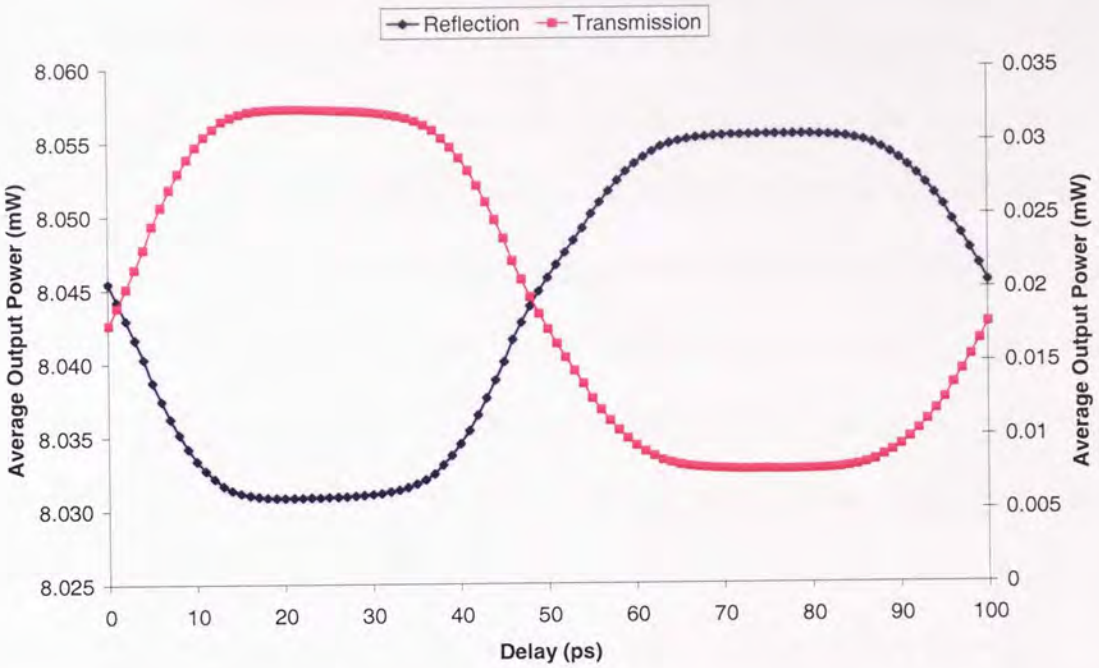

Figure 3.9: With both the data and the control having a fixed power, the relative timing offset, $\Delta\tau$, is varied over the entire bit period (the output power of the reflection refers to the left-hand axis whereas the output power of the transmission is shown in the right-hand axis)

Figure 3.9 shows the effect that the timing displacement between the data and the control, $\Delta\tau$, has on the output of the loop. Both the data and control power remained constant throughout, 0.5W peak power and 38W peak power respectively, and $\Delta\tau$ varied over the entire 100ps bit period in 1ps intervals. As the control pulse is swept through the data (it is this way around because in this case, the data never moves) once again, the output moves from one arm of the loop mirror to the other. The output is at a maximum in the reflected

arm for the second half of the timing window. Thus, the centre of this, 75ps, is chosen as the ideal point which will produce the best results.

With $\Delta\tau$ = 75ps and the control peak power at 38W peak power (equivalent to 4.05W of average power) the effect that the control pulse has on the output of the transmission arm of the loop was investigated. By applying a 4-bit word (we will use the following data pattern, 0111) to the data, in the absence of a control pulse) there is almost no output (Figure 3.12. However, a small amount of the original data does "leak through". This is due to the extinction ratio of the NOLM. The extinction ratio can be increased (which would decrease the level of leak through) by increasing the offset of the loop (in this particular case this would require increasing the attenuation on one side of the loop). However, for the purposes of this experiment, a small amount of leak through is of no consequence. Comparing now with Figure 3.11, with the addition of a control pulse, the output on the same transmission arm shows the original 0111 4-bit word. As before, we obtain a decent extinction ration between a '0' and '1' which could be further improved by increasing the attenuation in the aforementioned NOLM.

From this we can conclude that unless there is a control pulse of required power incident to the NOLM at the correct timing displacement, the loop will produce no output on the transmission arm. This property makes the NOLM particularly useful, by manipulating the control pulse it is possible to "turn on or off" the data. This functionality is analogous to an electronic AND gate or transistor.

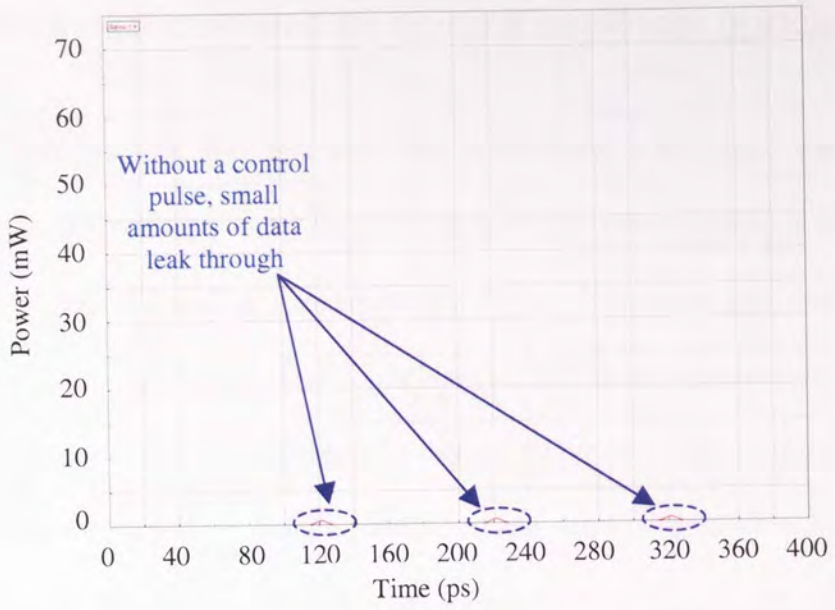

Figure 3.10: When there is no control pulse incident at the NOLM, there is no output on the transmission arm of the loop

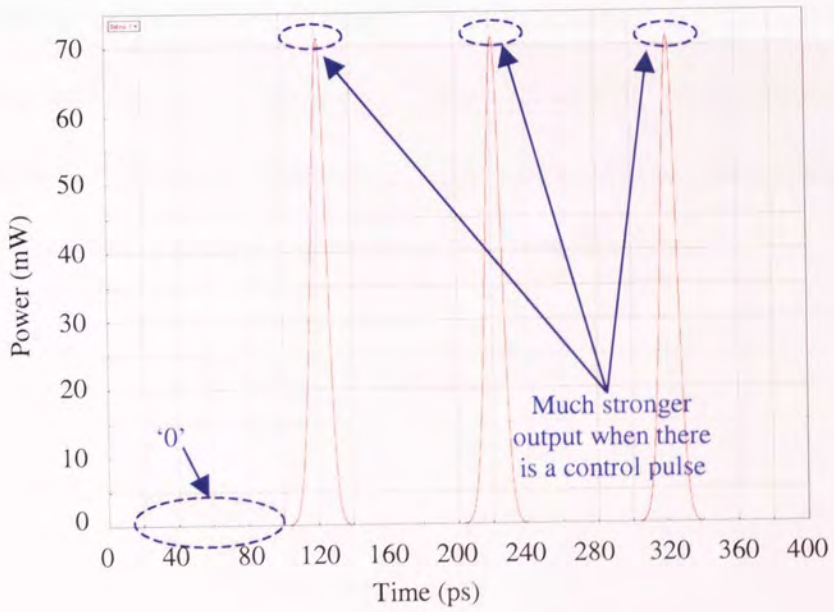

Figure 3.11: With control pulse with 4.05W of average power and $\Delta\tau = 75$ps, the data pattern 0111 is transmitted

3.4 Wavelength conversion using a nonlinear optical loop mirror

In the previous section, the data was only transmitted when there was a control pulse present. Optical filtering was employed to remove the control pulse at the output and the original data was allowed to propagate. However, if the data and control are swapped around (so that the control, or clock is incident on the "main" input to the NOLM) then the optical filters can be used to eliminate the data pulse and the so only the original clock wavelength is allowed to propagate (instead of the data). Because the NOLM acts like an AND gate, now the clock will only be transmitted when there is data present and so the pattern of the data is effectively "mapped" onto the clock [103]. Thus, a completely "new" copy of the data, but at the original clock wavelength, is transmitted. This principal is illustrated in Figure 3.12, the data power was increased for a fixed timing offset and the output produced at both the reflection and transmission arm measured. The NOLM configuration was changed slightly in order to achieve all of the following results. The SMF inside the NOLM was replaced with 1km of nonlinear fibre whose properties are based on commercially available nonlinear fibre from Sumitomo.

Figure 3.12: By varying the average power of the input data, the "clock" can be switched out of either of the two arms of the NOLM

As $\Delta\tau$ is fixed at 25ps, we are always sampling the control at exactly the same point in time. Whilst the control pulse remains at a constant power, with an increase in data power (average power) the output switches from the reflected arm to the transmission arm of the NOLM. A further increase in optical power would result in the pattern repeating itself. This works in exactly the same manner as in the previous section, the difference here is that it is the locally generated control (or clock) that is propagated, not the original data.

As before, the data and clock input powers were fixed and the timing delay, $\Delta\tau$, varied over the entire but period (100ps).

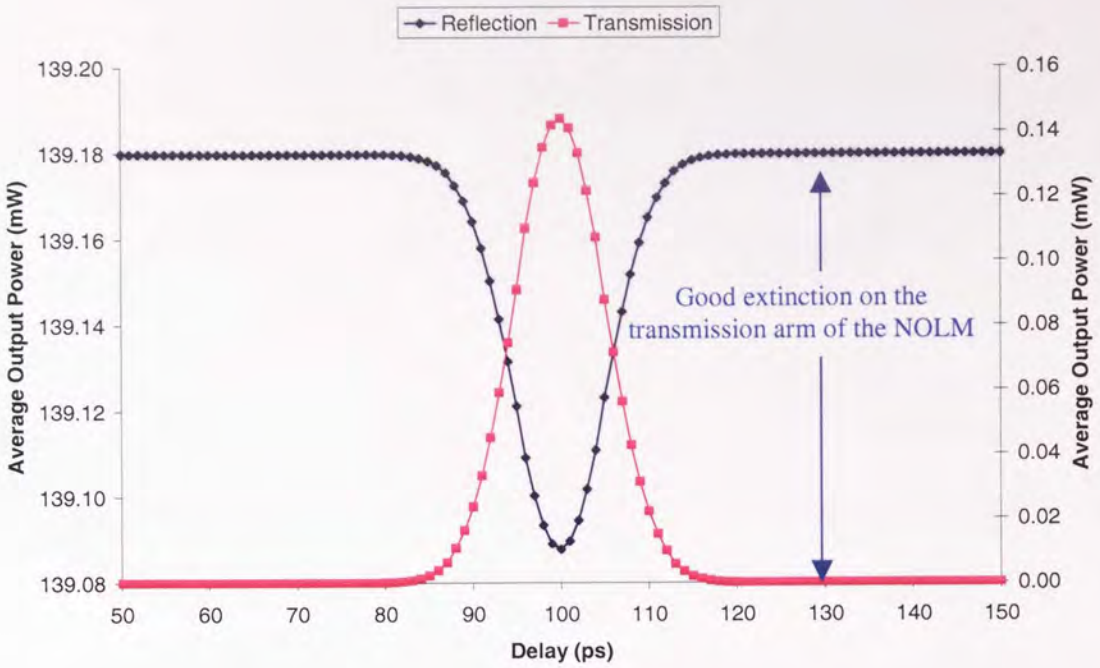

Figure 3.13: When the data is swept through the control the maximum output on the transmission arm of the NOLM occurs when there is a timing delay of 100ps

With fixed input powers on both the control and data channels, as the data is swept through the clock the output shifts from one arm of the NOLM to the other. This is clearly what would be expected (and is works in exactly the same way as Figure 3.9). Thus, we can determine if the control pulse is propagated by ensuring that both inputs to the loop were kept constant and varying $\Delta\tau$.

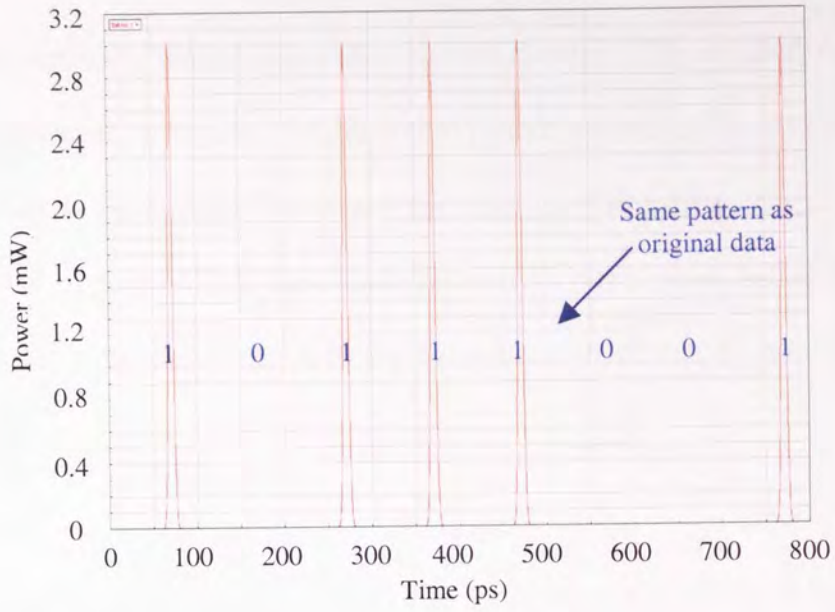

Figure 3.14: A "copy" of the data is mapped onto the control pulse and then transmitted

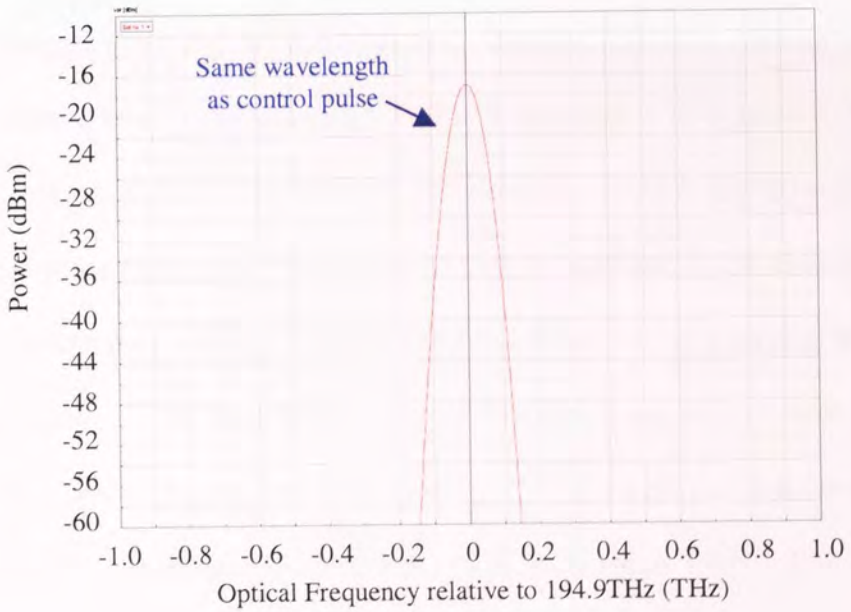

Figure 3.15: The new "data" is at the original clock wavelength

We can confirm that it is actually the clock that is now transmitted from the NOLM by measuring the frequency or wavelength that is produced Figure 3.15. The corresponding

temporal output is also shown (Figure 3.14) where it can be seen that the PRBS pattern has been successfully mapped onto the control channel. The original data pattern was 01110011. However, in Figure 3.14 the output pattern appears to be 10111001, which may initially appear to be wrong. This is not the case, the simulation only runs for "8bits of time" and then repeats. Thus, the output pattern is correct, just shifted in time by 1bit. Although this may be a problem when trying to measure BER's, for this illustration this is not the case.

If the clock that is generated (also referred to as the control pulse) is chirped (a change in frequency across the pulse), depending on the relative timing displacement between the clock and the data, a different portion of the clock will be sampled (through the effects of XPM). As the data samples different, discrete sections of the now chirped clock pulse, different discrete wavelengths are produced. Thus, any timing displacement is directly transferred into a change in wavelength (this is analogous to section 2.3 where optical filtering was used to select the desired wavelength). To test this hypothesis a linearly chirped clock pulse (section 2.2) was used as the clock source in the already tested NOLM configuration and data swept through it (this was achieved by applying varying amounts of temporal delay to the data source so that the data samples different sections of the chirped clock source). Firstly, we see that as the data is swept through the clock pulse, the output power on the transmission arm of the NOLM increases when XPM happens (Figure 3.16) but where there is no XPM, the data and the clock no longer temporally align) there is no output. This shows where the timing window will occur.

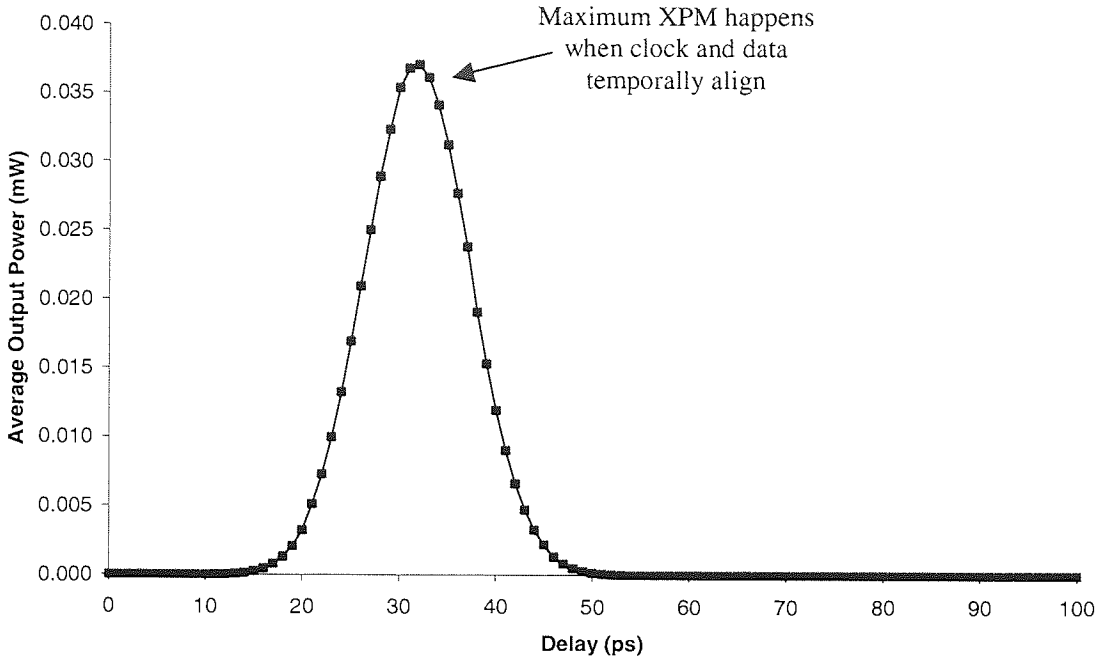

Figure 3.16: With a chirped clock pulse, XPM still occurs and maximum output on the transmission arm of the NOLM occurs at 32ps

At the same time, the frequency or wavelength shift that is produced at the transmission arm of the loop was measured and the results shown in Figure 3.17. It can be seen that for a change in optical timing delay, $\Delta\tau$, the wavelength that is produced at the output of the loop changes. Although it is not shown in the following graph, the relationship is not linear at the very extremities of the clock pulse. Beyond the clock pulse, no wavelength conversion occurs at all.

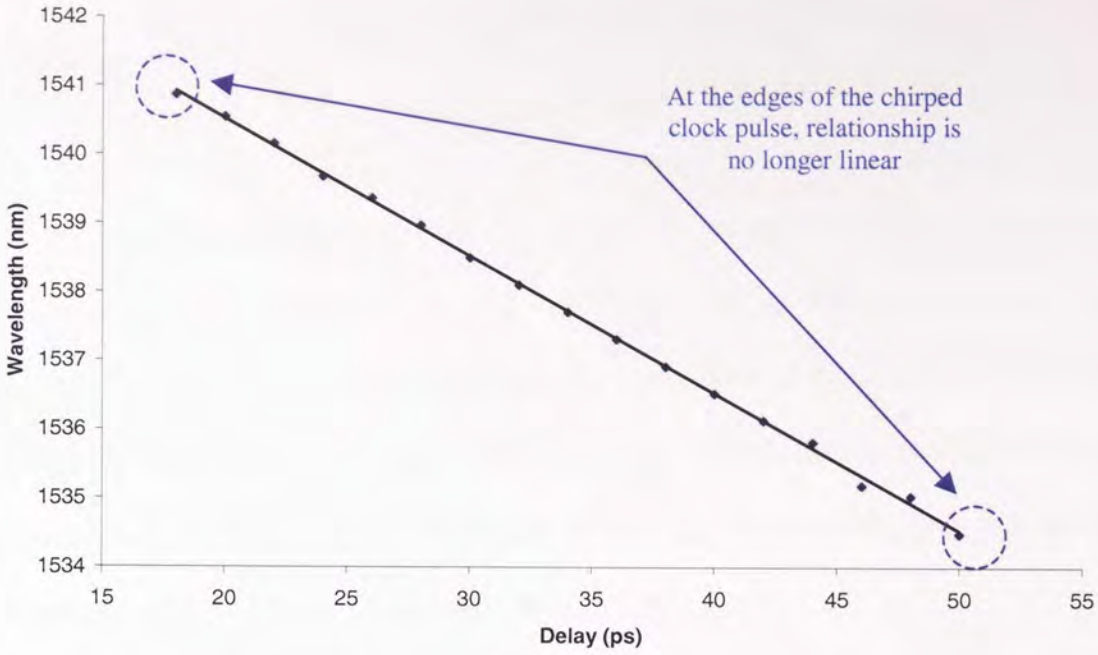

Figure 3.17: As the timing delay, $\Delta\tau$, increases the wavelength that is produced decreases

The above relationship is linear and thus, for a given timing delay, it is possible to generate a specific wavelength. It is possible to generate almost 7nm of wavelength shift over a timing range of more than 30ps (note, this does not necessarily imply that 30ps of phase wander can be removed error-free). The relationship is only true for the timing region where XPM occurs. Outside this region, if no XPM occurs then clearly there will be no wavelength conversion

3.5 Phase Wander reduction using a Nonlinear Optical Loop Mirror

To achieve phase wander reduction, the dynamically wavelength converted signal is then subjected to dispersion compensation such that the level of dispersion is opposite to the timing displacement which resulted in the specific wavelength shift. The way in which the dispersion is applied is irrelevant, any dispersion compensation module with the appropriate level of dispersion would suffice; the method chosen throughout this thesis is to use lengths of dispersion compensating fibre.

Wavelength conversion was achieved in the manner described in the previous section (a linearly chirped clock pulse is generated through propagation along 2.2km of nonlinear fibre. Data is then used to sample the linearly chirped clock pulse when the two channels exhibit XPM inside a NOLM. The resulting wavelength shift is proportional to the amount of timing displacement, see Figure 3.17). The level of dispersion required to achieve the maximum phase wander reduction can be found by simply varying the lengths of dispersion compensating fibre at the output of the NOLM and finding the point at which the chirped clock pulse's FWHM is at a minimum. This was achieved by turning off the data source and measuring the pulse duration out of the reflected arm of the NOLM (because the NOLM is set up to produce no output at the transmission arm of the NOLM when there is no data pulse, the clock will be produced at the reflection arm of the NOLM. Using this method, the NOLM does not have to be re-biased). The results of the simulation are shown in Figure 3.18.

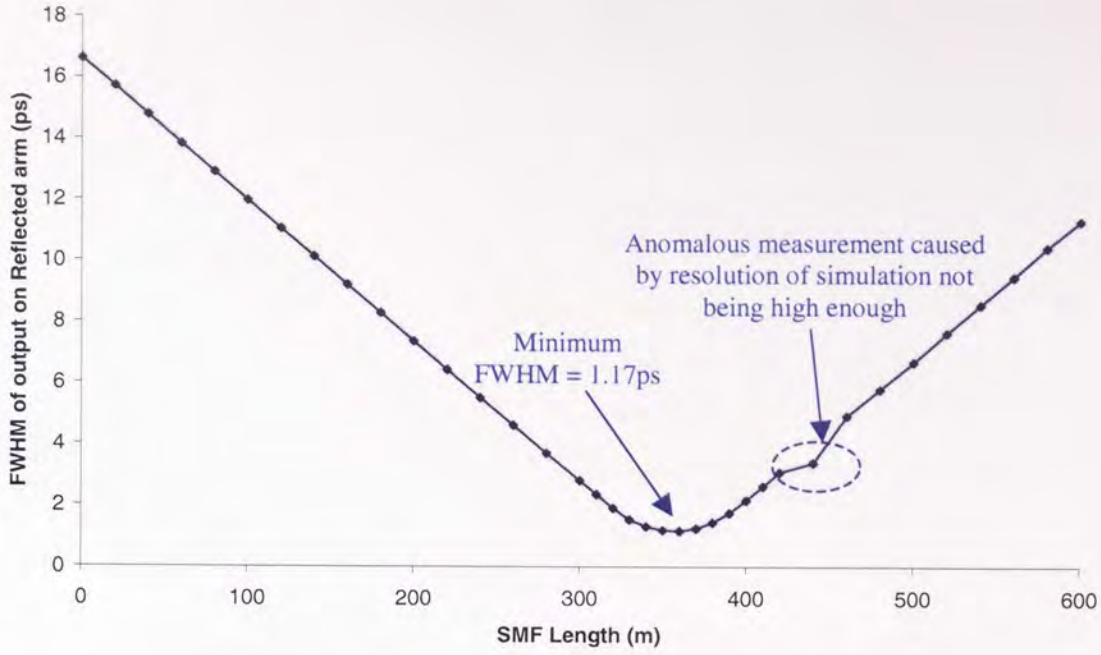

Figure 3.18: As the level of dispersion increases, the pulse duration reaches as minimum before increasing once more

Thus, we see that using just 360m of SMF will produce the minimum pulse duration on the reflected arm of the NOLM (SMF is used as the dispersion compensation module because of the sign of the chirp that was generated). The final pulse duration was 1.17ps which is significantly shorter than the initial clock FWHM of 10ps.

The SMF was then added after the transmission arm of the NOLM (after optical filtering, which is used to remove the unwanted original data channel) and the data re-applied to the NOLM. Phase wander can be "manually" applied to the system by adding controlled amounts of timing delay, $\Delta\tau$, to the input of the NOLM and then measuring the exact timing position of the data after propagation through the system. This is more readily understood by once again superimposing all of the timing displacements onto one

oscilloscope. Thus, the input data containing 20ps of phase wander is shown in Figure 3.19.

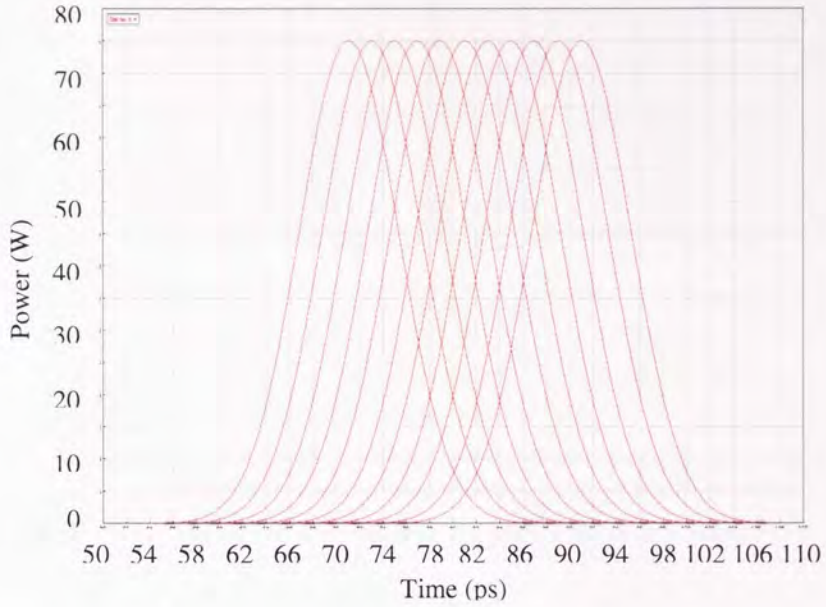

Figure 3.19: Input to the phase wander reduction scheme showing 20ps of phase wander applied to the data

The outputs produced by the NOLM are superimposed together and shown in Figure 3.20. By comparing Figure 3.19 and Figure 3.20 it can clearly be seen that the phase wander has been reduced. The timing, x-axis, of both figures is purposely shown over the same range to illustrate further, the reduction in phase wander. There is however one problem, phase wander has been translated into amplitude jitter with a peak power difference of 1.28mW. This is because we are actually trying to compensate for too much phase wander compared to duration of the chirped clock. Provided XPM occurs, wavelength conversion will occur. In order for phase wander to be reduced to approximately 1ps, the data must fall within the centre part of the chirped clock pulse.

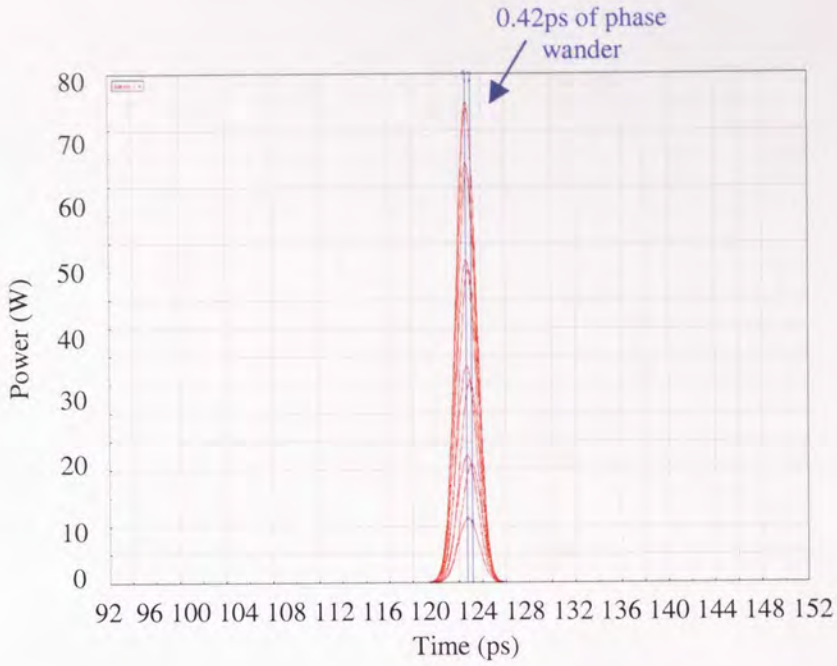

Figure 3.20: After propagation through the system, the phase wander was reduced to 0.42ps

As the data approaches the edge of the chirped clock pulse, not only will we be left with phase wander after the system, amplitude jitter will have also been generated. Thus, by increasing the chirped clock pulse duration, we can actually compensate for more phase wander. This is shown by increasing the clock input power (the FWHM of the generated clock pulse is increased to 50.02ps) and comparing how much phase wander can be reduced to >0.5ps.

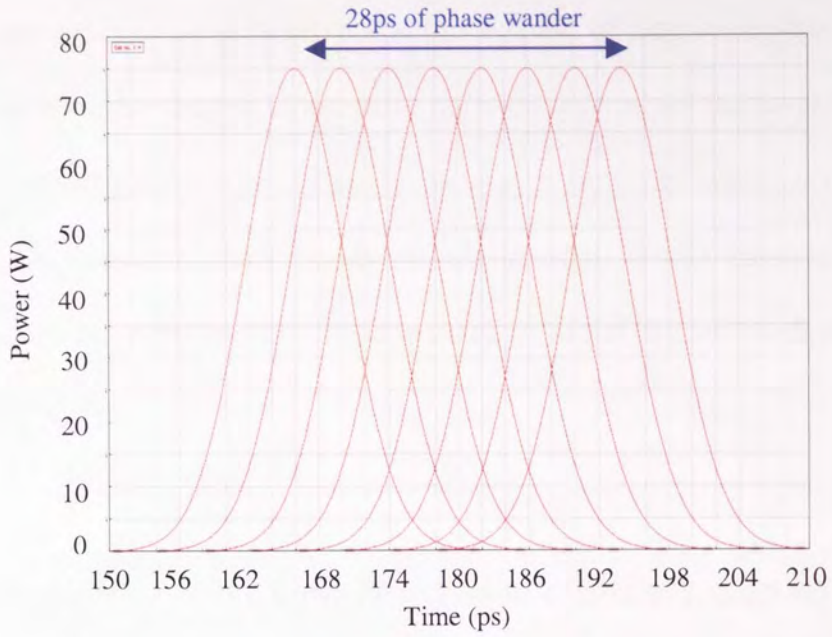

Figure 3.21: There is a total of 28ps of the phase wander applied at the input of the system

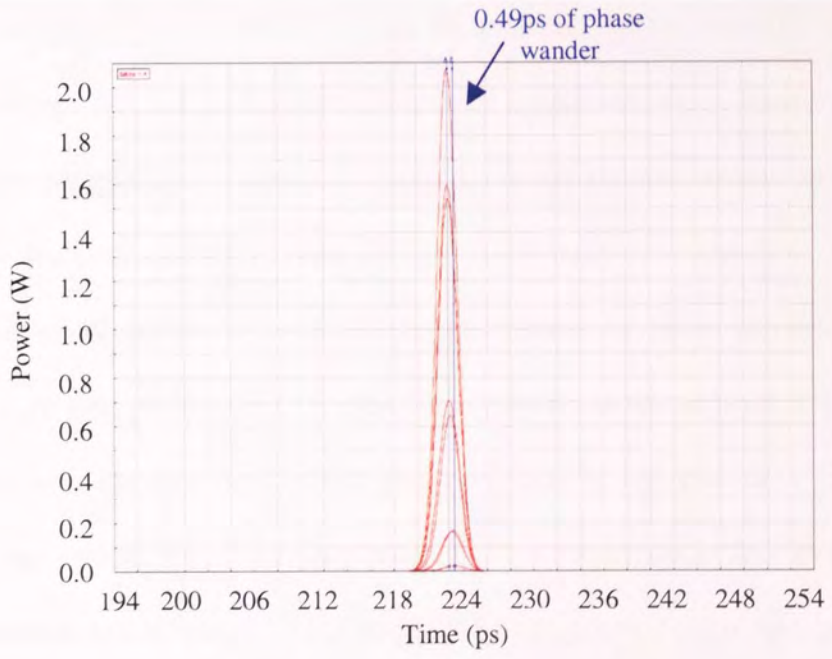

Figure 3.22: After propagation through the system, the phase wander is reduced to 0.49ps

Here we find that the increase in FWHM implies that up to 28ps, an increase of 8ps, of phase wander can now be reduced, but at the expense of amplitude jitter, to 0.49ps. This demonstrates how the chirped clock pulse duration determines the level of phase wander that can be effectively reduced. Clearly there is a limit, as previously discussed, it is imperative that adjacent clock pulses do not overlap. If this happens, errors will be generated when the sampling falls at the extremities of the chirped clock pulse.

3.6 3R regeneration using Nonlinear Optical Loop Mirror

It now has been shown that phase wander can be reduced using the principle of wavelength conversion (section 3.5). However, if we extend a slight modification to the previous model, full 3R regeneration can be achieved. In the previous section the phase wander was reduced (all be it at the expense of amplitude jitter). However, as the system relies on wavelength conversion to achieve the desired phase wander reduction, it should be obvious that each section of data, after phase wander compensation, will have its own unique wavelength (if timing jitter were compensated for, each individual successive bit would have its own unique wavelength). This problem is not an issue if the device were to be used as say, an all-optical clock recovery unit at the end of a transmission link. However, the system could not be placed inside a transmission link as propagation after the said system would re-introduce any timing irregularities that had been compensated for (due to the effects of dispersion, propagation of light at different wavelengths travel at different speeds). Thus, in order for further propagation to occur, the corrected data must all be at the same wavelength. If this occurs, 3R regeneration will have been achieved.

We now add a second stage to the previously discussed scheme. The output of the first stage is used as the data input to a second separate NOLM. A second local clock is generated and it will be the wavelength of clock 2 that is produced at the output of stage 2 (which is the final output of the new device). As it is this new clock that will be transmitted, by choosing a specific wavelength for the second clock, the final wavelength of the device can be controlled. Thus, in the case of the 3R regeneration where the original wavelength of the initial data needs to be preserved, by setting the second clock to the same wavelength as the original data, the wavelength will be maintained. Figure 3.23 shows the simulation schematic used to evaluate the 3R regenerator.

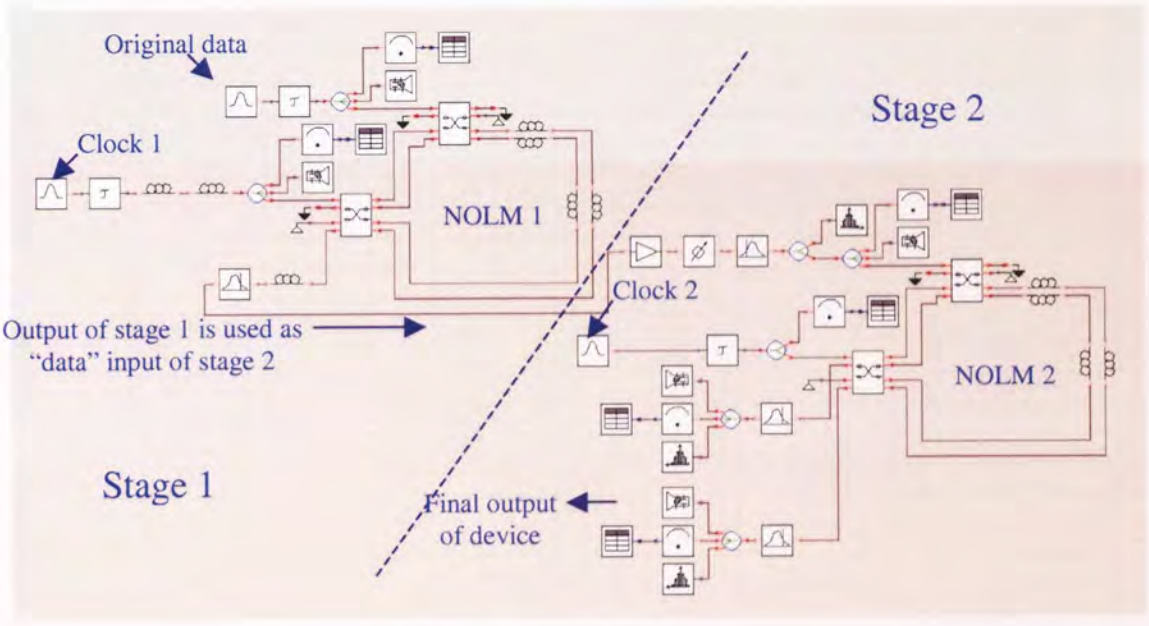

Figure 3.23: Schematic diagram of the 3R regenerator which utilises two wavelength converters

An input phase wander of 10.00ps was generated and used as the input to the system, Figure 3.24. It can also be seen that the data all has a single wavelength of 1550.1nm.

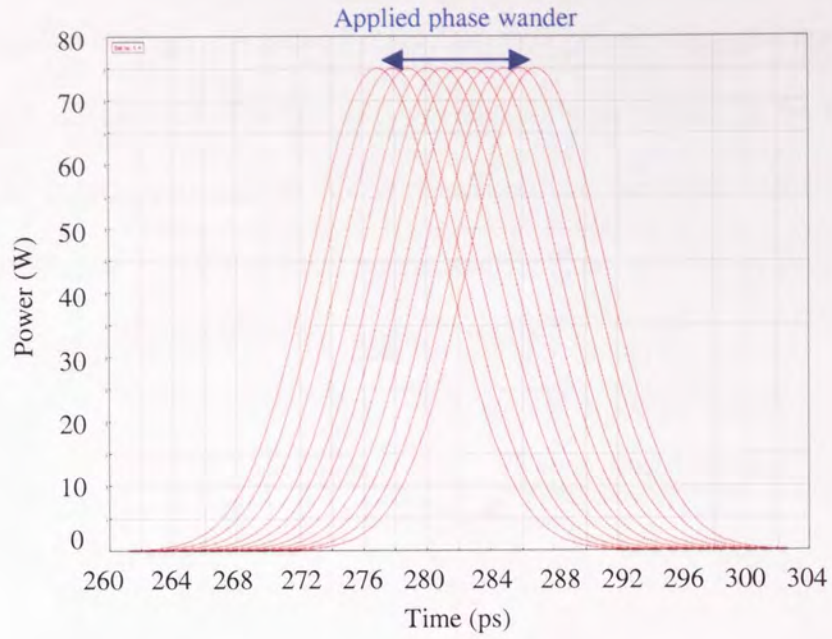

Figure 3.24: The input to the 3R regenerator has 10ps of phase wander applied

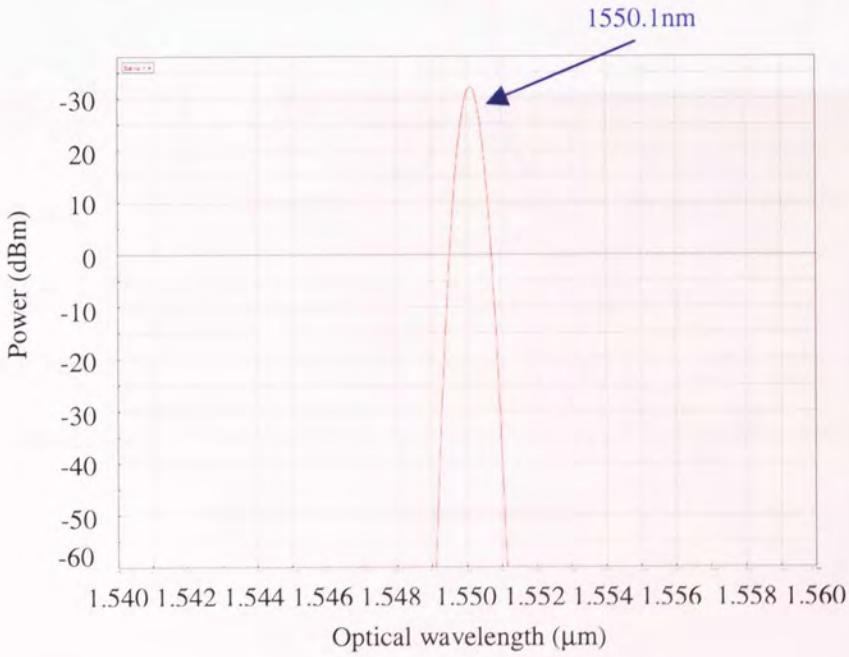

Figure 3.25: Optical spectrum of the original input data

At the output of stage 1, the phase wander has been reduced, but multiple wavelengths have been generated (not shown) making the system useless as a regenerator. However,

after propagation through the second stage, the multiple wavelengths are converted back into a single wavelength. The second wavelength was chosen to be the same as the original data (1550.1nm) and so 3R regeneration has occurred. As well as the single wavelength (Figure 3.27), the final output has a phase wander of only 0.05ps (Figure 3.26), significant reduction from the original 10.00ps.

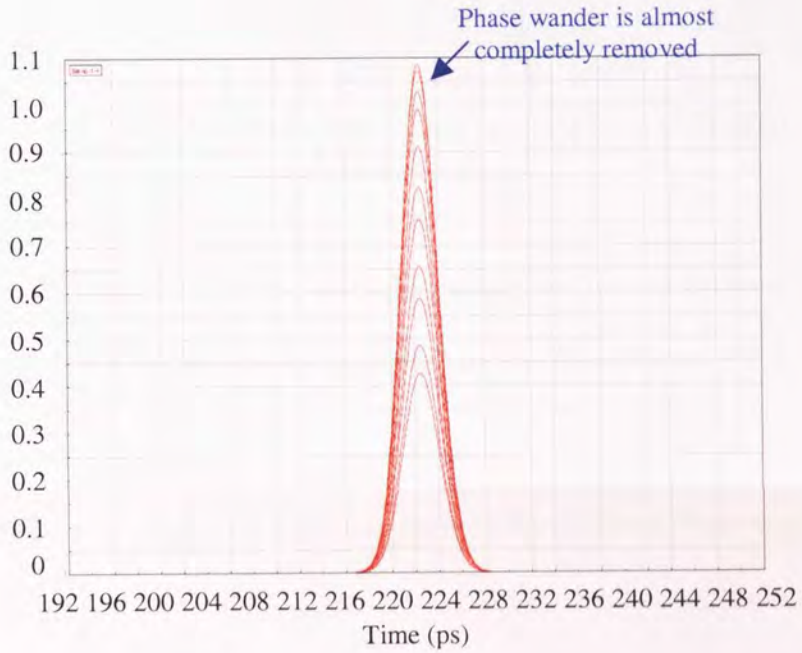

Figure 3.26: The phase wander at the output of stage 2 has been reduced to 0.05ps, although amplitude jitter has occurred (the peak power of the various outputs is no longer constant)

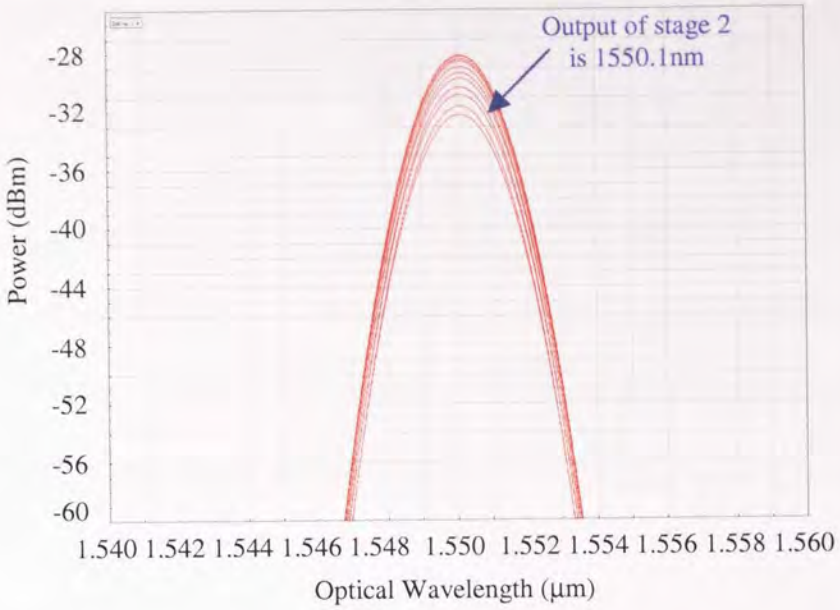

Figure 3.27: After stage 2, all of the individual pulses are now at the same wavelength as each other and the same as the original data (Figure 3.25)

It should be noted that amplitude jitter has once again occurred. This would of course be less than ideal in the case of 3R regeneration where we would be expecting further propagation after the system. The amplitude jitter has occurred as a result of the original chirped pulse not being square and has nothing to do with the principle of 3R regeneration.

The second non-chirped clock pulse's initial FWHM is now increased to 50ps and the previous simulation repeated. With the increase in FWHM, the results are almost identical (with further investigation we find that the final FWHM after propagation through the 3R regenerator is unchanged. The FWHM of the clock pulses doesn't matter providing of course that adjacent clock pulses do not overlap in time and so are shorter than the bit period). The single wavelength produced is always the same (that of the second clock) and the FWHM is always 3.60ps. Also note that the second clock delay (which is used to

temporally align the data and the clock in the second NOLM) is also always required to be the same, no matter what the FWHM of the second clock is.

As a comparison, the average output power, of stage 2 (which is of course the final output power of the 3R regenerator) was measured as a function of initial data delay (applied phase wander). The FWHM of the second clock was then changed and the simulation repeated. The results are shown in Figure 3.28.

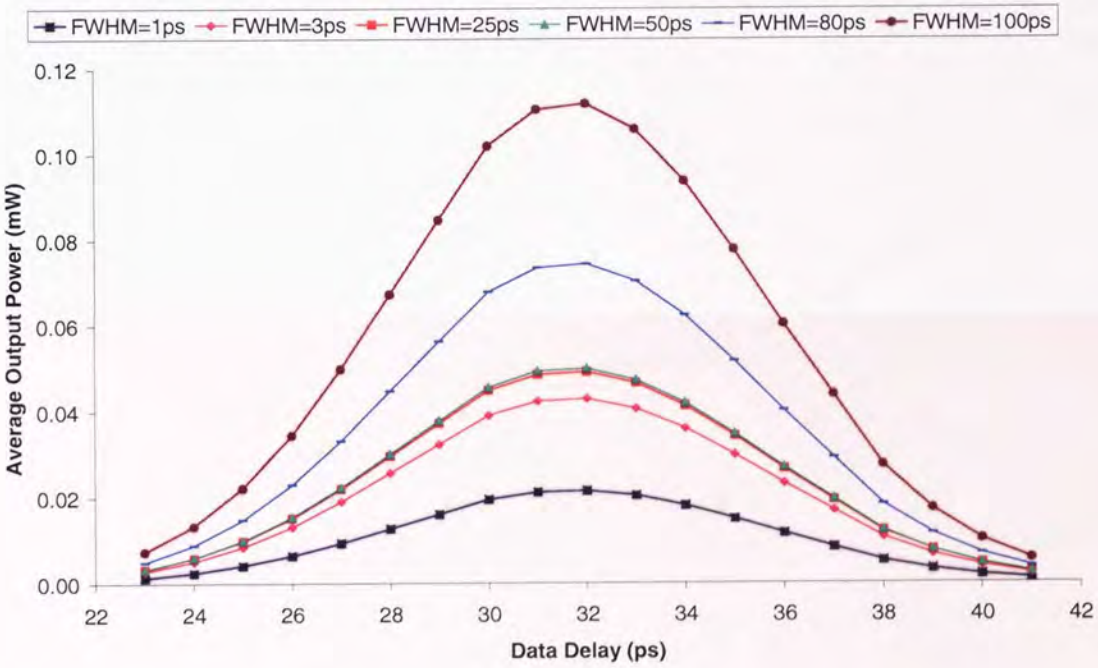

Figure 3.28: The average output power changes as the data is swept through the system and is also dependant on the FWHM of clock 2

As the FWHM of the second clock pulse is increased, because of the associated increases in energy, the average output power of the system also increases. We now determine a point at which we will say is the "edge" of the first clock (which is chirped) as our maximum range of timing compensation. In this case we define the range as an initial

timing delay of between 23ps and 41ps (it should be noted that this is not the maximum timing range that can be compensated for with this particular set-up, the range that is chosen here is arbitrary). The average output power at the edge of the timing range, $\Delta\tau_2$ = 23ps, is measured for a given clock 2 FWHM and then subtracted from the maximum average output power that occurs (which is in the centre of the chirped clock pulse when $\Delta\tau_1$ = 32ps). This leaves the average amplitude jitter over the given timing range for each successive clock 2 FWHM.

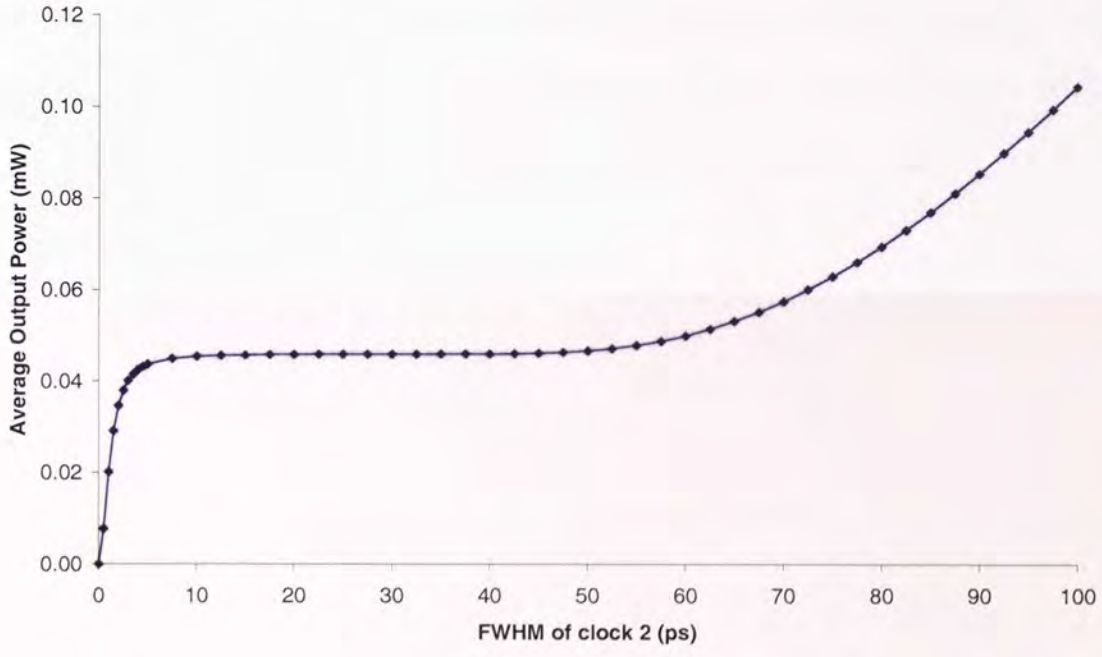

Figure 3.29: The output amplitude jitter changes as the FWHM of the second clock changes

Increasing the FWHM of clock 2, causes the average output amplitude jitter to also increase. Clearly in most cases this would be an undesirable effect and so clock 2 should be as short as possible. Thus, the only effect that changing the FWHM of the second clock has is to change the amplitude jitter that will be produced on the final output.

3.7 3R regeneration with dynamically controllable wavelength selector

In the previous section it was shown that a 2-stage 3R regenerator could be constructed out of 2 separate wavelength converters. The final output of the device is determined by the wavelength of the un-chirped second clock. However, a more "useful" approach would be to be able to control the final output of the device by some other method. If we now chirp the second clock pulse, then in the same way as stage 1, changing the input delay to stage 2 should change the wavelength that is produced after stage 2. The second chirped clock pulse was created using identical nonlinear fibres to that used to generate the first chirped clock source (namely 2.2km of Sumitomo nonlinear fibre). Of course the input wavelength is different in stage 2 compared to stage 1 and so the two chirped clock's will exhibit different properties.

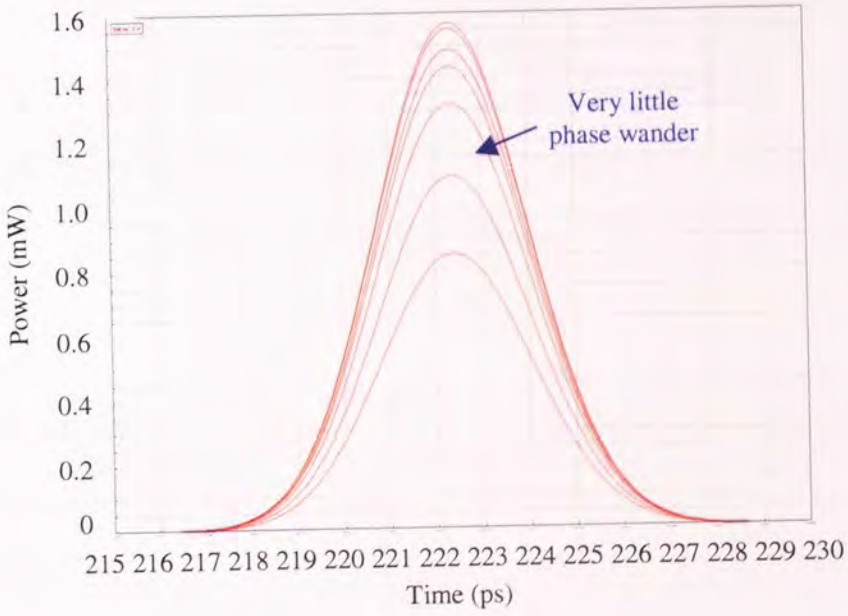

Figure 3.30: Final output of the 3R regenerator with a second timing delay of 73ps. The phase wander is almost completely removed

An initial input delay is varied over a range of 6ps (equivalent of 6ps of phase wander) and the second, now chirped clock source is delayed such that $\Delta\tau_2$ = 73ps. Figure 3.30 shows the temporal output of the after the 3R regenerator with the phase wander reduced from 6ps to almost 0ps. The corresponding optical spectrum is shown in Figure 3.31 where the wavelength produced is measured to be 1550.10nm

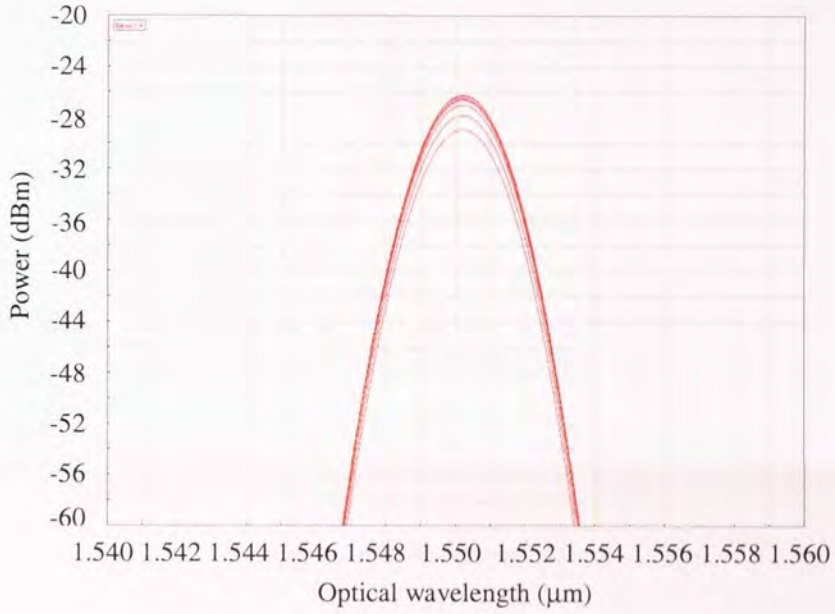

Figure 3.31: 3R regeneration has occurred resulting in one single wavelength, 1550.10nm, being produced

The previous simulation was repeated (with the same 6ps of phase wander applied at the input) but this time the second chirped clock source was delayed by 1ps less such that $\Delta\tau_2$ = 72ps. The new temporal profile that is produced is shown in Figure 3.32 and is almost identical to when $\Delta\tau_2$ was 73ps (Figure 3.30).The wavelength that is now produced (shown in Figure 3.33) is measured to be 1549.96nm. Thus, by simply changing the

optical timing delay to of clock 2, it has been shown that the wavelength that is produced can be controlled.

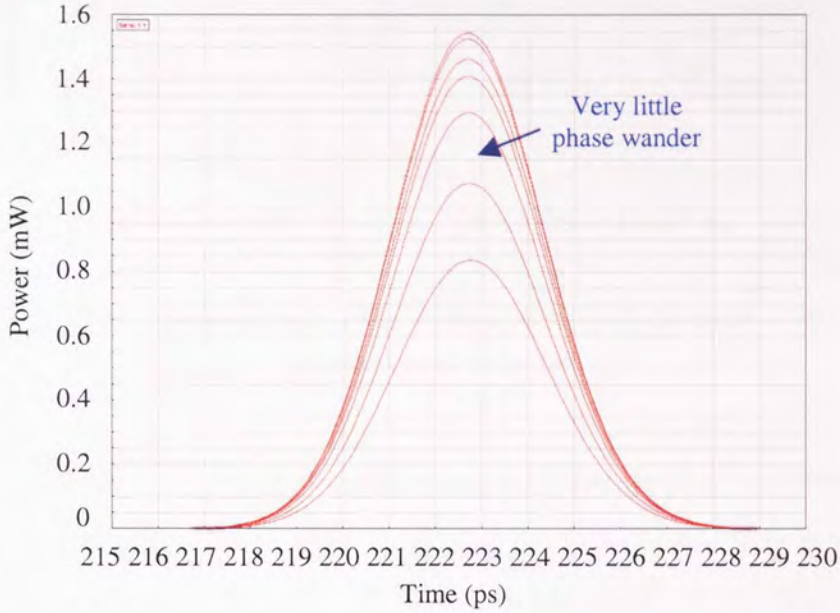

Figure 3.32: With $\Delta\tau_2$ = 72ps, a difference of 1ps, there is almost no change in the temporal response that is produced

To illustrate this point further, the amount of wavelength shift that can be produced by varying $\Delta\tau_2$ whilst still retaining the 3R characteristics is shown in Figure 3.34.

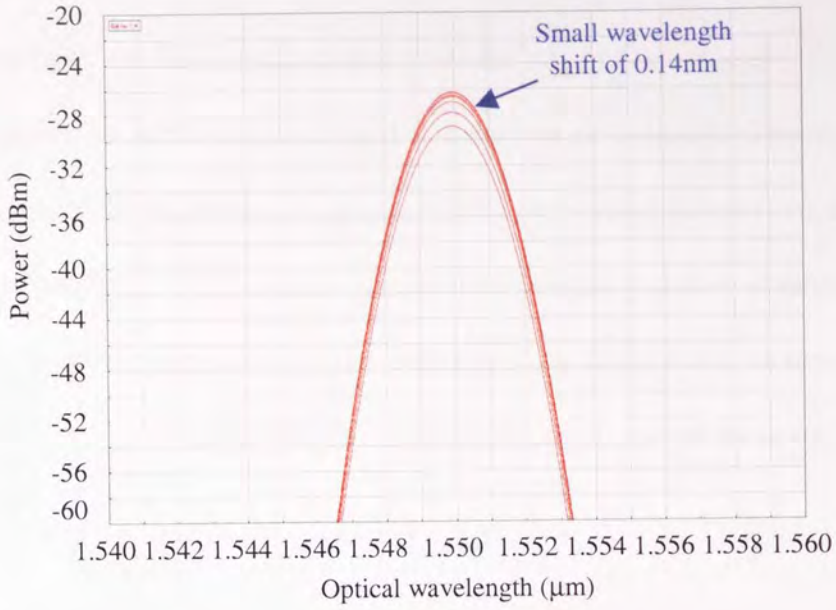

Figure 3.33: $\Delta\tau_2$ = 72ps, only one wavelength is produced but has been shifted to 1549.96nm

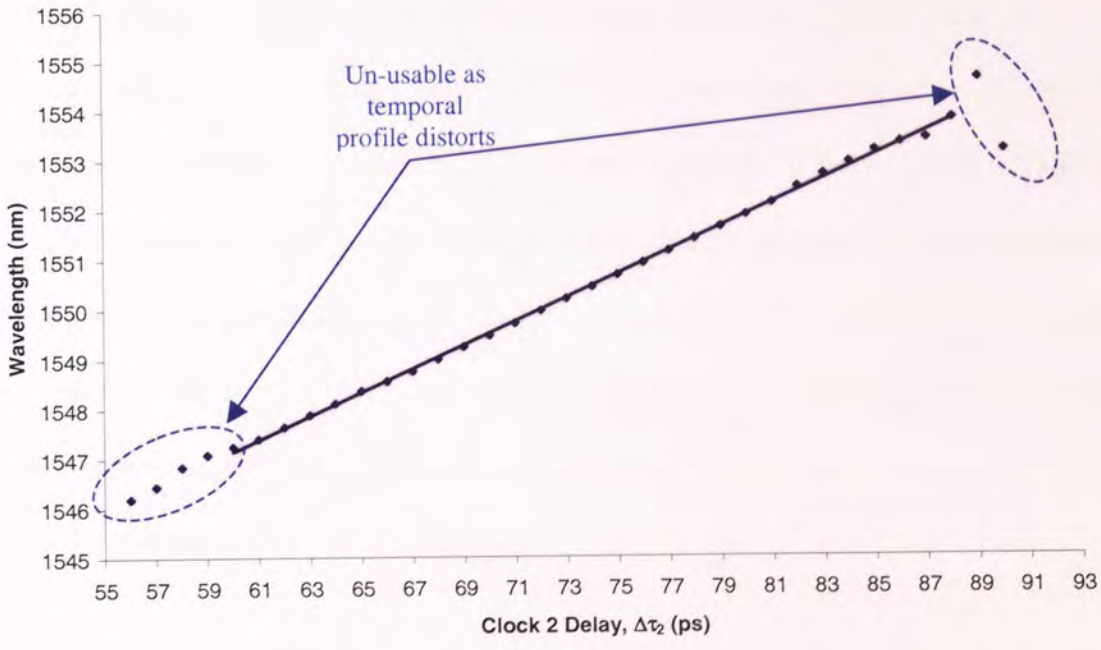

Figure 3.34: Increasing the timing offset between stage 1 and stage 2 increases the wavelength that is produced at the output. Total wavelength range is 6.57nm

The wavelength that is produced as a function of clock 2 timing delay is shown above. As one would expect, the relationship is linear. At the edge of the second chirped clock pulse, the temporal profile starts to distort and is therefore not useable. The wavelength range could be increased by changing the parameters of the second chirped clock pulse by either changing the nonlinear fibre used to generate the chirped pulse or alternatively, changing the peak power propagated through the said nonlinear fibre. Note, as there is no need for dispersion compensation at the output of the device, the shape of the graph is irrelevant.

3.8 Discussion

By using computer simulation, it has been shown that phase wander can be significantly reduced using the proposed scheme utilising dynamic wavelength conversion followed by dispersion compensation. The amount of phase wander that can be significantly reduced is entirely dependant on the duration of the locally generated chirped clock source. Increasing the FWHM of the clock source increases the timing window of the device and hence, more phase wander can be reduced. It has also been shown how the temporal profile of the locally generated chirped clock source has an effect on the results produced. It has been seen that if the clock is not temporally "square", the phase wander is directly converted into amplitude jitter. This may or may not be a problem depending on the situation that the device is to be used for.

Full 3R regeneration was also demonstrated by using two similar wavelength converters to construct a "2-stage" or "dual stage" device. Not only was it possible to convert the data back to the original wavelength (as is the case conventional 3R regenerators) but it was

also shown that it was possible to convert the output to a single, new wavelength. This was firstly achieved by simply changing the wavelength of the second clock source which resulted in a corresponding change in produced wavelength. Secondly, and potentially more useful, the ability to use optical timing delay to control the final wavelength was shown. The change in optical delay could easily be controlled remotely which would negate the need to re-installation of new hardware when a communications links wavelength needs to be altered. This device also has several potential uses in all optical metro style networks. Placing such a device at a node in say a local area network (LAN) would only allow for very specific wavelength conversion to occur whilst simultaneously regenerating the signal.

In reality we can conclude that the level of phase wander produced at the output can only ever be as small as the phase wander that produced by either of the clock sources. Of course in a computer simulation the clock source is ideal and so contains no phase wander. This implies that we should be able, inside a computer simulation, to reduce the phase wander to 0.00ps. The reason that the minimum phase wander that was ever produced was only slightly less than 1.00ps was because of compromises in the resolution of the computer simulation. Both the amount of samples contained within the simulations and the level of dispersion compensation could have been increased. However, this increase was considered unnecessary as it would have greatly increased simulation time.

It should be noted that as it is not possible to apply timing jitter to an optical source in VPI, timing jitter reduction has not been investigated. However, it is clear that this scheme would be able to compensate for applied timing jitter.

Chapter 4 - BER simulations

4.1 Introduction

In the previous chapter it was shown that by using a nonlinear optical loop mirror (NOLM) to sample a linearly chirped, locally generated clock pulse, phase wander could be reduced from an incoming data stream. This is an improvement over chapter 2 where an optical filtering technique was used as an analogy to demonstrate the principle of operation. It was also shown that by adding an almost identical second stage to the device, 3R regeneration could be achieved. This rather simple addition to the scheme increases the flexibility of the device as all-optical 3R regeneration is undoubtedly more useful. However, to date we have assumed the system works correctly by visually comparing an input codeword with that if the output codeword produced at the end of the system (Figure 3.11 and Figure 3.14). This now needs to be taken a step further and bit-error-rates (BER's) need to be measured.

It is at this stage that we run into a slight problem. It would have been desirable to use the previous NOLM configuration and add a photo-detector and BERT at the output. However, in order to obtain a "sensible" BER measurement, the time window that the simulation runs over has to be dramatically increased. Previously most of the basic simulations were only ran over 4 bits, only increasing when the input codeword and output codeword needed to be compared. When carrying out BER measurements the time window needs to be increased by 16 times at the very least. Of course, if the simulation is ran with a longer time window, the amount of samples taken needs to be increased appropriately (if we have too few samples the integrity of the pulses breaks down and

significant errors occur). All of this leads to a massive increase in the time taken to calculate the simulation results. In fact, a simple simulation, with no parameter sweeps, can easily take several hours of calculation time. This is clearly inappropriate as many multiple parameter sweeps will be needed in the following chapter. Thus, the configuration of the system has changed slightly (this does not effect the way in which the system works or the validity of the results). By adding lengths of SMF inside the loop, the point at which π switching occurs decreases. A decrease in required switching power will decrease the simulation time (it is the massive input peak powers of the previously chapters which caused such long simulation time) and so a manageable compromise can be reached, the results of which are shown in the following section.

The results that are shown in the following chapter were achieved entirely using VPI.

4.2 Basic operation of the new NOLM

As previously stated, the system has to be changed slightly so that the simulation time is manageable. These small changes do not affect the idea behind the system or the principle of operation. Figure 4.1 shows the configuration used to produce the following results. There are two new and identical receiver sections used to simultaneously measure the BER of firstly the back-to-back signal of the original data and secondly, the output signal of the timing jitter and phase wander reduction scheme (the back-to-back signal is used as a benchmark and to provide a comparison to the output of the system).

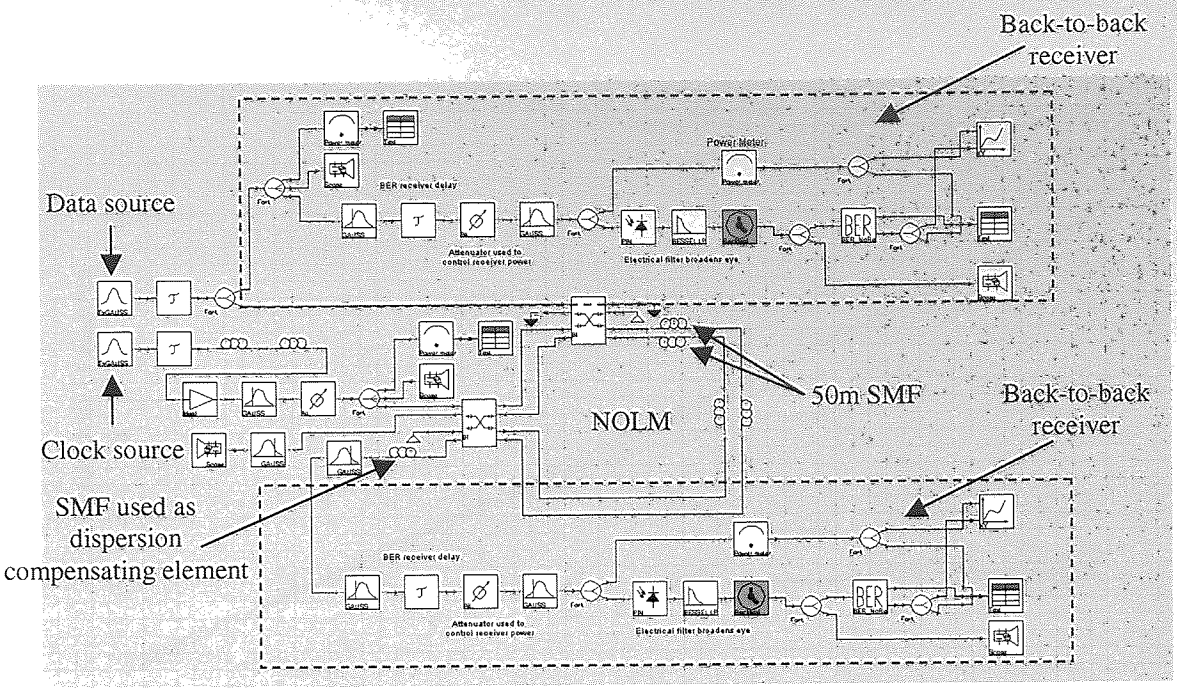

Figure 4.1: New schematic of timing jitter and phase wander suppression scheme. Included is the 50m of SMF which provides the nonlinear elements offset within the NOLM

Both the self-switching curves (where the clock power is increased without the presence of data in the NOLM), for firstly the reflection arm of the NOLM and secondly transmission are of the NOLM are shown in Figure 4.2 and Figure 4.3 respectively. Here we see how increasing the length of SMF inside the loop changes the switching characteristic of the NOLM. The increase in length of fibre effectively controls the offset of the nonlinear element (in this case the same 1km length of nonlinear fibre that has been previously used) inside the loop. Thus, the longer the length of fibre, the greater the offset and the lower the switching power is required to achieve π switching.

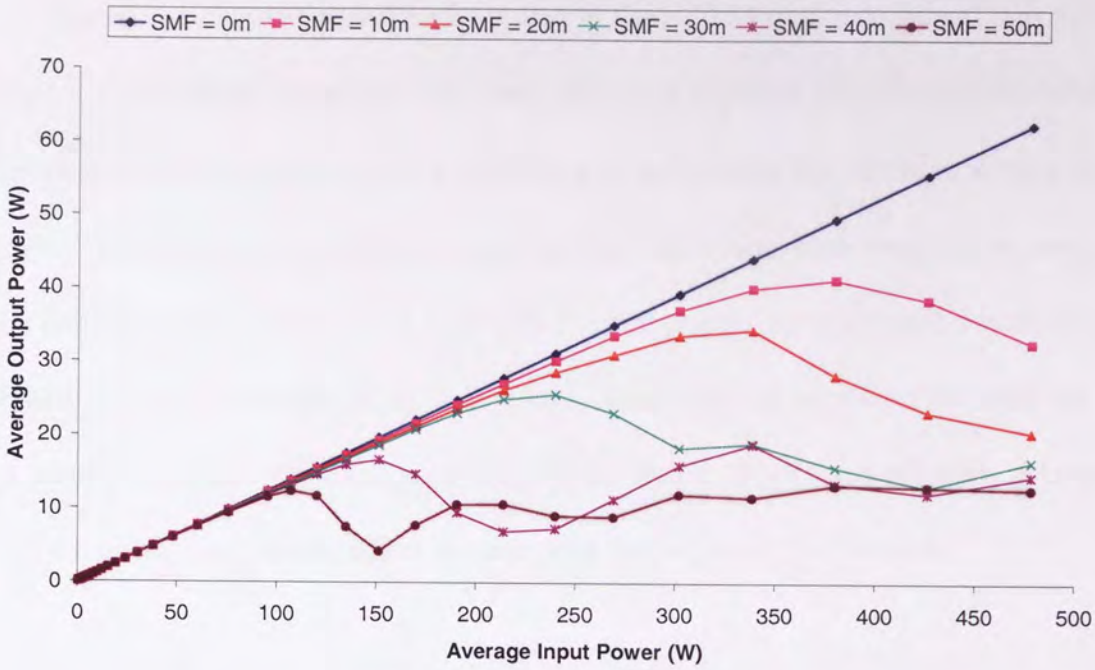

Figure 4.2: Self-Switching curve for reflection arm of the new NOLM which contains an added 50m of SMF

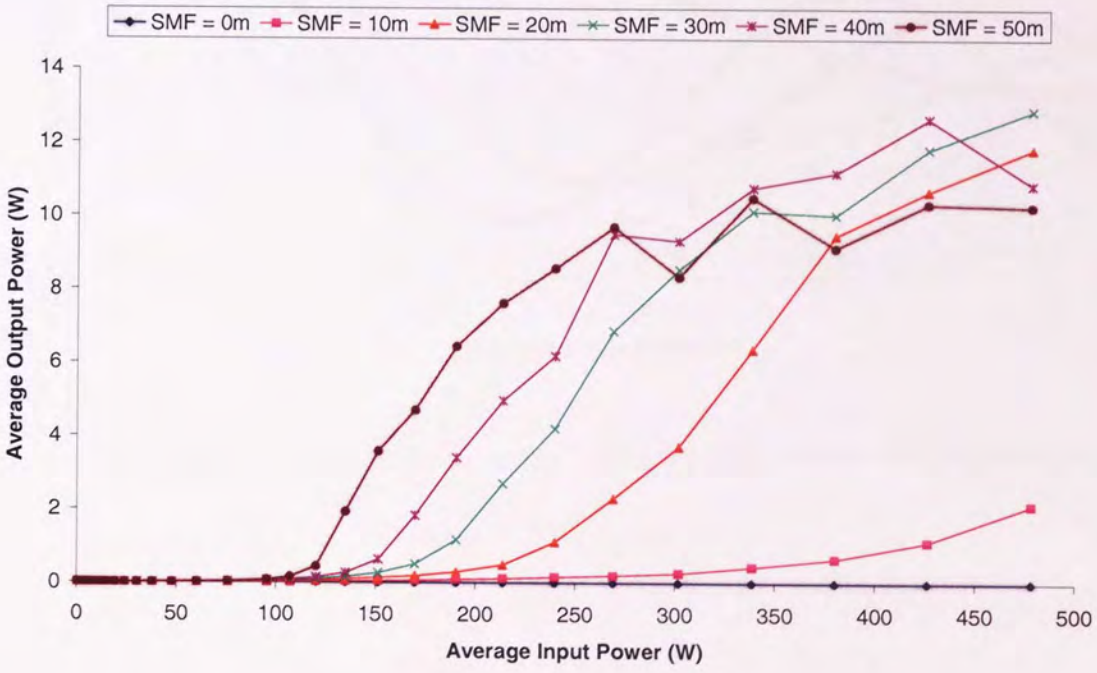

Figure 4.3 Self-Switching curve for transmission arm of the new NOLM which contains an added 50m of SMF

The controlled switching curves(data is applied to the NOLM with a constant clock power and then the data power is increased, the data pattern is imparted onto the clock) is shown in Figure 4.4 and Figure 4.5. Full π switching is achievable but requires a very large switching power. This would further increase the simulation time required to measure BER's (which is what we are trying to avoid). For this reason, an input peak power of only 10W will be used in the following simulations. This may not appear to be ideal (as we could further maximise the extinction ratio of the output if we used a higher data peak power) but again, this will not affect the principle that we are trying to show.

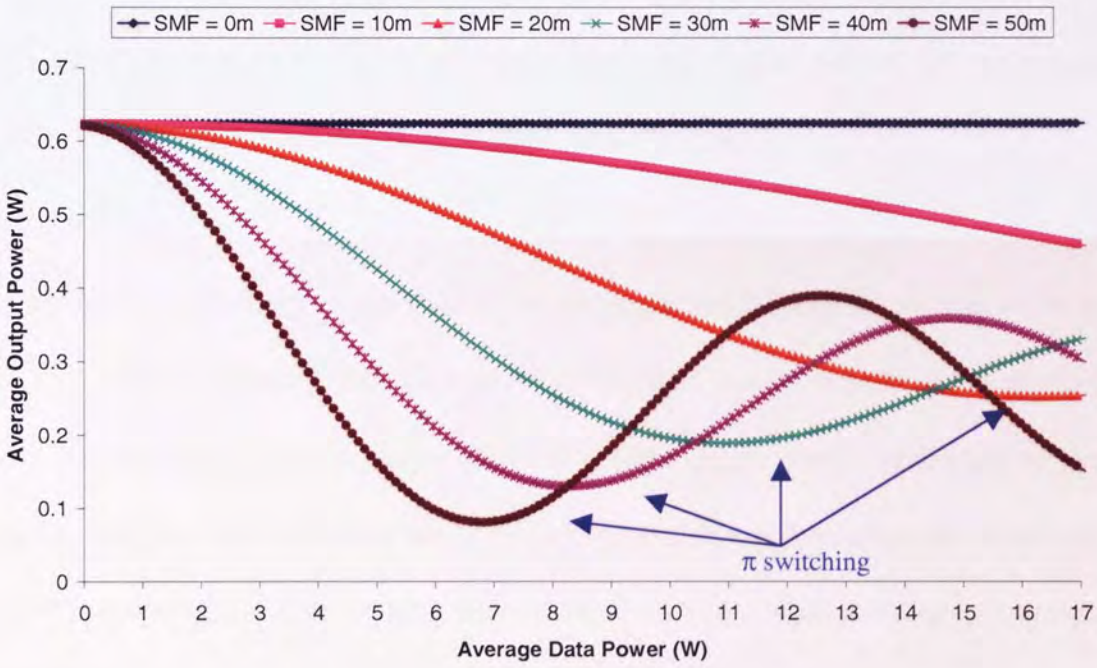

Figure 4.4: Controlled switching curve (reflected arm) for the new NOLM with varying amounts of SMF inside the loop

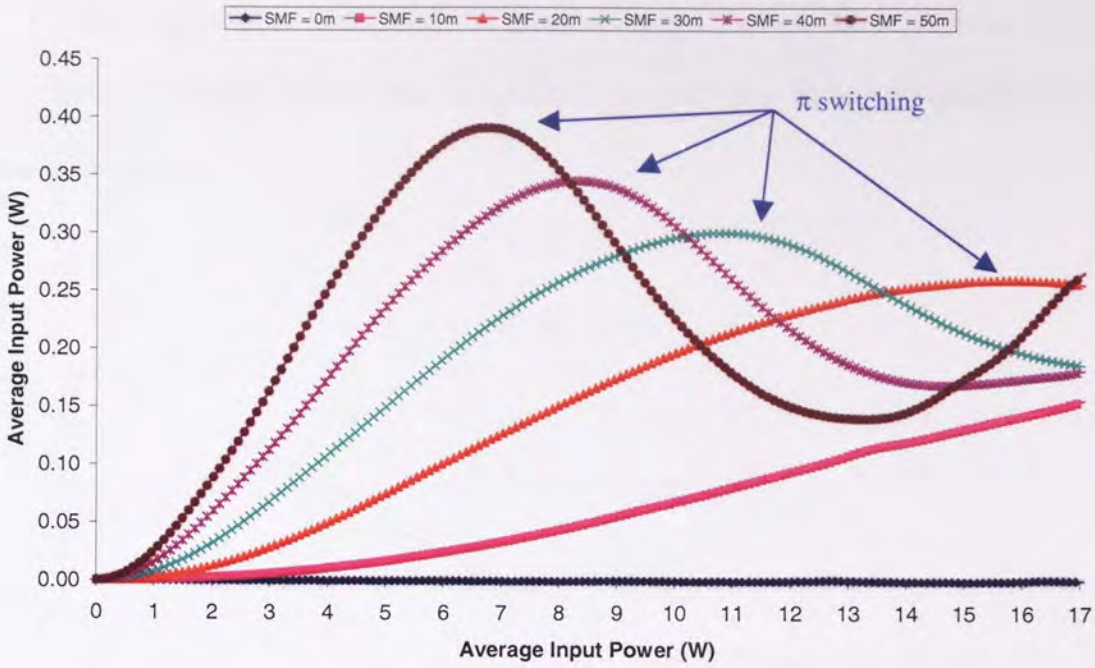

Figure 4.5: Controlled switching curve (transmitted arm) for the new NOLM with varying amounts of SMF inside the loop

As one might expect, the increase in SMF length inside the NOLM means that we require much less input switching power (the power of the data source, not the clock source) to achieve π switching. Clearly a further increase in fibre length (here I have stopped with a maximum length of SMF of 50m) would further serve to lower this value. However, this is a property of the NOLM that has long been understood and so does not require any further investigation.

The point at which switching occurs for the varying different lengths of SMF is shown in Figure 4.6. Thus, by extrapolating the results we are now able to determine the level of power required that will achieve π switching for any length of SMF. However, in the simulations which follow in the next sections, an input power which is less than that which will achieve π switching inside the NOLM is used. This is simply because of

overall simulation time. Even with the increase in SMF inside the loop, which decreases the required switching power, the simulations can still take an unmanageable amount of time to compute.

Figure 4.6: As the SMF inside the NOLM increases the power of the data which is required to achieve π switching also decreases

4.3 Error free operation

Now that it has been demonstrated that the new NOLM behaves in a sensible manner, it is time to carry out some BER measurements. Firstly the BER is measured out of the system as a function of BER delay (because there is no clock recovery is used in the simulation a timing offset, or BER delay, is applied in order for the data to arrive at the BERT at the appropriate time). This is achieved by connecting the output of the system (note, at this stage no phase wander or timing jitter is present on the original data and so it can therefore be considered that we have a "perfect" source) to the "BER receiver". The receiver consists of an optical delay unit (which is used to add optical timing delay, $\Delta\tau_{BER}$) along with an optical filter (which has a Gaussian profile). A photo detector then converts the signal from the optical domain into the electrical domain and is then followed by an electrical filter (the electrical filter is used to broaden the "eye" and has a bandwidth of 70% of the bit rate, so for a 10Gbit/s signal, the filter would have a bandwidth of 7GHz). One of the uses of this system would negate the need for an electrical clock recovery unit which is used to lock the original data to the BERT. If no electrical clock recovery is used, we must manually find the start of the data pattern in order to measure and BER's. Here we effectively remove the latency time that has occurred thus far by propagation through the system. As the data propagates through the phase wander reduction scheme it will encounter a certain relative timing delay which needs to be removed before BER measurements occur. This is vital as if we do not do this, BER measurements will be impossible as the BERT will not know where the start of the codeword or data pattern is.

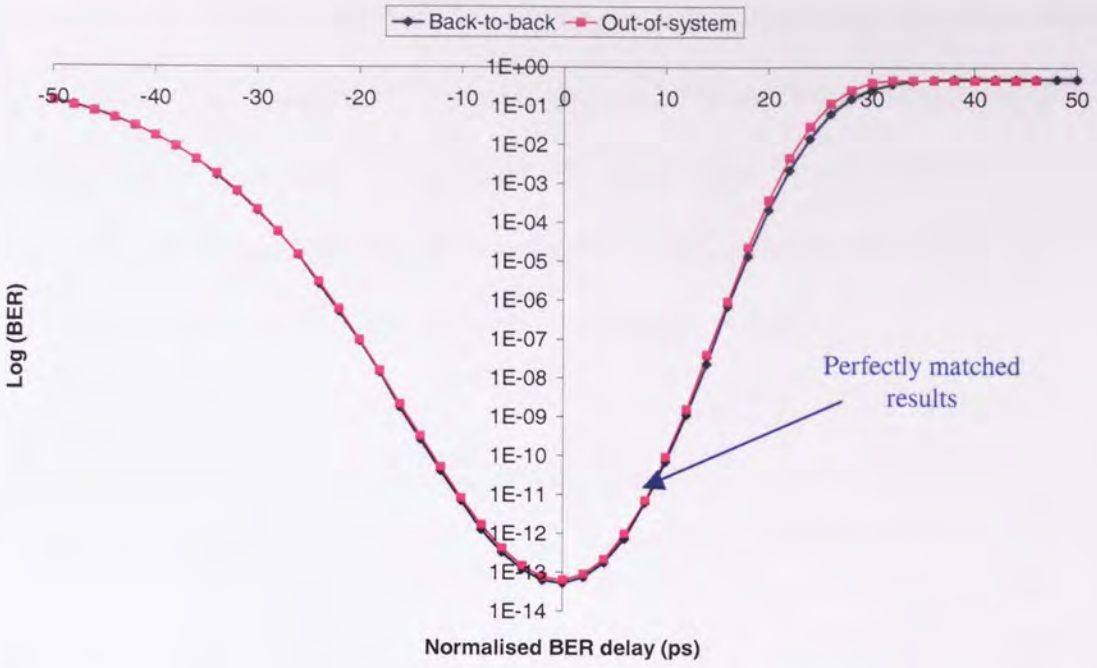

Figure 4.7: Comparison of BER as a function of $\Delta\tau_{BER}$ for both back-to-back and out of the system

By normalising $\Delta\tau_{BER}$, we can superimpose the two curves (each of which show effectively the same thing, the effect that $\Delta\tau_{BER}$ has on the received BER) on top of each other. From this we can conclude that there are no detrimental effects applied to the data by propagating it through the phase wander reduction system. We should also note in Figure 4.7 that we have a timing range of 100ps, this range was chosen for convenience, not because it is the bit period of the 10Gbit/s source. Because, as previously stated, $\Delta\tau_{BER}$ is just used to temporally align the BERT with start of the codeword, the bit period is irrelevant. If the simulation were increased in time, in either direction, the output would always remain at a minimum.

Now that we know where the codeword starts, by adding +10ps of optical delay after the system and -32.5ps to the back-to-back signal, the two sets of data can be independently

aligned with their respective BER modules. $\Delta\tau_{BER}$ is now left constant and phase wander, $\Delta\tau_{data}$, is applied to the data source. For each picosecond of applied phase wander the BER is measured out of the system. At the same time the average output power of the system will be measured. Because the output is optically sampling the chirped clock source, we should be able to get an idea of the temporal profile of the clock.

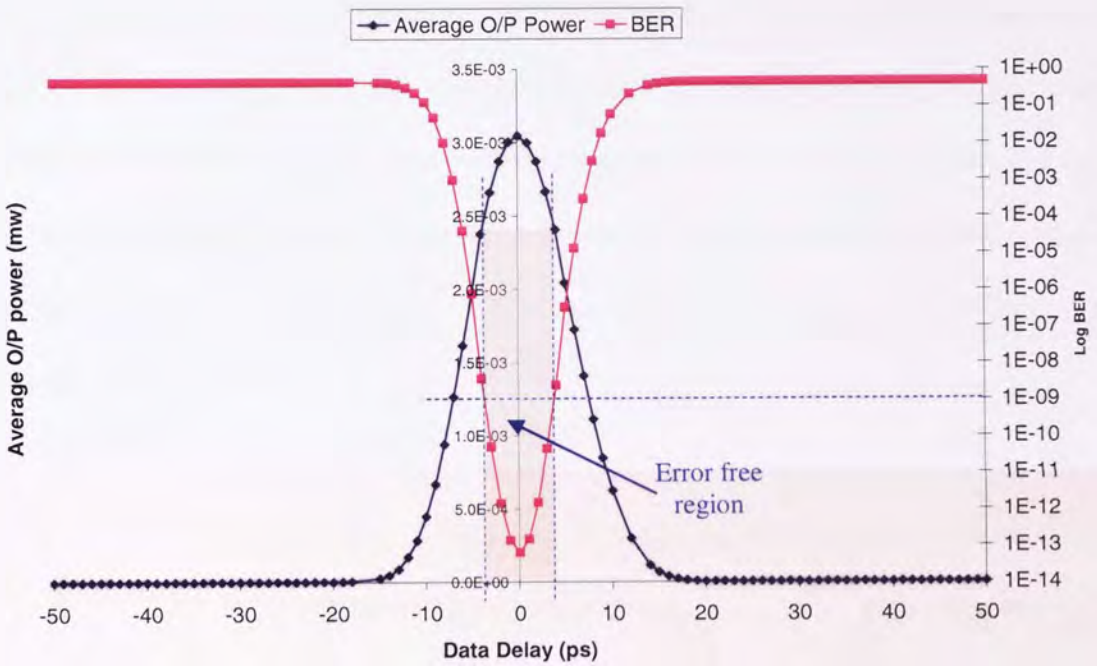

Figure 4.8: Variation in BER and average output power as a function of data delay or phase wander

Providing that the received power is above $2.66\text{x}10^{-3}$mW, an error free signal is achieved. This implies that we have approximately 6ps of phase wander that can be removed whilst maintaining an error free signal (we will define error free as a signal that has only 1 error in every 10^9 bits). This is the maximum level of phase wander that can be suppressed whilst simultaneously remaining error-free. One might have assumed that we would have been able to maintain the desired error-free operation for more than 6ps. However, this

value is small because of the relatively low average power that is incident on the photodiode section of the BER receiver (illustrated by the average received power curve in Figure 4.8). If we were to either increase the average received power or increase the sensitivity of the receiver, we would see an increase in the region for which error-free operation is achieved.

The next thing to consider is how the FWHM of a signal affects the BER that is being measured. This is important as we will later see that the back-to-back signal will usually be greater in duration (and therefore FWHM) than that of the signal emerging out of the phase wander reduction scheme. This was achieved by varying the FWHM of the back-to-back signal and at the same time, the BER was measured as a function of the BER delay, Figure 4.9.

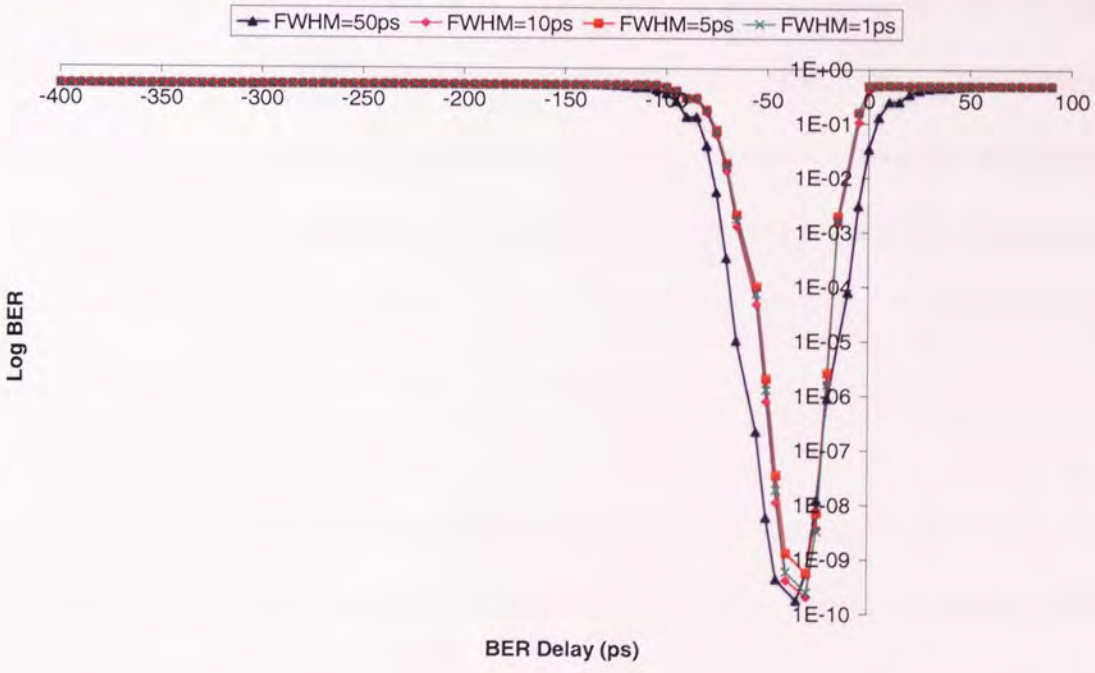

Figure 4.9: The FWHM of a signal only affects the BER for the most extreme case when there is a large FWHM

Thus, we can assume from the previous result that although the FWHM of the back-to-back signal and that out of the system may be slightly different, this should not have a detrimental effect when we are testing the validity of the system. However, the variance in peak power will still affect the results.

Throughout this chapter a 7GHz low-pass filter has been used in the BER receiver section of the model. The low-pass filter is used to broaden the pulse after the photo-diode but before the BERT. This would usually give a "better" BER (more tolerance to timing irregularities). However, if we compare the BER tolerance to applied phase wander for the back-to-back signal with that of the BER signal out of the system the opposite to what one might expect occurs (we always try and maintain that for both signals the average received power will be the same). There is actually more tolerances to phase wander when the system is not used (clearly this is less than ideal!). The reason for this is simple; it is an artefact of VPI (the simulation tool used throughout this thesis). Even without the use of electrical clock recovery, VPI always tries and measures the BER at the centre of each bit. Because the 7GHz low-pass filter broadens the eye by so much, we obtain an unusually high BER. Although the BER out of the system is also improved, the BER of the back-to-back signal will be better than that out of the system. By removing the aforementioned 7GHz filter the opposite occurs, this is illustrated below.

In the same manner as before the back-to-back signal and that out of the phase wander reduction system are compared. When doing the comparisons the same average received power (at the BERT module) is maintained throughout. This is achieved by starting with a single, constant data source and splitting it into two channels (the same basic model as Figure 4.1) where the two channels power can be independently controlled at the receiver

(as well as $\Delta\tau_{BER}$, the timing control for the two receivers). Firstly we compare the received power as a function of data delay (Figure 4.10).

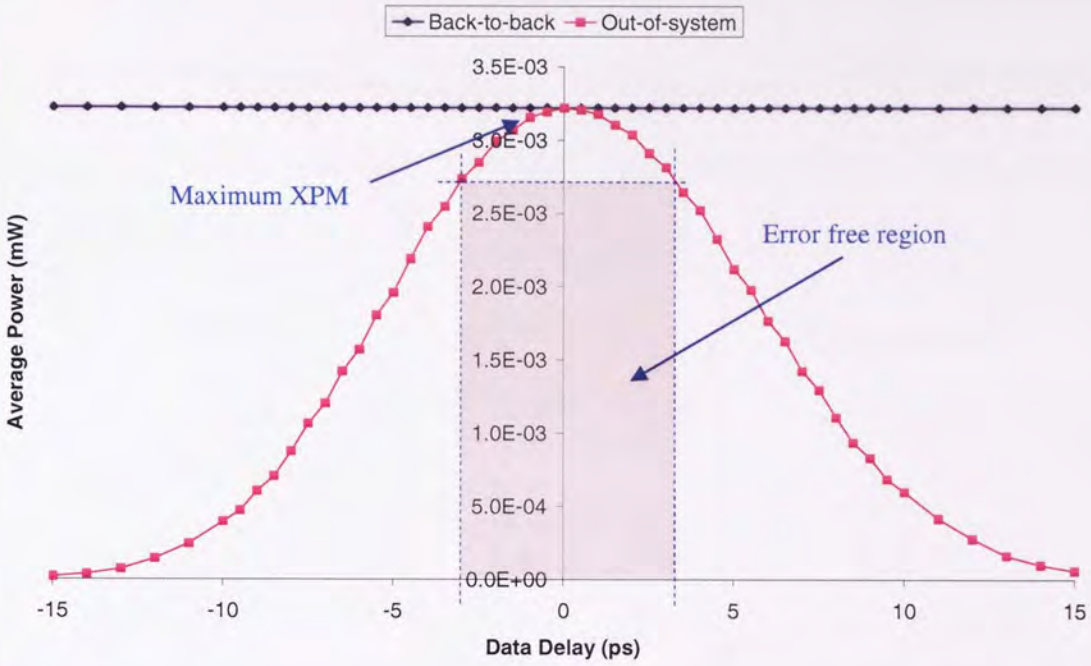

Figure 4.10: As delay, or phase wander, is applied to the data there is a change in received power after propagation through the system

If we look at the back-to-back received average power, we notice that it is constant throughout. This is because although the data is being shifted in time with respect to the BERT, the original data is not affected and so the power never changes. The average received power of the phase wander suppressed signal (after propagation through the system) does however vary with time. Because the loop mirror acts as an optical sampling gate (sampling the chirped clock pulse) the timing displacement of the data with respect to the clock implies that a different portion of the clock is sampled and then re-transmitted. The important thing to notice here is that average received powers of the two channels are

the same when maximum XPM occurs (and that they were both a product of the original data source).

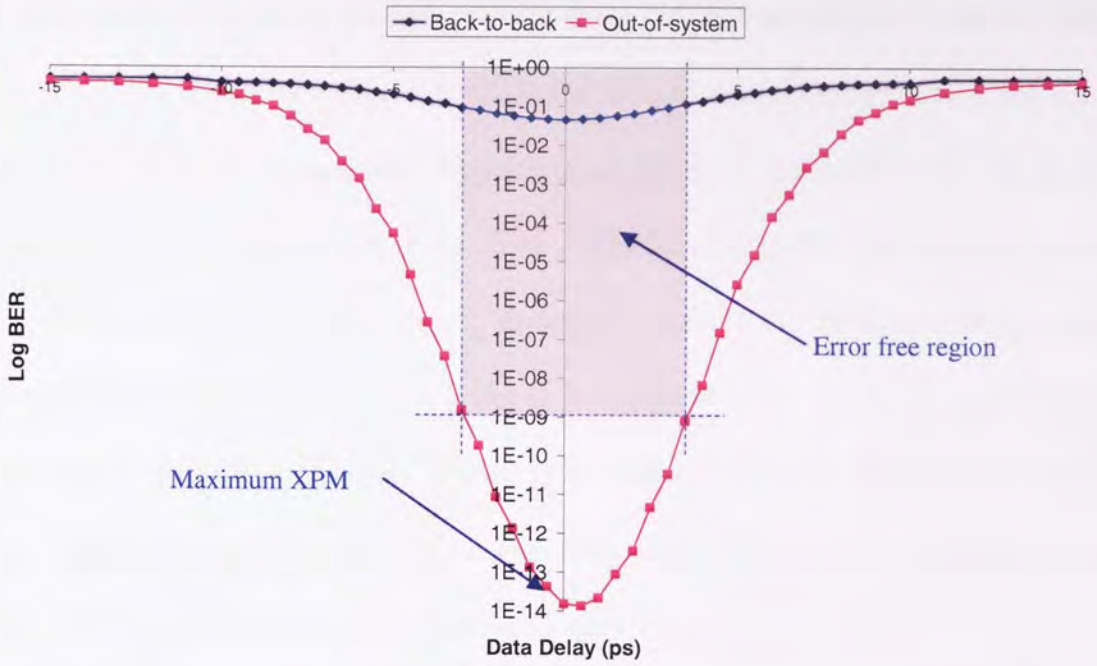

Figure 4.11: The corresponding BER curve (relating to Figure 4.10) shows that the back-to-back signal never reaches error free and that the best error free signal occurs when maximum XPM occurs

At the same time that the received power as a function of timing data, or applied phase wander, was measured, the BER of the two channels was also measured. Remembering that the two average received powers are of the two individual channels are the same, we notice the back-to-back channel never reaches error free (naturally both the BER receivers are identical and have identical settings). However, the channel which propagates through the phase wander reduction scheme does reach error free, in fact, it reaches significantly better than error free (the region for which error free occurs is illustrated on both of the previous two graphs by the shaded region). Thus, our original signal will never be error

free (under these conditions) but after the system, error free is achieved. This is incredibly significant as we have been able to "improve" on the original data signal. As long as after the system the received power is above 2.75×10^{-3}mW (average) the signal is error free. This corresponds to a timing window (where error free is maintained) of approximately 6ps. It is now necessary to see the effect that the level of phase wander, $\Delta\tau_{BER}$, has on the bit-error-rate. This can be evaluated by measuring either the BER or the Q, the latter in this particular case, as a function of received power (note, it is the received power that is changed here not the initial data power, the power entering the NOLM or power of the locally generated clock source). Firstly, the Q is measured when there is no applied phase wander, $\Delta\tau = 0$ps. $\Delta\tau$ is then varied and the Q is measured again as a function of received power. This is measured for both the back-to-back channel, Figure 4.12, and the channel that has been propagated through the system, Figure 4.13.

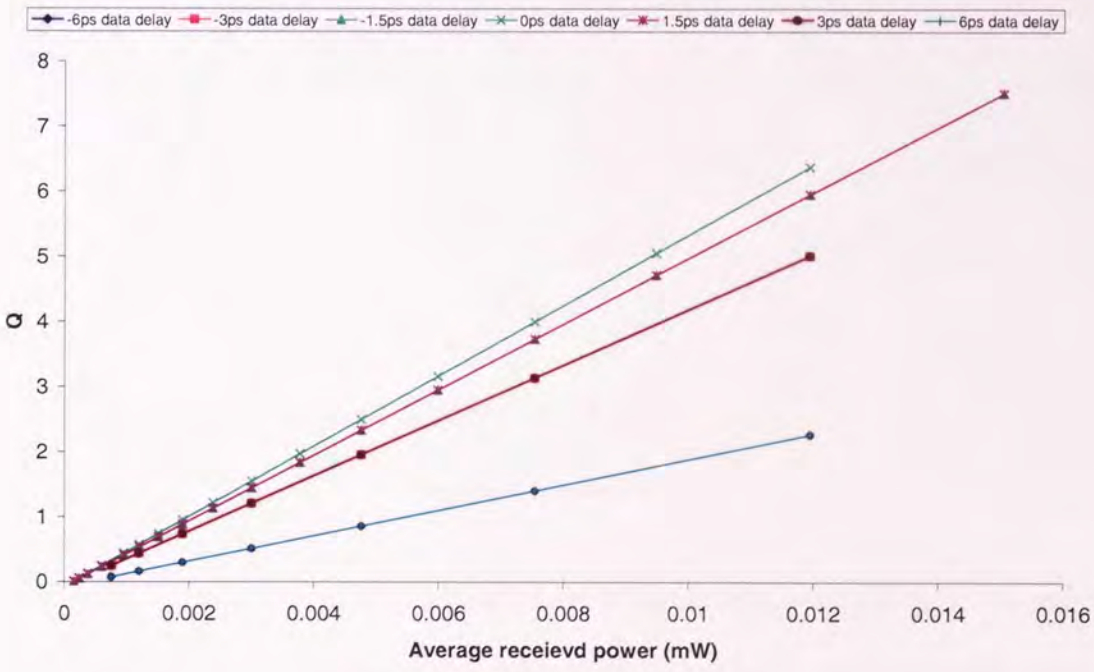

Figure 4.12: The variation of Q as a function of received power with varying degrees of applied phase wander is shown for the back-to-back signal

In Figure 4.11 it was seen that error free operation is never achievable for the back-to-back signal. However, as stated, this statement is only true under certain circumstances. If the received power were to be increased we would find that eventually error free operation would be achieved (the channel is deemed to be error free with a Q of 6 or above). This actually happens with an average received power greater than 0.0119mW (when there is no applied phase wander). As the integrity of the output is never compromised, Figure 4.11 shows us that in theory, an error free signal will always be achievable but at the expense of high received power. We also see that the effect of applied phase wander on the data source is quite large showing that even small amounts of phase wander will degrade the BER significantly.

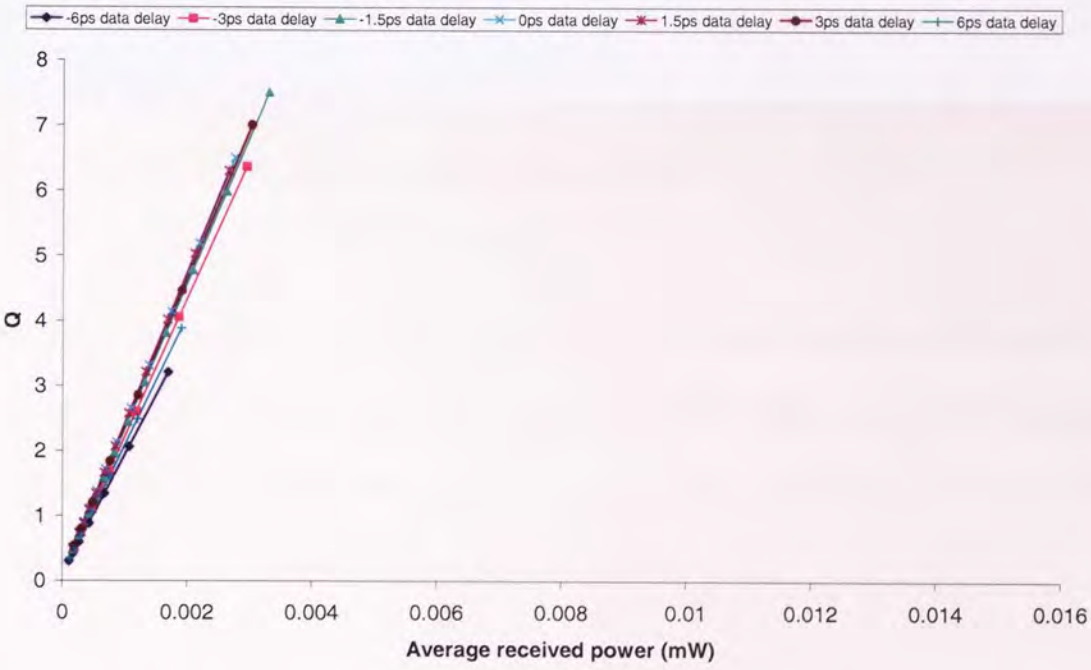

Figure 4.13: The variation of Q as a function of received power with varying degrees of applied phase wander is shown for the channel which has been propagated through the phase wander reduction system

In the same way, the output of the phase wander reduction system is measured. Here we see that the level of received power required to achieve error free operation is much less than before. Now we only require the average received power to be greater than 0.0028mW in order to achieve error free operation (a decrease in received power of 0.0091mW). Another very important feature of this channel is that there is significantly less influence on the BER as phase wander is applied. For lower levels of applied phase wander, between -1.5ps and +1.5ps, there is virtually no effect at all on the BER. This demonstrates that the phase wander reduction system removes some of the detrimental effects associated with the said, applied phase wander. Taking this a step further, although the received power drops slightly, the bigger range of -3ps to +3ps only has a small effect on the BER with extra plots almost falling on top of one another (decrease in received power is due to the profile of the chirped clock pulse. With a more temporally "square" profile, this difference would be eliminated). Thus, propagation through the system improves the BER and tolerance to applied phase wander.

A further example of the limitation of the back-to-back signal Figure 4.14 compared to that after propagation through the system. Whilst the BER is being measured, it is possible to also view the eye diagram that is produced (this is again, without any filtering in the BER section), Figure 4.14 and Figure 4.15 respectively.

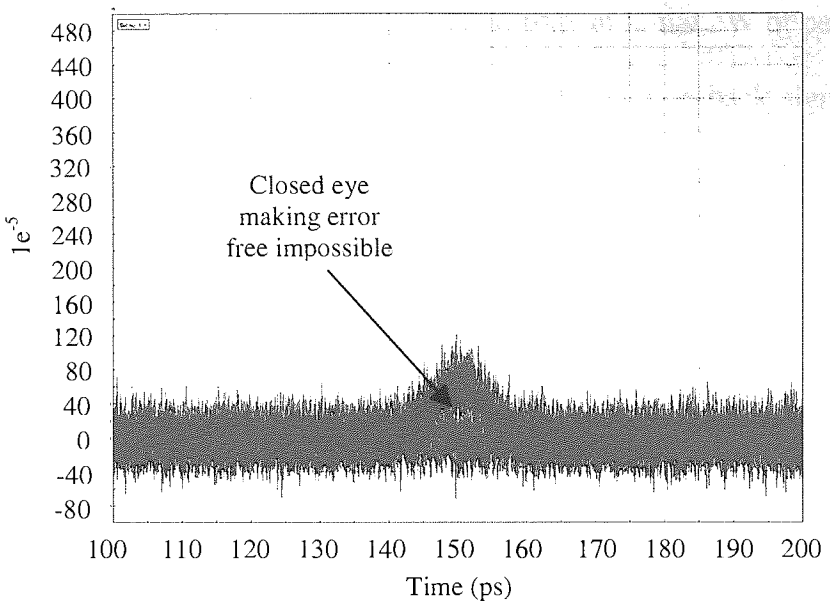

Figure 4.14: Without the 7GHz low-pass filter in the BER receiver section the eye diagram produced is almost completely closed

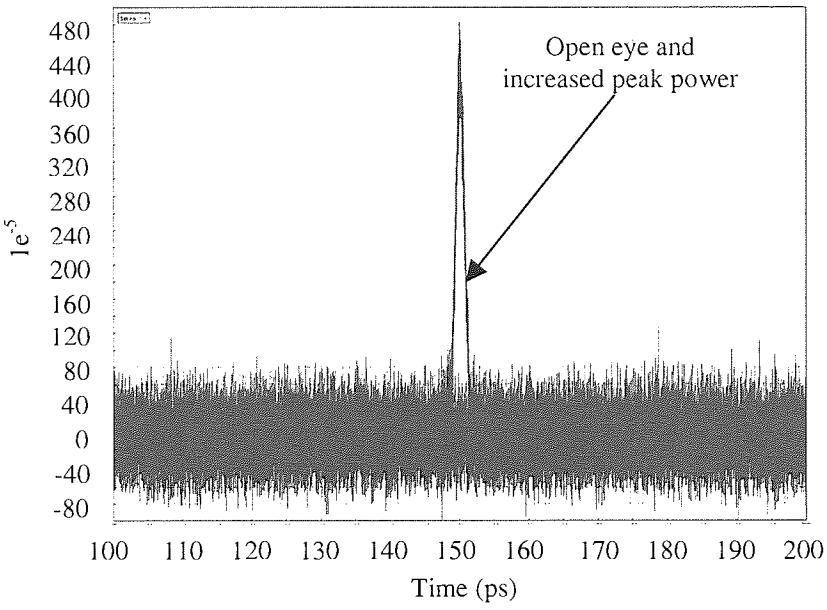

Figure 4.15: After propagation through the phase wander reduction system, the eye is open and the peak power increased significantly

Using the shorted chirped clock pulse (generated from an initial 2W of peak power) as the source we can clearly see why it is impossible for the back-to-back signal to achieve an error free signal. The two eye diagrams shown are for when there is no phase wander on the input data source, $\Delta\tau_{data}$ = 0ps, the point at which the "best" or "most open" eye should be produced. Even with this ideal condition, the back-to-back channel contains high levels of noise, low peak output power and the eye is very closed. The output that is produced when the same data source has been propagated through the system is significantly improved. We see a good open eye (Figure 4.15), all be it a very short eye, which has only a small amount of noise. It is for this reason that we can achieve better than error free operation (where we have defined "error free" as having a bit error rate of 10^{-9}) but only for a small amount of phase wander, a total of 6ps can be compensated for).

By adding a 7GHz filter to the BER section (this can be done either during the simulation by actually adding a component to the model, as before, or by applying a filter post simulation, this case) we see that the two eye diagrams that are produced, again with no phase wander added to the data source, are almost identical (Figure 4.16 and Figure 4.17 respectively).

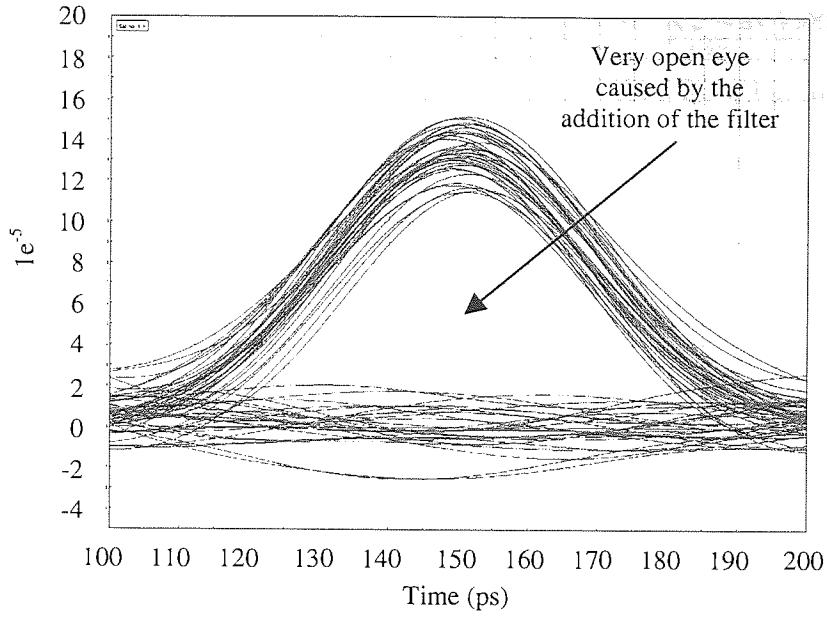

Figure 4.16: By adding the 7GHz filter to the BERT, the back-to-back channel the eye is dramatically opened

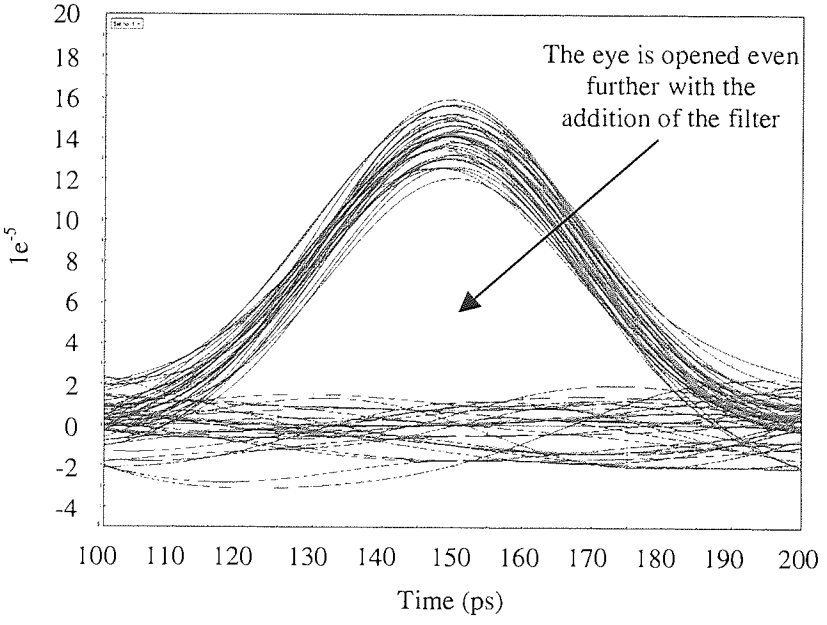

Figure 4.17: The eye produced after propagation through the system is almost identical to that of the back-to-back channel

The peak power of the original, locally generated clock source was then increased to 5W (previously the peak power of the clock was 2W) whilst all other parameters remain constant. After propagation through the 2.2km of nonlinear fibre the clock changes both in temporal profile and increases in duration (as discussed in previous chapters). The now new chirped clock source has a FWHM of 51.43ps (with 2W of peak power the chirped clock produced had a FWHM of 33.46ps), an increase of 17.97ps. The increase in FWHM should mean that if we maintain the same average received power as that used in Figure 4.11, we should find that there will be a greater region of error free operation. Thus, to test this hypothesis, phase wander was applied to the data, with the new broader chirped clock and both the average received power and BER measured (see Figure 4.18).

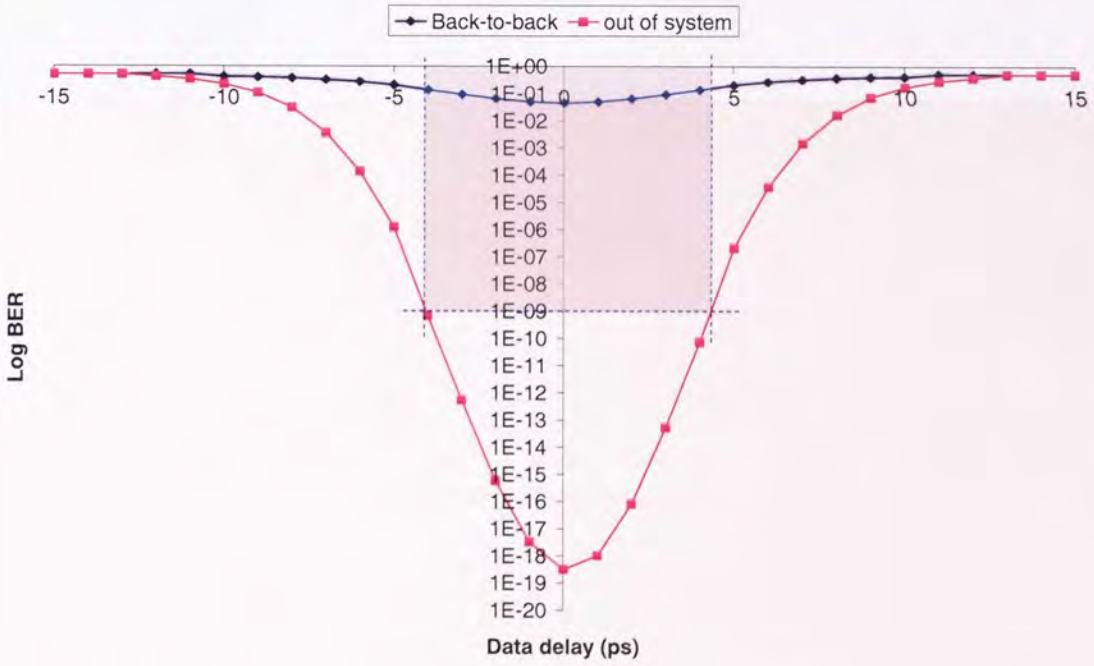

Figure 4.18: As phase wander is applied to the data source, the BER is measured for both the back-to-back channel and as well as the channel which is propagated through the system

As suspected, the increase in chirped pulse duration does increase the error free timing window (illustrated by the grey shaded box). We now find that there is an 8ps window for which the system is error free (note, we can make the same comparisons as before with the back-to-back channel as chirped clock duration has no effect on the back-to-back signal at all). As before, we can now measure the Q for the system as a function of received power (in the same was as before, only the power at the receiver is varied and all of the other parameters remain constant) for several different levels of applied phase wander, Figure 4.19.

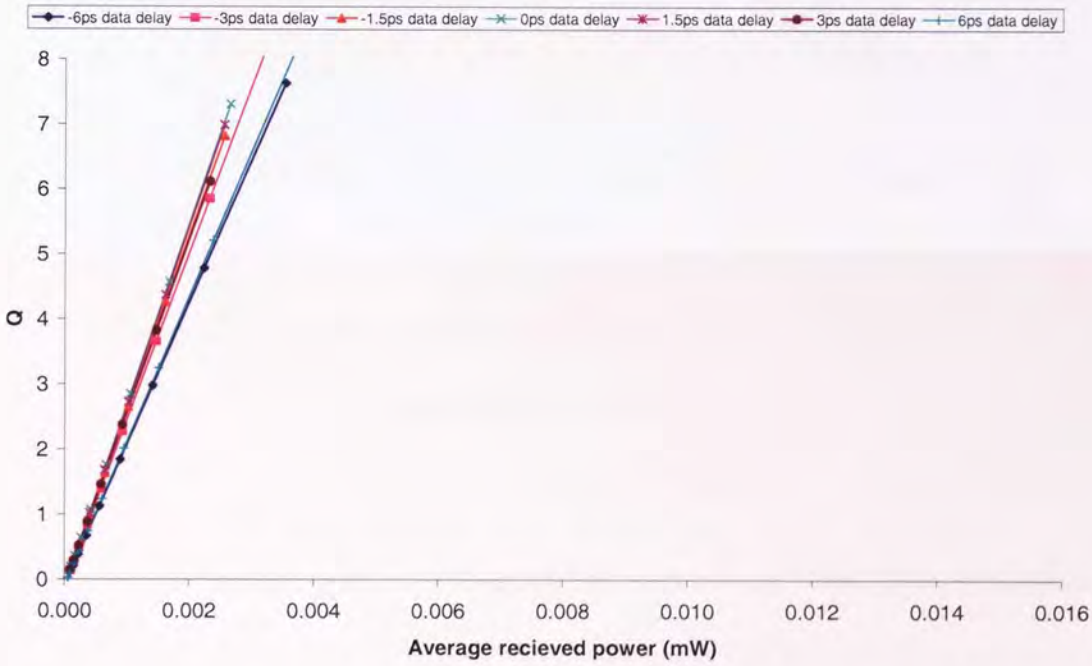

Figure 4.19: The variation of Q as a function of received power for an increased chirped clock duration for the channel propagated through the phase wander reduction system

In Figure 4.18 the increase in the FWHM of the chirped clock pulse increases the error free timing window. Taking this a step further, the increase in clock duration means that the BER produced is less sensitive to a variation in phase wander. From this we can

assume that if the chirped clock duration was to be increased even further, the system would become yet more tolerant to phase wander (assuming that the chirped clock pulse is not so big that it overlaps with the next adjacent pulse).

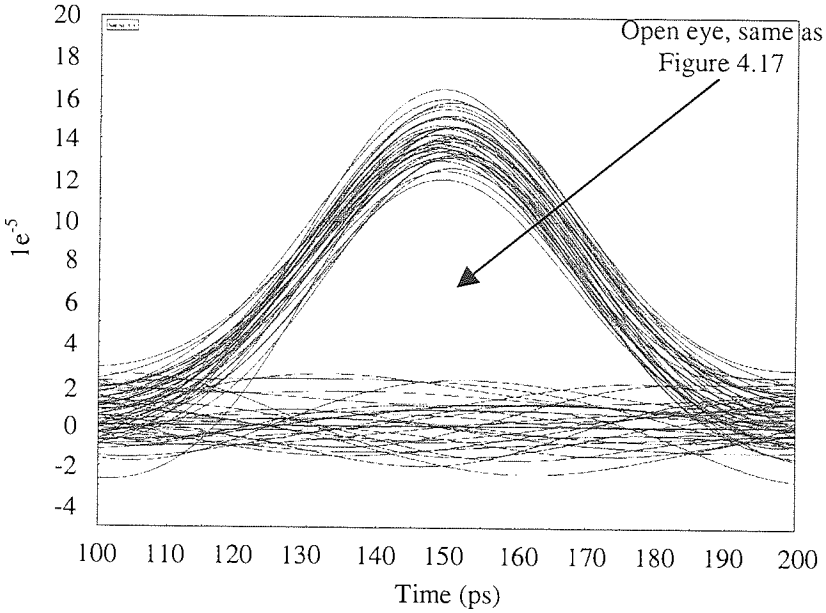

Figure 4.20: Increasing the chirped cock duration has no effect on the open eye when it is broadened by a 7GHz filter

As a comparison, looking at the eye diagram that is produced when there is the broader chirped clock pulse (and with the inclusion of the 7GHz low-pass filter) we see that the there is little or no difference compared with the previous, shorter chirped clock source. This is due to the effects of the 7GHz low-pass filter.

4.4 Error free operation using the 3R regenerator

Although it has been shown that the phase wander reduction scheme can operate error free and in fact improve the quality of the signal whilst increasing the tolerance to timing irregularities, the 3R regenerator from section 3.6 has not yet been tested for error free operation. It is important at this stage to show that the 3R regenerator can operate error free as otherwise there would have been little point in demonstrating its functionality. Thus, we firstly look at the tolerance to phase wander (in the same way in which the single stage phase wander reduction scheme was tested. Remember that this device is different from before in that it actually has 2, almost identical stages to the device. Stage 1 corrects for the applied timing irregularities using wavelength conversion before stage 2 converts the signal back into the original wavelength). Phase wander was applied to the data source and the received power and BER measured for both the back-to-back channel and the channel propagated through the phase wander reduction scheme. The results are shown in Figure 4.21.

(Note, whilst testing the 3R regenerator, the data source used had a FWHM of 10ps, this is different to previous BER simulations where the data source had a FWHM of 3ps. It should also be noted that the 7GHz low-pass filter was turned off throughout the 3R regenerator BER testing).

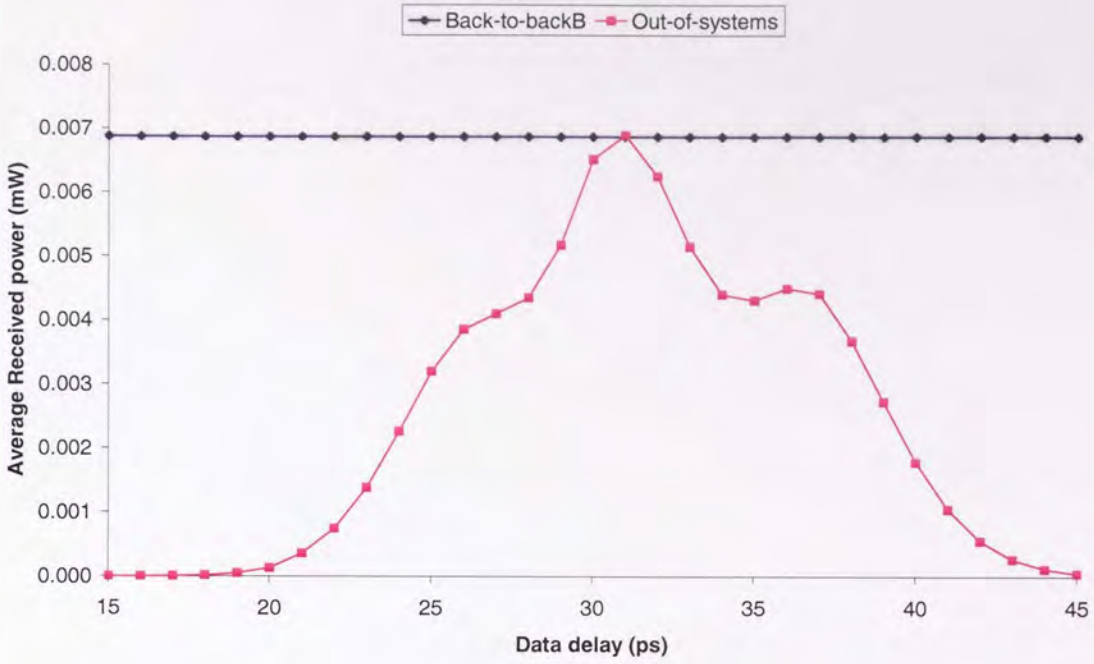

Figure 4.21: The non-square temporal profile is an artefact of the second stage to the device. This could be improved by varying the profile of the second chirped clock

For the back-to-back signal, the received power remains constant no matter how much phase wander is applied to the data source. The result is consistent with previous observations where this has occurred. This is because applying phase wander simply shifts the data in time (with respect to the clock or any other fixed timing point) only. If we now look at the received power after propagation through the 3R regenerator (which therefore has the same wavelength as the original data input) we see that the there is a clear maximum when there is no applied phase wander to the data source, $\Delta\tau_{data} = 0$ps, and then a drop in received power. The drop in received power is reflected in a corresponding drop in measured Q for the same level of applied phase wander.

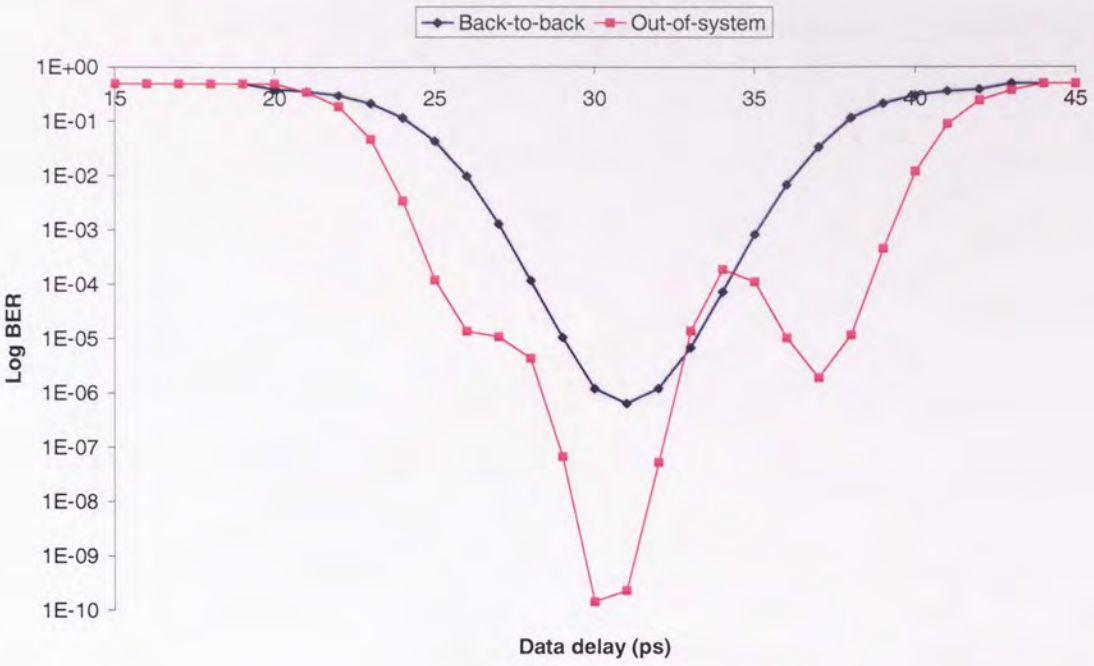

Figure 4.22: Measuring the BER as a function of timing delay reveals that the second stage affects the results

The Q is now measured as a function of received power, again, this is repeated with varying amounts of phase wander applied to the original, 10ps data source. A further comparison with the back-to-back channel is included because of the change in FWHM of the data source (an increase to 10ps from the 3ps used for the single stage simulations).

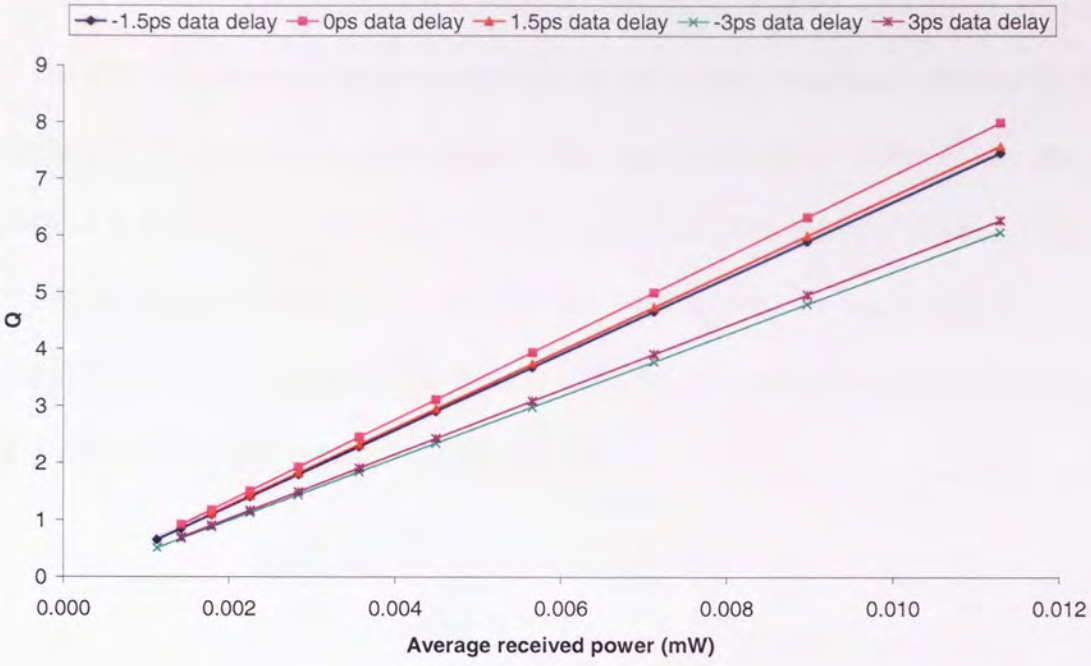

Figure 4.23: The BER of the back-to-back signal is shown as a function of received power

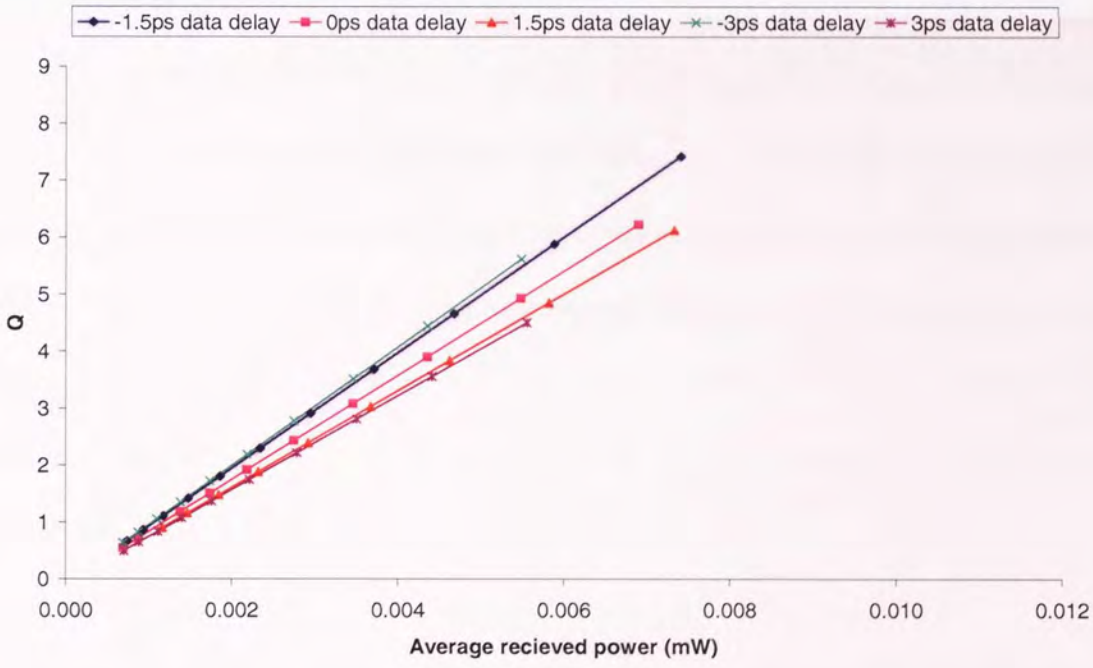

Figure 4.24: After 3R regeneration, the data is now at the original wavelength and error free operation is obtainable

Figure 4.24 reveals that less average received power is required to achieve error-free operation when the data is propagated through the 3R system, compared with the back-to-back channel (it should be noted again, that the "new" data produced by the 3R regenerator is at the same wavelength as the original data). The effect of the phase wander on the BER curve is also reduced because the BER curves are more tightly grouped together. From this we can imply that there is an increase in tolerance to phase wander (in much the same way as the single stage system did).

4.5 Dependency of BER on time window and resolution

It is important to realise that in the previous sections of this chapter, when we use VPI to calculate the Q of a system, or in fact the BER of a system (the BER is inferred from the calculated Q value), the importance that the global parameters have on the obtained results. Although the global parameters will effect such results as the average output power of channel (both back-to-back and out of either the single or dual stage system) the greatest discrepancy will be in the measurement of the Q. This variation is shown in Figure 4.25 where the dual stage 3R regenerator is used. The "time window" of the simulation is varied from 0.8ns to 102.4ns whilst all local parameters of the simulation remain constant.

The first point to make when looking at the following results is that we are unable to measure the Q when the time window is below 400ps. This is because VPI only uses one symbol to try and estimate the Q and BER and so fails to produce a result (because we are using a PRBS code word, in this case, only one bit is generated. Thus, it is possible in

other simulations that more than one bit could be generated and so a result could be obtained). As the time window increases, VPI uses more and more symbols to calculate the Q and BER and so hence, the accuracy of the approximation increases. We also see that doubling the time window has a dramatic effect on the Q initially, when the time window is relatively small, but conversely, has little effect when the time window is greater than 24ns.

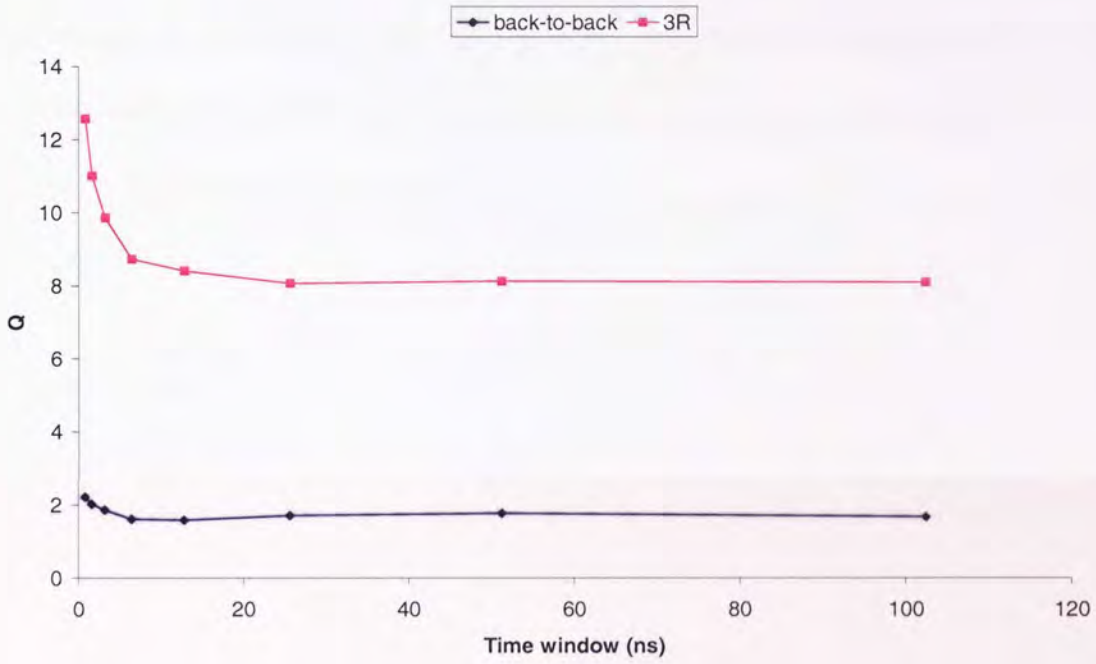

Figure 4.25: As the time window of a simulation is increased, the calculated Q changes giving a more "accurate" result

Although the size of the simulation time window may seem critical when trying to obtain "accurate" results, throughout this thesis this is not really critical. All of the simulations in this thesis are merely used to show trends and so for this reason, this issue is not a problem. It is also important to note that whenever two channels, the back-to-back and the out-of-system, are compared, in all cases the global parameters remained constant. By

ensuring this level of consistency we can always compare two channels whilst maintaining the integrity of the simulation.

However, when the simulation time is increased, we need to be aware that we actually have enough "samples" in the simulation to cope with the bigger time window. Because the amount of samples is always fixed, it is important that we start with enough that if the timing window is increased, it won't be a problem. If there are not enough samples in the simulation, erroneous results will be obtained and the integrity of the pulses will break down, this is illustrated in Figure 4.26.

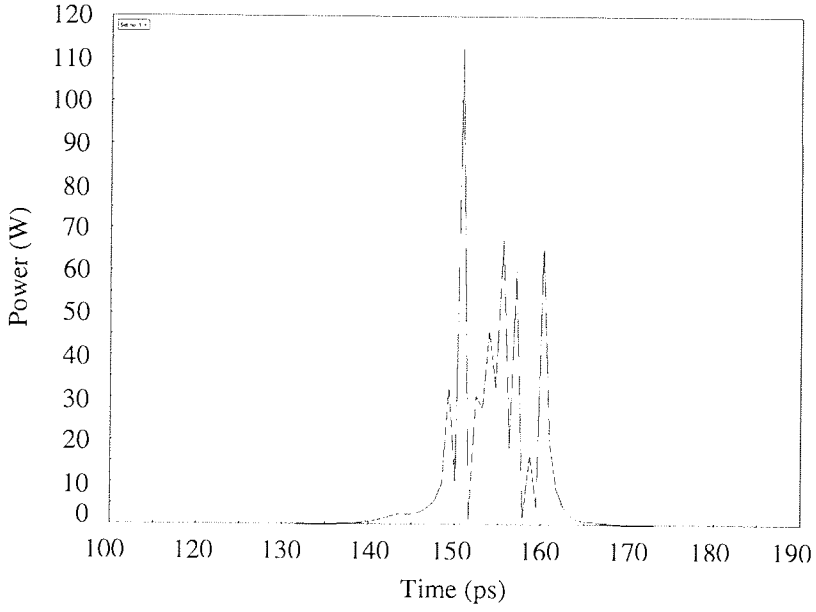

Figure 4.26: If the simulation has too few samples then the temporal profile of the clock is changed and the measured Q will be effected dramatically

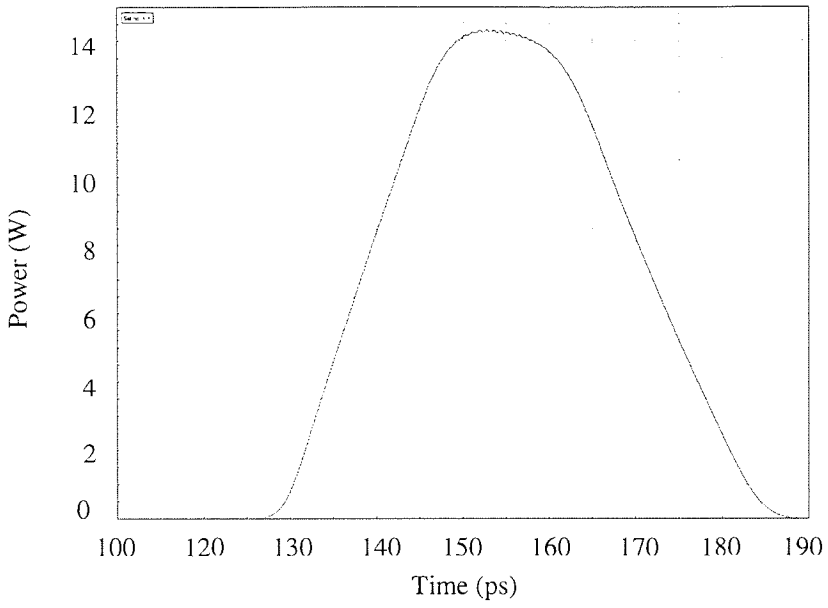

Figure 4.27: By ensuring that the simulation has enough samples, the clock's temporal profile is maintained

In Figure 4.26, the temporal profile of the chirped clock changes. We are always trying to strive for a temporally square profile, this is clearly not obtained here. If the amount of samples used is increased, Figure 4.27, we obtain the chirped clock profile that we would have expected, given the input parameters. This change is also reflected in the measured Q. When there are too few samples Figure 4.26, the measured Q out of the single stage device is 2.82 where as when there are more samples taken Figure 4.27, the Q is measured at 12.57. This illustrates the need for ensuring that enough samples are used in the simulations.

4.6 Discussion

The primary function of this chapter was to try and demonstrate that within the confines of the VPI simulation tool, error free operation (error free was defined as 1 in 10^9 errors or better) can be achieved using the previously discussed timing jitter and phase wander reduction scheme. Prior to this chapter, both the functionality and the principle of operation had been discussed, however, we still needed to demonstrate that under certain conditions error free operation could be achieved. Thus, simultaneously phase wander is reduced (in exactly the same manner as earlier chapters) whilst maintaining error free operation.

A large degree of care needs to be taken when using the simulation tool to evaluate bit-error-rates. It is vital that enough samples are taken in order to achieve an "accurate" measurement. However, the simulation time increases as the amount of samples increases and so we quickly arrive at a stage where the simulation is simply unmanageable and impractical because of the length of actual time the simulation will take. It is for this reason alone that certain compromises were taken when obtaining the BER results. Because the simulations are simply used to prove the principle and the exact numbers produced are not relevant, this does not affect the usefulness of this chapter. However, it should be noted that whenever two results have been directly compared, the simulation parameters for both sets of results were the exactly the same (for example the amount of samples or size of timing window). This enables us to directly and accurately compare results.

The initial goal of this chapter has been successfully achieved. It was shown that the "simple" single stage timing jitter and phase wander reduction system could operate error

free whist compensating for applied timing irregularities (phase wander. Although previously it may have seemed that relatively large amounts of phase wander could be compensated for, here it has been shown that the tolerance to the effect of phase wander is smaller than one might have expected. There is little or no point implementing a system that can not operate error free, so this test is vital and shows us the true level of useful phase wander that can be compensated for. Under the conditions outlined in this chapter a maximum of 8ps of phase wander could be corrected for whilst satisfying the error free criteria. It was also shown how the FWHM of the locally generated chirped clock source effectively determines the level of phase wander that can be compensated for. Thus, increasing the FWHM of the clock further would increase the error free timing window further. It was also shown that the temporal profile of the chirped clock has an effect on the BER as well. This is simply because the profile of the clock determines the average output power that will be received at the BERT, which in turn determines the BER that is measured. It was finally shown that by propagating the data channel through the phase wander reduction system the BER curves are very similar when there is only a small amount of phase wander (with an increase in chirped clock duration this level would also increase). This is an important improvement over the back-to-back channel (not propagated through the system) again, demonstration the advantage of using the said, phase wander reduction system in the first place.

Although it had been shown that the single stage phase wander reduction system could operate error free, it was still necessary to repeat the same measurements using the more complicated 2-stage, 3R regenerator. Thus, through BER measurements (simulations) we were able to show that the 3R regenerator could also compensate for applied phase wander

whilst maintaining error free and importantly (for this device) maintain the wavelength of the original incoming data.

It should also be mentioned here that all of the BER measurements that have been calculated in this chapter are of course subject to the receiver settings that were used. One can argue that the exact settings are irrelevant and that provided that the settings are consistent throughout all of the simulations (which is the case in all of this thesis) there is no problem. By changing say the sensitivity of the photodiode in the receiver we would no doubt have been able to increase the error free timing window available for both the one and two stage device. However, this would have also improved the results obtained from the back-to-back channel and so there would have been no net increase in performance for the two comparisons. Thus, for this reason at the start of this chapter parameters were chosen and they have remained constant throughout.

The effects of changing some global parameters were also examined in this chapter. It was shown that care needs to be taken when deciding how big the simulation time window should be. By increasing the simulation time window more samples can be used to calculate the Q and in turn the BER of a specific channel giving us a more "accurate" result. However, simulation run-time increases linearly and we easily find simulations taking an unmanageable amount of time. One also needs to consider the amount of samples taken as well. It is imperative that there are sufficient samples in the simulation to accommodate for the chosen time window.

Throughout the simulation chapters of this thesis there has been the problem of not being able to simulate timing jitter and this chapter suffers from the same problem. Because of

this limitation, it was not possible to measure the BER with respect to applied timing jitter. However, it is important to remember that this is a limitation of the simulation tool used, not the principles being tested.

Chapter 5 - Laboratory experiments

5.1 Introduction

Until this juncture in the thesis, the results have been largely based on either numerical modelling techniques or achieved using computer simulations. In the following chapter the author will demonstrate, in a purely laboratory environment, some of the principles of the proceeding chapters. It is vitally important to show that both the previously discussed "principle of operation" actually physically works and that we confirm the validity of some of the techniques that have been discovered and tested with the use of computer simulations. It will also be shown that the timing jitter/phase wander reduction system can be fabricated inside the laboratory whilst simultaneously operating error free.

Chapter 5 starts by constructing the all-optical timing jitter and phase wander reduction scheme in the laboratory. The basic experiment is based on the simulations from chapter 3 and the experimental set-up mirrors that of Figure 3.7. We will then explore what happens when with different sources operating at different repetition rates (this differs for the simulation sections of the thesis where all of the sources used are ideal and perfect) before finally moving onto full 3R regeneration (this technique was proved to be viable in section 3.7). All of the principles used within this section have been previously discussed and demonstrated in the preceding simulation chapters. The same "principle of operation" applies, the data undergoes dynamic wavelength conversion by optically sampling a linearly chirped clock pulse (where a wavelength is assigned depending on the relative timing displacement between the data and the clock). The new data is then propagated

through a dispersion compensation module (in this case SMF) where an appropriate level of dispersion is applied and the timing irregularity is removed.

A full investigation into the characterisation of the NOLM and a more detailed analysis of the chirp generation principles are contained within a Masters thesis [104]. The laboratory results in this section assume the characterisations found within the Masters thesis.

5.2 All-optical jitter suppression using one GS-DFB and one actively mode locked fibre laser

In the following section a GS-DFB was used as the "data" source for the experiment. The laser had a central wavelength of 1553nm and an actively mode locked laser operating 1538nm was used as the clock source. The clock source was then propagated through the 2.2km of nonlinear fibre (this is the Sumitomo nonlinear fibre that some of the simulations were based upon, the parameters of which can be found in Appendix C) to generate the chirped clock pulse. As previously discussed (section 2.2) we can control the parameters of the chirped clock pulse by careful control of the input power and pulse duration (in the following instances the fibre length and properties will not be changed, as they were in some of the simulations, and the initial pulse duration will also be kept constant). The actively mode locked laser provided a short, Gaussian pulse of <4ps FWHM which was used for the chirp generation (because of the high peak power that the short pulse duration provides). The clock pulse was then amplified by means of an EDFA and then optical filtered using a tuneable FBG filter (it is important to remove the ASE from the EDFA

before propagation through the nonlinear fibre) and was then propagated through the said nonlinear fibre. Due to the effects of SPM (as discussed in chapter 1) this arrangement will produce the required nominally square, linearly chirped clock pulse.

In order for jitter suppression and phase wander reduction to occur, we firstly need to know how to compress the clock pulse down to as short a duration as possible (as this will determine the minimum amount of jitter that will be produced at the end of the system). Because the chirped pulse was generated in the normal regime (chapter 1) pulse compression will occur after propagation through standard fibre, SMF (it is important to realise that if the chirp had the opposite sign, i.e. was anomalous, then propagation through DCF would have the same result, pulse compression). As pulse compression needs to occur at the end of the system, the now chirped clock pulse (as it has already propagated through the 2.2km of Sumitomo nonlinear fibre) is propagated through the NOLM (which is biased to transmission. The bias of the NOLM is achieved by manipulating the polarisation controllers so that a maximum output power occurs at the transmission arm of the NOLM) and then through changing lengths of SMF. The basic experimental arrangement is shown in Figure 5.1.

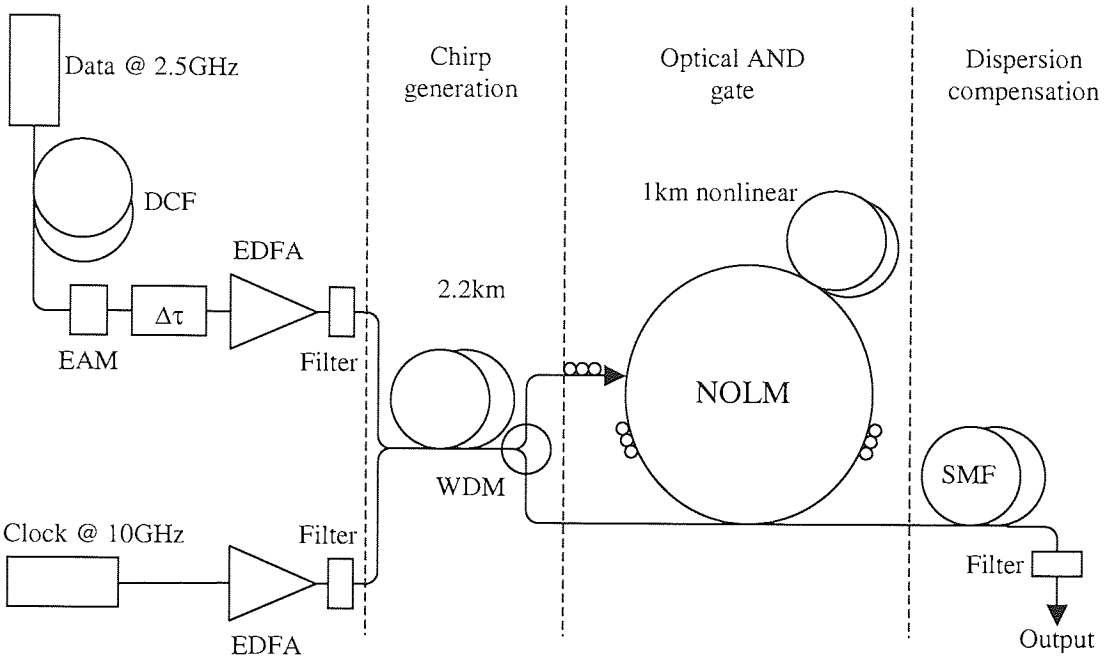

Figure 5.1: schematic of the timing jitter/phase wander reduction scheme utilising a nonlinear loop mirror which is used to perform the "and gate" function

At this point there is no need to actually have any "data" present in the NOLM, it has been included in the previous schematic just for completeness. The optical filters (used to filter off either ASE, if placed after an EDFA, or used to filter off any unwanted channels) are left in the system just ensure that they don't have any adverse effects on the results. A graph of the results was produced (Figure 5.2).

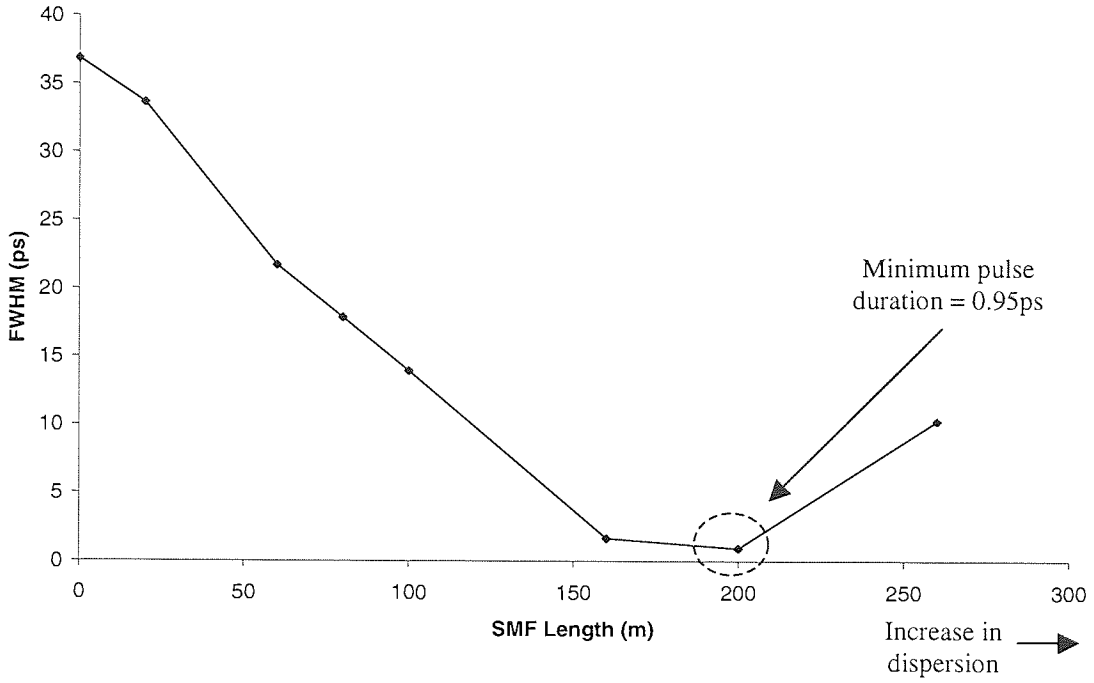

Figure 5.2: By changing the length of SMF we effectively change the level of dispersion compensation and therefore can find the minimum obtainable pulse duration

As one would expect, as we add more dispersion (which has the opposite sign to that of the chirped pulse), the output pulse duration approaches a minimum and then broadens again. This shows that with an SMF length of 200m we are able to obtain a minimum pulse duration of 0.95ps.

The GS-DFB, used as the data source, was nominally tuneable (it is possible to control the wavelength that is produced from the GS-DFB by simultaneously manipulating both the drive current of the device and its operating temperature). The actual wavelength of the data source is not particularly important so long as it is sufficiently higher in wavelength than the chirped clock pulse and is kept constant throughout the experiment. For this particular case the GS-DFB was set to have a wavelength of 1553nm. "Data" was applied to the GS-DFB by propagation through an electro-absorption modulator, EAM, which was

connected to a pattern generator (we are able to control the pattern placed on the pattern generator and therefore the pattern of the EAM and on the subsequent produced data).

It is important to note at this point that as the total fibre length of the overall system has now reached in excess of 3km (2.2 km of fibre was used for the chirped pulse generation and an additional 1km for the nonlinear fibre was used in the NOLM, which provided the nonlinear element to the device. As well, we have to remember that there are also further lengths of SMF used for dispersion compensation. Finally we should also note that we have short lengths of SMF which are used as patch cords). Because of this, the system has become inherently unstable. Due to the ambient temperature surrounding the system randomly fluctuating the fibre either expands (as the temperature increases) or contracts (as the temperature decreases) thus, we have a constantly changing overall propagation length (this is also known as extrinsic fluctuations). The extent of the problem is illustrated in Figure 5.3 where a sampling oscilloscope has been allowed to capture 1,000,000 samples (which equates to a capture time of ~30seconds). The output is taken out of the transmission arm of the NOLM and the NOLM is biased so that the chirped clock pulse it as at a maximum output power (no data was applied to the system).

It is clear from the temporal profile shown on the sampling oscilloscope that this random "drift" is clearly going to be a problem. The problem will become most apparent when trying to take BER measurements. Problems will also be encountered when trying to actually measure the output timing jitter or applied phase wander of the system, as the relative timing position of the output is constantly changing. It is possible to apply some thermal shielding to the long lengths of fibre involved, however, even a small change in

temperature (<1°C) will cause significant variations in temporal displacement and complete removable of this problem is not feasible by this method.

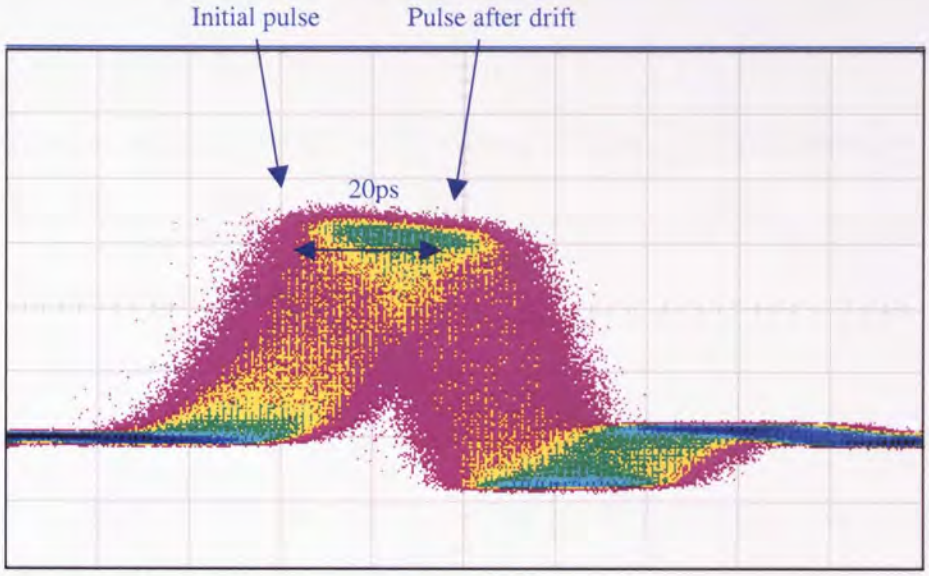

Figure 5.3: The extent of the temporal drift can be seen. 1,000,000 samples were taken over a period of approximately 30seconds, a temporal drift of more than 20ps is produced

The problem of drift at the output of the system can however be eliminated by the use of an electrical "clock-recovery" unit. The optical output of the system is converted into an electrical signal by means of a lightwave converter or photo-detector. This electrical signal is then passed into the clock recovery circuit (the one used throughout this thesis was an Agilent 83491A "plug in" which is a module that plugs into the front of the sampling oscilloscope). Because the operating frequency of the clock recovery unit is 2.488GHz, the GS-DFB and the EAM had to be matched exactly to this frequency. The clock source then had to be operated at exactly 4 times this frequency, 9.952GHz. This device therefore completely removes the temporal drift caused by temperature fluctuations which were seen at the output of the system illustrated in Figure 5.3. The temporal drift caused by the

extrinsic fluctuation (the change in ambient temperature) is of course phase wander (one of the timing anomalies that the system is designed to compensate for). However, by using an external clock recovery unit we can separate and remove the phase wander from the timing jitter and so we are able to analyse the system with just timing jitter applied. Another consideration is that we cannot control the level of this phase wander, making it difficult to do a systematic analysis of the system (in section 5.5 an alternative method of applying phase wander to the data that can be controlled is shown. This enables us to apply varying amounts of phase wander).

It should be noted here that at this point timing jitter is not actually manually applied to the data source, instead, when we look at just the output of the source we see that timing jitter is present (Figure 5.4). This means that this level is not directly controllable and so this is used as a simple test to verify the principle of operation.

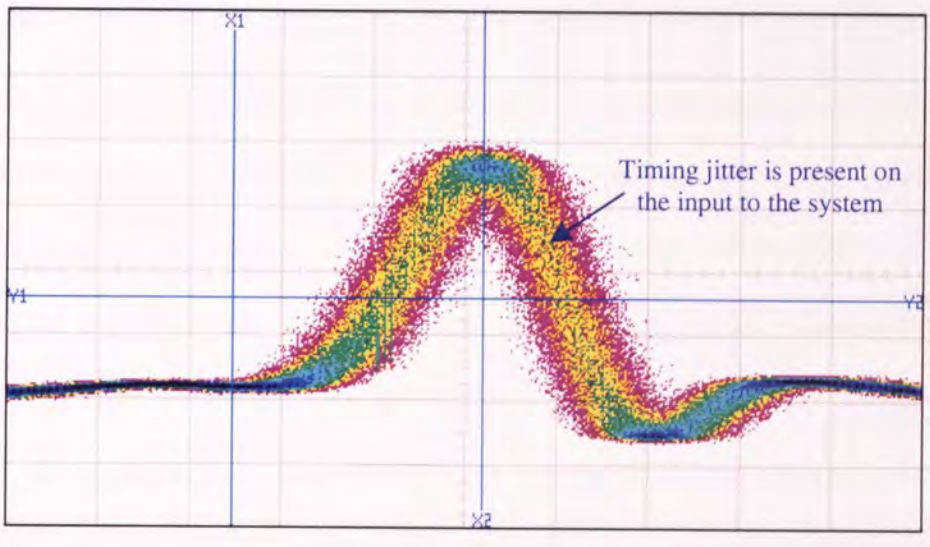

Figure 5.4: A relatively small amount of timing jitter (2.20ps) is seen at the input system

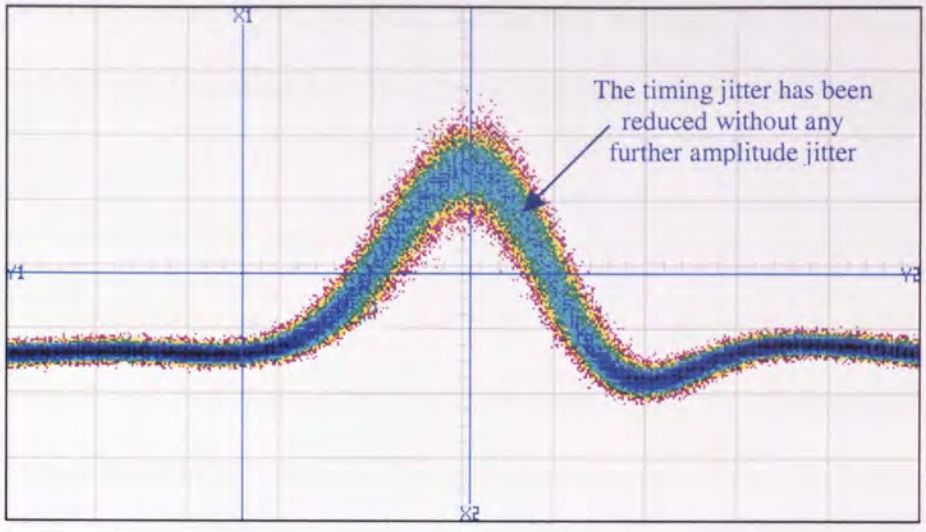

Figure 5.5: After propagation through the system the timing jitter has been reduced to 1.20ps. The temporal drift has been reduced by use of an external electrical clock recovery unit

By looking at the output of the system, Figure 5.5, we see that the timing jitter has been slightly reduced and the signal improved. This, we have now demonstrated experimentally that the system can successfully reduce small amounts of timing jitter. However, this cannot be assumed to be a "useable" system without first validating the results by looking at some BER measurements. In order to obtain the required BER results the output of the aforementioned clock recovery unit is connected directly to the BERT. It should be pointed out at this stage that because we are using both the clock recovery unit and the GS-DFB, the BER measured will be at 2.488Gbit/s (the base rate of the GS-DFB). However, we should also remember that the locally generated chirped clock pulse is operating at 9.952GHz, which is the actual speed that the scheme is operating at. This will not effect the BER's as the data will simply sample every fourth chirped clock pulse. Thus, the final BER measurement at the end of the system will actually be at 2.488Gbt/s

(the reason for the mismatch in operating frequencies is simply one of convenience. The GS-DFB and the ring laser used both have fixed data rates which cannot be altered).

In order to demonstrate the effectiveness of the scheme, we can measure the BER as a function of timing delay, $\Delta\tau$. We can define $\Delta\tau$ as the relative timing displacement of incoming data stream with respect to the chirped clock pulse. $\Delta\tau$ is controlled by varying the optical delay line, thereby shifting the relative timing position of the data with respect to the clock This is equivalent to manually adding phase wander to the system, where the entire word is shifted by the same amount, showing the tolerance to this problem (rather than timing jitter where the displacement is at a bit-by-bit level). The range of "error free operation" will help us determine the maximum timing range that can be compensated for ("error free" is dependant on how long the BER is measured for. Throughout this thesis we assume that the system is error free at $1x10^{-9}$, one error in every 10^9 bits. Error free could of course be defined over a longer period of time, in this case error free will be $1x10^{-10}$ or lower).

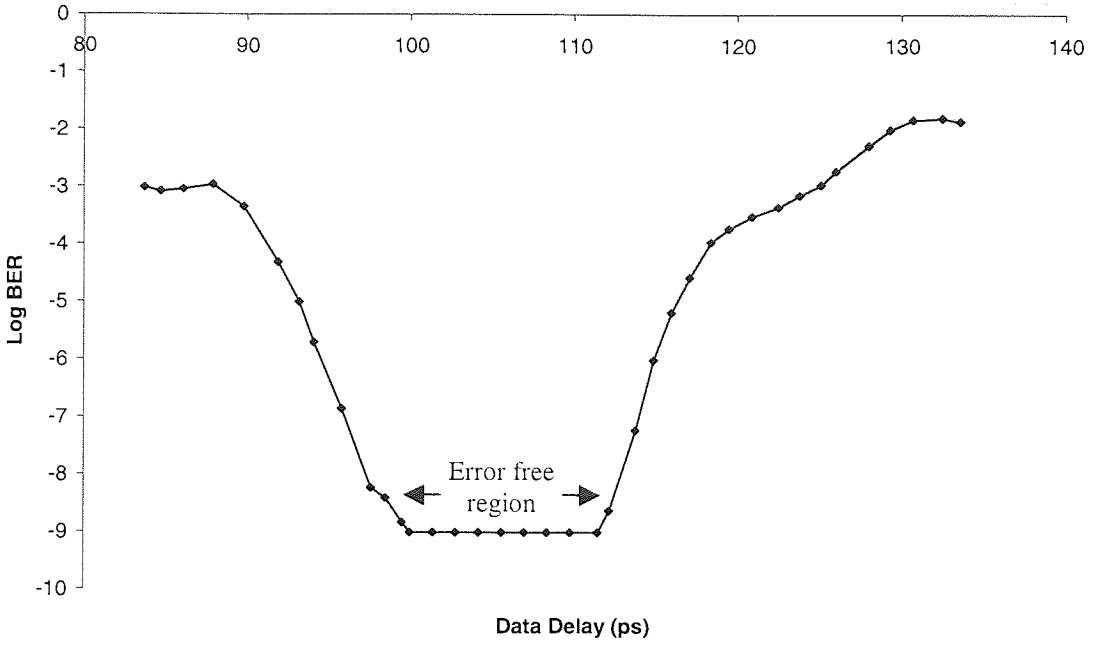

Figure 5.6: As we sweep through the bit period, as the data "samples" the chirped clock pulse error free operation can be obtained

We now move $\Delta\tau$ through 100ps, the bit period of the 10GHz chirped clock pulse (note, the BER for the entire bit period is not shown in the above figure. Outside the 60ps region shown, we would see that the system contains nearly all errors). From Figure 5.6 we see that there is approximately 12ps of error free operation, which determines the timing window of this device for the particular configuration used. If we assume that the data source used to obtain this result is free from timing jitter (clearly there will always be timing jitter in any source which can be seen in Figure 5.4, but we will assume that is negligible in this particular case) and this scheme were to be used as a pre-receiver at the end of a transmission link, a timing window of 12ps would mean that there would be 12ps of tolerance to such effects as temporal drift and phase wander. It is important to remember that the shape of the graph, and therefore the region of error free operation, is dependant on the receiver sensitivity how much optical power it receives. If the overall

output power of the system was increased, one would expect the overall region of error free operation to also increase. This will scale linearly until increasing the receiver sensitivity will have no effect and on the timing window. At this point we have the maximum timing window and can infer the exact temporal profile of the chirped pulse.

We now need to know how the BER of the system varies as a function of the received power (this being the power received after the system, at the BERT). In order to achieve this, we must firstly measure the back-to-back BER (the back-to-back measurement is a direct measurement of the data source straight into the receiver via the clock recovery unit, which is used in order to maintain consistency when comparing to the results after the jitter reduction system). The back-to-back signal was then measured directly after the EAM, by varying the input power to the receiver with an optical attenuator. One would assume that this should produce a linear result and is shown in Figure 5.7. If we now go back to the jitter reduction scheme we firstly need to set $\Delta\tau$ so that we sample the chirped pulse at the centre of the timing window (the centre of the timing window shown in Figure 5.6). This will ensure that we obtain the best possible BER result, with the most tolerance to timing irregularities. The received power is varied at the receiver and the BER measured.

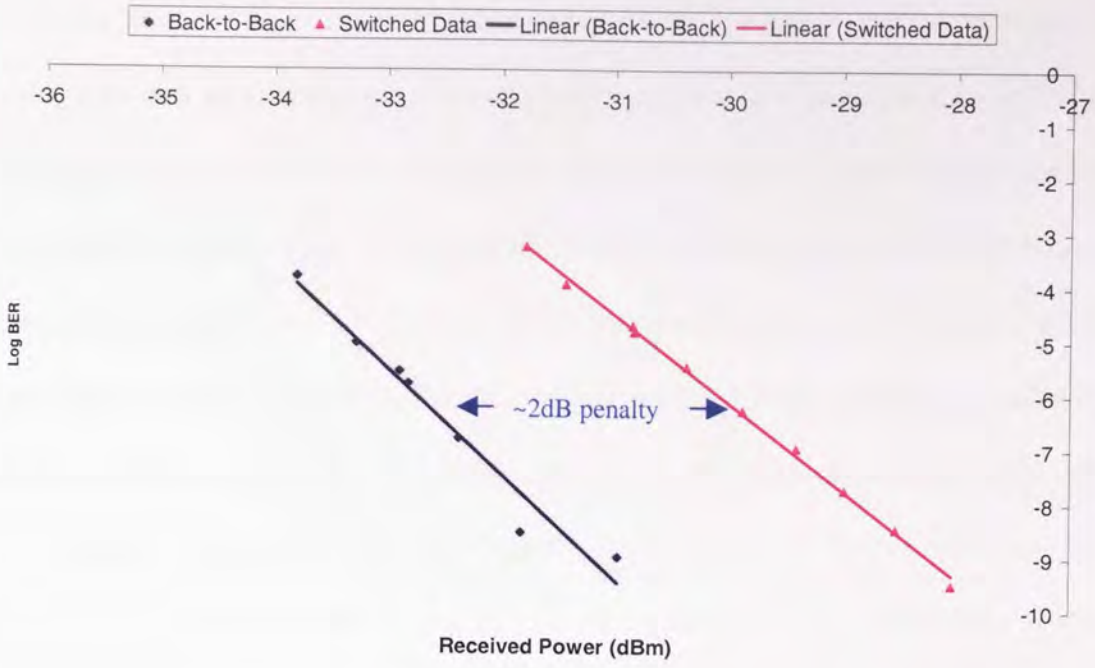

Figure 5.7: A comparison of the two BER curves shows that there is a penalty for having the jitter reduction scheme

A comparison of the back-to-back measurement and that of after the jitter reduction scheme shows that both measurements produce a linear result. However, the second trace, after the jitter reduction system, is offset by 2dB, this is known as a 2dB penalty. The penalty is most likely due to the ASE build up from the EDFA's contained within the system, which is unavoidable. Thus, we can conclude that the system will operate error free (although of course at this stage there hasn't been any significant timing jitter applied to the data source).

It is also possible at this stage to "map out" more accurately the temporal profile of the chirped pulse. These measurements can actually be taken at the same time as the results are taken for Figure 5.6. At the same time that the BER is measured, by adding a optical coupler at the output, the average received power can be measured. As we are effectively

sampling the chirped pulse (the XPM interaction between the chirped clock pulse and the incoming data pulses) then a graph of average output power as a function of $\Delta\tau$ will show the chirped pulse profile (this is a particularly useful technique as without the use of high speed sampling oscilloscopes, we cannot accurately ascertain a temporal profile of the chirped pulse. Because we are limited by the bandwidth of a photo-detector, simply looking at the temporal profile of the chirped pulse on a 10GHz sampling oscilloscope produces a Gaussian profile, not the profile that we actually generate through propagation of the nonlinear fibre which is nominally square). Of course, we do have to remember that the chirped clock pulse has also propagated through a further 1km of nonlinear fibre (the nonlinear fibre which provides the nonlinear element of the NOLM), and also propagates through a length of SMF (used to add dispersion compensation). These extra components will of course affect the profile of the pulse. By increasing or decreasing the power of the pre-nonlinear fibre (chirp generating fibre) EDFA we change the launch power into the fibre thereby changing the profile of the pulse produced (Figure 5.8).

Not only does the FWHM of the chirped pulse increase as we increase the average input power to the 2.2km of nonlinear fibre, the pulse starts to lose shape and also the pedestals from the chirped pulse in the adjacent bit slot start to overlap. This again demonstrates the need to be cautious when choosing the input power to the nonlinear fibre and thereby the FWHM of the produced chirped clock pulse. One would always like to have as large a pulse duration as possible (without sacrificing temporal profile) as this would imply that more timing jitter/phase wander could be potentially be suppressed or corrected for. However, if the pedestals overlap, errors will start to be produced and a "double sample" effect will happen (section 5.10).

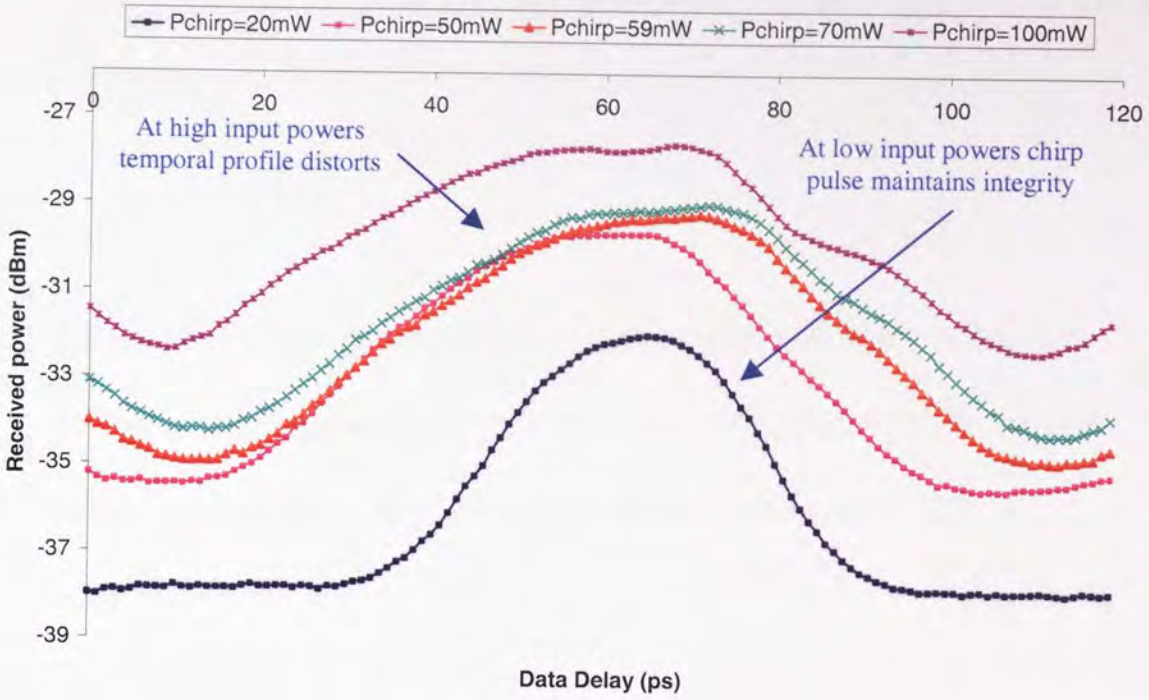

Figure 5.8: Increasing the input power to the nonlinear fibre increases the FWHM of the chirped pulse. Note that $\Delta\tau >$ bit period. After bit period, pattern repeats

In this section we have demonstrated that the system can operate error free using a GS-DFB, a ring laser and a NOLM. However, because of the way that the GS-DFB operates, it is not possible for us to easily apply timing jitter to the said GS-DFB and show that the system can both compensate for timing jitter/phase wander and maintain error free operation. This is because as we vary say the bias current of the GS-DFB (which will temporally shift the starting position of the data pulse with respect to any fixed clock) or change the temperature of the device (which will have similar effects), the GS-DFB starts to "drop out". Dropping out is where the GS-DFB fails to function properly and a '0' will be produced instead of a '1' (and vice-versa). Thus, if our starting of data pulses truly randomly contains 0's or 1's then the PRBS word produced after propagation through a modulator will in fact wrong and so we can never apply anything other than low level

timing jitter. Unfortunately it is impossible to correct for an initial error and thus, error free operation will never be achievable. The solution is to replace the data source with a more appropriate laser.

5.3 All-optical jitter suppression and phase wander reduction using one passively mode-locked external cavity tuneable laser, an actively mode-locked fibre laser and a NOLM

The same experimental arrangement as before (Figure 5.1) is used except that the GS-DFB is replaced with a passively mode-locked external cavity laser (produced by a company called LKF) which had a tuneable wavelength range between 1490nm and 1590nm. Because the pulses that the LKF source produced were relatively short (~3ps FWHM) we no longer need to do any pulse compression prior to the NOLM (thus the initial length of fibre before the EAM can be removed). In order to still be able to use the previously described Agilent clock recovery unit, both the LKF (data source) and the Pritel (clock source) need to operate at exactly 9.952GHz (four times that of the clock recovery unit which operates at 2.488Gbit/s). Thus, although both data and chirp are at ~10GHz, we have to say the system is only operating at 2.5GHz. The LKF data source was tuned to 1553nm and the Pritel clock source's wavelength remains unchanged at 1538nm.

As in section 5.2, by varying $\Delta\tau$ we are able to sweep the data source through the chirped clock source (using the NOLM as the optical AND gate, which once more performs the

optical sampling function) we are able to define the "error free timing window". The chirped clock pulse can be further broadened (in time) by adding a short length (50m) of dispersion compensating fibre (Lycom dispersion compensating fibre) after the combined 2.2km of Sumitomo nonlinear fibre. Because the chirp is produced in the normal regime, the dispersion compensating fibre works the opposite way around to what we might call convention and so broadens the pulse in time. Figure 5.9 shows both the received power and BER as a function of $\Delta\tau$.

Figure 5.9: With the broadened chirped clock pulse we obtain 60ps of error free operation

Although it might first seem that broadening the pulse in time increases the error free time window, because the increase in pulse duration is due to dispersion broadening, not nonlinear pulse broadening, the chirped clock pulse loses it's "square" profile which in fact could lower our tolerance to timing jitter and phase wander. However, as seen in Figure 5.9, as long as the received power is above a certain threshold level (in this

particular case -26.5dB) then error free operation is achieved and we have an error free timing window of 60ps.

To obtain a BER curve for the system, as previously discussed, if $\Delta\tau$ is set such that the data is sampling somewhere in the centre of the error free operation (as $\Delta\tau$ is only a relative measure of the data pulse's initial starting position compared to that of the starting point of the chirped pulse, the exact value of $\Delta\tau$ is of little or no consequence) and the received power varied whilst the BER is measured. The specific value of $\Delta\tau$ is now changed (although we still remain within the parameters of the chirped clock pulse) and a new BER curve produced. The back-to-back result is compared with the results produced for the two differing time delay settings, $\Delta\tau_1$ and $\Delta\tau_2$ and the produced results are shown in Figure 5.10.

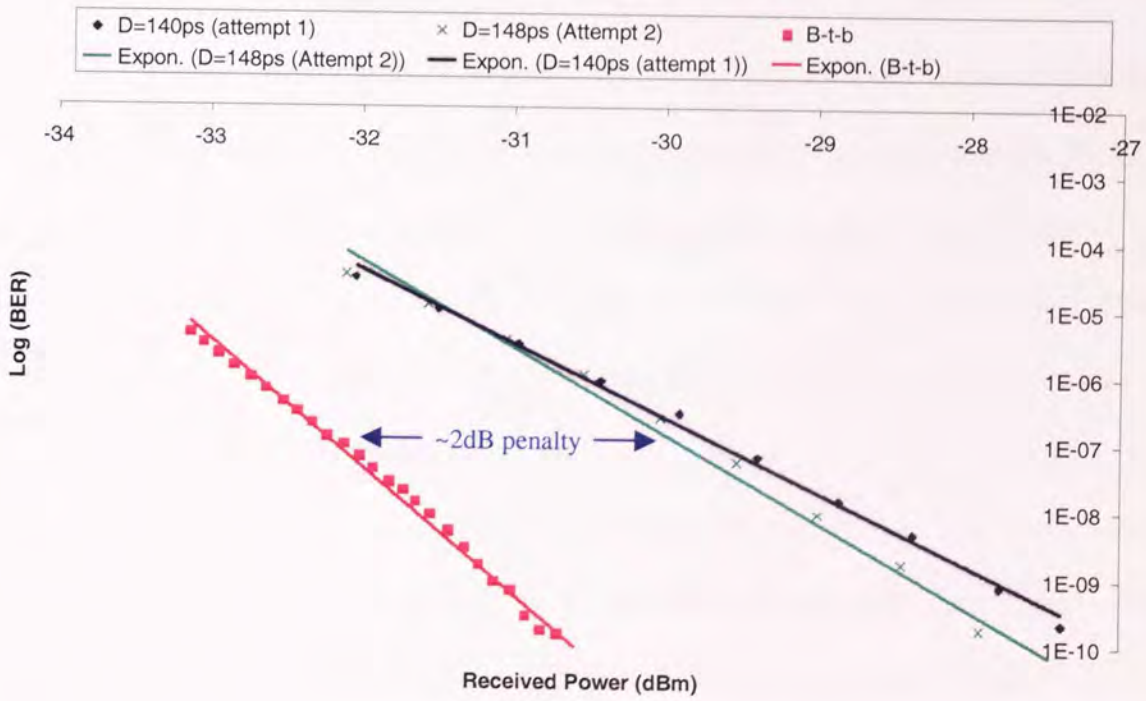

Figure 5.10: BER curves taken at two different sampling points on chirped clock source

If we look at the above figure, we see that for the two different $\Delta\tau$ settings (which are separated by 8ps) have nominally the same BER curve, both of which exhibit a ~2dB penalty when compared to the back-to-back measurements. Just like in Figure 5.7 the 2dB penalty is caused by the build up of the ASE from the several EDFA's which provide optical amplification throughout the system, this is unavoidable. The significant result is that using different $\Delta\tau$ timing positions, the BER curve's are almost the same. We can infer from this that provided that our relative timing position is within the error-free timing window, we shall always obtain a receiver power greater than that of -26.5dBm, which in turn will mean that the system will be error free and we will also obtain the same BER curve, and therefore the same 2dB penalty (this is exactly what happened in Figure 4.13). Although we discretely sample the chirped clock pulse, clearly any point could be sampled and therefore as long as we fall between the limits of the timing window then the system can be said to be continuous. This gives a total error free timing window of 60ps.

A direct comparison should now be looked at comparing chirped clock pulses of differing durations (this was also looked at in chapter 4, a computer simulation chapter). Without changing any of the major component parameters or settings, if we simply remove the 50m of Lycom (DCF) then we instantly shorten the duration of the chirped clock pulse (removing a propagation length by 50m will mean that $\Delta\tau$ will change as will the bias of the NOLM and thus, the polarisation state will need to be altered to achieve full transmission bias. These setting changes will not affect the comparison of the two systems and this is an excellent way of looking at what happens for different chirped clock durations whilst maintaining sources, amplifiers and modulator settings). Clearly opposite dispersion (again, SMF) will be required to achieve the desired effects, the two SMF lengths (with and without the 50m of DCF) will of course be different (because of the

different chirped clock profiles that will be produced) and the appropriate one is chosen here. In exactly the same way as before, $\Delta\tau$ is varied over the entire bit period (100ps as both sources are operating at 10GHz) and a graph of both received power and BER as a function of $\Delta\tau$ produced.

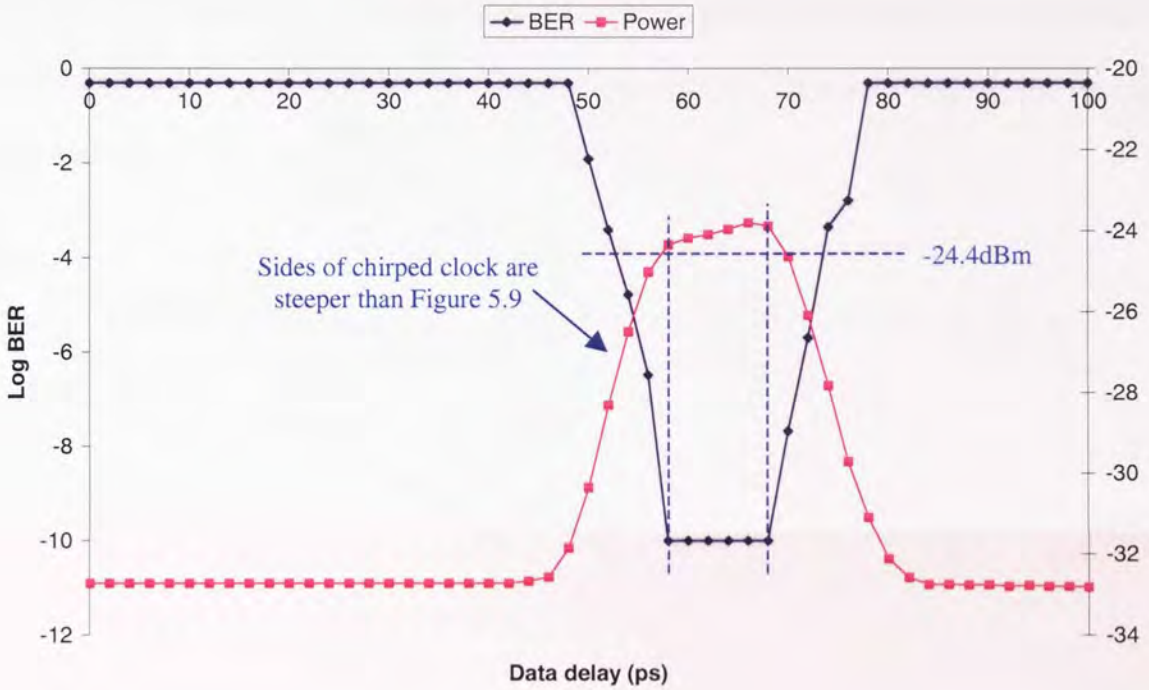

Figure 5.11: The removal of the DCF (used to broaden the clock) reduces the error free region

The differences seen in Figure 5.11 show that by removing the 50m of DCF, the chirped pulse does in fact dramatically shorten in duration (60ps to 22ps) and also changes the temporal profile (a much squarer pulse profile is seen when there is no DCF as the pulse broadening is due to the nonlinear broadening effects of the 2.2km of nonlinear fibre rather than the dispersion effects of the DCF). It should of course be pointed out that error free operation is readily achievable, providing that the average received power is greater than -24.4dBm. However, this time the error free window is significantly reduced to 10ps

(compared to 60ps with the 50m of DCF). This shorter chirped pulse duration (FWHM) combined with the steeper chirped pulse sides naturally means that the tolerance to timing displacements and therefore $\Delta\tau$ will be significantly lowered which all means that the timing of the data pulses with respect to the chirped clock pulses will be all the more critical. Once more, if we pick two different timing positions (i.e. two different $\Delta\tau$ values) that fall within the error free timing window and measure the BER as a function of received power, we can compare the output of the system with that of without the system, back-to-back.

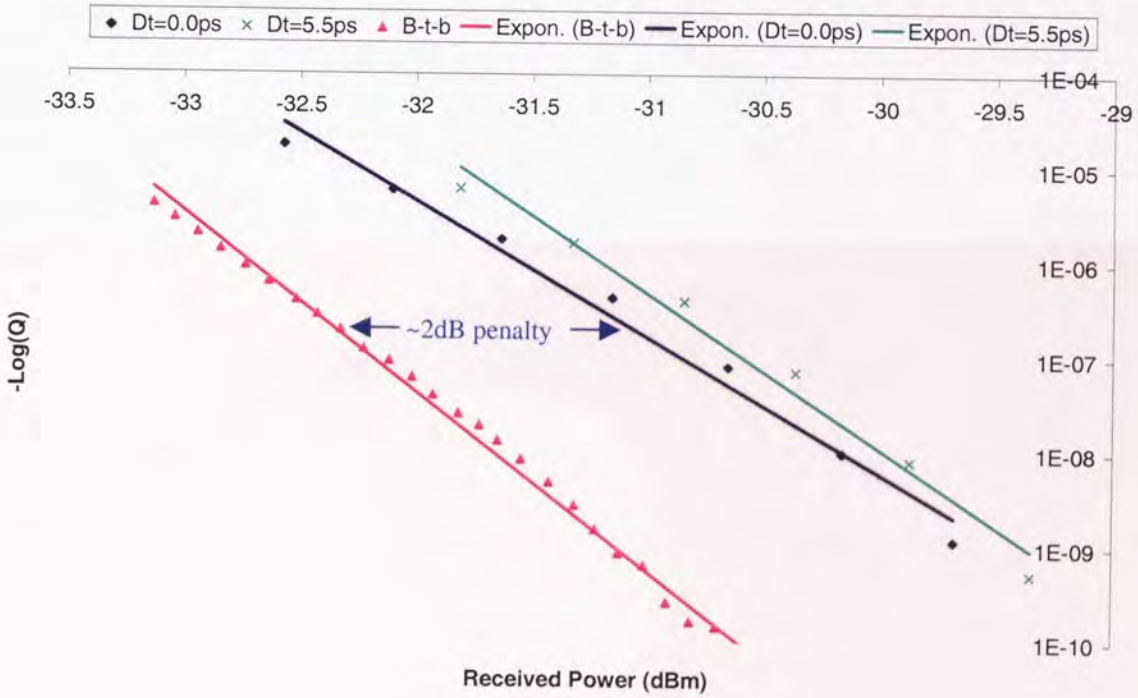

Figure 5.12: Even with the shorter chirped clock pulse BER curves can still be obtained

In Figure 5.12 we see that once again, as expected, there is a penalty of ~2dB which is caused by the ASE noise from the EDFA's within the jitter reduction system. Because the two curves obtained using the two different $\Delta\tau$ settings (separated by only 5.5ps this time) are very similar, we again conclude that so long as we sample the chirped clock pulse

within the predetermined error free timing window, we will have an error free system that will always produce the nominally same BER result. It is also interesting that both with and without the extra 50m of DCF (and therefore significantly larger timing window) the same characteristic result and the same 2dB penalty seen in the BER curve taken are both the same. This demonstrates that the only advantage gained from the larger chirp clock pulse duration is a larger tolerance to timing irregularity. One should also point out again at this juncture that we are still only dealing with an "ideal" data source, one that we are assuming has little or no timing jitter.

We can also measure the wavelength shift as a function of applied timing delay (Figure 5.13)

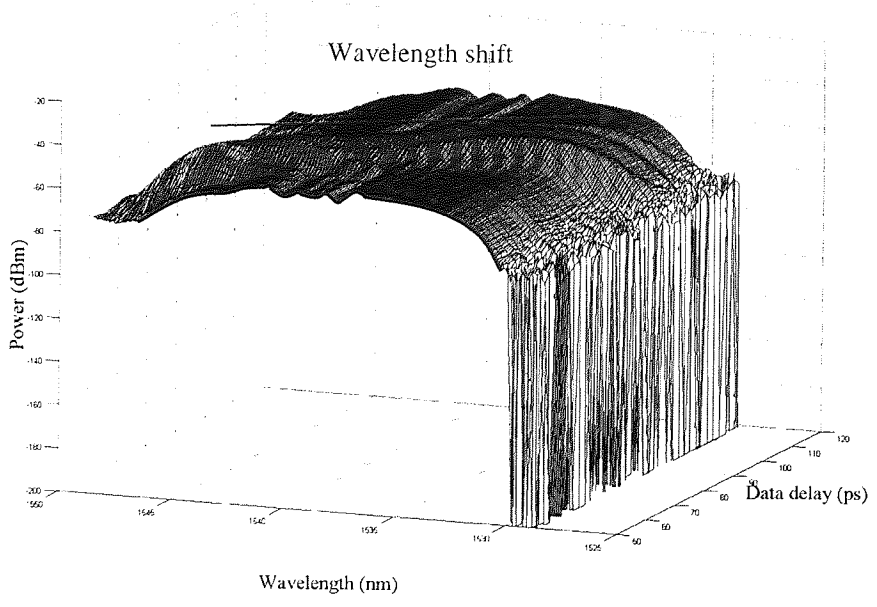

Figure 5.13: The wavelength sampled changes as the data delay is varied

Here we see that the wavelength shift is linear whilst the main temporal profile of the chirped clock source remains constant.

5.4 Application of timing jitter to data source

Previously in this chapter we have concentrated on demonstrating the basic principle of operation and that the system can operate error free under specific conditions. However, to date, we have only used an "ideal" data source to demonstrate this (low-level timing jitter). After all, as the point of this system is to compensate for timing irregularities, its time that we apply some!

By connecting one of the outputs of the BERT to an electrical phase shifter, to achieve synchronicity, which is in turn connected to a noise generator we can apply Gaussian noise to the data source. The Gaussian noise produces timing irregularities which randomly change the relative temporal position of the data pulses on a bit-by-bit level. This, as previously described, is known as "timing jitter". By varying the applied voltage to the noise generator we are able to control the amount of timing jitter experienced by the data source (see Appendix D, section 8.4). Thus, we now have an excellent, controllable way of generating and applying timing jitter to the data source. Using this it is possible to see how our timing jitter reduction scheme will be able to compensate and remove the said timing jitter whilst maintaining error free operation. This has an advantage over the previously discussed scheme were a GS-DFB was used as the data source as now when the level of timing jitter is increased, the source should not "drop-out" which caused errors which could never be compensated for (note, at this juncture we are still using the clock recovery unit before the receiver and BERT). It is now possible to compare the initially input timing jittered data source (before the scheme) with that of the output after the jitter reduction scheme to see if any improvements have been made. As we are now going to be adding relatively large amounts of timing jitter to the data source, the 50m of DCF (Lycom) has been re-added to the system in order to broaden the duration of the chirped

clock pulse. This should help us keep the timing jitter within the larger error-free timing window.

We now apply an rms voltage of 100mV to the noise generator (Appendix D, Figure 8.1). The output of the data source is connected directly to the sampling oscilloscope and the timing jitter measured (by "slicing" through the pulse at approximately half the peak power point we can measure the timing jitter for an infinitely thin slice for both the leading and trailing edge of the pulse. The average of these two values is taken which gives a good approximation of the relative timing jitter. This measurement is always carried out for the same amount of samples).

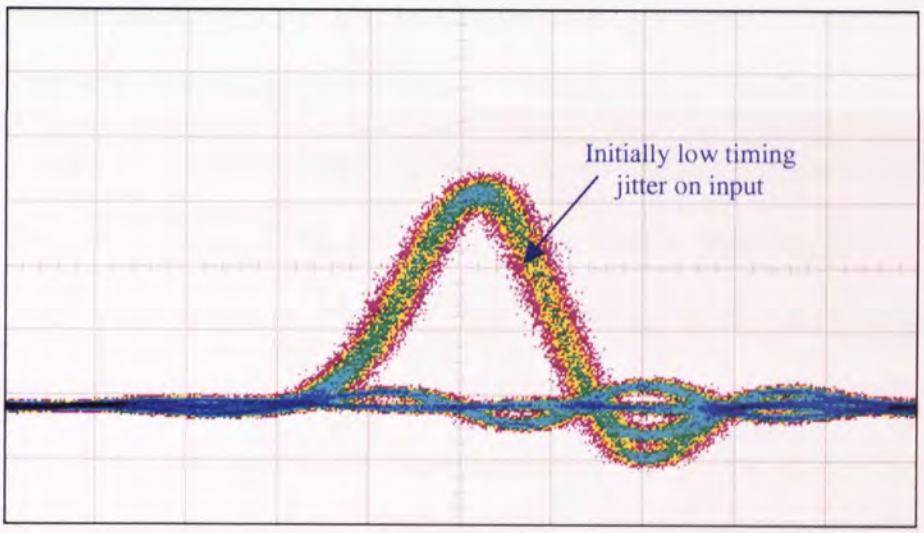

Figure 5.14: The input to the system has 1.12ps of timing jitter. This relates to V_{rms} of 100mV

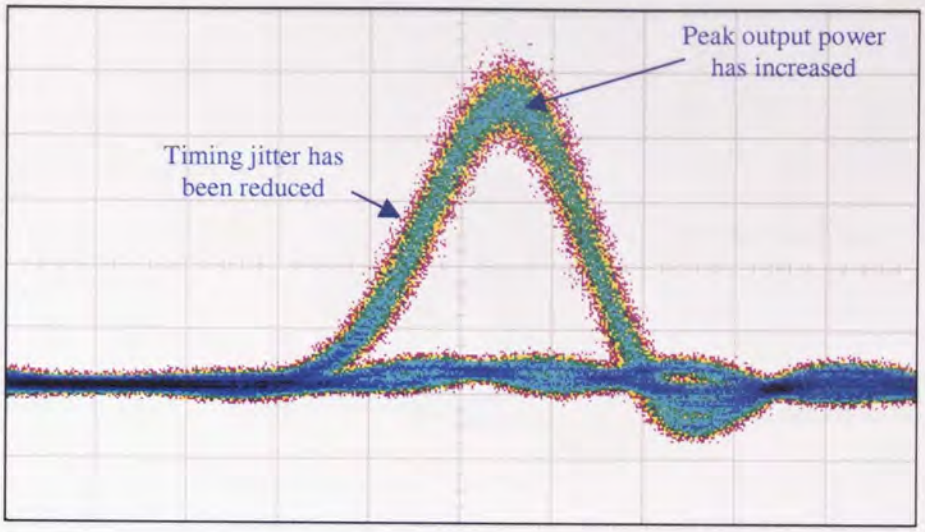

Figure 5.15: At the output of the system the timing jitter has been reduced by 7% to 1.04ps

Here we are starting with a relatively small amount of timing jitter, 1.12ps, which in many systems would not be considered a problem or particularly excessive. However, if we look at Figure 5.15, after the timing jitter reduction scheme, we see that the timing jitter has been reduced to 1.04ps, a reduction of 7%. Although this reduction is small, we do need to remember that we only started with a relatively small amount of timing jitter. We need to remember that we can only ever reduce the level of timing jitter to that of the initial clock pulse. This will always determine the minimum timing jitter as we effectively "lock" the data stream to this clock source, an improvement on this can never be made without improving the timing jitter of the initial clock). Thus, using the current clock source, ~1ps will be the minimum timing jitter produced at the output.

If we now apply 750mV to the noise generator, which is the maximum voltage that can be applied using the current equipment configuration, we see in Figure 5.16 that there is a significant increase in timing jitter produced on the input to the system (3.12ps).

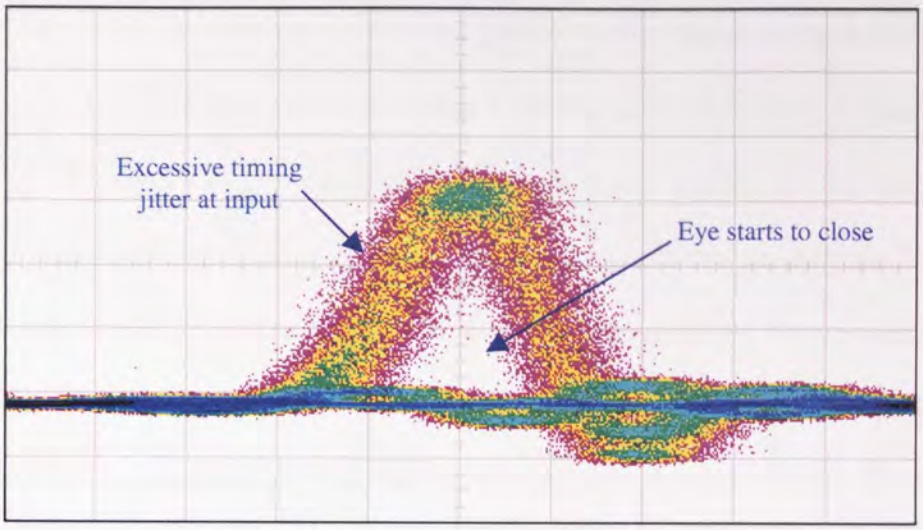

Figure 5.16: The input to the system has a timing jitter of 3.12ps which was generated with a V_{rms} of 750mV

We now compare this to the output of the system (note, there has been no change to the configuration of the system, it is the same as for the previous test), Figure 5.17.

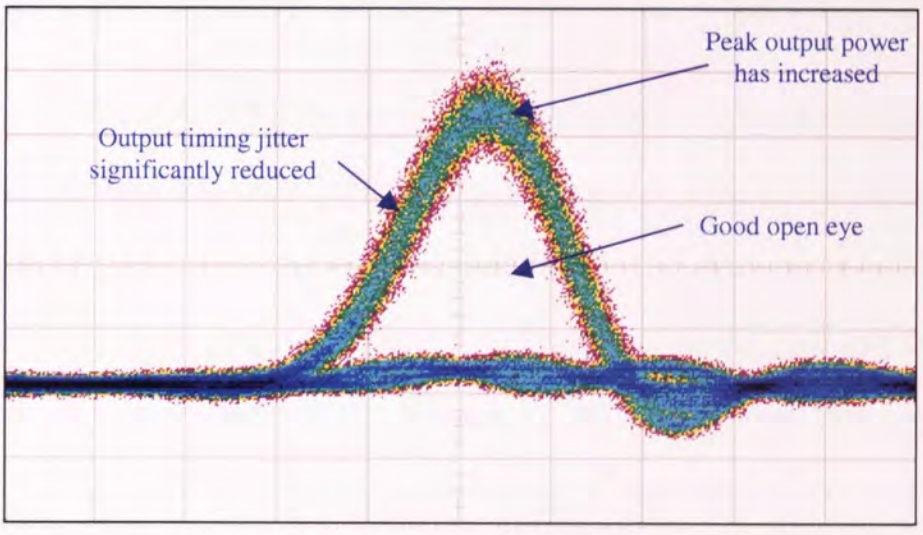

Figure 5.17: There has been a reduction in timing jitter of 70%. The output timing jitter is 0.93ps

After the jitter reduction scheme, we see that there has been a reduction in timing jitter of 70% (Figure 5.17). The data source now has a timing jitter of 0.93ps, which is close to what we would expect (as previously discussed, we would expect the timing jitter to be reduced to that of the clock source, ~1ps). We may have expected that the final timing jitter reduction shown in Figure 5.15 and Figure 5.17 would have been exactly the same and in theory this should have been the case. However, whilst carrying out the experimentation to demonstrate that the jitter reduction scheme works, the author has discovered that ring laser used to produce the initial clock pulses, which after propagation through the nonlinear fibre produce our chirped source, does not always produce an identical clock stream. The variation in initial clock pulses explains the variation in the timing jitter reduction. As well as the results shown here, further demonstration of the initial timing jitter can be seen in Appendix D, section 8.4 where applied voltages, V_{rms}, of 250mV and 500mV produce initial timing jitters of 1.57ps and 2.21ps respectively, both of which were reduced to ~1ps of timing jitter after the reduction scheme.

Previously we have shown that the jitter reduction scheme can operate error free (section 5.3) and we have now shown that the system can in fact reduce the effects of timing jitter, however, in order for this system to be considered effective, we must also demonstrate that it can operate error free, whilst under the influence of timing jitter and remove the said, timing jitter. In essence, we will combine the last two sections. This can easily be achieved by simply measuring the BER as a function of input timing delay, as in previous sections, whilst applying various amounts of timing delay to the data (clearly BER as a function of $\Delta\tau$ is measured over the entire bit period, 100ps, the timing jitter is then increased and the process repeated).

Note, for the following results we have an average clock pre-chirp input power of 60mW, 2.2km of nonlinear fibre and the same 50m of DCF in the system which is added to further broaden the chirped clock pulse in time. The results can be found seen in Figure 5.18.

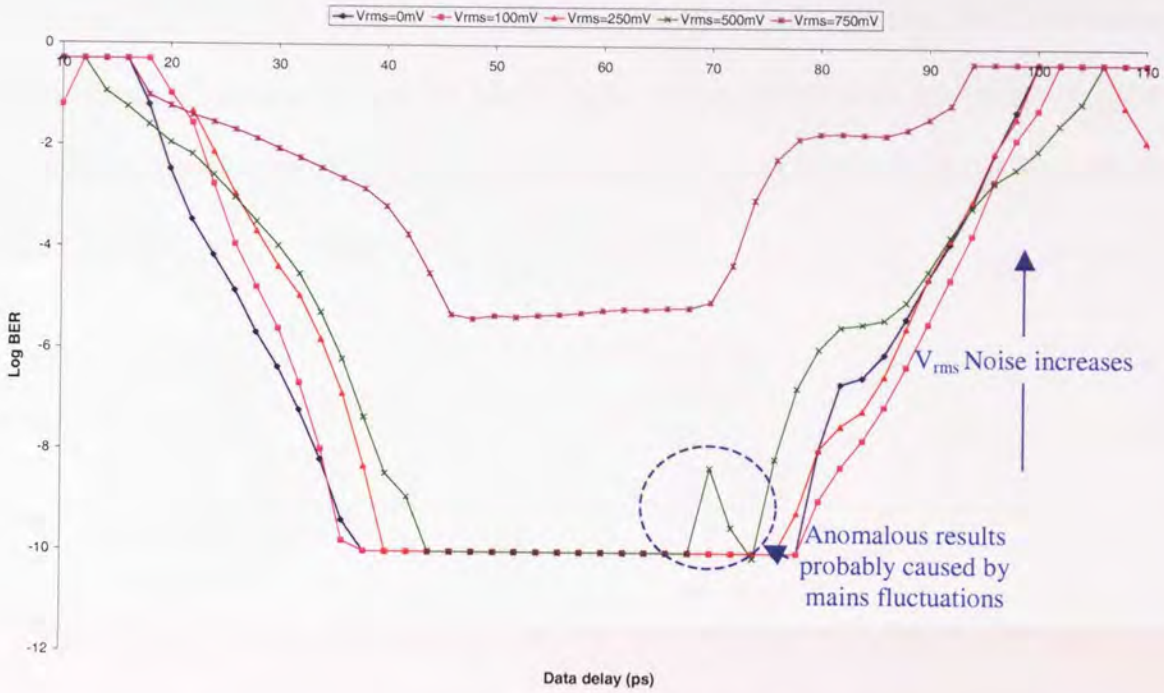

Figure 5.18: As the applied noise increases, the error free region decreases

When there is "no noise", i.e. 0mV, and low noise applied to the noise generator (100mV) we see that the switching windows are almost identical. This is to be expected as the base state, 0mV and 100mV give us almost identical initial timing jitters (~1ps). Thus, we would expect these two settings to produce the same result. As the applied voltage is increased, the level of noise is increased and therefore so is the timing jitter on the data source. As this happens the error free region decreases. This was to be expected as the larger the timing jitter, the longer the effective data pulse potentially is and in order to be error free, the entire effective data pulse must fall within the timing window and so the tolerance to applied timing jitter decreases. This naturally implies that we have a smaller

compensate able window, the higher the initial timing jitter. What is interesting is that for an applied rms voltage of 750mV (the largest voltage that we can apply) to the noise generator (which gives an input timing jitter of 3.12ps) error free operation is never achieved. One might have assumed that because the pulse, along with the timing jitter, is significantly smaller than the FWHM of the chirped clock pulse, timing jitter suppression would occur. What actually happens is that as the applied noise has a profile which fits a Gaussian distribution, there is still a possibility that the data pulse will appear somewhere at the extremities of the Gaussian profile (Figure 5.19).

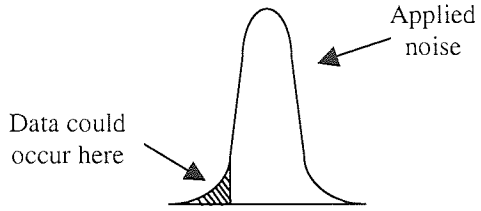

Figure 5.19: With the application of rms noise to the data source, there is always, in theory, the possibility that the timing jitter can never be compensated for

If we look at this from a purely theoretical point of view we could say that the Gaussian "tail" tends of to infinity and therefore if we apply Gaussian noise at the input, the timing jitter will never be compensated for (if this were the case, then one would need in an infinitely large chirped clock pulse in order to be able to compensate for any timing jitter no matter how small, this is clearly impractical!). What actually happens is that we need to impose some physical limitations on the system, if the timing jitter exceeds these limits, then although the timing jitter may appear to be suppressed, the system will not operate error free. When dealing with timing jitter, we actually find that it would appear as though a very large amount of timing jitter can be suppressed. However, if the timing jitter falls outside our limits, we find that errors occur. This happens because the system can

potentially take a wayward '1' and turn it into a re-timed '0'. This is clearly wrong and an incorrect code word would be transmitted. It is impossible to detect this type of error by eye (using the sampling oscilloscope to measure the timing jitter) this type of error can only be detected by measuring the output BER.

Thus, for our particular system under these specific conditions it has been found that the maximum input timing jitter that can be suppressed (back to ~1ps) is 2.21ps. Timing jitter greater than this will be suppressed but would not be error free.

5.5 Application of phase wander to data source

We now need to look at a slightly different timing irregularity, phase wander. As previously discussed, phase wander is where an entire codeword is shifted in time (rather than the individual bits). Thus, a different test needs to be analysed. In the last section we applied Gaussian noise to the data source using a noise generator, if we replace this noise generator with a sine wave generator we can actually shift an entire codeword backwards and forwards in time, thus, we can apply the aforementioned phase wander in a controllable way. This simple substitution now means that we can controllably emulate the effects of phase wander and investigate how this will have an effect on the BER in the same way as before.

It is important to realise that timing jitter has been replaced by phase wander and that these two distinct timing irregularities are tested separately. However, the initial system remains the same and only minor adjustments to the system are needed (naturally we

would expect $\Delta\tau$ to change and so the timing alignment within the NOLM we need to be adjusted as well as the bias of the loop mirror). To date the author has not found a way to apply both timing jitter and phase wander in a controllable manner at the same time. As before the 50m of DCF is kept within the system in order to maximise the duration of the chirped clock pulse and an average input power of 60mW used.

If we now apply a small amount of phase wander, 2.63ps, Figure 5.20, we can instantly see why this could be potentially such a large problem.

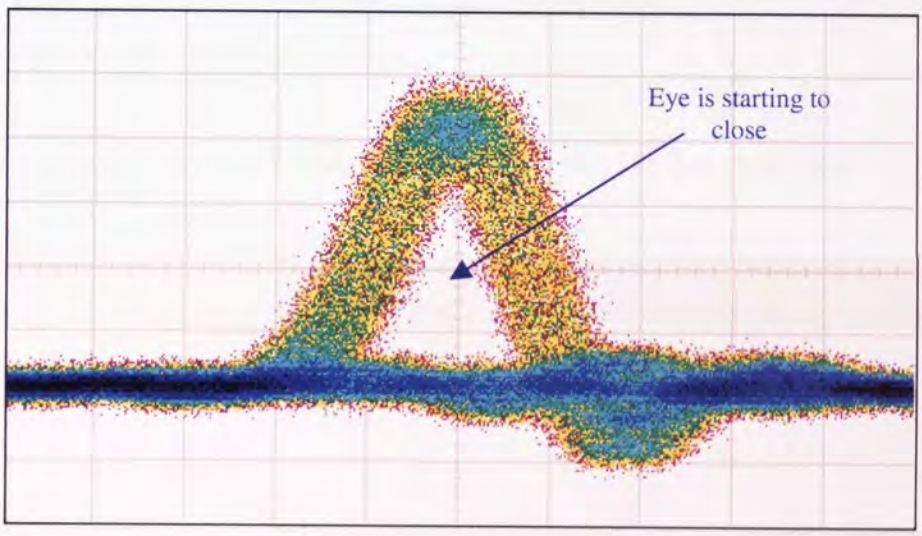

Figure 5.20: Just 2.63ps of phase wander could cause errors to be produced

Large amounts of phase wander is obviously a very serious problem, unlike timing jitter where only a few bits of a codeword might be misinterpreted, with phase wander an entire codeword could potentially be missed altogether!

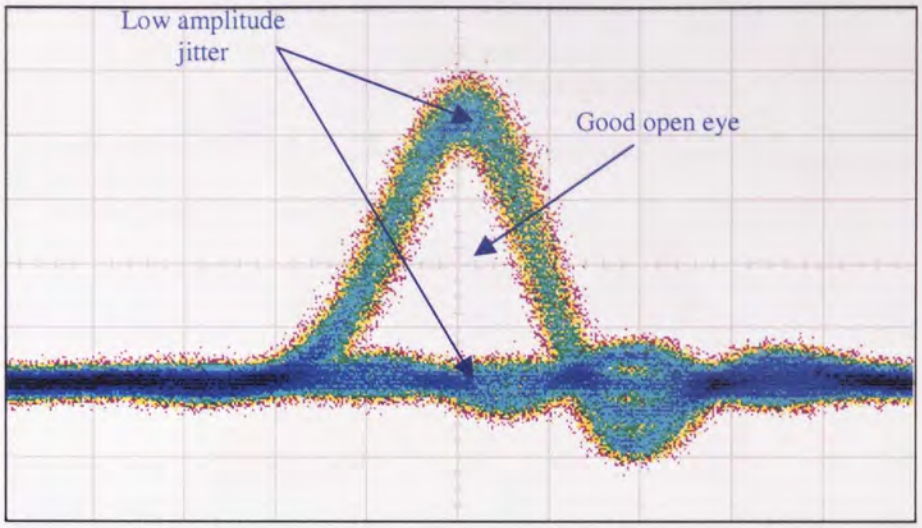

Figure 5.21: The phase wander is reduced to 1.51ps after propagation through the system. A clear improvement can be seen

Looking at the system output, Figure 5.21, the phase wander has been suppressed and the usual pulse profile is seen. Of course this was for only a small amount of phase wander. By increasing the sine wave generator so that we now have 33ps of phase wander, the data source which has almost an unrecognisable temporal profile (Figure 5.22).

It would be impossible to connect this output to a receiver and try and measure the BER or detect a code word. However, if we propagate this "blurred" word through the system we see that this excessive phase wander can be suppressed.

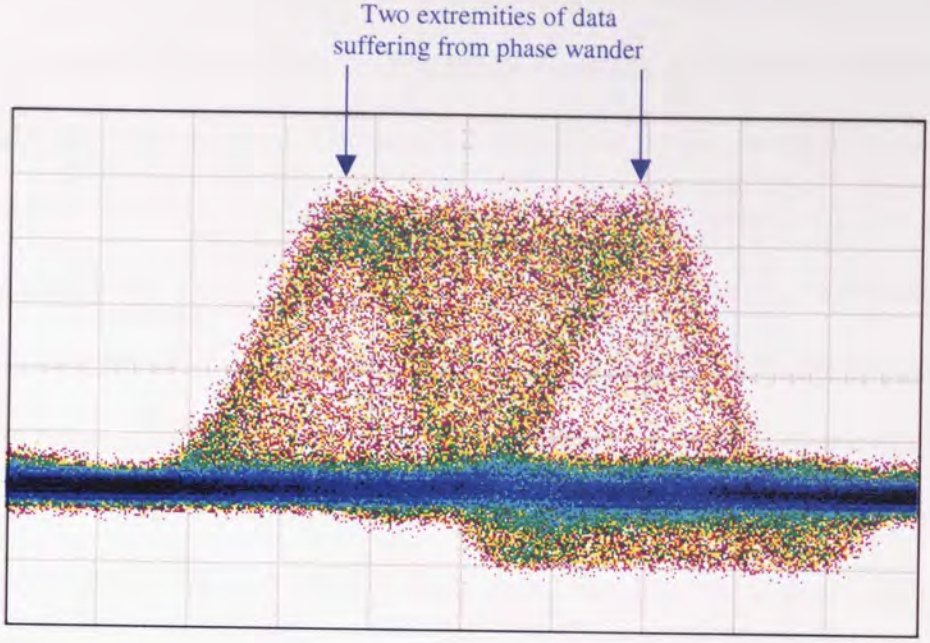

Figure 5.22: Excessive amounts of phase wander make it impossible to understand the transmitted code word

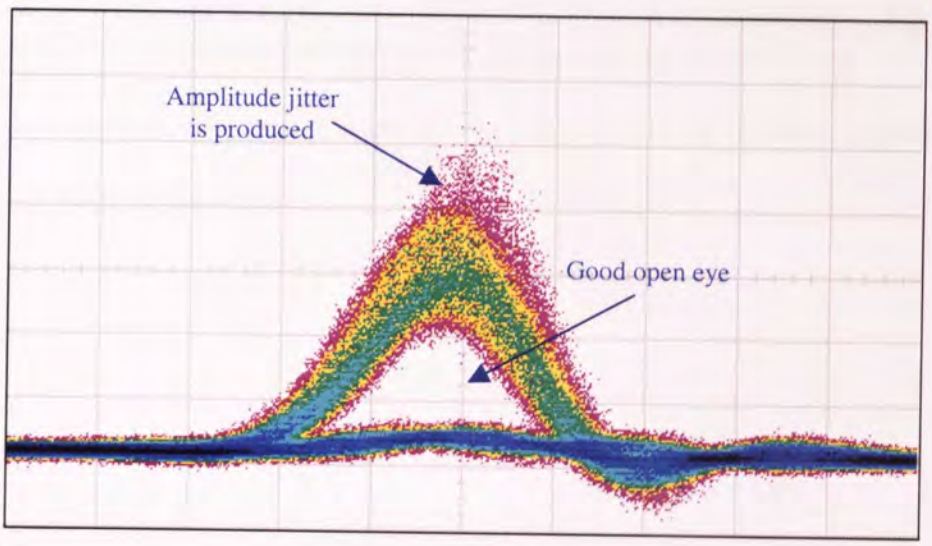

Figure 5.23: After propagation through the system, a clear and open eye is formed. The amplitude jitter could be removed by propagation through another similar device such as a 3R regenerator

Figure 5.23 shows that the blurred and elongated pulse shape (Figure 5.22) has been resolved to something which starts to represent a Gaussian pulse profile and most of the phase wander has been removed. The output is clearly not perfect, but it is however a vast improvement on the excessive case that we started with. Unfortunately we have generated some amplitude jitter. This can be attributed to the imperfections in the initial chirped clock pulse. In order to generate the large FWHM required to be able to compensate for such a large phase wander, we have to sacrifice the temporal profile of the chirped clock pulse (by the addition of the DCF). We know that the chirped pulse does not have a constant amplitude or "square" temporal profile and this imperfection will unfortunately always be translated directly into amplitude jitter.

We now measure the BER as a function of $\Delta\tau$ for varying amounts of phase wander in exactly the same manner as when we applied timing jitter to the data source. In the case of phase wander, one would expect that we would be able to achieve error free operation provided that the level of phase wander is less than the timing window provided by the chirped clock pulse (Figure 5.24).

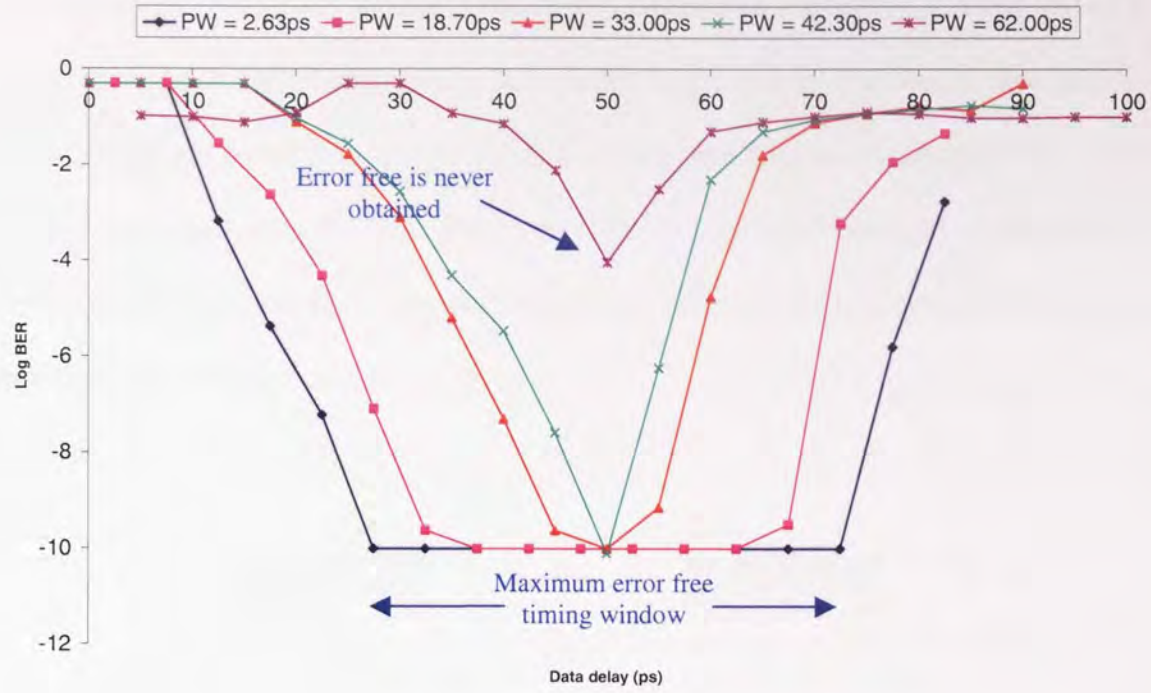

Figure 5.24: As the phase wander increases, the error free timing window decreases and so does the tolerance to relative timing position

For the lower levels of phase wander, we see that a large error free timing window is produced which means that we have a large tolerance to any further timing irregularities. As the phase wander increases the error free window decreases. This effect occurs because all of the phase wander must fall within the timing window (which is ultimately determined by the duration of the chirped clock pulse) and so for large amounts of phase wander we find that we cannot achieve error free operation. This principle is illustrated in Figure 5.25. We now just concentrate on one, individual bit period anywhere in the time shifted code word. In the first diagram (a), the phase wander is significantly shorter than the timing window and so the word can be shifted back into the centre of the timing window. The same applies to case (b), the phase wander is only just shorter than the maximum timing window however, the phase wander can be still eliminated. Finally we

look at case (c). The phase wander is potentially larger than the timing window and so the pulse falls outside the timing window and cannot be recovered. We should note here that this is not always possible to spot when looking at an eye diagram as adjacent bits will get dragged into the wrong bit slot. However, they will be re-shaped and re-amplified so usually a very open and clean eye will be produced although the code word would now be incorrect and will contain errors.

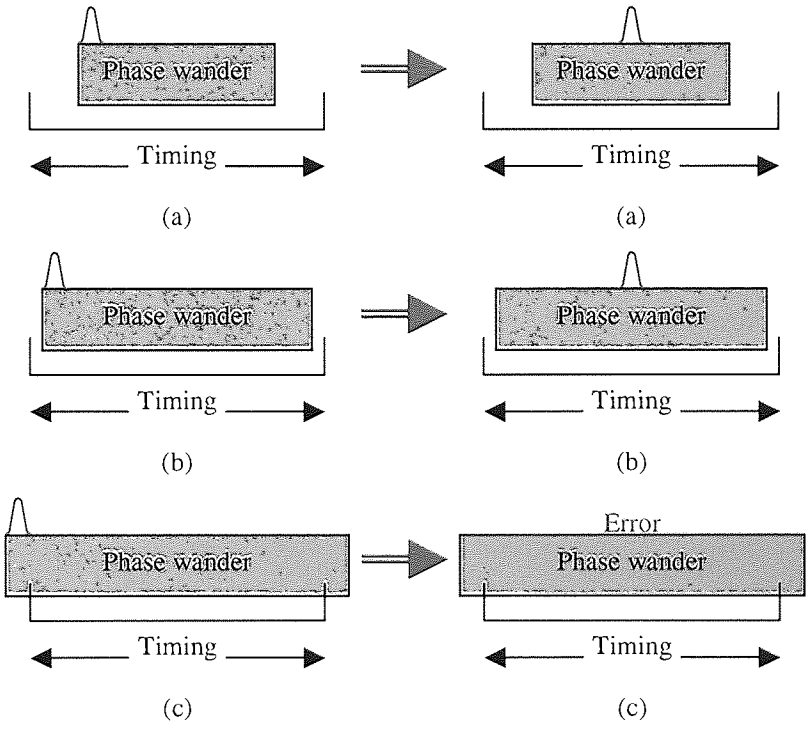

Figure 5.25: Providing that the level of phase wander falls within the timing window, determined by the locally generated chirped clock pulse duration, the phase wander can be compensated for

If we were to now increase the chirped clock pulse duration then error free operation would be achievable for even the largest amounts of applied phase wander (clearly if we were to be able to increase the phase wander past the bit period, 100ps, then we would

never be able to compensate for the phase wander as we would get interference between adjacent clock bits). Thus, using the current configuration, provided that the phase wander is less than 42.30ps (which equates to 42% of the bit period being taken up by phase wander), then the system will remove the phase wander whilst still remaining error free. As stated earlier, this figure is only limited by the FWHM of the chirped clock pulse and so the phase wander has to be only slightly less than the FWHM of the chirped clock pulse in order that the data pulse to be recoverable (this is in contrast to when applying timing jitter where the chirped pulse must be significantly larger than the level of timing jitter applied). As the data pulse used has an initially short FWHM, one only needs ensure that the "centre" of the heavily phase wandered data pulses aligns temporally with the centre of the chirped clock pulse. If the alignment is incorrect, then clearly errors will occur. This demonstrates that there will be some tolerance to the temporal alignment for low levels of phase wander, but for high levels the initial alignment must be very accurate.

5.6 10Gbit/s re-timing and jitter suppression without the use of clock recovery

Until now we have always used a clock recovery unit at the output of the system (in between the photo-detector and the BERT). Although when using this device both of the laser sources (data and clock) were actually operating at 10GHz, the maximum rate of the clock recovery unit was 2.5Gbit/s and so the system effectively had to be scaled down to accommodate this device. By removing the clock recovery unit we are now able to operate at a full 10Gbit/s (note, both the sources already ran at this speed and the EAM used can

also operate at 10Gbit/s so scaling the system is trivial. It was however found that a 20GHz RF amplifier was needed after the receiver in order to increase the input power to the BERT and the receiver itself had to be upgraded as well, to one with a greater bandwidth). It is now easy to repeat some of the previous experiments at the higher data rate (clearly the BERT had to be replaced with another model which was capable of operating at 10Gbit/s). One of the uses of this system is as an all-optical clock recovery unit which would be used at the end of a transmission link or optical network. Clearly if this were the case then we would not want to have to use an electrical clock recovery unit there as well, thus, it is important that the system can operate in a stand-alone manner without the need for its electronic counterpart.

In the same manner as previous sections, the system was first tested by measuring the BER and received power as a function of an input timing delay, $\Delta\tau$ (in this particular case $\Delta\tau$ was actually extended past 100ps, the bit period, to show that oscillatory nature of the system). The results are found in Figure 5.26.

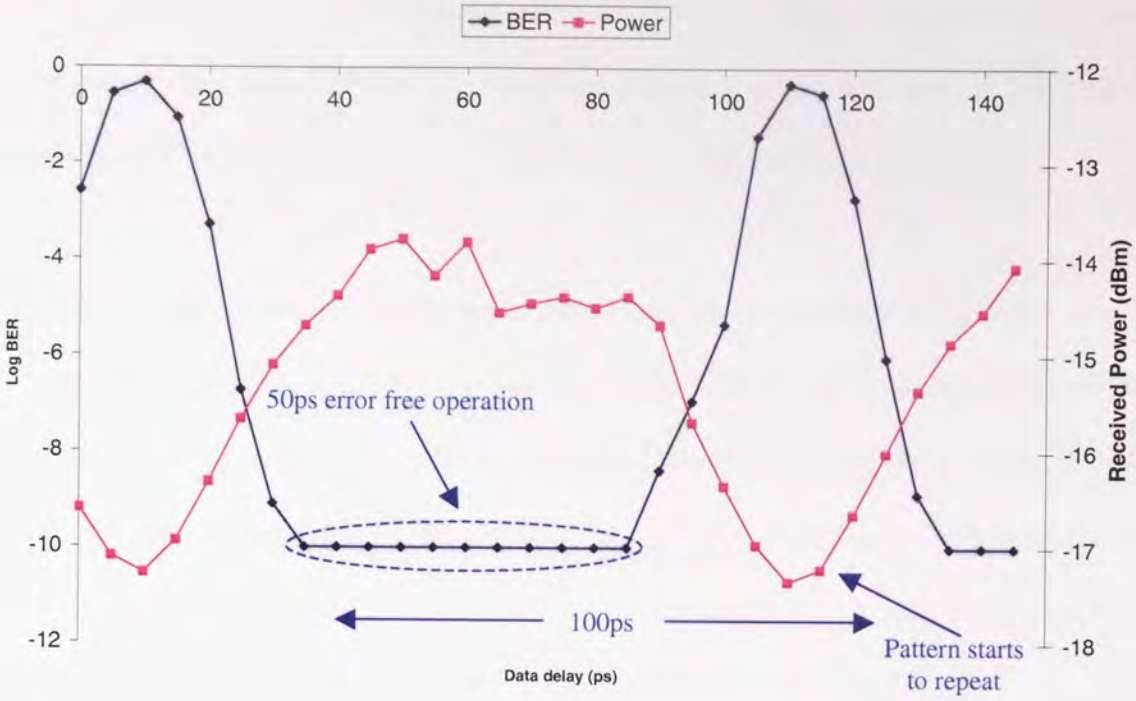

Figure 5.26: Even without the use of clock recovery, 50ps of error free timing operation can be easily achieved

The above figure clearly demonstrates that the system operates sufficiently well at the increased repetition rare of 10Gbit/s with the important factor being that there is no electronic clock recovery used at all. Of course, at this stage we have returned to having a "perfect" data source for which we make the assumption that there is nominally no timing jitter or phase wander. Thus, one might have expected the system to work, it is still important to demonstrate that it does. One can also make the hypothesis that the only true limiting factor on the repetition rate at which the device can operate at is the speed at which the NOLM can switch (which is determined by the recovery time of the silica fibre). This implies that speeds in the Tbit/s region should possible. In reality of course, the faster the system operates, the shorter the chirped clock pulse would need to be to fit within one bit period and so the less toleration to timing jitter and phase wander there would be (because the duration of the chirped pulse effectively determines the switching

window of the system). It is interesting, although maybe obvious, but as we extend past the bit period, the results of one bit period are identical to the next and so the pattern repeats. This should always be the case when there are identical adjacent bits.

When timing jitter is applied to the input, the system should produce comparable results with previous experiments (at lower repetition rates) and should be independent of the repetition rate of the said system. This is shown to be the case by applying timing jitter at a level of 2.66ps to the input of the system (Figure 5.27). With this timing jitter on the PRBS input, the trace produced looks very similar to Figure 5.16 which was effectively operating at the slower speed of 2.5Gbit/s (with slightly more timing jitter)

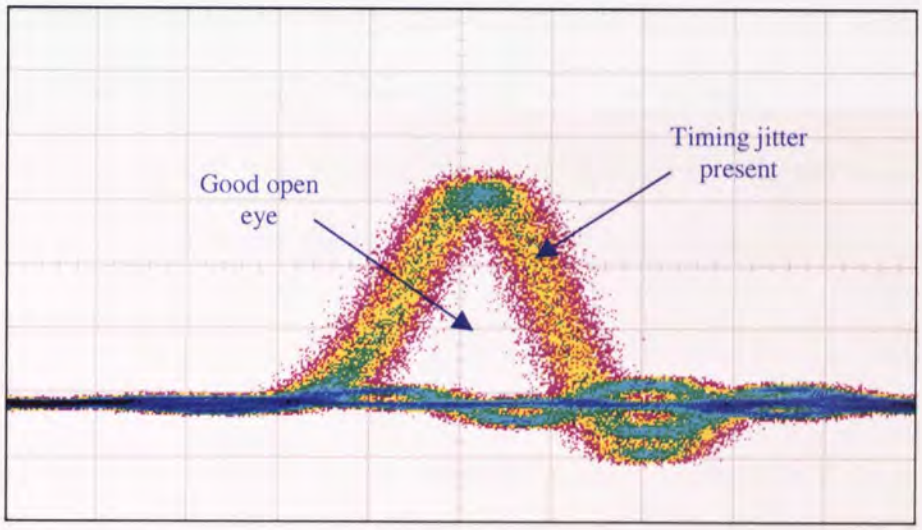

Figure 5.27: With 2.66ps of timing jitter, the eye remains open

The output of the new 10Gbit/s system (which has no electronic external clock recovery), Figure 5.28, looks exactly the same as the output of the system when it was operated at a 2.5Gbit/s, Figure 5.15, which illustrates that the initial speed of either the data source or in fact the initial clock source, does not effect the operation of the device.

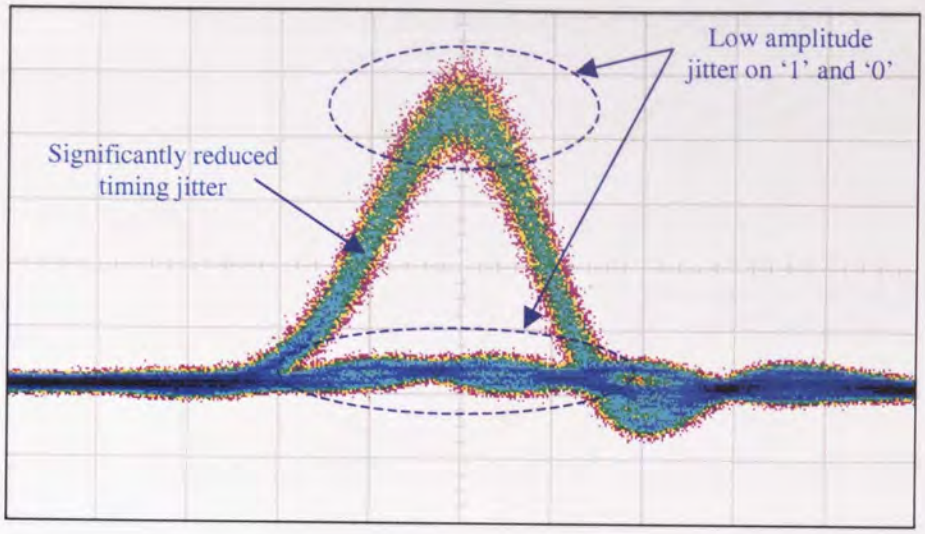

Figure 5.28: After timing jitter suppression, the timing jitter is reduced to 0.86ps (a reduction of 68%) and there has also been an increase in peak output power

The timing jitter is reduced by 68% and there is minimal amplitude jitter. Although it can be seen that there is little or no difference to the result for differing repetition rates, it is important to point out that some of the variables do have to be adjusted to each specific case (such as the input power of the data to the NOLM, the polarisation and therefore bias of the NOLM and $\Delta\tau$).

In the same manner as before, we vary $\Delta\tau$ and measure the BER as a function of $\Delta\tau$. However, this time we are using a set level of timing jitter (V_{rms} = 300mV which is equivalent to an input timing jitter of 1.73ps) and no electrical clock recovery at all. We can also investigate at this point what happens if the receiver power (at the BERT) is changed and see how this affects the potential error free timing window (the results are shown in Figure 5.29).

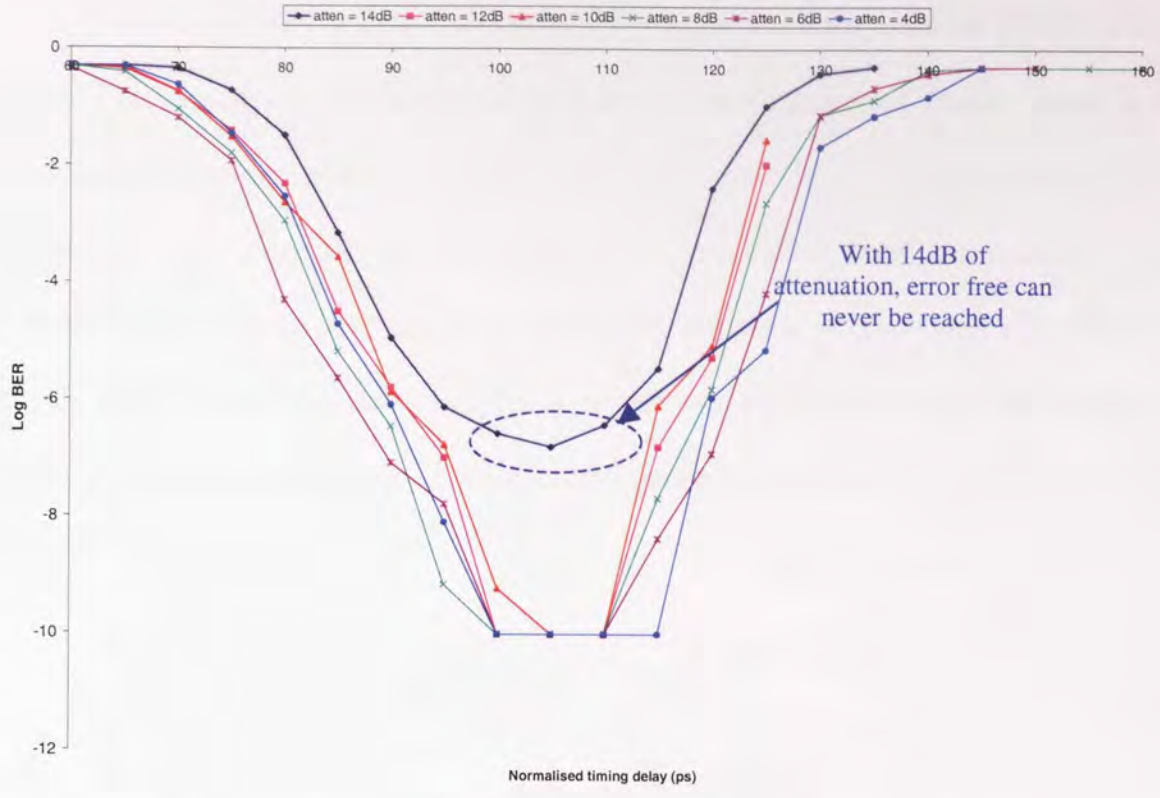

Figure 5.29: With the decrease in attenuation at the receiver, the error free region increases to a maximum of 15ps

The first thing to note in the previous graph is that we have yet more confirmation that the system works error free with no external or electrical clock recovery at all. A maximum error free timing window of 15ps is obtained when there is the minimum amount of attenuation and so maximum received power (which demonstrates that this system could indeed be used as an all-optical clock recovery unit). As the power received by the BERT decreases, the error free timing window also decreases to the point that there quickly becomes no error free timing window at all. From this we learn that it is important to always obtain the maximum output power out of the jitter reduction scheme in order to maximise the effectiveness of the device.

Finally, we can now look at how both the optical spectrum and the temporal profile at the output of the system changes as a function of $\Delta\tau$ (clearly the temporal profile, shown as a sampling oscilloscope trace, will be effected by the bandwidth of the photodiode which proceeds the said device and also the bandwidth of the sampling oscilloscope itself). This will show that by using the NOLM we effectively sample a different part of the broad chirped clock pulses spectrum when $\Delta\tau$ is varied. We will also see how the temporal profile of the output changes for a corresponding sampling point.

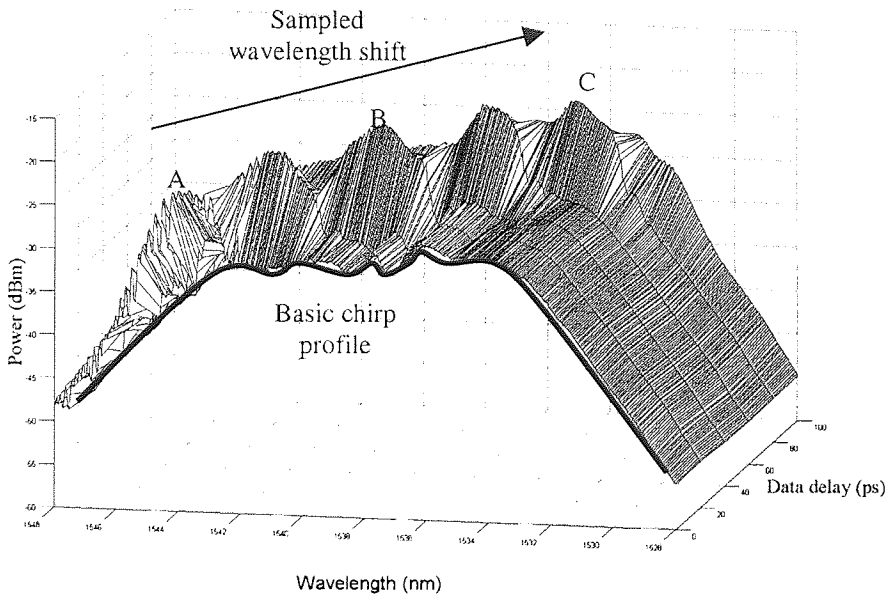

Figure 5.30: As the data delay is increased, we sample a different section of the chirped pulse which corresponds to a specific wavelength

In the above figure, $\Delta\tau$ is incremented by 20ps, the OSA traces have been grouped together which generates a 3D plot showing how the optical spectrum changes as $\Delta\tau$ is increased. The three points correspond to the following sampling oscilloscope traces.

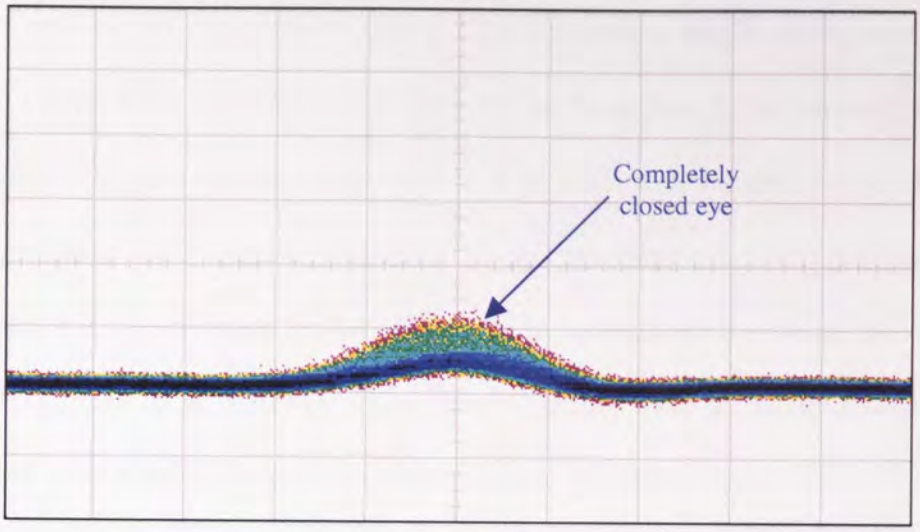

Figure 5.31: Sampling at the edge of the chirped clock pulse produces hardly any output on the sampling oscilloscope. No eye can be seen (position A)

If we define this as the "start" of the chirped clock pulse (this is simply an arbitrary point which has been chosen), as would be expected, there is no significant output on the sampling oscilloscope. This is because we are only just sampling on the edge of the chirped clock pulse, corresponding to point A on Figure 5.30.

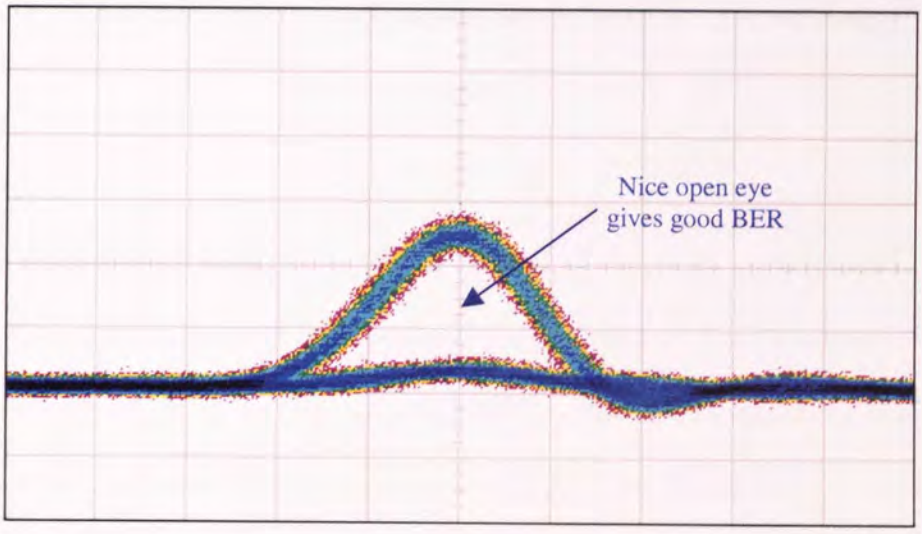

Figure 5.32: At the "centre" of the chirped clock pulse (position B) the eye is fully open

As $\Delta\tau$ is increased, an eye starts to appear on the sampling oscilloscope, corresponds to point B on Figure 5.30. It can be clearly seen that as we approach the centre of the chirped pulse, the eye produced becomes more open and prominent. It should be noted here that it doesn't necessarily follow that the centre of the chirped clock pulse will produce the most open eye and maximum output power. This is because although we would ideally like the chirped clock pulse to be perfectly square (and therefore have a flat and uniform plateau with an even output power across the entire temporal profile) it clearly isn't.

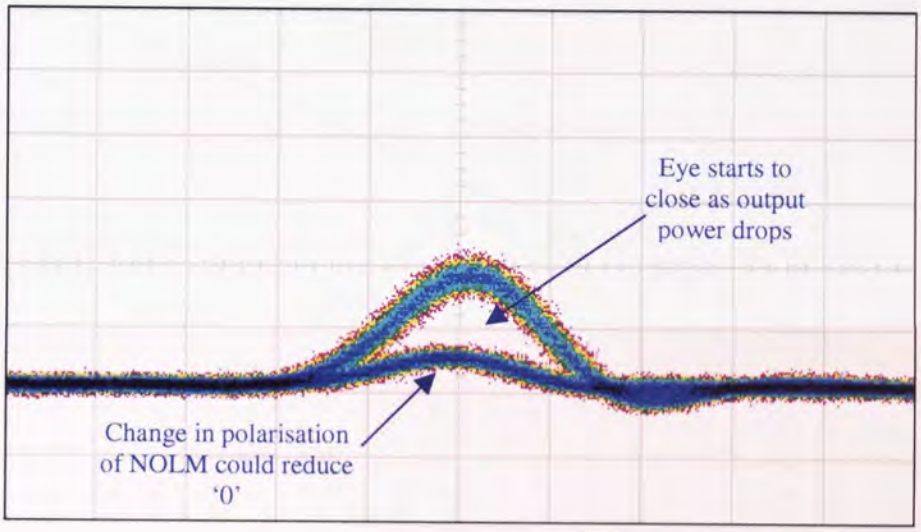

Figure 5.33: As the data tends towards the opposite edge of the chirped clock (position C) the output power decreases

Finally, as $\Delta\tau$ reaches the extremity of the chirped clock pulse again (point C on Figure 5.30) the eye starts to close again and the average output power is reduced. Eventually there will be no eye at all on the sampling oscilloscope. However, if $\Delta\tau$ was increased even further, an eye would start to appear once again as we would start to sample the next chirped clock pulse and the cycle would repeat. It is now possible to show the relationship between $\Delta\tau$ and the wavelength produced at the output of the system. This is simply

achieved by measuring the wavelength for which the maximum output power is produced for any given sampling point. Naturally if $\Delta\tau$ was at 100ps then we would be back at the start of the next chirped clock pulse (as the bit period at 10GHz is 100ps) so there is no need to show this. The following pattern is simply repeated.

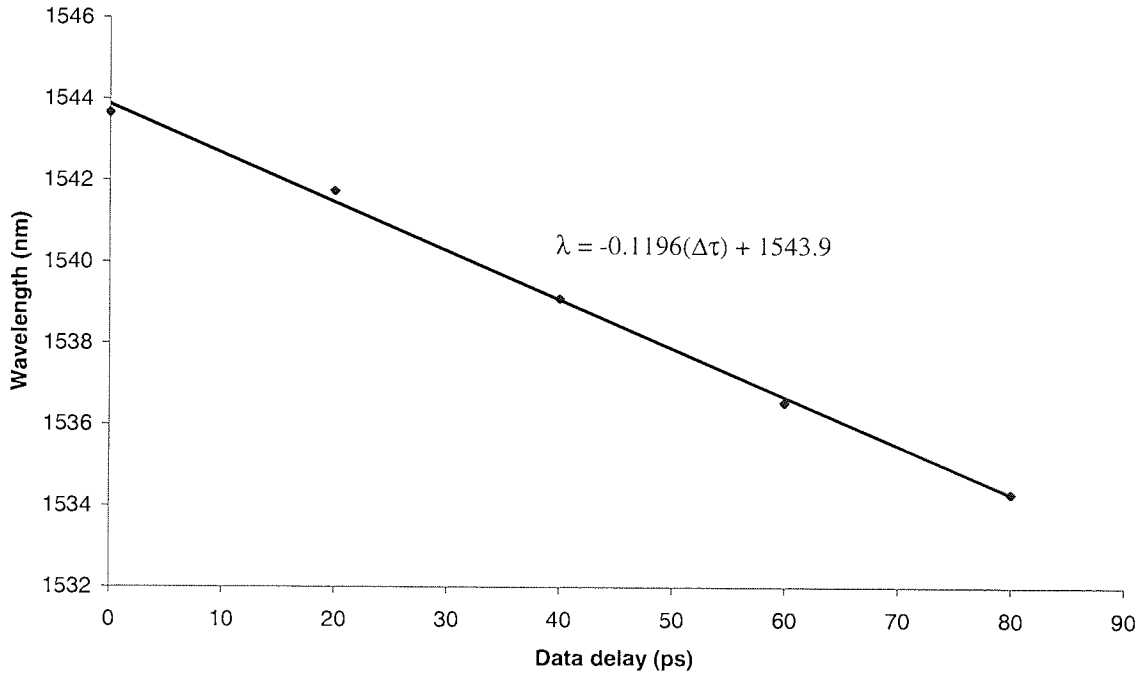

Figure 5.34: As $\Delta\tau$ increases the wavelength produced decreases

As one would expect, the wavelength conversion is linear (Figure 5.34). By simply controlling $\Delta\tau$, we can control the wavelength translation and therefore the wavelength that is produced. This throws up another possible use for the single stage system. Here we have shown that all optical controllable wavelength conversion has been achieved.

5.7 All-optical jitter suppression using two GS-DFB's at 2.5GHz

We would ideally like the chirped clock pulse to be perfectly temporally square, however, this is highly unlikely to happen. We have already seen the effects that having a locally generated chirped clock pulse which does not have a uniform and flat top will have on the output that is produced (section 3.4). We can now take this one stage further and show that the system will still work if the chirped clock pulse actually has a Gaussian profile and that it doesn't have to be square at all. However, it will be impossible to obtain a particularly good eye opening as the timing jitter will be directly translated into amplitude jitter during the wavelength conversion.

The basic experimental arrangement described in Figure 5.1 is used except that the clock source is a 2.5GHz GS-DFB operating at 1538nm (the same wavelength as the 10GHz source that has been previously used) and 600m of dispersion compensating fibre is simply used to broaden the clock pulse instead of the 2.2km of Sumitomo nonlinear fibre. However, as we now start with a relatively low peak power in the Gaussian pulse, propagating through the length of DCF we will never be able to generate a square clock pulse, the pulse will merely be broadened in time. We will now take a purposely highly timing jittered data input to the system, Figure 5.35.

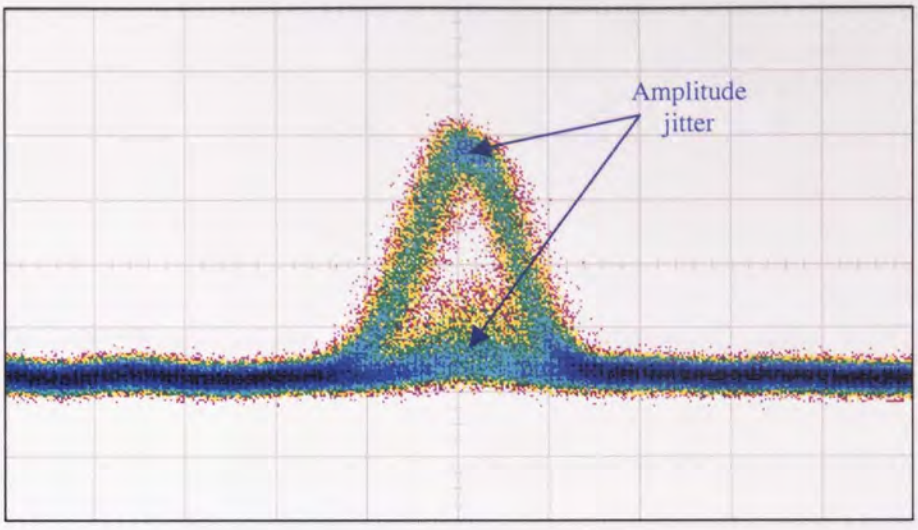

Figure 5.35: The initial eye is closed and the input suffers from timing jitter

The data is then propagated through the system and the output is shown in Figure 5.36. The first thing to note is that the timing jitter which was applied has only slightly been reduced. This is because the clock pulse is only slightly chirped, therefore there is only a small amount of wavelength conversion (this could be rectified by using a clock source that produces an initially chirped pulse). We also note that because of the profile of the clock, we will always have amplitude jitter. It is impossible to remove this amplitude jitter demonstrating why we would always prefer to have as temporally square clock pulse.

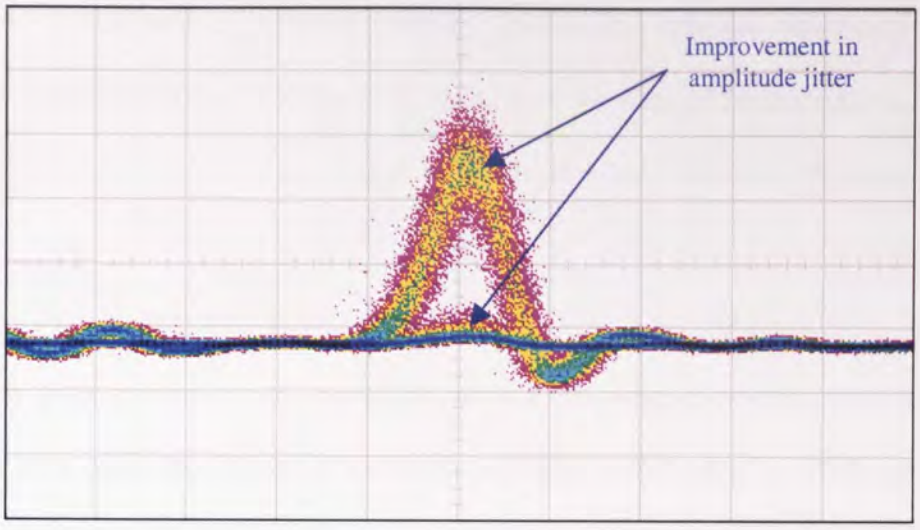

Figure 5.36: The output that is produced still suffers from timing jitter but has less amplitude jitter than the input

Thus, we find here that in order for wavelength conversion to occur, some chirp must of course be present in the initial clock. However, providing that there is a small amount of chirp present, the temporal profile of the clock only effects the level of amplitude jitter that is produced.

5.8 Demonstration of 20Gbit/s operation using 2 ring lasers and two SOA's in an optical waveguide

It has been demonstrated both experimentally and through numerical simulation that the timing jitter reduction/phase wander suppression system can operate error free at 10Gbit/s. However, it has also been suggested that there is no reason why this scheme cannot operate at significantly higher repetition rates. To demonstrate this we will now show, within a laboratory environment, that 20Gbit/s is readily achievable (note, there was only

an increase of 10Gbit/s as we were unable to obtain the required equipment needed to operate at 40Gbit/s and beyond). In order to achieve the desired increase in repetition rate to 20Gbit/s it was decided to use a dual SOA based Mach-Zehnder interferometer [105] optical waveguide [106-108] to perform the optical AND gate function instead of the NOLM, which has been used prior to this juncture. This is simply because of the required increase in peak power which would be needed to optically switch data through the NOLM is very high. In Chapter 1 we discussed how when using an SOA based, device such as a TOAD, the required peak power needed to achieve full π switching would generally be significantly less than the peak power required to achieve the same π switching in a NOLM. As the repetition rate doubles (from 10Gbit/s to 20Gbit/s) the peak power required to reach the π phase shift in the NOLM also doubles. Thus, it is easier if we use the MZI as it requires much less power in order to switch (the MZI was a proprietary design and was manufactured at Corning Research Centre. At the time of usage, this device was not commercially available). Another advantage of this device is that it will not suffer from extrinsic fluctuations in the same way that the NOLM did.

A schematic of the dual SOA based Mach-Zehnder interferometer is shown in Figure 5.37. All though this particular device was not commercially available at the time of usage, similar devices have been reported [58, 86, 109-113].

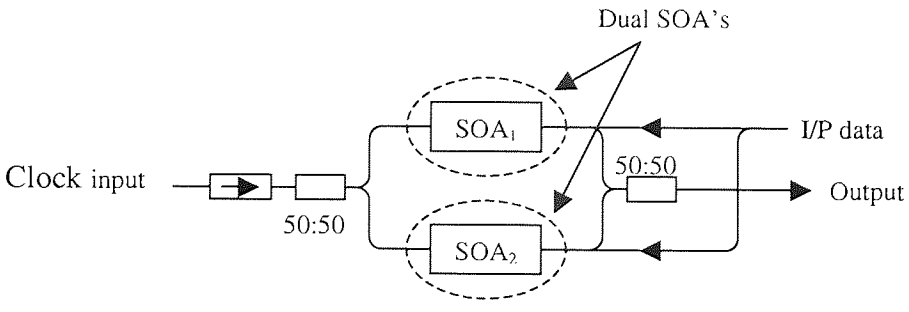

Figure 5.37: Schematic of integrated SOA based all-optical switch

Figure 5.37 only shows the new optical sampling device, clearly the locally generated clock still needs to be propagated through the 2.2km of nonlinear fibre in order to generate the chirp and at the output of the Mach-Zehneder interferometer, an appropriate level of dispersion compensation will still be required. By applying the data in the opposite direction to the clock, we remove the need to filter of the unwanted original data pattern. Thus, this device simply replaces the NOLM used in previous experiments and simulations.

To achieve the initial 20Gbit/s data rates, two different Pritel ring lasers were used, both multiplexed to 20Gbit/s (one ring laser was used as the locally generated clock source, operating at 1538nm and the other was used as the data source operating at 1558nm. Figure 5.38 shows the configuration required to achieve 20Gbit/s switching in the MZI.

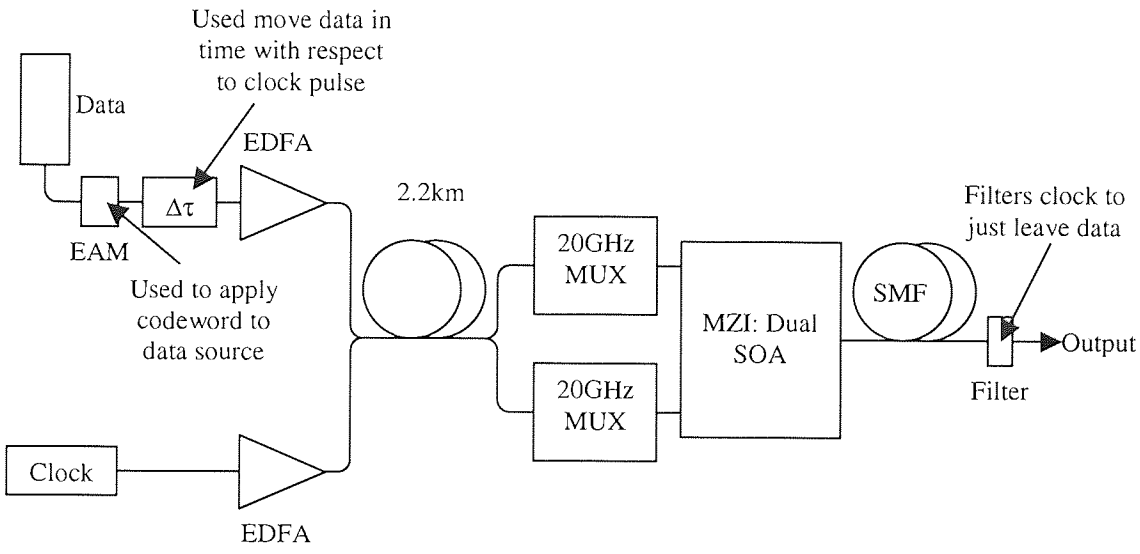

Figure 5.38: Schematic of the experimental arrangement used to achieve 20Gbit/s switching using two ring lasers and a dual SOA based MZI optical waveguide

An 8-bit word is applied to the data source (operating at 1558nm) via the EAM. This is then propagated through the 20GHz MUX to produce a 16-bit 20Gbit/s code word of '1111110011001100'. Because the data pattern was multiplexed, we naturally get a repeated pattern; hence each individual bit is effectively seen twice. This is why we always have two successive 1's or 0's. However, the output pattern, at 20Gbit/s is exactly the same as the input pattern. Thus, we can say that we are now operating at a full 20Gbit/s (Figure 5.39).

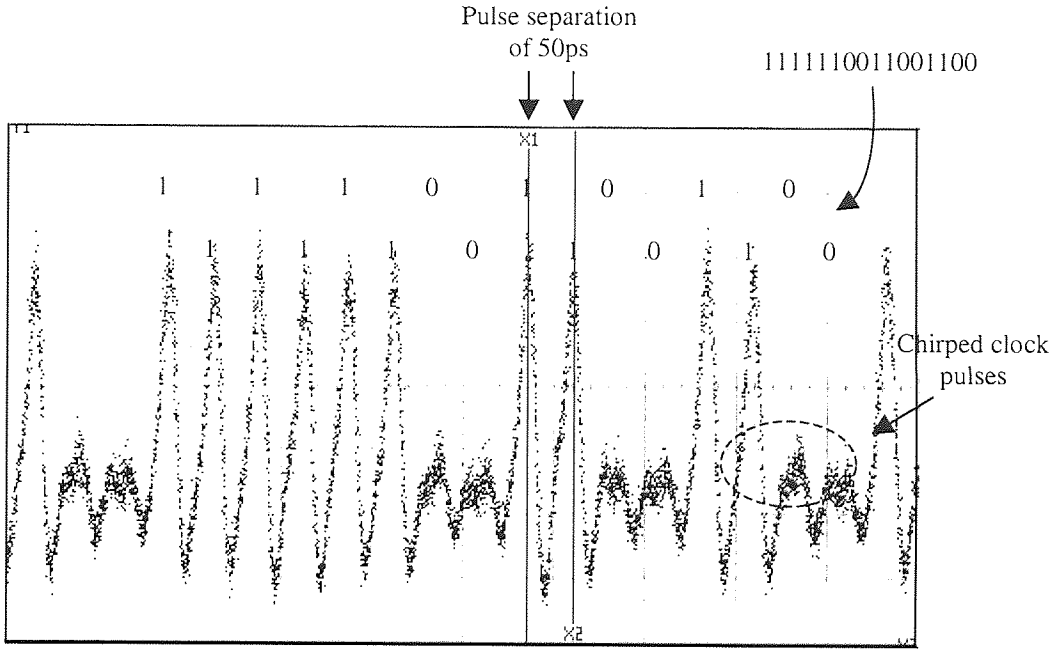

Figure 5.39: 20Gbit/s operation is achieved using two ring lasers (initially operating at 10Gbit/s but then multiplexed up to 20Gbit/s) and the MZI

The two markers seen on the sampling oscilloscope trace in Figure 5.39 (X1 and X2) are separated by exactly 50ps which further confirms that the system is operating at 20Gbit/s (as 50ps is the equivalent bit period). We do however see that the chirped clock pulse leaks through at the output. This is why our '0' base line is not completely flat. Providing that there is an appropriate threshold level at the receiver, this is not a problem, with

further investigation and tailoring of some of the parameters this could be minimised. One possible reason for why these extra peaks appear is that the polarisation of MZI was not correctly balanced to produce the maximum extinction ratio between the '0' and the '1'. It can be noted that no BER's at 20Gbit/s (or higher) are found within the experimental section of this thesis. This is because at the time that the experimentation was carried out, a 20Gbit/s BERT was unavailable.

5.9 2-stage 3R regenerator

It has been previously discussed that the all-optical, timing jitter/phase wander reduction scheme has several different uses. It has been shown that device could be used as both a jitter reduction scheme as well as an all-optical clock recovery unit which would be used at the end of either a long-haul transmission system or at the nodes in an optical network. However, with the addition of a second stage, the device could also be used as an all-optical 3R regenerator (simulations in sections 3.6 and 3.7 showed that a 2-stage device would be feasible). The same schematic, discussed in the previous section, is used as the first section of the device and the output of stage 1 is then fed into the input of a dual SOA Mach-Zehnder interferometer (another NOLM, identical to stage 1 could be used here instead of the MZI. The MZI was used purely for convenience), Figure 5.40. It should also be obvious that there is no reason why stage 1 and stage 2 could not be used the opposite way around, if this were the case, the following results would look pretty similar.

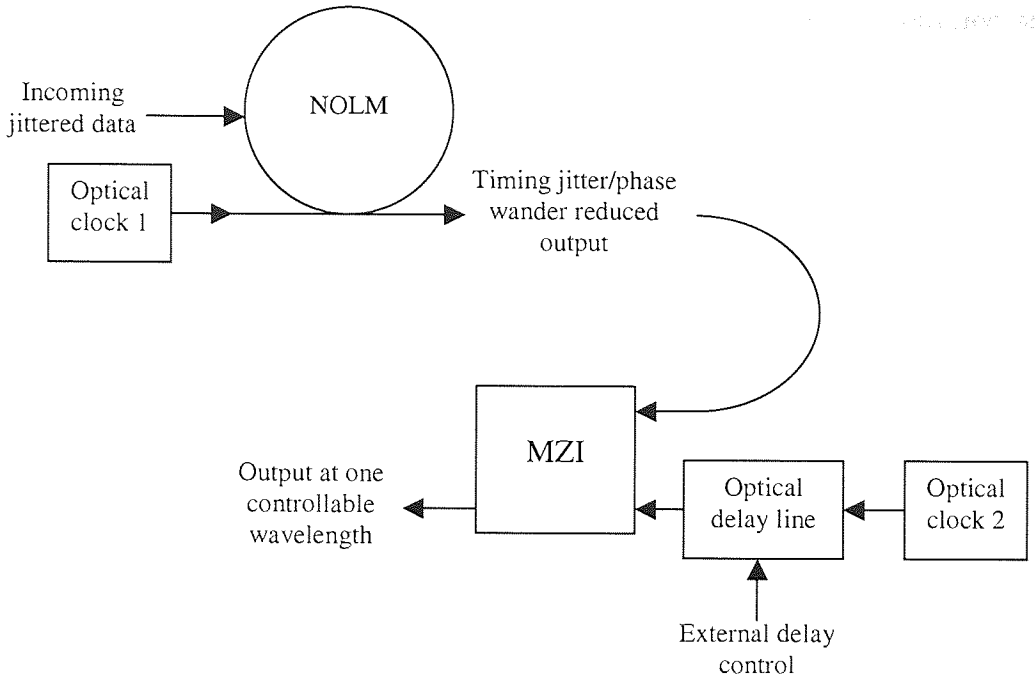

Figure 5.40: Schematic diagram showing how a 2 stage device could be used to produce a full, all-optical 3R regenerator

The second stage is required as the output of stage 1 does not have a constant wavelength (as the timing jitter and phase wander is reduced by means of wavelength conversion, there is the potential that each individual bit, or in fact word, will have its own unique wavelength. This is not a problem if the output is then simply passed into a BERT for example, but would be disastrous if it were instead allowed to propagate as the dispersion effects of any subsequent fibre would introduce yet more timing jitter and phase wander). We can however, use the wavelength conversion to our advantage once more by allowing the second stage to convert all of the data back to one wavelength (because we now know the exact timing position of the data, we are able to convert all of the data to any given wavelength that falls within a second locally generated chirped optical clock pulse). Of course one could easily convert, within stage 2, to the original incoming data's wavelength, pre-stage 1, and so we would have a "conventional" 3R regenerator.

However, another level of flexibility is incorporated by adding a controlled amount of timing delay, a brand new, completely different wavelength could in fact be produced. There is of course no reason why this new delay, $\Delta\tau_2$, could not be controlled remotely using, for example, a change in electrical power to alter $\Delta\tau_2$. This extra flexibility could be incredible useful in an optical network situation where at a node the data could be regenerated and at the same time a new wavelength formed for further propagation through the network.

It would appear as though demonstrating a practical laboratory device would be trivial and indeed it should be, however, there were many problems with the electrical timing of the 2-stage device. Problems occurred when trying to electrically synchronise together all the signal generators and detectors, however, these teething problems were related to laboratory problems rather than to problems associated with the principles of operation.

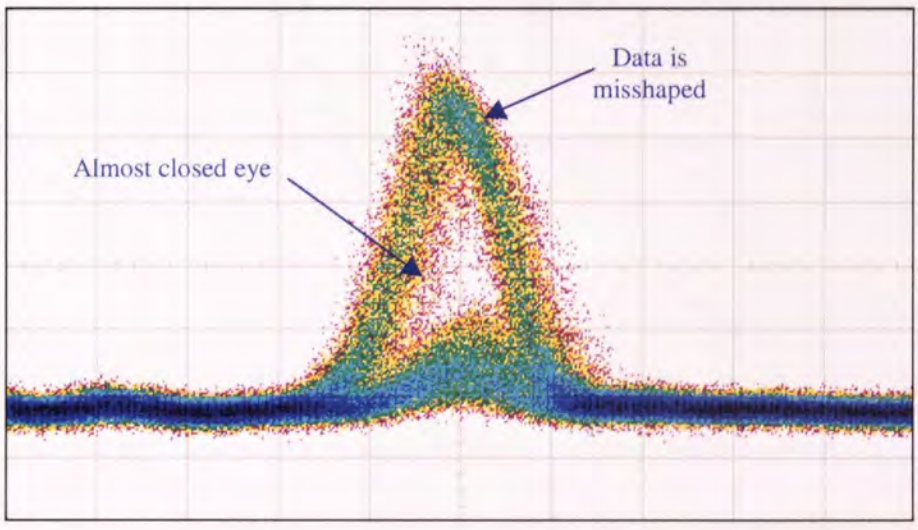

Figure 5.41: The closed eye and misshaped data makes error free transmission impossible

This means that the second clock pulse (chirped in this particular case) moves with respect to the initial data input making BER measurements impossible. If we now take a badly timing jittered and almost closed eye as the input to the 2 stage device (Figure 5.41) we can see that we would not be able to accurately distinguish the initial transmitted word. Comparing Figure 5.41 with the final output of the 2 stage device, Figure 5.42, we see that there has been a clear improvement over the shape and integrity of the eye. However, due to the "breathing" effect of the 2 stage device, BER curves were not obtainable.

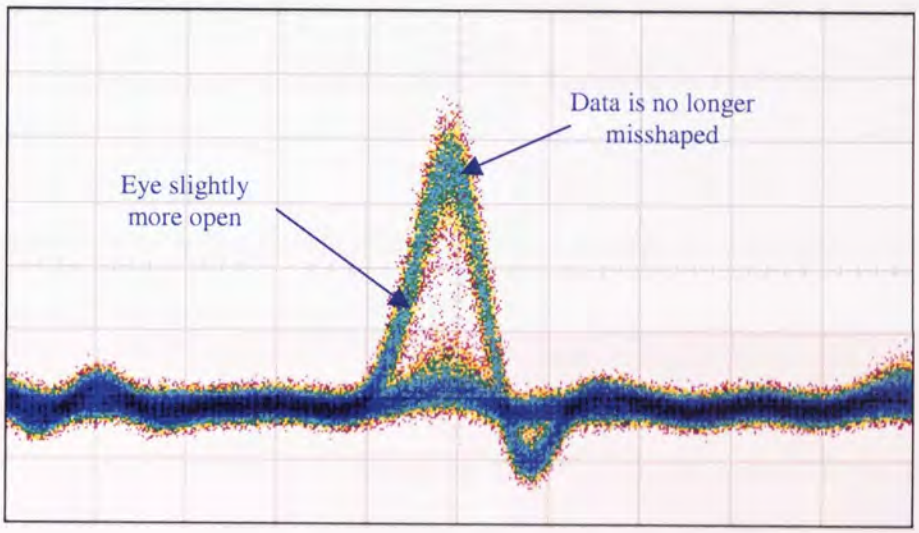

Figure 5.42: After the 2-stage device the data has undergone full 3R regeneration

It can also been seen in Figure 5.43 that using this 2 stage device a very clean eye can be achieved (although the input to the initial system was distinctly better than that of Figure 5.41). Because it was not possible to obtain BER's, a known word was propagated through the 2 stage device and the triggering altered so that the full output word could be observed rather than the eye. By matching the two words, it was confirmed that the propagation through the 2 stage device could potentially be error free.

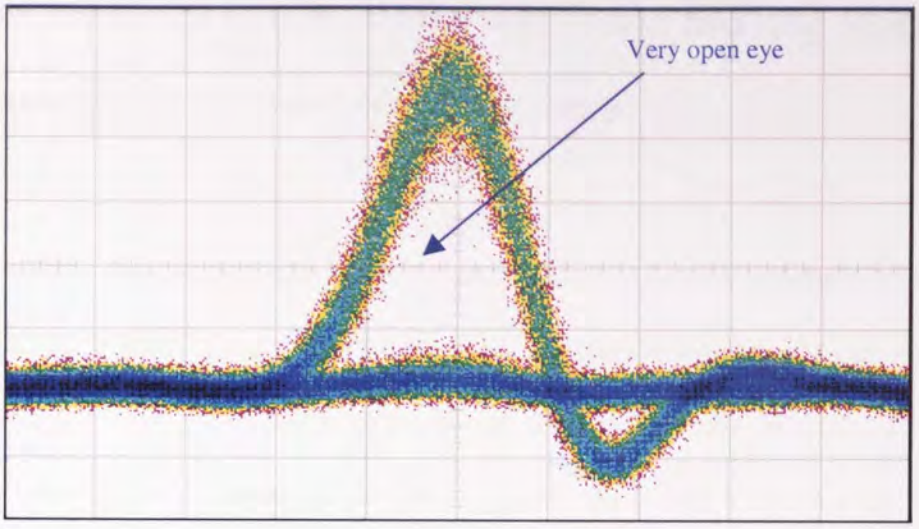

Figure 5.43: With careful set-up of the 2-stage device and better quality input than before, a very good eye can be produced at the output of the device

Another useful feature is that the chirped clock pulse of stage 2 of the device doesn't have to be square at all, or in fact contain any chirp. There is no reason why this second clock pulse couldn't simply have a Gaussian profile generated from any one of a whole host of sources. If this were the case, then changing the delay of the second clock pulse with respect to the output of stage 1 would have no effect and the new wavelength. In this instance the final produced wavelength would always be at the same wavelength of the second clock source.

5.10 Generation of errors using a NOLM and two ring lasers operating at different repetition rates

We now need to ask the question, what happens when the locally generated chirped clock pulses overlap in time? More importantly, what happens when the chirped clock pulses overlap and the data pulse happens to fall at that exact point in time? One way of achieving this is to use a mismatch in repetition rates. By letting the data source operate at 10Gbit/s but at the same time letting the chirped clock pulse operate at 20GHz (using the previously discussed MUX) we have a mismatch in repetition rates. This mismatch in rates is used to demonstrate how errors can potentially arrive and now we can actually see the problem physically arise. As the chirped clock source now only has a pulse separation of 50ps (at 20GHz), using the optical delay associated with the MUX unit, we can manipulate the chirped pulses so they do in fact overlap in time slightly at the edges (the chirped clock pulse is not allowed to broaden too much so that we can control the amount of overlap that occurs). The data is now given a specific 8-bit code word of '01000000'. This is to ensure that we only ever have one specific '1' that we are dealing with, this is used to minimise any confusion. We now start with the data sampling what we define as the "start" of the first chirped clock pulse, Figure 5.44.

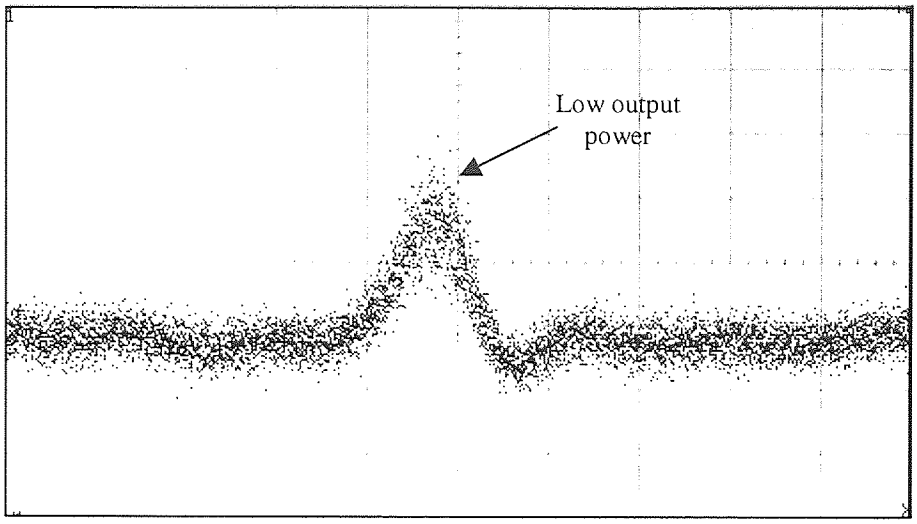

Figure 5.44: $\Delta\tau$ = 5ps. The point in time where we first start to sample clock 1

The data is then moved with respect to the clock pulse by increasing $\Delta\tau$. As we move further toward the centre of the chirped clock pulse the output power increases, which gives us an indication that clock 1 is not entirely square (this is not important for this demonstration).

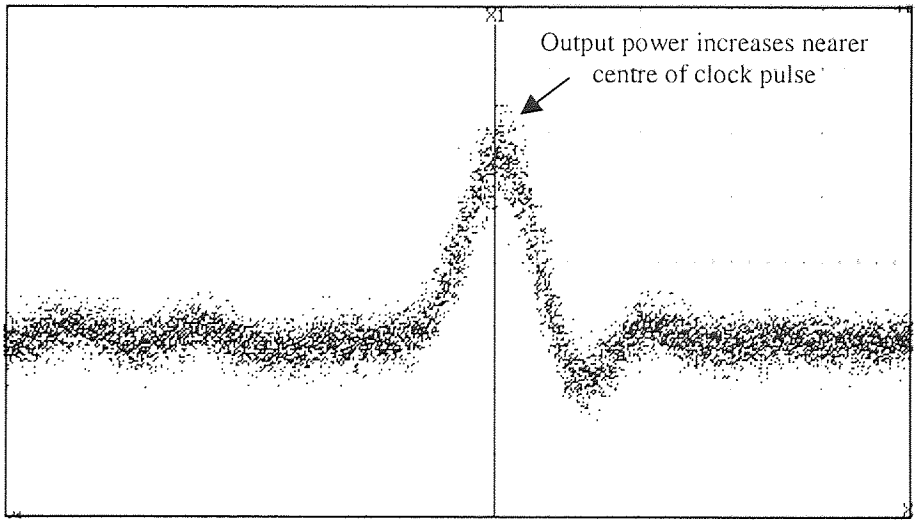

Figure 5.45: $\Delta\tau$ = 8ps. The increase in timing delay shifts the sampling point nearer to the centre of the chirped clock pulse and so the output power increases

A further increase of 8ps pushes the data even further through clock 1, up to the point at which clock 1 and clock 2 overlap. Because of the overlap, the data actually samples both clock 1 and clock 2 simultaneously and so thus, two 1's are generated instead of the desired single '1' (this is illustrated by a "double pulse" shown in Figure 5.46). This is clearly a problem as we have now actually generated an extra '1' thereby changing the initial codeword that we were actually trying to transmit in the first place. The original codeword was '01000000', but due to the error that has just been generated, the new codeword would be '01100000'.

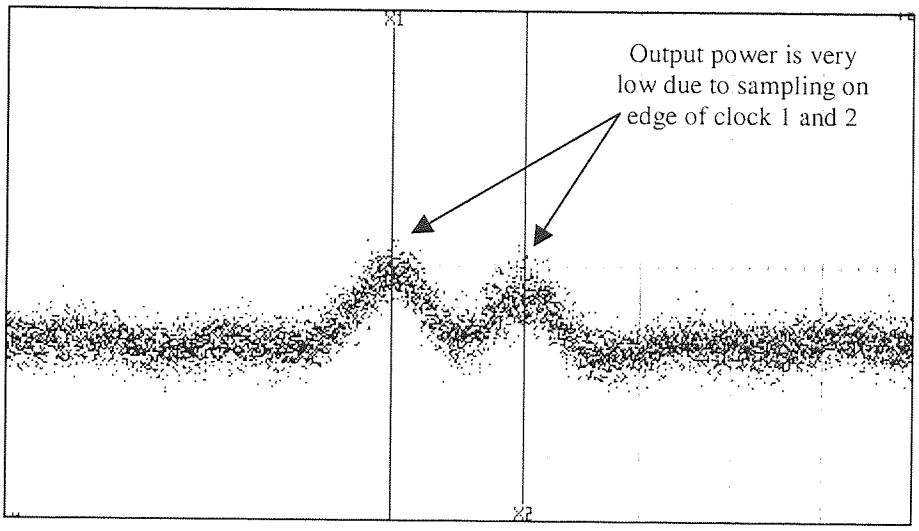

Figure 5.46: $\Delta\tau$ = 15ps: The double pulse produced illustrates that the newly generated codeword is now wrong, the output should only contain one single pulse

With yet another increase in $\Delta\tau$, we now only sample the second clock pulse (clock 2) shown in Figure 5.47. The new pulse is approximately 30ps away from where the first pulse (clock 1) was produced (we should note that $\Delta\tau$ has only moved by a change of 20ps, not 30ps. The reason for this apparent discrepancy is simple. Although sampling clock 2 may seem like an error, both jitter reduction and phase wander suppression will

still occur as clock 1 and clock 2 are effectively identical. Thus, the SMF at the end of the system, used for the dispersion compensation, will drag the second '1' into the desired place, the centre of the clock pulse).

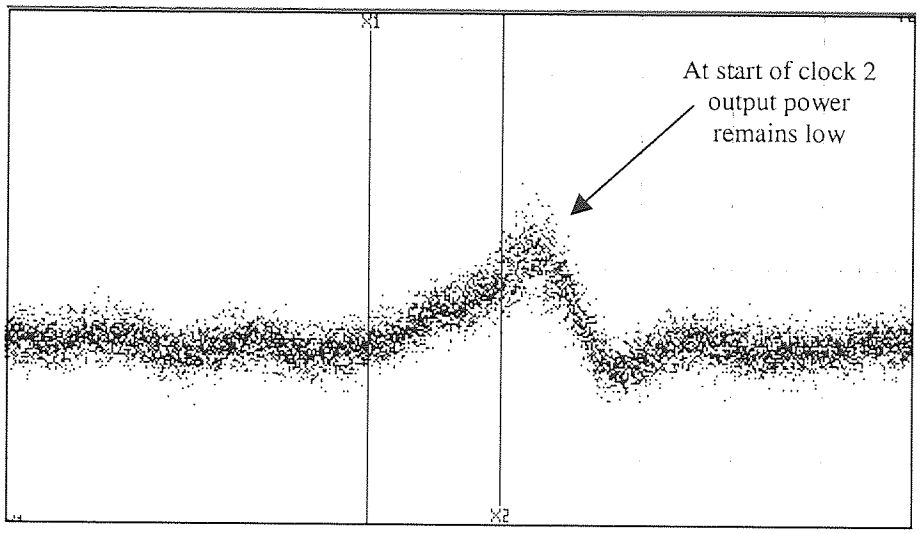

Figure 5.47: $\Delta\tau = 28$ps. The edge of clock 2 is now being sampled instead of clock 1. As it is at the edge, the output power remains low

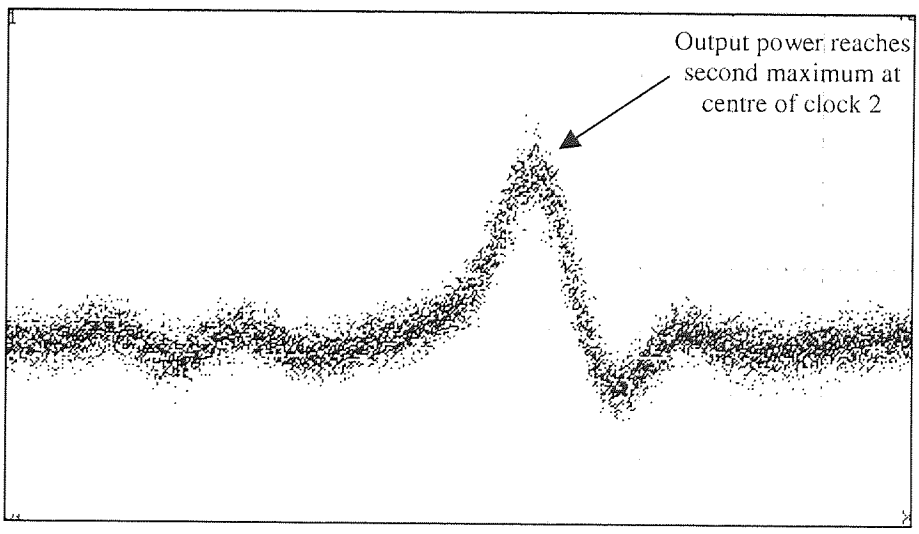

Figure 5.48: $\Delta\tau = 31$ps. The sample now occurs in almost the centre of clock 2 and hence, the received output power is once again at a maximum

By increasing $\Delta\tau$ further still, the output power reaches a maximum at the centre of clock 2, Figure 5.48.

If $\Delta\tau$ were to be increased even further (by another 74ps) we would see the exact same pattern repeat. At first glance it may seem as if the pattern should be repeated before this, however, we should remember that the two clock pulses are not evenly spaced in time because the second clock pulse was shifted as it passed through the MUX.

We need to remember that although this limitation was demonstrated using a NOLM, the same error will be incurred when using any switching device to sample the chirped clock pulse. Thus, simply switching to say the dual SOA based Mach-Zehnder interferometer will not elevate this problem.

5.11 Discussion

In this chapter the author has demonstrated the feasibility of the timing jitter and phase wander reduction scheme. It has been shown, experimentally, that firstly the scheme works and secondly, and more importantly, that it works error free. It has been shown that this scheme can be utilised as an all-optical clock recovery unit which would be placed at the end of an optical point-to-point link or in an optical network. This would remove the need for the relatively slow electronics (an all-optical clock recovery unit could not only operate at significantly higher data rates compared to an electrical clock recovery unit, but also suffers from far less latency) and potentially costly electronic counter part. It has also been shown that with the addition of a second stage to the device, we are left with an all-

optical, single channel, 3R regenerator that could be used in say, an undersea transatlantic optical transmission. The device successfully exhibits the three characteristics required to be a 3R regenerator, re-amplification, re-timing and re-shaping whilst simultaneously reducing both timing jitter and phase wander. The second stage is required, however, if it is to be used as 3R regenerator as the timing irregularities are translated into wavelength conversion. This means that each successive section of data could easily leave the device with a unique wavelength.

It has also been shown experimentally that practically, the device can operate at higher repetition rates, 20Gbit/s, and still maintain its functionality (although of course some parameters have to be adjusted to facilitate this increase). This is important as in the future, significantly higher data rates will dominate the globe. It is at this stage that an all-optical approach to both regeneration and clock recovery becomes much more attractive than the current, conventional electrical approach.

Some limitations were also discovered within this chapter that had previously not been considered. In the simulation chapters, the problem of extrinsic fluctuations such as temperature changes had not been investigated. It is almost trivial to overcome this problem and simply encasing the all-optical device inside an insulated, temperature maintained chamber removes this problem entirely. An alternative to this would be to use the dual SOA based Mach-Zehnder device (discussed in chapter 5.8). The small packaged device will only suffer from extrinsic fluctuations in the extremists of cases and the nonlinear fibre required to produce the chirped clock pulse can be accommodated inside another small package. We have also seen experimentally that care needs to be taken when setting up the device to ensure that the locally generated chirped clock pulses do not

overlap in time with the next successive time slot. When this happens, and the data falls at this intersection, errors will be generated. Although this is a limitation of the system, with care this can easily be avoided.

Chapter 6 - Phase wander reduction using single length of fibre

6.1 Introduction

There are of course many different ways in which wavelength conversion can be used to compensate for both timing jitter and phase wander. So far we have concentrated on using different types of optical AND gates to sample a linearly chirped, nominally square clock pulse. In this chapter we will look at a slightly different method which does not rely on either generating a chirped clock pulse or using an optical AND gate. Instead we use XPM (which is also the basic fundamental operating principle in the previously used optical AND gates) between a locally generated clock pulse and the incoming data stream. This is used to apply wavelength conversion in a single length of nonlinear fibre. The clock is removed using an optical filter and after propagation through a length of fibre used for dispersion compensation, timing jitter and phase wander is found to be reduced. All of the following results were achieved using computer simulation, using VPI, and are presented without any laboratory results for corroboration.

6.2 Wavelength conversion a single length of nonlinear fibre

Before we address the problem of trying to reduce either timing jitter or phase wander we must firstly attempt to produce a system that can achieve wavelength conversion using a single length of nonlinear fibre (without the aid of an optical AND gate to perform the optical sampling function). The following experimental setup was created in VPI. The

data source produced Gaussian pulses at 1576.2nm with a FWHM of 3.3ps. The clock source also produced Gaussian pulses with a FWHM of 10.0ps and at a wavelength of 1530.2nm.

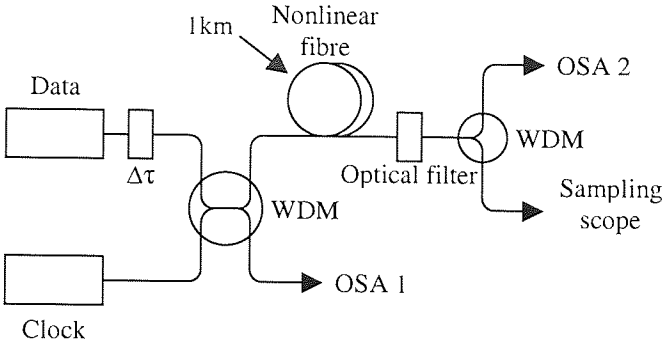

Figure 6.1: Schematic of wavelength conversion scheme

OSA 1 is included so that we can easily compare the output of the system with that of the input. By varying $\Delta\tau$ (the timing difference between the data and the clock) we are able to walk the data through the clock pulse. The optical filter then removes the clock from the data. The nonlinear fibre parameters are based on a short length (300m) of highly nonlinear fibre (HNLF) provided by Sumitomo. By monitoring the output produced at OSA 2 we can see if any frequency shift has occurred. All of the results are superimposed on top of each other and shown in Figure 6.2 (each trace corresponds to a change in $\Delta\tau$).

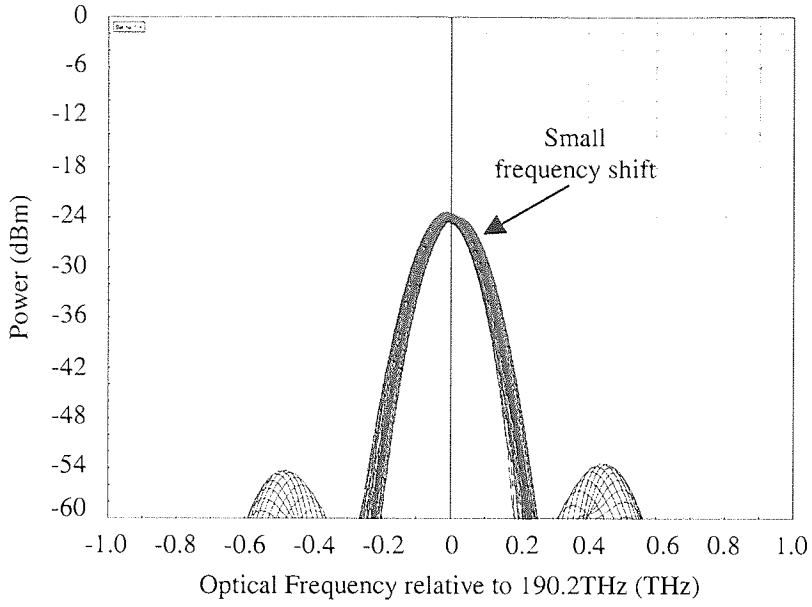

Figure 6.2: As the data and the clock walk through each other, the data is shifted in frequency because of the effects of XPM

This simple demonstration shows that as the data is walked through the clock, the frequency of the data produced changes. This frequency shift (or wavelength shift) is dependant on the timing offset of the data with respect to the clock and so the timing offset is dynamically converted into a specific wavelength shift (which is the foundation of the timing jitter and phase wander reduction scheme used throughout this thesis). From this we can hypothesise that with the addition of a dispersion compensation module, we could compensate for both timing jitter and phase wander. The corresponding sampling oscilloscope traces are shown in Figure 6.3. Again, all of the results are superimposed on top of one another, however, the entire bit period (100ps) is not shown.

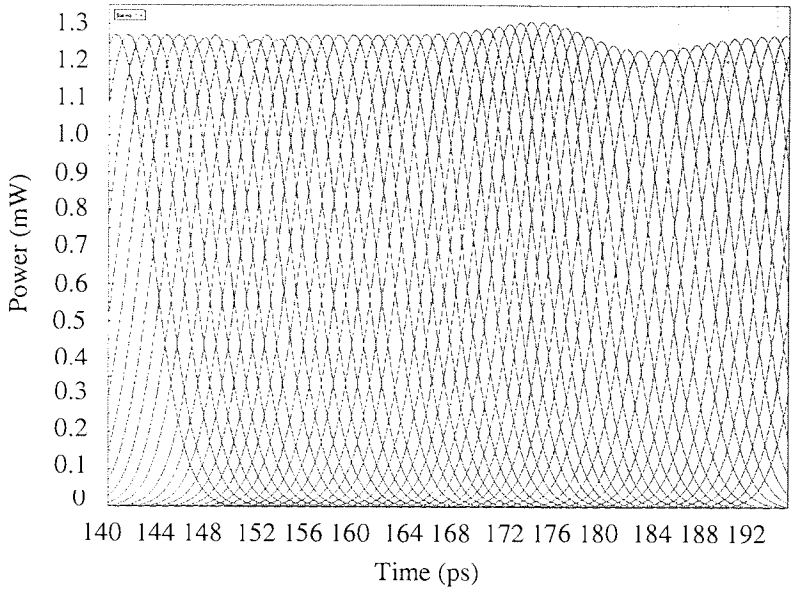

Figure 6.3: The temporal profile at the output of the system shows that there is hardly any change in produced peak power irrespective of timing delay

From the previous two graphs we can exactly measure both the wavelength shift that is produced by the XPM and the peak power change that is produced. These results can be seen in Figure 6.4.

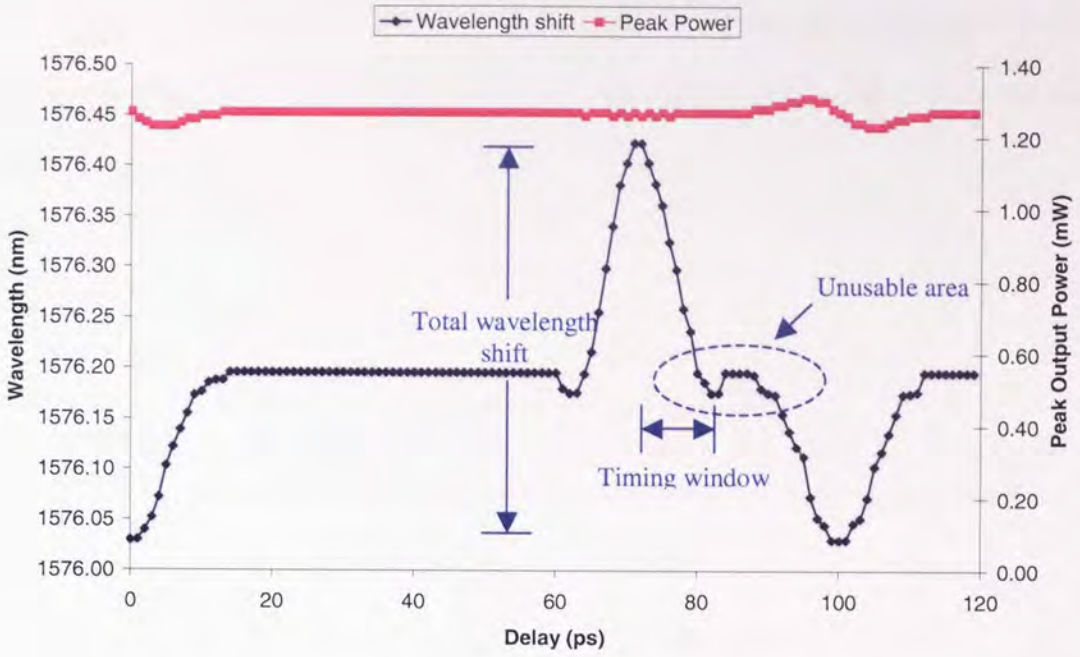

Figure 6.4: As the data sweeps through the clock pulse wavelength conversion occurs

There are two potential problems with the above graph. Firstly the maximum wavelength shift is very small (only 0.39nm in total). This could however be increased, if so desired, by increasing the nonlinear element (which in this case would involve either increasing the length of the nonlinear fibre or increasing its nonlinear coefficient by say reducing the core area of the fibre). Secondly, we cannot use the timing window which spans the total wavelength shift as in the centre of the shift there suddenly is no wavelength shift at all. This not only means that this portion of the timing window is not useable, it also implies that we will only be able to use the region where there is either a positive, or negative wavelength shift. Thus, the maximum available timing window is reduced to only 11ps. This is because the data and the clock propagate at different speeds along the fibre and so walk-off occurs between the two channels. The overall lack of wavelength shift occurs because of the dispersion in the nonlinear fibre.

The length of the nonlinear fibre was then doubled to 600m (from the previously used 300m) and the simulation repeated (note, all other parameters were exactly the same as before).

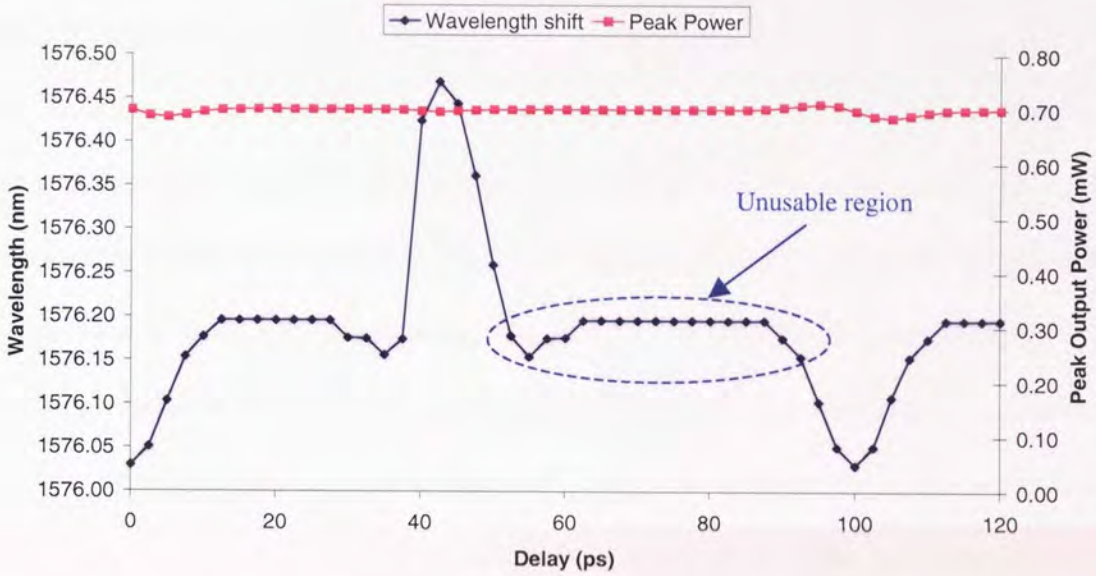

Figure 6.5: With an increase in fibre length there is even more walk-off because of the increase in dispersion

The increase in fibre length has naturally increased the level of dispersion. Thus, this has increased the amount of walk-off that occurs between the two different channels. This can be seen by comparing the unusable region in Figure 6.4 with that of Figure 6.5. In Figure 6.5, the unusable region is significantly increased to 32.5ps. Even though the length of fibre has been increased, there is still only a relatively small total wavelength shift of only 0.44nm.

6.3 Wavelength conversion using nonlinear fibre with zero dispersion and dispersion slope

The problem of walk-off occurs between the data and the clock pulse because during propagation the two pulses, at different wavelengths to each other, experience different levels of dispersion and hence, propagates at differing speeds to one another along the fibre. This appears to have the effect of increasing the FWHM of the clock as there is an increased amount of time where interaction between the two channels occurs. This effect can easily be removed by choosing a fibre with a zero dispersion slope, D' = 0ps/nm/km (if this were a laboratory experiment, obtaining fibre with D' = 0ps/nm/km over the wavelength range in which we are operating could be tricky and as alternative, choosing a fibre with an appropriate dispersion slope and D_0 falling in the centre of the two pulses so that both the normal and anomalous channels experience the same net dispersion is an option). However, as the following results were obtained using computer simulation, the simplest approach is to set both D_0 and D' to be zero. The peak pump power was set to 2W with a FWHM of 10ps and $\Delta\tau$ was varied in 1ps steps over 120ps range. As the repletion rate for both the data and the clock was 10GHz, the 120ps range means that we cover slightly more than one single bit period. The simulation schematic shown in Figure 6.1 was used to produce the following results.

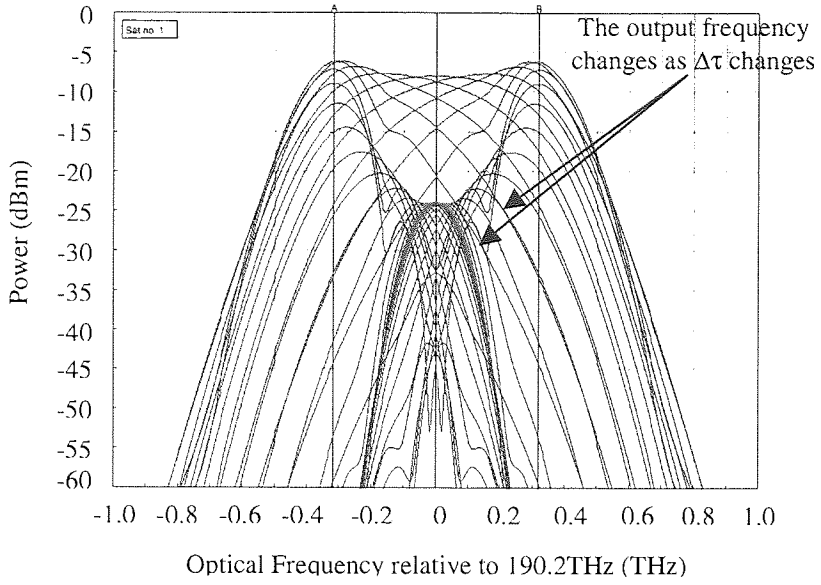

Figure 6.6: Optical spectrum showing how the frequency of data changes after XPM in the nonlinear fibre

The optical spectrum of the output of the system is shown Figure 6.6. The figure shows all of the 120 output traces produced all superimposed on top of each other (as $\Delta\tau$ was increased in 1ps increments). As $\Delta\tau$ changes, the output frequency (and therefore wavelength) changes accordingly. From this we are able to obtain a fixed output wavelength simply by fixing $\Delta\tau$ to a desired value. The corresponding sampling oscilloscope traces are shown in Figure 6.7. As in the previous figure, all of the 120 traces have been superimposed on top of each other and show the evolution of the output.

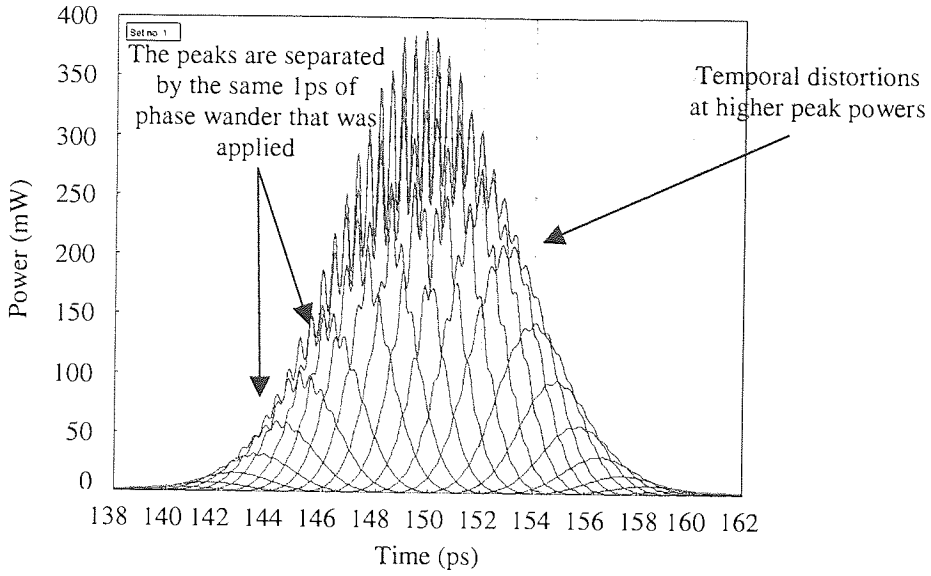

Figure 6.7: The output power changes as $\Delta\tau$ and therefore the produced frequency changes

The distortion that has occurred on the temporal profile of the shifted data is due to the filter used at the output of the system but for this demonstration, this aberration is not a problem. At the point at which we go from a positive to a negative frequency shift the maximum peak power is produced. As there was no dispersion compensation used at the output, we see that there is still the 1ps of phase wander between each successive pulse, which was applied by $\Delta\tau$, is present at the output. The frequency shift and peak power variation that is obtained from the previous two figures is translated into the following graph.

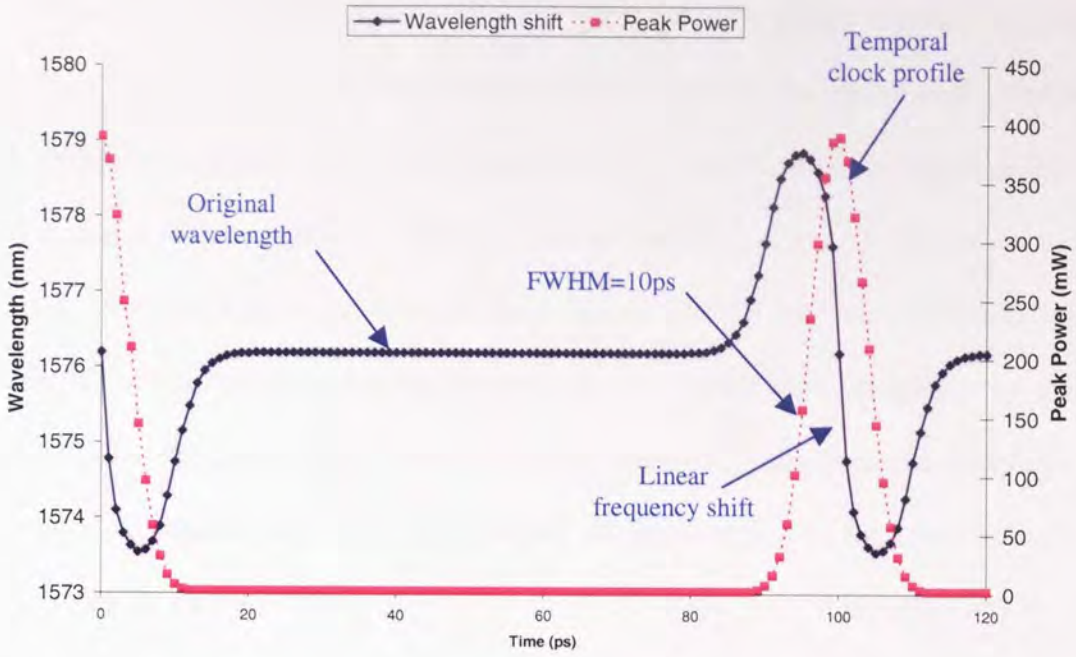

Figure 6.8: As $\Delta\tau$ is swept through 120ps, the temporal profile of the clock is measured at the same time as the wavelength that is produced

As $\Delta\tau$ is increased, because of the effects of XPM in the length of nonlinear fibre, the data undergoes a wavelength shift. If we measure this wavelength shift and plot it as a function of $\Delta\tau$ we see that there is a positive wavelength shift followed by a negative wavelength shift. This is as exactly what we would expect after XPM and the principle is explained in chapter 1. At the same time we can measure the peak power as a function of $\Delta\tau$. Because the dispersion of the nonlinear fibre, along with the dispersion slope of the fibre, has been set to zero, the clock pulse's duration does not increase and so the profile that we are left with is the same as that of the original clock pulse (the fibre does still contain a certain amount of attenuation and so the peak output power that is produced has dwindled). In the previous simulation we were able to obtain a maximum of 5.31nm of wavelength shift.

It is interesting to note that if we compare Figure 6.4 with Figure 6.8 and specifically looking at the frequency shift, we see that there is a point in the centre of the frequency shift, which corresponds to the same timing delay as the centre of the pulse in the time domain, that it is not linear and in fact the frequency shift goes to zero. This is because of the walk off caused by the dispersion in the nonlinear fibre. If we were to think ahead and consider the phase wander reduction problem, we will realise that it is imperative that we have a linear frequency shift over our timing window. Thus, we can conclude that although it may appear that the timing window will be increased by the effect of walk off, as the region in which XPM happens is increased, the converse will happen and we will in fact have half of the useable timing window.

6.4 Phase wander reduction using a single length of nonlinear fibre

We have now shown, in section 6.3, that it is possible to take an incoming data channel and by propagating it along side a local clock (through the same length fibre), we can dynamically shift the wavelength according to the relative timing displacements of the two channels. We now need to see what happens if we choose an appropriate level of dispersion compensation to try and re-time the data channel suffering from the applied phase wander. Using the same computer simulation as before, the FWHM of the clock pulse was increased to 50ps (an increase of 40ps from the previous section) while the dispersion and dispersion slope of the nonlinear fibre were kept at 0.

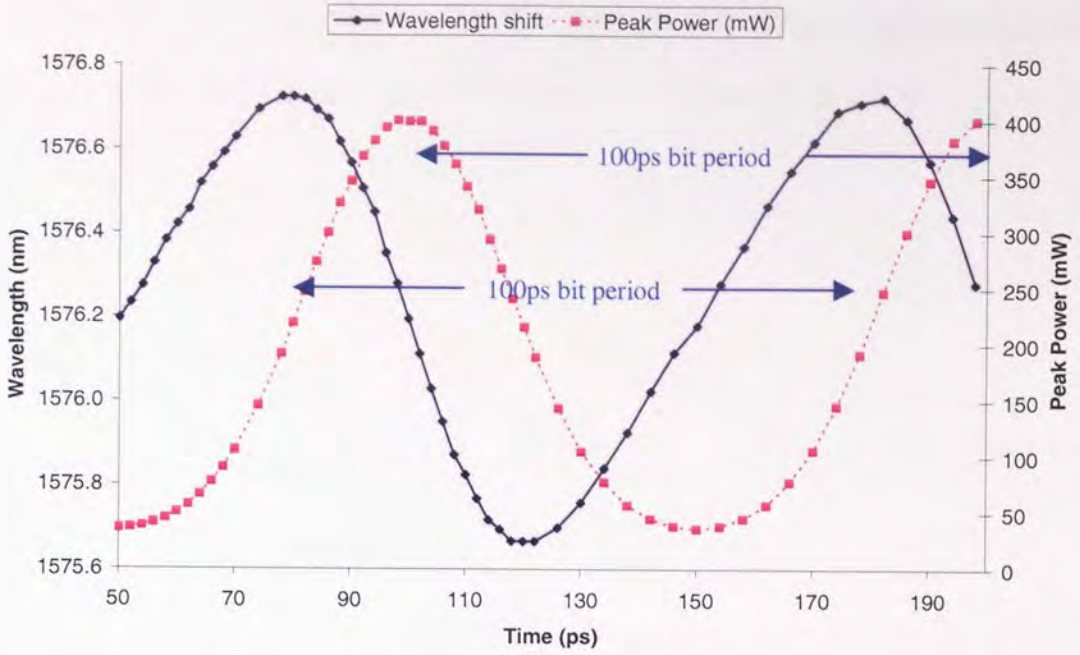

Figure 6.9: Because the FWHM of the clock has increased, adjacent pulses start to overlap in time. The maximum wavelength shift produced is 1.06nm

$\Delta\tau$ was swept through 150ps and the wavelength shift and peak power measured (the results are shown in Figure 6.9). As $\Delta\tau$ goes through the bit period, which is 100ps as the system is operating at 10Gbit/s, the pattern produced at the output repeats. We also see that with the increases in FWHM of the clock, the timing window is naturally increased. As there was no dispersion present in the nonlinear fibre we don't have to worry about the inflection point that would have been present, caused by walk-off, if dispersion was left in the fibre.

We now need to know how much dispersion compensating fibre to use to resolve any timing displacement (any dispersion compensating element will suffice, optical fibre was used in this case). This was achieved by adding 20ps of phase wander to the input data channel, using the optical delay unit to temporally align the data and the clock, and adding

6 individual bits, each separated by 4ps. The temporal displacement was measured after the various lengths of DCF and a graph of the results produced, Figure 6.10.

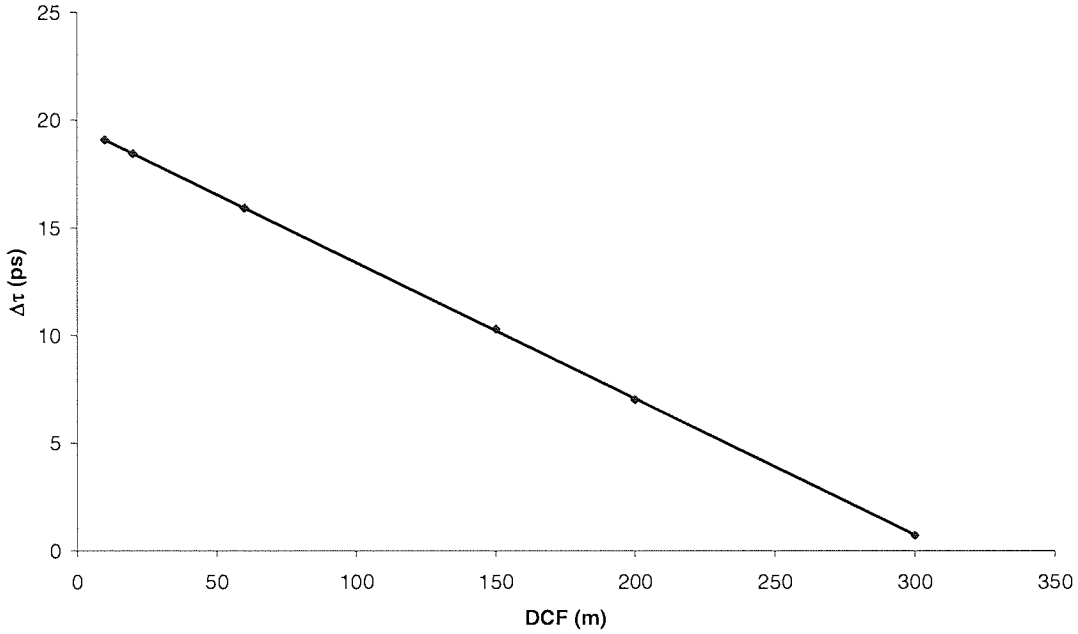

Figure 6.10: As the level of dispersion is increased, the phase wander at the output decreases and a linear relationship is found

A linear relationship is produced with the minimum phase wander of 0.74ps. If the level of dispersion had been increased further we would have seen that there would have been a clear minimum before the phase wander at the output would start to increase. The initial input to the system is shown in Figure 6.11 where the six input data pulses, which were separated in time by 4ps giving a total input phase wander of 20ps, are all shown together on one graph.

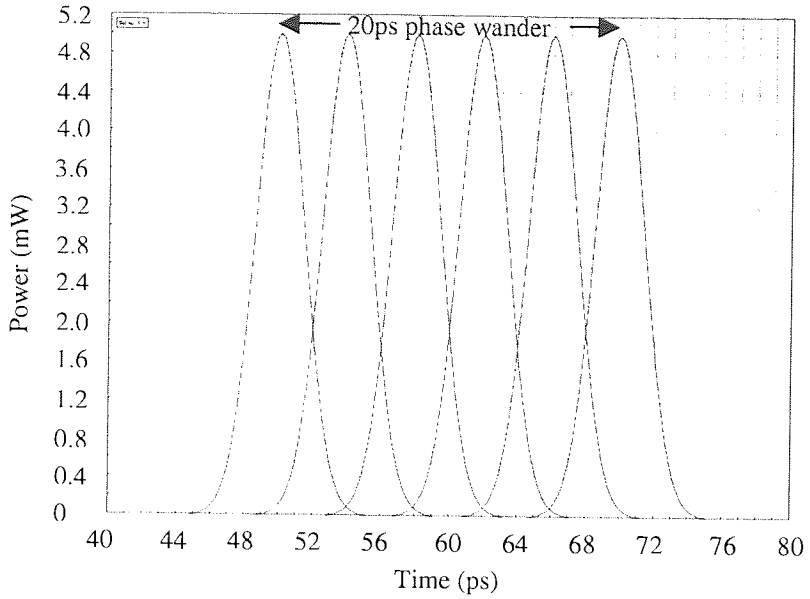

Figure 6.11: There is 20ps of phase wander on the input to the system

The initial input to the system (taken directly after the optical delay unit) contains no amplitude jitter. These six bits are used to represent 20ps of phase wander. For the system to work, at the output there should be no temporal displacement between the six pulses at all and the phase wander will have been reduced. The output of the system is shown in Figure 6.12.

Although the input phase wander has been significantly reduced (virtually no phase wander is present at the output), it has been at the expense of amplitude jitter. As our initial clock pulse had a Gaussian profile, rather than the nominally square chirped clock pulse used in previous chapters, the phase wander (or in fact timing jitter), will be directly translated into amplitude jitter. Of course this problem could be removed by generating a square clock pulse through SPM in highly nonlinear fibre as before, but there would be little point. We could also reduce the amount of phase wander reduction that we can

compensate for compared to the FWHM of the clock. Thus, if we either need to say that we can compensate for less phase wander, or we need to increase the FWHM of the clock.

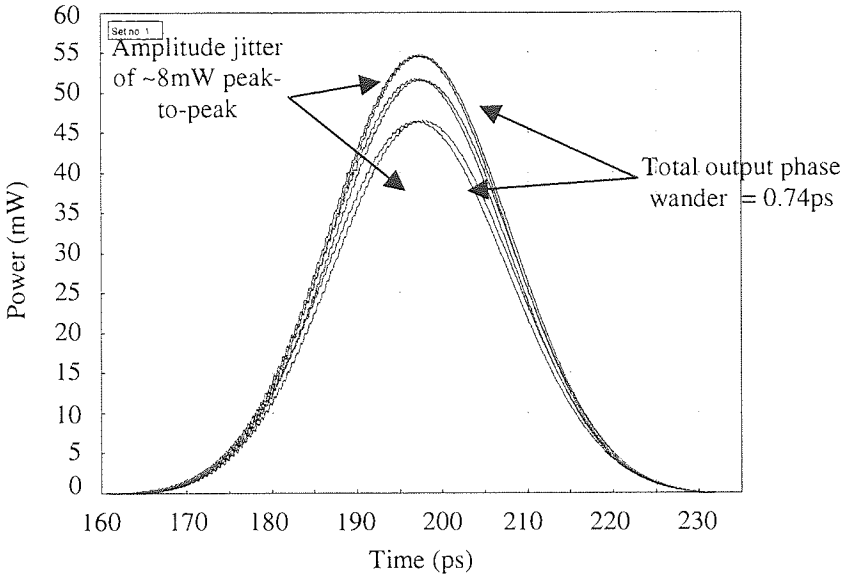

Figure 6.12: The phase wander has been reduced from 20ps down to 0.75ps but at the expense of amplitude jitter

6.5 3R regenerator based on a 2-stage device

It was shown in the previous section that phase wander can be reduced using a single length of nonlinear fibre and a high powered clock pulse. As this is the case, we can make the hypothesis that with a second stage to the device, we should be able to achieve full 3R regeneration. For exactly the same reasons as before, a second stage to the device is required in order to convert the now phase wander suppressed data, back into its original wavelength (or a new wavelength is so desired). By suppressing the phase wander, we have actually converted the data into an entirely new wavelength or set of wavelengths which would cause severe problems if propagation along more fibre were to ensue.

The most obvious way to transform the phase wander suppression schematic into a 3R regenerator is to simply add an almost identical section at the output (the form of section 2 is identical but the wavelength of the second clock source and also the delay of $\Delta\tau_2$ will be different). This is illustrated in Figure 6.13.

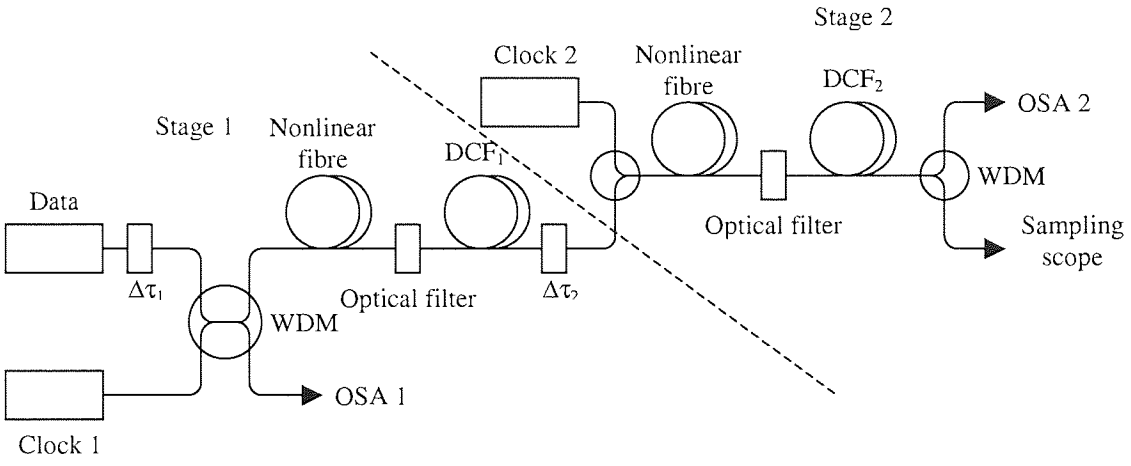

Figure 6.13: 3R regenerator utilising a 2-stage device. The second stage controls the final wavelength produced

By applying phase wander, in the same manner as before, to the input of stage 1 we can test the 3R capability of the system. Initially only a small amount of phase wander is applied, 2ps. With this low level of phase wander we find that the temporal output of stage 1 contains virtually no amplitude jitter. This is then propagated through stage 2 of the device. Initial results (in the time domain) suggest that the 3R regeneration has worked. There is little amplitude jitter and the phase wander has been completely removed. However, closer inspection of the optical spectrum shows that we no longer have a single output frequency (Figure 6.14).

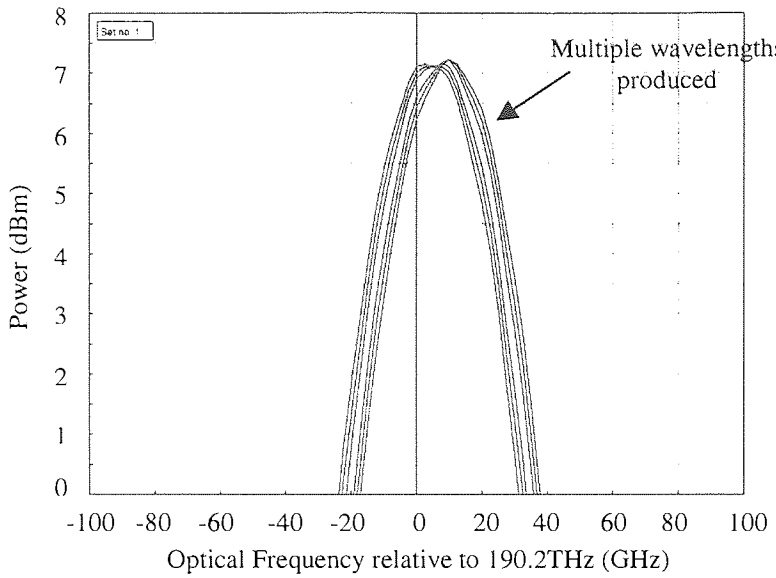

Figure 6.14: At the output of stage 2 of the 3R regenerator multiple wavelengths have been generated instead of the desired single wavelength

These results clearly show a problem. although stage 2 hasn't had any detrimental effect on the output, it hasn't done what it was intended to do and create a single frequency at the output. This not only means that there is no point in having a second stage (which simply adds extra level of un-required complexness) but it also means that this system cannot be used as a 3R regenerator.

Unfortunately it is now apparent that a 2-stage device used as an all-optical 3R regenerator using a single lengths of nonlinear fibre will never work. There are actually two reason why this is the case. Firstly, any slight amplitude jitter that is present after stage 1 will be translated back into phase wander and timing jitter in stage 2, thus rendering stage 2 useless. Because the clock sources in this particular set-up have a Gaussian profile, after XPM there will always be amplitude jitter. We have seen that increasing the FWHM of the Gaussian clock source will reduce the produced amplitude jitter but as the clock

increases, adjacent pulses will start to overlap in time and errors will potentially occur at the output of the system. Thus, if any significant amount of phase wander were to be reduced, this system would prove impractical. Secondly, after stage 1 each bit, or code word, will have a different wavelength. This will be a problem when we try and convert all of the different wavelengths back to a single wavelength using XPM in stage 2 as the level of wavelength conversion that occurs is dependant on not only the relative peak powers of the two channels, the relative timing displacement of the two channels but also on the wavelength difference. Thus, using this method it will never be possible to use a second stage to convert the data back to the original wavelength. This problem can easily be illustrated by generating four different discrete channels and applying XPM to each of them. The optical spectrums of the four channels are shown in Figure 6.15.

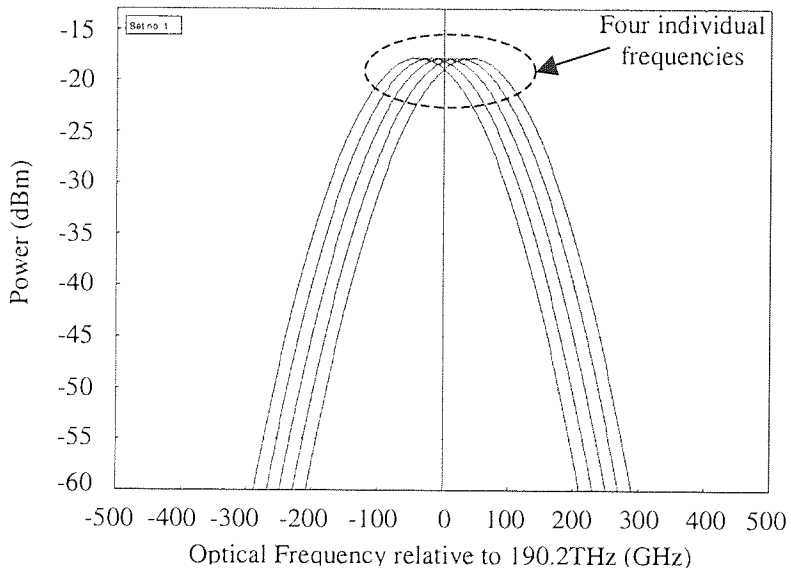

Figure 6.15: The four different frequencies represent the output of stage 1 after phase wander reduction

Each channel is then propagated through a single stage system (the four channels represent what the output of stage 1 might be like. There is no timing irregularities on any of the data, but four discrete wavelengths have been generated). The same amount of XPM is then applied to each channel and the timing delay, $\Delta\tau_2$, is kept constant throughout. With the exception of the wavelength, each channel is identical.

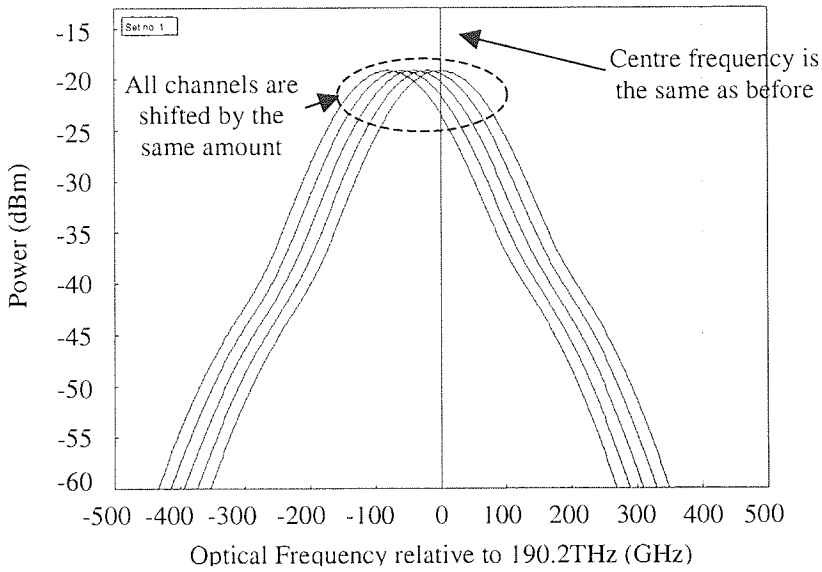

Figure 6.16: After propagation through stage 2 we still have four discrete frequencies that have all been frequency shifted by the same amount

Looking at the output of this single stage device, Figure 6.16, we actually find that although $\Delta\tau_2$ was kept constant throughout, the initial wavelength of the data to be converted has had an effect on the wavelength that is produced. Each individual frequency was converted by exactly the same amount and so the outputs have all just been shifted a little. This demonstrates that using this scheme as a second stage in order to produce a constant, single wavelength will never work.

6.6 Discussion

It has been demonstrated during the previous chapter that it is in fact not necessary that an optical AND gate be employed in order to apply wavelength conversion to data. The basic principle that applying dynamic wavelength conversion followed by dispersion compensating to data can reduce both timing jitter and phase wander has once more been shown. Indeed at first glance this adapted scheme shows some distinct advantages over previously discussed schemes, but overall it may prove difficult to implement. For example, by not having to generate a chirped clock source we instantly have a much shorter propagation length for the device. This would clearly help when trying to overcome the problems of temporal drift. Also, as the device is once again passive (not electrical components such as SOA's) we potentially have a device which would be capable of operating at a very high repetition rate. However, there will always be one fundamental flaw with this scheme that has not yet been considered during this chapter and that is external variables. Extrinsic fluctuations, such as ambient temperature change, will be a severe problem. Instability will occur as the propagation length of the nonlinear fibre changes. Although temperature changes have been a problem in previous chapters, the problem has been because of the long length of fibre used for the chirp generation and not necessarily because of the 1km of nonlinear fibre used in say the NOLM. Because all of the results in this chapter have been generated entirely by computer simulation, this problem has not been addressed but I would hypothesise that it would be a severe limitation if the device were to be fabricated inside a laboratory. As has been previously stated, housing the entire device inside a temperature controlled chamber would help alleviate this problem but may prove impractical.

It has also been shown that using this arrangement, it will not be possible to convert the phase wander reduced output back into a single wavelength. This does mean that this system cannot be converted into a 3R regenerator or used in a transmission link. However, there is no reason why this arrangement could not work perfectly well as an optical clock recovery unit which is placed before a photodiode at the end of a transmission link where the wavelength of the output is incidental.

It should also be noted that although the timing irregularity that has been considered throughout this chapter is phase wander, it is obvious that the exact same setup would also compensate for timing jitter. The problem of timing jitter was not considered here simply because it is difficult to apply timing jitter within the simulation tool.

Chapter 7 - Conclusions

7.1 Conclusion

This thesis has combined both optical numerical simulations with actual laboratory results. Both the numerical simulations (the results for which were obtained using the computer modelling tool VPI) and experimental results were all obtained by the author. There is a distinct advantage in having one person performing both tasks and that is simply one of understanding. The use of simulations in research (all-optical processing in this particular case) is incredibly valuable. Firstly we are able to simulate non-practical models which can be used to demonstrate say a principle of operation (we can think of non-practical models as ones which would be impossible to re-create in a laboratory environment. For example, in a computer model it is possible to say have no noise in a system or a parameter that is simply unfeasible). Secondly, we are able to easily create massive or complex systems whose only draw back is simulation time. It is for these reasons that numerical simulations prove an invaluable tool. However, at the same time, one can never underestimate the need for practical laboratory results and so an experimental section has been included in this thesis.

The main purpose of this thesis was to investigate the potential usefulness and practicability of all-optical processing for current and future optical communications networks. The author was able to postulate a possible solution to this issue by utilising various optical loop mirror configurations to produce a device that could compensate for both timing jitter and phase wander simultaneously. This was achieved by taking the incoming data channel (which contained the timing problems that needed to be

compensated for) and optically sampling a locally generated chirped optical clock source. The sampling function was achieved by using a nonlinear optical loop mirror (NOLM) and the chirped clock source was generated by propagating a short, high peak powered clock source through a length of nonlinear fibre. An appropriate length of fibre was then used to apply dispersion compensation. The timing compensation scheme works by dynamic wavelength conversion. Depending on the relative timing displacement of the data with respect to the clock (we use the clock to define what we will call the "ideal" timing position), the data is converted to a new corresponding wavelength (this conversion is continuous in nature, not discrete). By applying dispersion compensation, the timing displacement is then removed and hence, timing jitter and phase wander is suppressed.

The above outlined "principle of operation" was conceived and then tested using computer simulation (the simulation tool used exclusively throughout this thesis was VPI). Early simulations showed that the chirped clock pulse could be tailored, in temporal profile and chirp, by manipulation of certain parameters (such as core effective area, fibre length and peak power used), this is an essential element of the system. It was also shown how changing the temporal profile of the chirped clock affected how the final system performed. By increasing the duration of the clock, the tolerance to timing jitter and phase wander can be increased. However, if the chirp of the clock source is changed, the level of dispersion compensation required to remove the timing irregularity must also be changed accordingly. It was then shown that by using an optical filtering technique, an analogous system could be constructed and tested. This showed that the basic principle could work and led to the construction of a full model in VPI. The full model incorporated a nonlinear optical loop mirror (NOLM) and the required dispersion compensation. However, before the full model could be used, testing of the said NOLM and following dispersion

compensation was undertaken (without the use of wavelength conversion). The NOLM behaved as one might expect, on this evidence it was deemed that VPI would be able to calculate the required results. Finally the full model, dynamic wavelength conversion using a NOLM, was tested which showed that the "principle of operation" worked and that by using this method, phase wander could be compensated for (at no point in this thesis are the effects of timing jitter simulated). A second stage was then added to the device and the possibility of 3R regeneration was investigated. For both the phase wander compensation and 3R regeneration, BER simulations were carried out showing that the devices could operate, whilst correcting for the applied phase wander, error free.

Once it had been shown that the device could be simulated, these principles were applied in a laboratory environment. The chirp generation and NOLM characteristics were tested and the results showed good agreement with the simulation results (note, the simulations were not designed to accurately re-create the numbers that would be achieved in the laboratory, they were designed to show applicable trends). The full single stage was then constructed and the "principle of operation" shown to work, applied timing jitter and phase wander were successfully reduced. BER measurements were also taken showing that the device could compensate for timing jitter and phase wander whilst remaining error free. The effects of the timing issues on bit error rate measurements were also investigated. Finally it was shown that a second stage could be added to the device, creating a 3R regenerator, and the wavelength produced controlled by simple manipulation of an optical delay line.

7.2 Future Work

Certainly one possible feasible extension to this thesis would be to continue with more experimental laboratory work. There have been several simulations that have been included in this thesis that don't necessarily have a similar corresponding experimental result. In terms of this thesis, this is not necessarily a problem as it is much easier to run simulations than to construct complex experiments (which is one of the reasons for doing the simulations in the first place). This explains the slight imbalance in quantity of presented results.

The results collated and presented throughout this thesis, either obtained by simulation or by experimental investigation, relied on synchronous functionality in order to perform their operations successfully. An extension to either the timing jitter/phase wander reduction system or the 3R regenerator would be to devise a method for creating asynchronous operation. The limitation of synchronous operation is that it relies on nominally knowing when the data, for either of the two discussed devices, will arrive at a certain point in time and then "locking" the system to that point. Clearly the advantage of both the proposed systems is that because they compensate for a certain level of timing offset (be that either timing jitter or phase wander) then there is a tolerance to how exact we need to be when locking on to the data (one of the reasons for using the device in the first place) but we still do need to know when the data will roughly arrive. By modifying the systems so that they could operate truly asynchronously, there would be no need to know at all when the data was to be transmitted. This would add an extra degree of functionality and to some extent "future proofing" as it would mean that the devices could be simply installed in a network and left to operate on its own (providing of course that the bit rate and transmission wavelength of the original data remained constant). A further

addition would be to introduce more than one channel to the system (at the moment one single channel operation is feasible and so any extra channels requiring timing jitter or phase wander reduction would require additional devices). This would potentially reduce costs and installation space which would surely increase the desirability of the system further.

Within the experimental chapters contained in this thesis, a proprietary waveguide device was tested which showed that when using such a device, timing jitter and phase wander could be compensated for. As discussed, this holds the advantage over the fibre based designs (NOLM) in that it is small and compact. However, the tested system still required further external large subsystems (such as the 2.2km of nonlinear fibre required to produce the locally generated chirped clock source, various lengths of SMF which were required for the dispersion compensation, not to mention the EDFA's and filters used). In theory in the future these could be miniaturized and included on the waveguide itself. This would lead to one waveguide and ultimately a small package for the entire device.

Finally the chirped clock pulse generation should be briefly mentioned. To date the simplest way of generating the required temporal profile and linear chirp of the clock is through propagation through lengths of highly nonlinear fibre. However, because of the high nonlinearity that is required, relatively long lengths of fibre are needed (or incredibly high peak power). With the advancements in photonic crystal fibre comes the potential for incredibly high nonlinearity over a very short length of fibre. This would be ideal as it would alleviate many of the temporal drift problems that were encountered due to extrinsic effects. A further development would lead to the use of another element to produce the desired clock pulse. This may mean that it would be easier to tailor the

characteristics of the generated pulse more accurately as we are currently limited by the clock pulse not being perfectly square in the time domain.

There is clearly a bright future ahead of optical processing. With the advancements in laser technology and the increased demand for ever faster and faster networks, a clear alternative to "conventional" electronic switching (which is considered to be relatively slow) needs to be found. All-optical processing is certainly a firm contender to fill this gap and it is for this reason that it is vital that the technology and research be allowed to continue.

Chapter 8 - Appendices

8.1 Appendix A: Publications

- "All-optical signal processing circuits" (invited paper), A.J. Poustie, R. Manning, R. Webb, J. Harrison, *Proc IEEE/LEOS Summer Topical Meetings 2002 - Fast Optical Signal Processing in Optical Transmission*, p.3 (2002)

- "All-optical retiming and jitter suppression using dynamic wavelength conversion and dispersion compensation" J. A. Harrison, A.J. Poustie, K. J. Blow, *Proc Photonics and Switching 2003*

- "All-optical bit-level retiming and jitter suppression", J. A. Harrison, K. J. Blow, A.J. Poustie, *Optics Communications, Vol 240, pp221-226, 1st October 2004*

8.2 Appendix B: Definitions and Symbols

3R	Regenerate, re-shape, re-time
α	Attenuation coefficient
β_n	Dispersion of the group velocity
Δ	Relative core cladding index difference
$\varepsilon(\omega)$	Dielectric constant
γ	Nonlinear coefficient
k_0	Wavenumber
θ_c	Critical angle
μ_0	Permeability of free space
ϕ_{NL}	Nonlinear phase shift
τ	Time
V	Normalised frequency
v_g	Group velocity
λ	Wavelength
A_0	Peak amplitude
ASE	Amplified spontaneous emission
BW	Bandwidth
BER	Bit-error-rate
c	Speed of light
C	Chirp parameter
dB	Decibels
dBm	Power calculated in dB with respect to 1mW

DCF	Dispersion compensation fibre
DFB	Distributed feedback laser
EAM	Electro-absorption modulator
EDFA	Erbium doped fibre amplifier
FBG	Fibre Bragg grating
FWHM	Full width half maximum
Gbit/s	Giga bit per second
GHz	Giga hertz
GNLSE	Generalised nonlinear Schrödinger equation
GS-DFB	Gain switched distributed feedback laser
L	Length
L_D	Dispersion length
L_{eff}	Effective length
L_{NL}	Nonlinear length
L_w	Walk-off length
mW	milliwatt
n	Refractive index
n2	Nonlinear index coefficient
n_g	Group index
NLSE	Nonlinear Schrödinger equation
NRZ	Nonreturn-to-zero
NOLM	Nonlinear optical loop mirror
OSA	Optical spectrum analyser
OTDM	Optical time division multiplexing
P_{in}	Input power

P_{out}	Output power
PRBS	Pseudo random bit sequence
ps	Pico seconds
RF	Radio Frequency
RMS	Root mean square
RZ	Return-to-zero
SMF	Single mode fibre
SOA	Semiconductor optical amplifier
SPM	Self phase modulation
Tbit/s	Tera bit per second
VPI	Virtual photonics interface
WDM	Wavelength division multiplexing
XPM	Cross phase modulation

8.3 Appendix C: Nonlinear fibre parameters

Below is a list of the parameters for the two lengths of nonlinear fibre used in the simulations of this thesis.

Parameter	Sumitomo 1	Sumitomo 2
Length (m)	1000.00	1200.00
Reference frequency (Hz)	193.41e12	193.41e12
Attenuation (dB/m)	0.57e-3	0.57e-3
Dispersion (s/m^2)	-1.57e-6	-0.60e-6
Dispersion slope (s/m^3)	0.03e3	0.03e3
Nonlinear index (m^2/W)	5.60e-20	5.60e-20
Core area (m^2)	11.34e-12	11.34e-12
Tau1 (s)	12.20e-15	12.20e-15
Tau2 (s)	32.00e-15	32.00e-15
Raman coefficient	0.00	0.00

Table 1.1: Parameters used for the generation of nonlinear fibre

8.4 Appendix D: Timing jitter applied to data source

The applied rms noise is shown for the four different noise settings. The noise is naturally seen to increase as the applied voltage increases. Also shown is the effect that the noise has on the original data's eye diagram

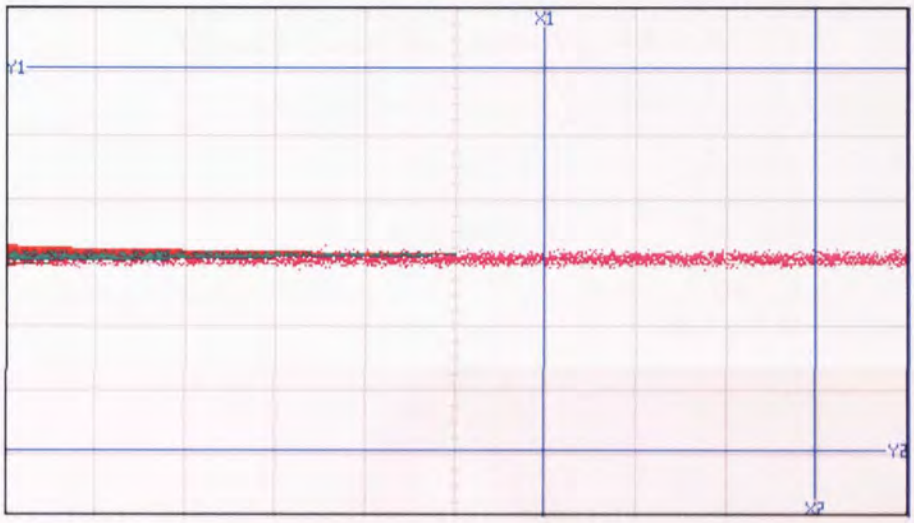

Figure 8.1: Applied voltage, V_{rms} = 100mV

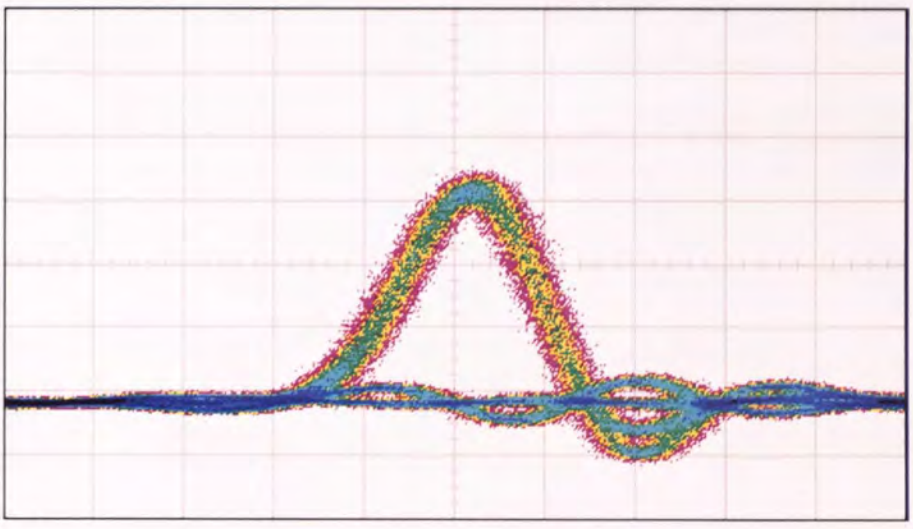

Figure 8.2: The eye diagram from the previous level of noise, V_{rms} = 100mV

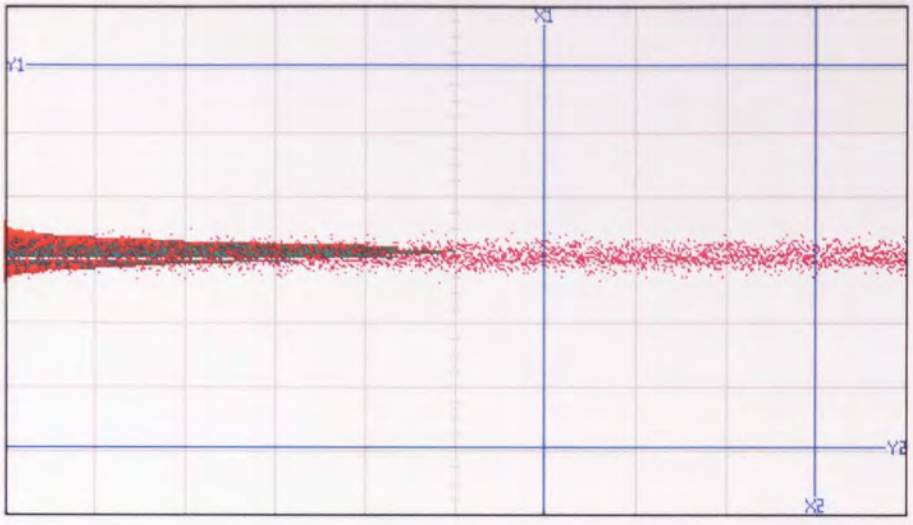

Figure 8.3: Applied voltage, V_{rms} = 250mV

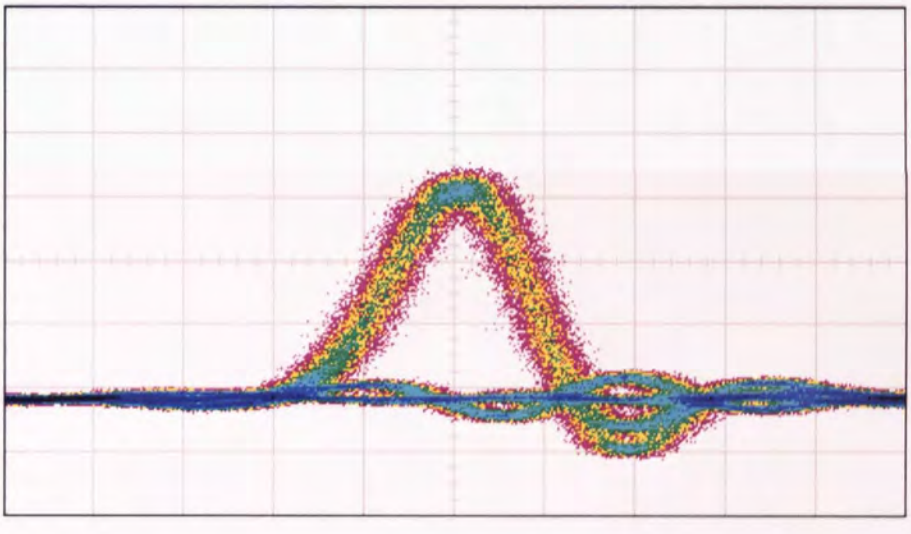

Figure 8.4: The eye diagram from the previous level of noise, V_{rms} = 250mV

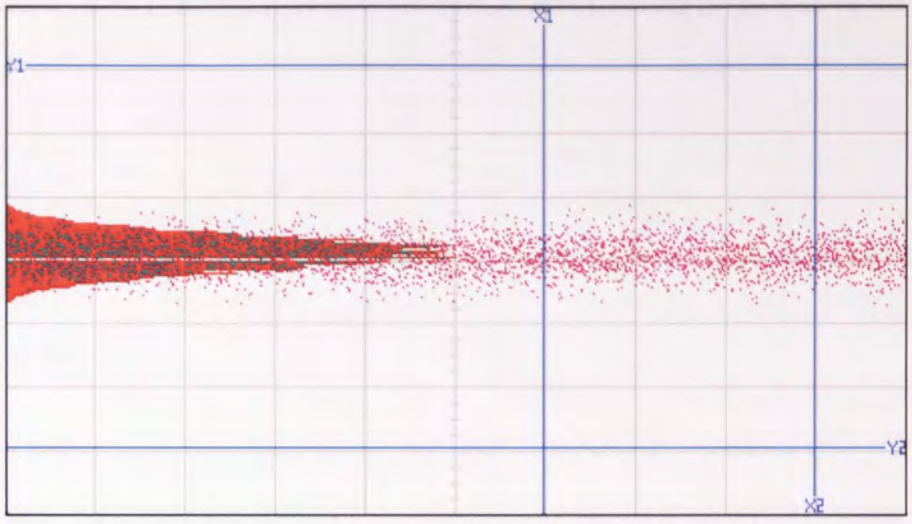

Figure 8.5: Applied voltage, V_{rms} = 500mV

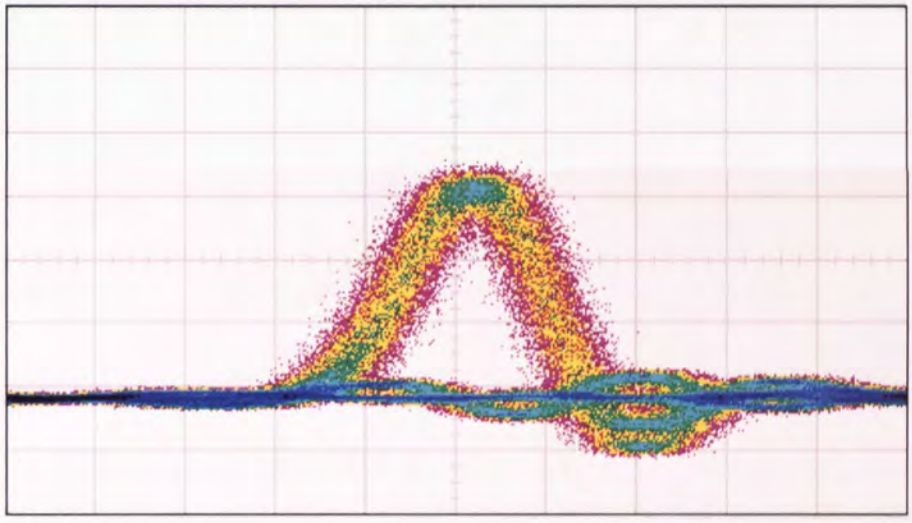

Figure 8.6: The eye diagram from the previous level of noise, V_{rms} = 500mV

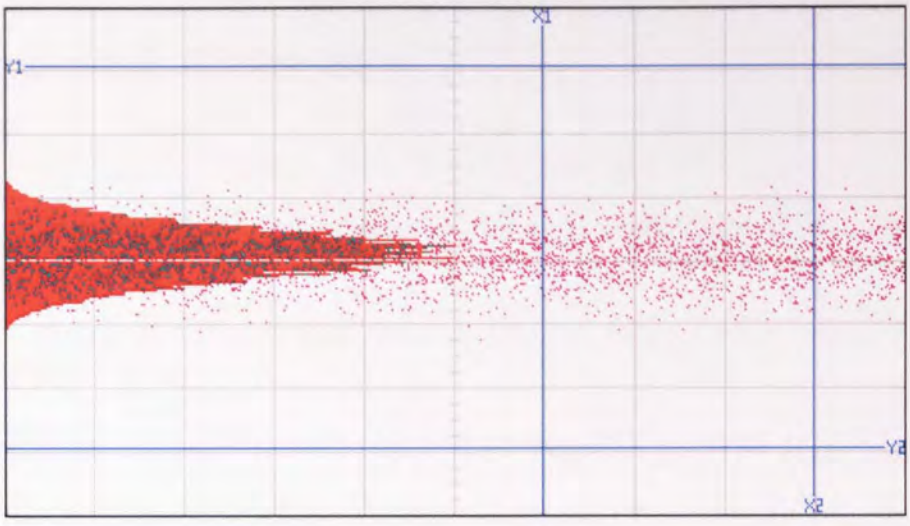

Figure 8.7: Applied voltage, V_{rms} = 750mV

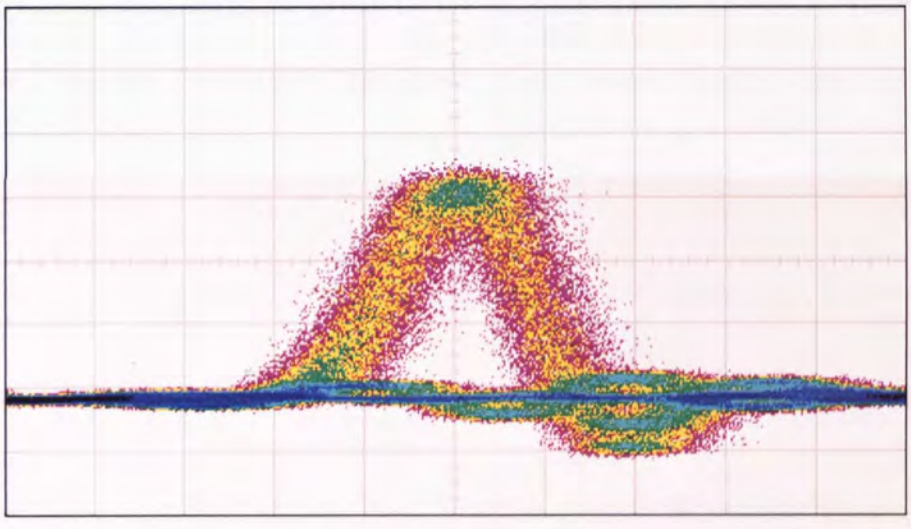

Figure 8.8: The eye diagram from the previous level of noise, V_{rms} = 750mV

8.5 Appendix E: Bibliography

1. G. P. Agrawal, *Fibre Optic Communications Systems*, Third, Editor. 2002, Wiley-interscience. p. 2.

2. A. Ghatak, K. Thyagarajan, *Introduction to Fibre Optics*. 1998, Cambridge University Press. p. 1-3.

3. D. Dyer, *A story of Discovery and Reinvention*. 2001, Corning. p. 100-117.

4. G. P. Agrawal, *Fibre Optic Communications Systems*, Third, Editor. 2002, Wiley-interscience. p. 13-15.

5. A. Ghatak, K. Thyagarajan, *Introduction to Fibre Optics*. 1998, Cambridge University Press. p. 29-31.

6. A. Ghatak, K. Thyagarajan, *Introduction to Fibre Optics*. 1998, Cambridge University Press. p. 31.

7. G. P. Agrawal, *Fibre Optic Communications Systems*, Third, Editor. 2002, Wiley-interscience. p. 55-56.

8. A. Ghatak, K. Thyagarajan, *Introduction to Fibre Optics*. 1998, Cambridge University Press. p. 34-35.

9. A. Ghatak, K.T., *Introduction to Fibre Optics*. 1998, Cambridge University Press. p. 39-40.

10. G. P. Agrawal, *Fibre Optic Communications Systems*, Third, Editor. 2002, Wiley-interscience. p. 56-58.

11. E. B. Brown, *Modern Optics*. 1965, Reinhold publishing corporation. p. 112-118.

12. A. Ghatak, K.T Thyagarajan, *Introduction to Fibre Optics*. 1998, Cambridge University Press. p. 97-100.

13. G. P. Agrawal, *Fibre Optic Communications Systems*, Third, Editor. 2002, Wiley-interscience. p. 29-30.

14. E. B. Brown, *Modern Optics*. 1965, Reinhold publishing corporation. p. 41-43.

15. M. Garbuny, *Optical Physics*. 1965, Academic press. p. 242-243.

16. G. R. Fowles, *Introduction to Modern Optics*. 1968, Holt, Rinehart and Winston, Inc. p. 35.

17. R. W. Ditchburn, *Light*. 1963, lackie and Son. p. 504-508.

18. D. Min, K. Chan, C. K. Chui, *A novel approach to solving the nonlinear Schrodinger equation bythe coupled amplitude-phase formulation.* IEEE Journal of Quantum Electronics, 1995. **31**(1): p. 177-182.

19. C. Monterola, C. Saloma, *Solving the nonlinear Schrodinger equation with an unsupervised neural network: estimation of error in solution.* Optics Communications, 2003. **222**(1-6): p. 331-339.

20. L. R. Watkins, Y. R. Zhou, *Modeling propagation in optical fibers using wavelets.* Journal of Lightwave Technology, 1994. **12**(9): p. 1536-1542.

21. K. V. Peddanarappagari, M. B-Pearce, *Volterra series approach for optimizing fiber-optic communications system designs.* Journal of Lightwave Technology, 1998. **16**(11): p. 2046-2055.

22. I. P. Kaminow, T. Lee, *Optical Fiber Telecommunications*. 2002, Academic Press. p. 247-248.

23. G. P. Agrawal, *Nonlinear Fibre Optics*, Third, Editor. 2001, Academic Press. p. 49-50.

24. A. Sano, Y. Miyamoto, S. Kuwahara, H. Toba, *A 40-Gb/s/ch WDM transmission with SPM/XPM suppression through prechirping and dispersion management.* Journal of Lightwave Technology, 2000. **18**(11): p. 1519-1527.

25. T. K. Chiang, N. Kagi, T. K. Fong, M. E. Marhic, L. G. Kazovsky, *Cross-phase modulation in dispersive fibers: Theoretical and experimental investigation of the impact of modulation frequency.* IEEE Photonics Technology Letters, 1994. **6**: p. 733-736.

26. K. Song, M. Premaratne, *Effects of SPM, XPM, and Four-Wave-Mixing in L-Band EDFAs on Fiber-Optic Signal Transmission.* Electronics Letters, 2000. **12**(12): p. 1630-1632.

27. H. Yoshiyama, Y. Shio, A. Imaizumi, H. Motoyama, M. Nakajima, S. Tanaka, H. Kobayashi, A. Watanabe, H. Saito, *Evaluation of intensity shape and phase change of light pulses with frequency chirp due to self-phase modulation.* IEEE Journal of Quantum Electronics, 1989. **25**(10): p. 2129 - 2134.

28. M. Stern, J. P. Heritage, R. N. Thurston, S. Tu, *Self-phase modulation and dispersion in high data rate fiber-optic transmission systems.* Journal of Lightwave Technology, July. **8**(7): p. 1009-1016.

29. G. P. Agrawal, N. A. Olsson, *Self-phase modulation and spectral broadening of optical pulses insemiconductor laser amplifiers.* IEEE Journal of Quantum Electronics, 1989. **25**(11): p. 2297 - 2306.

30. R. R. Alfano, Q. Li, T. Jimbo, J. T. Manassah, P. P. Ho, *Induced spectral broadening of a weak picosecond pulse in glass produced by an intense picosecond pulse.* Optics Letters, 1986. **11**(10): p. 626-628.

31. H. J. Thiele, R. I. Killey, P. Bayvel, *Influence of fibre dispersion and bit rate on cross-phase-modulation-induced distortion in amplified optical fibre links.* Electronics Letters, 1998. **34**(21): p. 2050-2051.

32. R. A. Saunders, A. Robinson, D. Garthe, R. Hui, M. O'Sullivan, *Method of compensating cross phase modulation in 10Gbit/s WDM systems over nonzero dispersion shifted fibre.* Electronics Letters, 1998. **34**(18): p. 1767-1768.

33. R. A. Saunders, B. L. Patel, H. J. Harvey, A. Robinson, *Impact of cross-phase modulation for WDM systems over positive and negative dispersion NZ-DSF and methods for its suppression.* Electronics Letters, 1996. **32**(24): p. 2206-2207.

34. T. K. Chiang, N. Kagi, M. E. Marhic, L. G. Kazovsky, *Cross-phase modulation in fiber links with multiple opticalamplifiers and dispersion compensators.* Journal of Lightwave Technology, 1996. **14**(3): p. 249-259.

35. G. P. Agrawal, R. R. Alfano, *Temporal and spectral effects of cross-phase modulation on co-propagating ultrashort pulses in optical fibres.* Physical Review A, 1989. **40**(9): p. 5063-5072.

36. G. P. Agrawal, *Nonlinear Fibre Optics*, Third, Editor. 2001, Academic Press. p. 18-19.

37. G. P. Agrawal, *Nonlinear Fibre Optics*, Third, Editor. 2001, Academic Press. p. 205-206.

38. G. P. Agrawal, *Nonlinear Fibre Optics*, Third, Editor. 2001, Academic Press. p. 69-71.

39. J. Jae-Hoon, S. Sang-Yung, L. Chang-Hee, *Effects of pre-chirping on the repeaterless dispersion-managedtransmission system.* Electronics Letters, 1996. **32**(9): p. 831-833.

40. T. Morioka, S. Kawanishi, K. Mori, M. Saruwatari, *Transform limited, femtosecond WDM pulse generation by spectral filtering of gigahertz supercontinuum.* Electronics Letters, 1994. **30**(14): p. 1166-1168.

41. A. Ghatak, K. Thyagarajan, *Introduction to Fibre Optics.* 1998, Cambridge University Press. p. 21-24.

42. B. J. Vakoc, M. J. F. Digonnet, G. S. Kino, *A novel fiber-optic sensor array based on the Sagnac interferometer.* Journal of Lightwave Technology, 1999. **17**(11): p. 2316-2326.

43. D. Zhao, X. Shu, Y. Lai, L. Zhang, I. Bennion, *Fiber Bragg grating sensor interrogation using chirped fiber grating-based Sagnac loop.* IEEE Sensors Journal, 2003. **63**(6): p. 734-738.

44. M. Jinno, T. Matsumoto, *Nonlinear Sagnac interferometer switch and its applications.* IEEE Journal of Quantum Electronics, 1992. **28**(4): p. 875-882.

45. P. Parolari, P. Boffi, L. Marazzi, M. Martinelli, *Two-stage Sagnac demultiplexer.* Journal of Lightwave Technology, 2003. **21**(8): p. 1808-1812.

46. T. Houbavlis, K. Zoiros, K. Vlachos, T. Papakyriakopoulos, H. Avramopoulos, F. Girardin, G. Guekos, R. Dall'Ara, S. Hansmann, H. Burkhard, *All-optical XOR in a semiconductor optical amplifier-assisted fiber Sagnac gate.* IEEE Photonics Technology Letters, 1999. **11**(3): p. 334-336.

47. Y. Zhou, J. Wu, J. Lin, *Novel ultrafast all-optical XOR scheme based on sagnac interferometric structure.* IEEE Journal of Quantum Electronics, 2005. **41**(6): p. 823-827.

48. G. P. Agrawal, *Applications of Nonlinear Fibre Optics*. 2001, Academic Press. p. 124.

49. G. P. Agrawal, *Applications of Nonlinear Fibre Optics*. 2001, Academic Press. p. 126.

50. M. Eiselt, W. Pieper, H. G. Weber, *SLALOM: Semiconductor laser amplifier in a loop mirror.* Journal of Lightwave Technology, 1995. **13**(10): p. 2099-2112.

51. G. P. Agrawal, *Applications of Nonlinear Fibre Optics*. 2001, Academic Press. p. 130.

52. O. Leclerc, B. Lavigne, E. Balmefrezol, P. Brindel, L. Pierre, D. Rouvillain, F. Seguineau, *Optical regeneration at 40Gb/s and beyond.* Journal of Lightwave Technology, 2003. **21**(11): p. 27792790.

53. M. Meissner, M. Rosch, B. Schmauss, G. Leuchs, *12dB of noise reduction by a NOLM-based 2R regenerator.* IEEE Photonics Technology Letters, 2003. **15**(9): p. 1297-1299.

54. T. Sakamoto, K. Kikuchi, *Nonlinear optical loop mirror with an optical bias controller for achieving full-swing operation of gate switching.* IEEE Photonics Technology Letters, 2003. **16**(2): p. 545-547.

55. S. Boscolo, S. K. Turitsyn, K. J. Blow, *All-optical passive 2R regeneration for N x 40Gbit/s WDM transmission using NOLM and novel filtering technique.* Optics Communication. 2003. **217**: p. 227-232.

56. F. Parmigiani, P. Petropoulos, M. Ibsen, D. J. Richardson, *All-optical pulse reshaping and retiming systems incorporating pulse shaping fibre Bragg gratings.* Journal of Lightwave Technology, 2006. **24**(1): p. 357-364.

57.. L. Xu, I. Glesk, V. Baby, P. R. Prucnal, *All-optical wavelength conversion using SOA at nearly symmetric position in a fiber-based Sagnac interferometric loop.* IEEE Photonics Technology Letters, 2004. **16**(2): p. 539-541.

58. T. Durhuus, B. Mikkelsen, C. Joergensen, S.L. Danielsen, K.E. Stubkjaer, *All-optical wavelength conversion by semiconductor optical amplifiers.* Journal of Lightwave Technology, 1996. **14**(6): p. 942-954.

59. A. Bogoni, P. Ghelfi, M. Scaffardi, L. Poti, *All-optical regeneration and demultiplexing for 160Gb/s transmission systems using a NOLM-based three-stage scheme.* IEEE Journal of Selected Topics in Quantum Electronics, 2004. **10**(1): p. 192-196.

60. T. Durhuus, C. Joergensen, B. Mikkelsen, R. J. S. Pedersen, K. E. Stubkjaer, *All optical wavelength conversion by an SOA in a Mach-Zehnder interferometer.* IEEE Photonics Technology Letters, 1994. **6**(1): p. 53-55.

61. K. S. Jepsen, A. Buxens, A. T. Clausen, H. N. Poulsen, B. Mikkelsen, K. E. Stubkjaer, *20Gbit/s optical 3R regeneration using polarisation-independent monolithically integrated Michelsen interferometer.* Electronics Letters, 1998. **34**(5): p. 472-474.

62. J. D. Merlier, G. Morthier, S. Verstuyft, T. V. Caenegem, I. Moerman, P. V. Daele, P. Baets, *Experimental demonstartion of all-optical regeneration using an MMI-SOA.* IEEE Photonics Technology Letters, 2002. **14**(5): p. 660-662.

63. Z. Hu, H. Chou, K. Nishimura, M. Usami, J. E. Bowers, D. J. Blumenthal, *Optical clock recovery circuits using travelling-wave electro-absorption modulator-based ring oscillators for 3R regeneration.* IEEE Journal of Selected Topics in Quantum Electronics, 2005. **11**(2): p. 329-337.

64. T. Otani, T. Miyazaki, S. Yamamoto, *40Gbit/s optical 3R regeneration using electro-absorption modulators for optical networks.* Journal of Lightwave Technology, 1996. **20**(2): p. 195-200.

65. E. S. Awad, P. S. Cho, C. Richardson, N. Moulton, J. Goldhar, *Optical 3R regeneration using a single EAM for all-optical timing extraction with simultaneous reshaping and wavelength conversion.* IEEE Photonics Technology Letters, 2002. **14**(9): p. 1378-1380.

66. H. Chou, Z. Hu, J. E. Bowers, D. J. Blumenthal, *Compact optical 3R regeneration using a travelling-wave electro-absorption modulator.* IEEE Photonics Technology Letters, 2005. **17**(2): p. 486-488.

67. S. Arahira, Y. Ogawa, *160Gb/s OTDM signal source with 3R function utilising ultrafast mode-locked laser diodes and modified NOLM.* IEEE Photonics Technology Letters, 2005. **17**(5): p. 992-994.

68. H. S. Chung, R. Inohara, N. Nishimura, M. Usami, *40Gb/s NRZ wavelength conversion with 3R regeneration using an EA modulator and SOA polarisation-discriminating delay interferometer.* IEEE Photonics Technology Letters, 2006. **18**(2): p. 337-339.

69. M. Cvijetic, *Progress toward multi-band high capacity WDM system.* in *Lasers and Electro-Optics Society (LEOS).* 2001.

70. Y. Yamada, S. I. Nakagawa, Y. Kurosawa, T. Kawazawa, H. Taga, K. Goto, *2 Tbit/s (200x10 Gbit/s) over 9240km transmission experiment with 0.15nm channel spacing using VSB format.* Electronics Letters, 2002. **38**(7): p. 328-330.

71. L.J. Richardson, W. Forysiak, K.J. Blow, *Single channel 320Gbit/s short period dispersion managed transmission over 6000km.* Electronics Letters, 2000. **36**(24): p. 2029-2030.

72. B. Mikkelsen, G. Raybon, R. J. Essiambre, J. E. Johnson, K. Dreyer, L. F. Nelson, *Unrepeated transmission over 150km of nonzero-dispersion fibre at 100Gbit/s with semiconductor based pulse source, demultiplexer and clock recovery.* Electronics Letters, 1999. **35**(21).

73. T. Tsuritani, I.Morita, N. Edagawa. *Ultra long-haul transmission with multi-terabit capacity.* in *Lasers and Electro-Optics Society (LEOS).* 2001.

74. N. Yoshikane, I. Morita, T. Tsuritani, A. Agata, N. Edagawa, S. Akiba, *Benefit of SPM-based all-optical reshaper in receiver for long-haul DWDM transmission systems.* IEEE Journal of Selected Topics in Quantum Electronics, 2004. **10**(2): p. 412-420.

75. M. Matsumoto, *Performance analysis and comparison of optical 3R regenerators utilizing self-phase modulation in fibers.* Journal of Lightwave Technology, 2004. **22**(6): p. 1472-1482.

76. T. Miyazaki, F. Kuboto, *All-optical reshaping in a 160-Gb/s OTDM receiver using an XAM gate followed by an SPM discriminator.* IEEE Photonics Technology Letters, 2004. **16**(8): p. 1909-1911.

77. X. Liu, C. Xu, W. H. Knox, M. F. Man. *Characteristics of all-optical 2R regenerators based on self-phase modulation in high-nonlinear fibers.* in *Laser and Elctro-optics Society, (CLEO).* 2002.

78. C. Ito, I. Monfils, J.C. Cartiedge. *Implications of signal chirp on the performance of an all-optical 2R regenerator based on self-phase modulation in a highly nonlinear fiber.* in *Lasers and Electro-Optics Society (LEOS).* 2004.

79. O. Leclerc, B. Lavigne, E. Balmefrezol, P. Brindel, L. Pierre, D. Rouvillain, F. Seguineau, *All-optical signal regeneration: from first principles to a 40 Gbit/s system demonstration.* Optical Telecommunications, 2003. **4**(1): p. 163-173.

80. G. Gavioli, P. Bayvel, *Novel 3R regenerator based on polarization switching in a semiconductor optical amplifier-assisted fiber Sagnac interferometer.* IEEE Photonics Technology Letters, 2003. **15**(9): p. 1261-1263.

81. S. Boscolo, S. K. Turitsyn, K. J. Blow, *Study of the operating Regime for all-optical passive 2R regeneration of dispersion-managed RZ data at 40 Gb/s using in-line NOLMs.* IEEE Photonics Technology Letters, 2002. **14**(1): p. 30-32.

82. R. J. Manning, I. D. Phillips, A. D. Ellis, A. E. Kelly, A. J. Poustie, K. J. Blow, *10 Gbit/s all-optical regenerative memory using single SOA-based logic gate.* Electronics Letters, 1999. **35**(2): p. 159.

83. N. Chi, L. Xu, L. Oxenlowe, T. Tokle, P. Jeppesen, *2R regeneration based on high nonlinear dispersion-imbalanced loop mirror.* Optics Communications, 2002. **206**: p. 295-300.

84. O. Leclerc, B. Danny, D. Rouvillain, P. Brindel, E. Desurvire, C. Duchet, A. Shen, F. Devaux, A. Coquelin, M. Goix, S. Bouchoule, L. Fleury, P. Nouchi, *Simultaneously regenerated 4x40Gbit/s dense WDM transmission over 10,000km using single 40GHz InP Mach-Zehnder modulator.* Electronics Letters, 2000. **36**(18): p. 1574-1575.

85. P. Leisching, H. Beck, A. Richter, D. Stoll, G. Fischer. *Reconfigurable all-optical networking at terabit transmission rates.* in *Optical Fiber Communication Conference.* 2000.

86. T. Goh, M. Yasu, K. Hattori, A. Himeno, M. Okuno, Y. Ohmori, *Silicon-based optical integrated circuits for terabit-rate optical networks.* Journal of Lightwave Technology, 2001. **19**(3): p. 371-379.

87. P. D. Townsend, S. J. D. Pheonix, K. J. Blow, S. M. Barnett, *Design of quantum cryptography systems for passive optical networks.* Electronics Letters, 1994. **30**(22): p. 1875-1877.

88. A. J. Poustie, R. J. Manning, K.J. Blow, *All-optical circulating shift register using a semiconductor optical amplifier in a fibre loop mirror.* Electronics Letters, 1996. **32**(13): p. 1215-1216.

89. Y. Horiuchi, M. Suzuki, *Optical label switch routing on wide-scale optical network using digitally encoded SCM label.* Electronics Letters, 2001. **37**(25).

90. A. J. Poustie, R. J. Manning, K.J. Blow, *All-optical circulating shift register using a semiconductor optical amplifier in a fibre loop mirror.* Electronics Letters, 1996. **32**(13).

91. R. J. Manning, A. J. Poustie, K.J. Blow, *All-optical clock division using a semiconductor optical amplifier loop mirror with feedback.* Electronics Letters, 1996. **32**(16).

92. N.J. Smith, N. J. Doran, K.J. Blow, W.J. Firth, *Gordon-Haus jitter suppression using a single phase modulator.* Electronics Letters, 1994. **30**(12): p. 987-988.

93. M. Hayashi, T. Otani, H. Tanaka, M. Suzuki, *Analysis on jitter tolerance of optical 3R regenerator.* IEEE Photonics Technology Letters, 2003. **15**(11): p. 1609-1611.

94. Q. Xu, V. R. Almeida, M. Lipson, *Micrometer-scale all-optical wavelength converter on silicon.* Optics Letters, 2005. **30**(20): p. 2733-2755.

95. S. L. Jansen, H. Chayet, E. Granot, S. Ben Ezra, D. den van Borne, P. M. Krummrich, D. Chen, G. D. Khoe, H. De Waardt, *Wavelength conversion of a 40-Gb/s NRZ signal across the entire C-band by an asymmetric Sagnac loop.* IEEE Photonics Technology Letters, 2005. **17**(10): p. 2137-2139.

96. A. E. Kelly, A. D. Ellis, D. Nesset, R. Kashyap, D. G. Moodie, *100 Gbit/s wavelength conversion using FWM in an MQW semiconductor optical amplifier.* Electronics Letters, 1998. **34**(20): p. 1955-1956.

97. G. P. Agrawal, *Applications of Nonlinear Fibre Optics*. 2001, Academic Press. p. 290.

98. G. P. Agrawal, *Applications of Nonlinear Fiber Optics*. 2001, Academic Press. p. 305-307.

99. H. Sotobayashi, W. Chujo, *Wideband tunable wavelength conversion of 10Gbit/s return-to-zero signals by optical time gating of a highly chirped rectangular supercontinuum light source.* Optics Letters, 2001. **26**(17): p. 1314-1316.

100. K. Uchiyama, H. Takara, T. Morioka, S. Kawanishi, M. Saruwatari, *100Gbit/s multiple-channel output all-optical demultiplexing based on TDM-WDM conversion in a nonlinear optical loop mirror.* Electronics Letters, 1996. **32**(21): p. 1989-1991.

101. T. Morioka, S. Kawanishi, H. Takara, M. Saruwatari, *Multiple-output, 100Gbit/s all-optical demultiplexer based on multichannel four-wave mixing pumped by a linearly chirped square pulse.* Electronics Letters, 1994. **30**(23): p. 1959-1960.

102. J. Yu, X. Z heng, C. Peucheret, A. T .Clausen, H. N. Poulsen, P. Jeppesen, *40-Gbit/s all-optical wavelength conversion based on a nonlinear optical loop mirror.* Journal of Lightwave Technology, 2000. **18**(7): p. 1001-1006.

103. Y. Zhao, P. Ye, *Impact of initial chirp on nonlinear optical loop mirror switches in switching solitons.* Optics Communications, 2001. **199**: p. 361-368.

104. J. A. Harrison, *All-optical re-timing and jitter suppression.* 2001, Aston University.

105. D. Wolfson, P. B. Hansen, A. Kloch, K. E. Stubkjaer, *All-optical 2R regeneration based on interferometric structure incorporating semiconductor optical amplifiers.* Electronics Letters, 1999. **35**(1).

106. R. P. Webb, R. J. Manning, G. D. Maxwell. A. J. Poustie, *40 Gbit/s all-optical XOR gate based on hybrid-integrated Mach-Zehnder interferometer.* Electronics Letters, 2003. **39**(1): p. 79-80.

107. Y. Ye, X. Zheng, H. Zhang, X. Teng, K. Wu, X. Ma, Y. Guo, *Theoretical analysis of all-optical 2R gegeneration in a SOA based Mach-Zehnder interferometer.* Optics and Laser Technology, 2002. **34**: p. 337-341.

108. J. De Merlier, P. Van. Daele, I. Moreman, R. Beats, *All-optical 2R regeneration based on asymmetric Mach-Zehnder interferometer incorporating MMI-SOA.* Electronics Letters, 2002. **38**(5): p. 238-239

109. R.P. Webb, R. J. Manning, G.D. Maxwell, A.J. Poustie, *40 Gbit/s all-optical XOR gate based on hybrid-integrated Mach-Zehnder interferometer.* Electronics Letters, 2003. **39**(1): p. 79-81.

110. D. Wolfson, A. Kloch, T. Fjelde, C. Janz, B. Dagens, M. Renaud, *40-Gb/s All-optical wavelength conversion, regeneration, and demultiplexing in an SOA-Based all-active Mach–Zehnder Interferometer.* IEEE Photonics Technology Letters,, 2000. **12**(3): p. 332-334.

111. C. Joergensen, S. L. Danielsen., M. Vaa, B. Mikkelsen, K.E. Subkjaer, P.Doussiere, F. Pommerau, L. Goldstein, M. Goix, *40Gbit/s all-optical wavelength conversion by semiconductor optical amplifiers.* Electronics Letters, 1996. **32**(4): p. 367-368.

112. K. K. Svidzinskiy, *Silicon-based optical integrated circuits for terabit-rate optical networks.* Microelectronic Engineering, 2003. **69**(2-4): p. 221-227.